PNNL-22677

Pacific Northwest
NATIONAL LABORATORY
Proudly Operated by Battelle Since 1965

PARENT Quick Blind Round-Robin Test Report

September 2014

BG Braatz
PG Heasler
RM Meyer

Prepared for the U.S. Nuclear Regulatory Commission
under a Related Services Agreement with the U.S. Department of Energy
CONTRACT DE-AC05-76RL01830

U.S. DEPARTMENT OF ENERGY

DISCLAIMER

PACIFIC NORTHWEST NATIONAL LABORATORY
operated by
BATTELLE
for the
UNITED STATES DEPARTMENT OF ENERGY
under Contract DE-AC05-76RL01830

Printed in the United States of America

Available to DOE and DOE contractors from the
Office of Scientific and Technical Information,
P.O. Box 62, Oak Ridge, TN 37831-0062;
ph: (865) 576-8401
fax: (865) 576-5728
email: reports@adonis.osti.gov

Available to the public from the National Technical Information Service,
U.S. Department of Commerce, 5285 Port Royal Rd., Springfield, VA 22161
ph: (800) 553-6847
fax: (703) 605-6900
email: orders@ntis.fedworld.gov
online ordering: http://www.ntis.gov/ordering.htm


This document was printed on recycled paper.
(9/2003)

PNNL-22677

PARENT Quick Blind Round-Robin Test Report

BG Braatz
PG Heasler
RM Meyer

September 2014

Prepared for
the U.S. Department of Energy
under Contract DE-AC05-76RL01830

Pacific Northwest National Laboratory
Richland, Washington 99352

Summary

The U.S. Nuclear Regulatory Commission has established the Program to Assess the Reliability of Emerging Nondestructive Techniques (PARENT) whose goal is to investigate the effectiveness of current and novel nondestructive examination procedures and techniques to find flaws in nickel-alloy welds and base materials. This is to be done by conducting a series of open and blind international round-robin tests on a set of piping components that include large-bore dissimilar metal welds, small-bore dissimilar metal welds, and bottom-mounted instrumentation penetration welds. The blind testing is being conducted in two segments, one is called Quick-Blind and the other is called Blind. The Quick-Blind testing and destructive analysis of the test blocks has been completed. This report describes the four Quick-Blind test blocks used, summarizes their destructive analysis, gives an overview of the nondestructive evaluation (NDE) techniques applied, provides an analysis inspection data, and presents the conclusions drawn.

For use in the Quick-Blind tests, four large-bore dissimilar metal weld test block segments were provided to PARENT by the Japan Nuclear Energy Safety Organization. Three of these test blocks contained laboratory-grown axially oriented stress corrosion crack flaws and the fourth test block was blank. Six testing organizations representing Sweden, Republic of South Korea, Japan, and the USA applied NDE test procedures that employed conventional ultrasonic, phased-array ultrasonic, and eddy current NDE techniques. The objective of the tests was to learn how the NDE procedures applied performed from the standpoint of flaw detection, flaw depth sizing, and flaw length sizing.

A destructive analysis of the three test blocks revealed that the laboratory-grown flaws formed in a complex cluster consisting of dozens of cracks. In particular, these axial flaw clusters have significant extent in the circumferential direction (flaw width). The clustered and volumetric nature of the flaws surely had an effect on the detection and sizing results; some readily discernible, others remain unknown as they were not quantified.

All six testing teams detected all of the flaws. Using detection and false call data, probability of detection (POD) curves were developed for flaw length and depth that have wide 95% confidence bounds due mostly to the limited amount of data. The clustered and volumetric nature of these flaws made them relatively easy to detect. This should be considered when interpreting the POD curves developed using the Quick Blind flaws.

The depth sizing analysis showed that testing teams tended to oversize the shallow (2.4 mm) flaw and to undersize the deeper flaws (13.6 mm and 20.1 mm). With a root mean square depth sizing error of 1.3 mm, team 113 had the best depth sizing performance. Team 113's performance is consistent with the conclusion reached in Program for the Inspection of Nickel Alloy Components where tests showed that a combination of conventional and phased-array ultrasound techniques provided the best performance for flaw depth sizing. Teams whose procedures accessed the test block from the inner diameter outperformed teams that accessed from the outer diameter.

Excluding one test team, the root mean square axial length sizing error range (7.3–11.4 mm) for the individual testing teams was reasonable considering that in the USA, to pass a typical weld qualification examination, the maximum difference between indicated and true-state values for flaw length is 19 mm. Team 108 had the lowest root mean square error (7.3) and applied a procedure that combined 1–2 MHz conventional and 2 MHz phased-array ultrasonic techniques.

Acknowledgments

This work was conducted by the U.S. Nuclear Regulatory Commission and the Pacific Northwest National Laboratory in partnership with the Japan Nuclear Energy Safety Organization (JNES), Japan Power Engineering and Inspection Corporation (JAPEIC), Mitsubishi Heavy Industries, Ltd. (MHI), Korea Institute of Nuclear Safety (KINS), Korea Hydro & Nuclear Power Company, Ltd. (KHNP), Swedish Radiation Safety Authority, and the Swedish Qualification Centre (SQC). Collectively, these organizations provided financial support in the form of PARENT participant personnel, test blocks, destructive analysis of test blocks, test teams, shipping, and program leadership.

Acronyms and Abbreviations

BMI	bottom-mounted instrumentation
DMW	dissimilar-metal welds
ECT	eddy current technique
FCP	false call probability
ID	inner diameter
IGSCC	inter-granular stress corrosion cracking
NDE	nondestructive evaluation
OD	outer diameter
PA	ultrasonic testing (phased-array)
PARENT	Program to Assess the Reliability of Emerging Nondestructive Techniques
PINC	Program for the Inspection of Nickel Alloy Components
POD	probability of detection
PWSCC	primary water stress corrosion cracking
RMSE	root mean square error
RRT	round-robin test
SCC	stress corrosion cracking
S/N	signal-to-noise ratio
TRL	transmit-receive longitudinal
UT	ultrasonic testing (conventional)

Contents

Summary iii
Acknowledgments v
Acronyms and Abbreviations vii
1.0 Introduction 1.1
1.1 Background 1.1
1.2 PARENT Quick Blind Round-Robin Tests 1.2
1.3 Guidance from PINC – Lessons Learned Adopted by PARENT 1.2
2.0 Test Block Descriptions 2.1
2.1 Coordinate System 2.1
2.2 Test Block Specifications, Dimensions, and Photographs 2.1
2.3 Flaw Fabrication Process 2.9
2.4 True-State Flaw Locations and Dimensions as Determined by Destructive Analysis 2.11
3.0 NDE Teams, Techniques, and Descriptions 3.1
3.1 Inspection Team and Inspection Procedure Qualifications 3.1
3.2 Summary of NDE Techniques Applied by Testing Teams 3.1
3.3 Combining NDE Techniques 3.2
4.0 Analysis of Performance 4.1
4.1 Scoring Procedure Used for the PARENT Round-Robin Tests 4.1
4.1.1 Calculation of False Call Probability 4.5
4.1.2 Logistic Regression Model for POD 4.5
4.1.3 Scoring Example 4.6
4.2 Evaluation of Detection Capability 4.8
4.2.1 Probability of Detection Results 4.8
4.2.2 Probability of Detection Curves for Flaw Depth and Length 4.9
4.3 Flaw Sizing Results 4.10
4.3.1 Evaluation of Sizing Performance 4.10
4.3.2 Flaw Data 4.11
4.3.3 Depth Sizing Analysis 4.13
4.3.4 Length Sizing Analysis 4.16
5.0 Conclusions 5.1
5.1 Destructive Analysis Results 5.1
5.2 Probability of Detection Performance 5.1
5.3 Depth Sizing Performance 5.1
5.4 Length Sizing Performance 5.1

6.0 Reference 6.1
Appendix A – Destructive Analysis of Quick Blind Test Blocks A.1
Appendix B – Inspection Plots of Quick Blind Test Blocks B.1

Figures

2.1 Coordinate System for Dissimilar Metal Weld Pipe Test Blocks 2.2
2.2 Coordinate System for Test Blocks P15, P16, P17, and P45 ..... 2.3
2.3 Schematic Diagram Showing 1 Axial Laboratory Grown PWSCC Flaw in Each of Test Blocks P15, P16, P17, and P45 ..... 2.4
2.4 Photograph of Test Block P15 ..... 2.5
2.5 Photograph of Test Block P16 ..... 2.6
2.6 Photograph of Test Block P17 ..... 2.7
2.7 Photograph of Test Block P45 ..... 2.8
2.8 Depiction of the Approach Used to Produce a Laboratory Grown PWSCC/IGSCC 2.9
2.9 Flowchart of the Process Used to Produce a Laboratory-Grown PWSCC/IGSCC 2.10
2.10 Stepwise Depiction of Coupon Extraction for Destructive Analysis 2.12
2.11 Cross Section and Crack Information for Test Block P15 at Y=−11 ..... 2.13
2.12 Fracture Surface for the Y=−5 to Y=−9 Segment of Test Block P15 ..... 2.14
2.13 Complex Stress Corrosion Crack Morphology of Stress Corrosion Cracks Found During 2007 in Japan in the Dissimilar Metal Weld of a Steam Generator Nozzle 2.15
4.1 Scoring Procedure for PARENT Quick Blind Round-Robin Tests 4.2
4.2 Probability of Detection versus Scoring Tolerance for Flaws in Test Blocks 4.3
4.3 Probability of Detection versus Scoring Tolerance for Test Teams 4.4
4.4 Scoring Examples for Test Blocks P15, P16, and P45 ..... 4.7
4.5 Probability of Detection versus Flaw Depth 4.9
4.6 Probability of Detection versus Flaw Length 4.10
4.7 Indicated versus True-Flaw Depth by Test Team 4.13
4.8 Indicated versus True Axial Flaw Depth by Test Team 4.15
4.9 Indicated versus True Axial Flaw Depth by NDE Technique 4.16
4.10 Indicated versus True Axial Flaw Length by Test Team 4.17
4.11 Indicated versus True Axial Flaw Length by NDE Technique 4.18
4.12 Indicated versus True Circumferential Flaw Length by Test Team 4.19

Tables

2.1 Actual (True-State) Flaw Locations and Dimensions 2.11
3.1 NDE Techniques Used for PARENT Quick Blind Round-Robin Testing 3.3
4.1 Typical PARENT Inspection Results 4.6
4.2 Probability of Detection by Team with 10-mm Tolerance 4.8
4.3 Probability of Detection by Flaw 4.8
4.4 Summary of False Calls Table 4.8
4.5 Flaw Size Data Reported by Testing Teams 4.12
4.6 Comparison Between Reported Indication Data and True-State Flaw Sizes 4.12
4.7 Flaw Depth Sizing Error by Team 4.14
4.8 Flaw Depth Sizing Error Summary 4.14
4.9 Flaw Depth Sizing Error by ID/OD Access 4.14
4.10 Flaw Axial Length Sizing Error by Team 4.17
4.11 Flaw Axial Length Sizing Errors 4.18

1.0 Introduction

1.1 Background

Worldwide, nuclear power plants have used nickel weld alloys (600, 182, 82, and 52) to facilitate welds of stainless steel cooling line pipes and instrumentation components to the carbon steel vessels. It is now known that these dissimilar-metal nickel-alloy weld joints are susceptible to stress corrosion cracking (SCC), a phenomenon that initiates at the weld/coolant-water interface. This cracking in dissimilar-metal welds (DMWs) has been referred to as primary water stress corrosion cracking (PWSCC), inter-dendritic stress corrosion cracking, and inter-granular stress corrosion cracking (IGSCC). The PWSCC acronym will be the term used throughout this report. PWSCC are generally very tight and they often exhibit complex branching. This morphology combined with the complex weld/component configurations and materials and geometries can make it challenging to achieve reliable detection and sizing by nondestructive evaluation (NDE) methods. PWSCC has occurred in nuclear power plants throughout the world and is a serious issue regarding the safe and reliable operation of nuclear power plants.

The U.S. Nuclear Regulatory Commission has established the Program to Assess the Reliability of Emerging Nondestructive Techniques (PARENT) as a follow-on to the international cooperative Program for the Inspection of Nickel Alloy Components (PINC). The goal of PINC was to evaluate the capabilities of various NDE techniques to detect and characterize surface-breaking primary water stress corrosion cracks in dissimilar-metal welds in bottom-mounted instrumentation (BMI) penetrations and small-bore (≈400-mm diameter) piping components. A series of international blind round-robin tests (RRTs) were conducted by commercial and university inspection teams. Results from these tests showed that a combination of conventional and phased-array ultrasound techniques provided the highest performance for flaw detection and depth sizing in dissimilar metal piping welds. The goal of PARENT is to continue the work begun in PINC and apply the lessons learned to a series of open and blind international round-robin tests that will be conducted on a new set of piping components including large-bore (≈900-mm diameter) DMWs, small-bore DMWs, and BMIs. The testing will include two main parts having the objectives stated below.

1. Blind RRTs

   The objective of the blind testing is to evaluate the latest commercially used NDE inspection techniques to determine which are the most effective for reliably detecting and accurately sizing PWSCC in small-bore DMWs, large-bore DMWs, and BMIs. Only qualified inspectors and qualified procedures will be employed.

2. Open RRTs

   The objective of the open testing is to evaluate novel and emerging NDE inspection techniques to determine which ones show the most promise for inspecting small-bore DMWs, large-bore DMWs, and BMIs. The tests are designed to learn how a variety of advanced techniques being developed by universities and new techniques being developed by industry respond to realistically simulated PWSCC in components that have realistic geometries.

1.2 PARENT Quick Blind Round-Robin Tests

Due to the limited availability of a subset of the large-bore DMW test blocks, during the test planning phase the decision was made to split the PARENT blind round-robin testing into two groups—Quick Blind and Blind. The Quick Blind test blocks were only available from October 2011 through September 2012. This report describes the four Quick Blind test blocks used, summarizes their destructive analysis to determine the true locations and dimensions of the flaws, gives an overview of the NDE techniques applied by the six test teams, provides an analysis of the 24 inspections performed, and presents the conclusions drawn. This report provides the U.S. Nuclear Regulatory Commission, the PARENT Invigilator/Data-Analysis-Group, and PARENT members with an initial view of the data, the data analysis, and the conclusions. The contents of this report will eventually be incorporated into a final report, which will include data from both the Quick Blind and Blind RRT groups.

1.3 Guidance from PINC – Lessons Learned Adopted by PARENT

There were a number of lessons learned during PINC about how to more effectively conduct international round-robin tests of the sort to be conducted in PARENT. Due to practical limitations associated with the compressed schedule for the Quick Blind tests, not all the lessons learned in PINC could be applied to PARENT Quick Blind RRT. The following is a summary of the PINC lessons learned that were applied.

1. Standardized Test Blocks – The Quick Blind test blocks were developed by one group. The test blocks employed the same geometries, materials, and flaw implantation technique. The test blocks utilized the coordinate marking system defined in the round-robin test protocol.
2. Clear Specification Drawings – Testing teams were provided drawings for the test blocks in conformance to the round-robin test protocol. This combined with the proper marking mentioned in (1) above made it possible for teams to correctly report their results, thereby avoiding having teams report data with reversed directions, incorrect units, and displaced locations.
3. Team and Procedure Qualifications – The qualifications of test teams and inspectors was confirmed by test invigilators prior to (or at the time of) data acquisition and data analysis.
4. Inspection Equipment Information – Non-proprietary information about inspection equipment was provided to Pacific Northwest National Laboratory by invigilators in the Procedure Summary Datasheets.
5. Apply Experimental NDE Techniques Only to Open Test Blocks – No experimental NDE techniques were used in the Quick Blind RRT.

2.0 Test Block Descriptions

The following sections provide an overview of the test blocks used in the Quick Blind RRT. The coordinate system used by testing teams to acquire and report data is reviewed in Section 2.1. The test blocks used and photographs for each one are provided in Section 2.2. A description of the fabrication process used to create the laboratory-grown PWSCC in the test blocks is provided in Section 2.3. The actual flaw locations and dimensions (true-state data) for the flaws as determined by destructive analysis is provided in Section 2.4.

2.1 Coordinate System

A round-robin test protocol was developed to provide testing teams with directions for conducting the round-robin tests and reporting results. Figure 2.1 shows the coordinate system defined for dissimilar metal weld pipe test blocks. The zero point is defined as that location on the test block where X=0, Y=0, and Z=0. Figure 2.1 also provides the definitions for the directional vectors X+, Y+, and Z+ in relation to the zero point and with respect to the material construction of the test block. The location for Z=0 is at the outer diameter surface of the test block, at the center of the weld, and is located a distance “D” from the face edge of the carbon steel pipe. Figure 2.2 is a three-dimensional depiction of the coordinate system in Figure 2.1 as applied to the Quick Blind test blocks P15, P16, P17, and P45.

2.2 Test Block Specifications, Dimensions, and Photographs

Figure 2.3 is a schematic diagram that provides the dimensions of test blocks P15, P16, P17, and P45. The coordinate system defined above in Section 2.1 is clearly depicted this diagram. As indicated by the red line with the PWSCC labeled arrow, each of the four test blocks has an axially oriented (Y direction) laboratory-grown PWSCC flaw within the weld region located approximately at the center of the inside diameter surface. The dimensions X1, X2, Y1, Y2, Z1, and Z2 define a three-dimensional box within which the flaw is completely enclosed. Figures 2.4–2.7 are photographs of each of the test blocks.

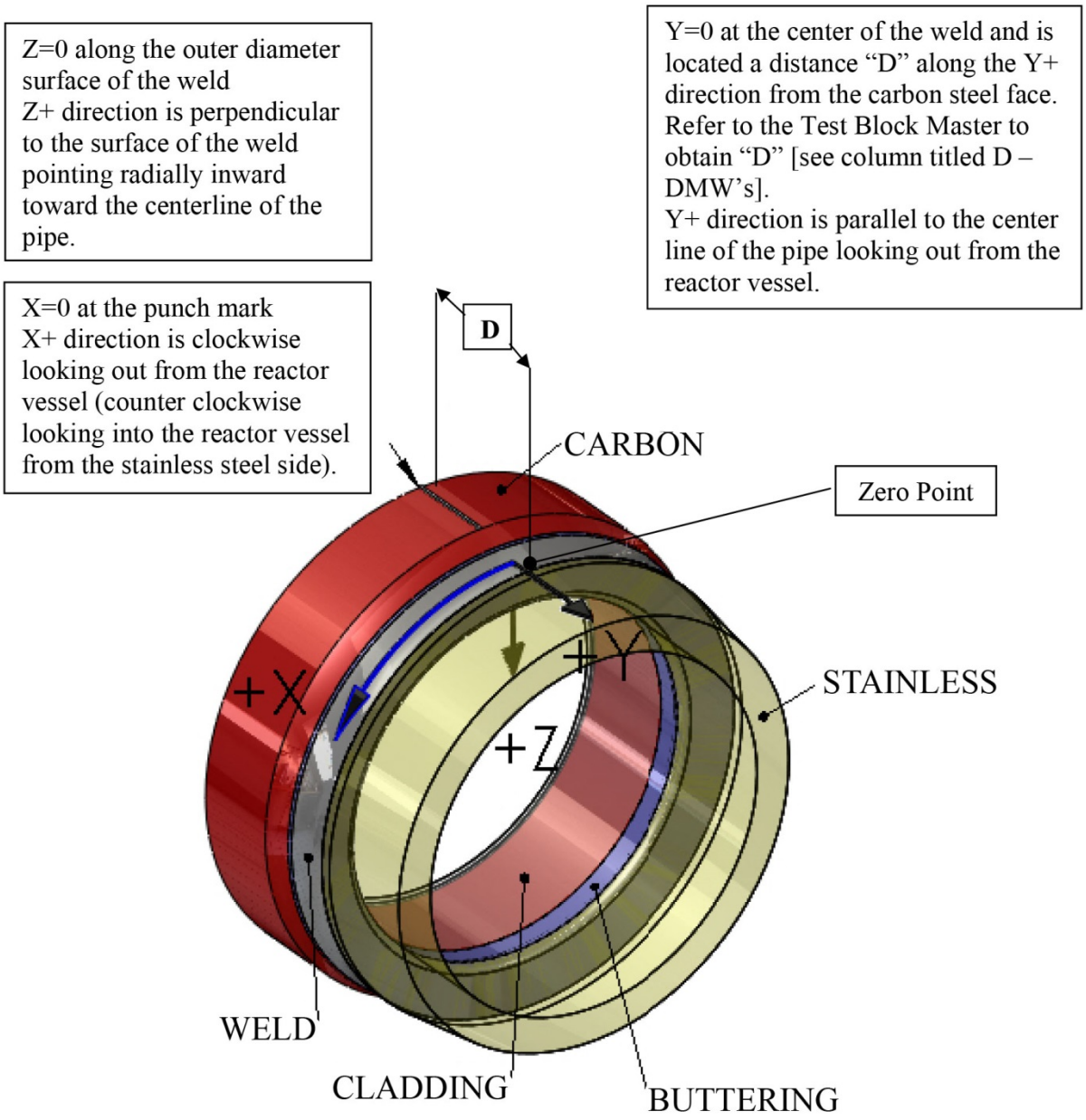

Figure 2.1. Coordinate System for Dissimilar Metal Weld Pipe Test Blocks

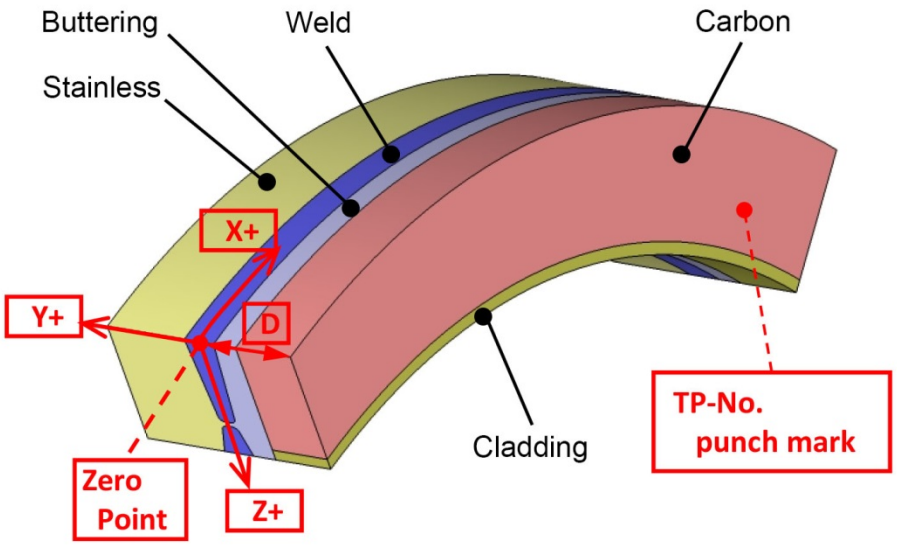

Figure 2.2. Coordinate System for Test Blocks P15, P16, P17, and P45

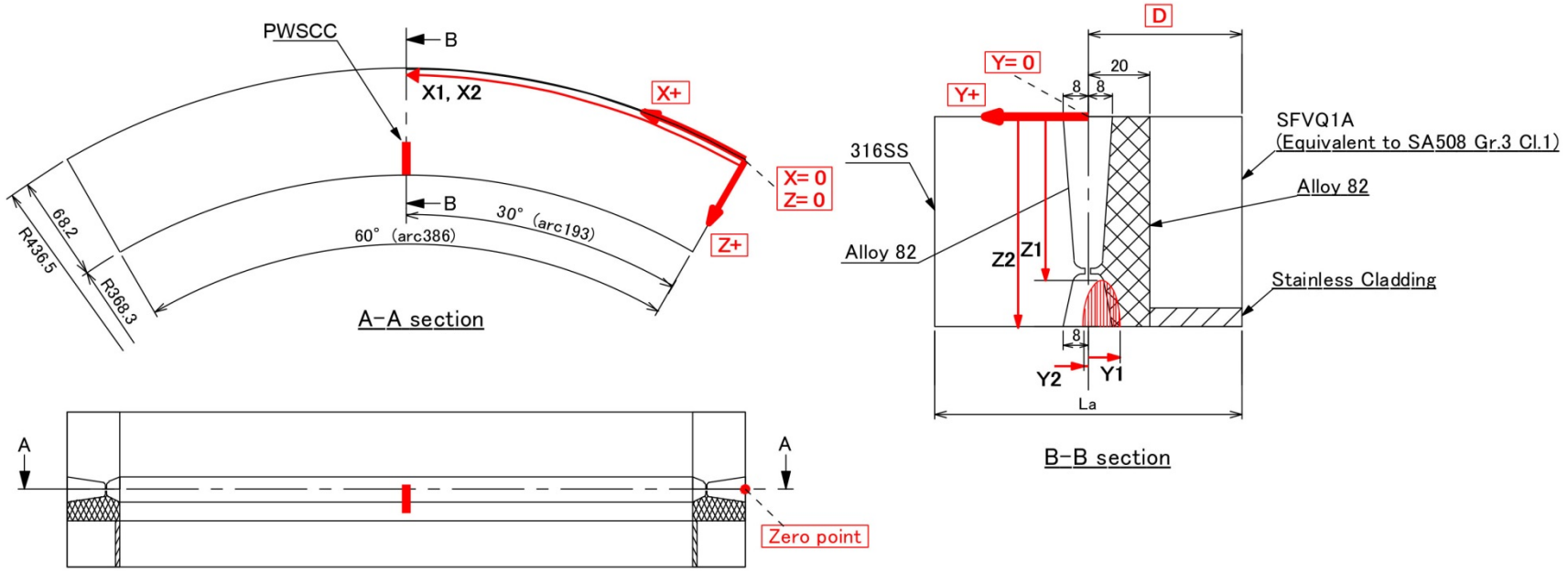

Test Block No.	Flaw	La	D	X1	X2	Y1	Y2	Z1	Z2
P15 (JRV-S1)	PWSCC	100.0	50.0	222.4	234.1	−15.0	6.0	48.1	68.2
P16 (JRV-S2)	PWSCC	100.0	50.0	211.7	236.1	−12.0	4.0	54.6	68.2
P17 (JRV-S3)	PWSCC	100.0	50.0	211.2	244.1	−15.0	6.0	65.8	68.2
P45 (JRV-S4)	No flaw	105.0	51.5	-	-	-	-	-	-

Dimensions are in millimeters

Figure 2.3. Schematic Diagram Showing 1 Axial Laboratory Grown PWSCC Flaw in Each of Test Blocks P15, P16, P17, and P45

Figure 2.4. Photograph of Test Block P15

Figure 2.5. Photograph of Test Block P16

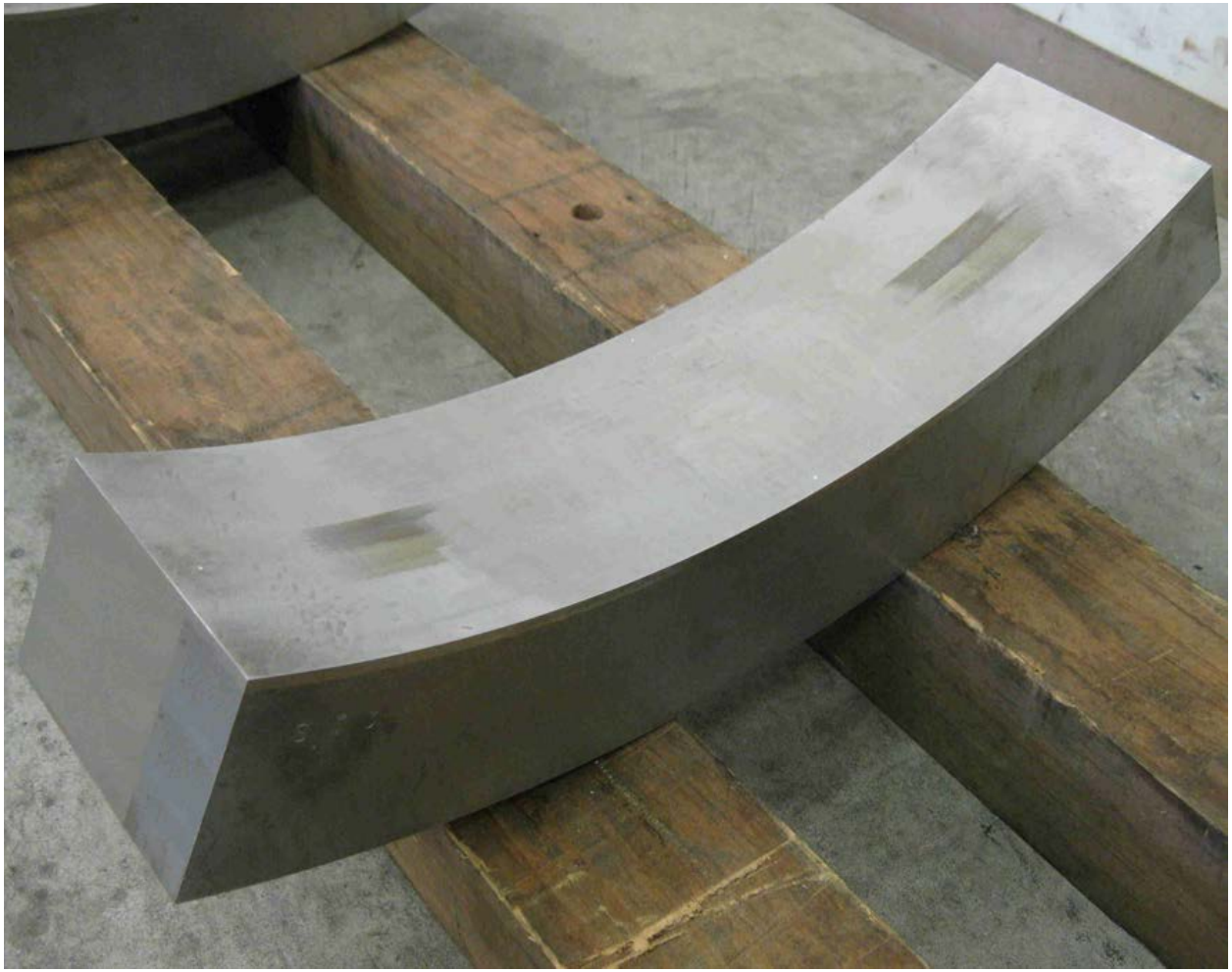

Figure 2.6. Photograph of Test Block P17

Figure 2.7. Photograph of Test Block P45

2.3 Flaw Fabrication Process

The two configurations shown in Figure 2.8(a) and 9(b) were used to fabricate laboratory-grown PWSCC in test blocks P15, P16, and P17. In order to grow a deep SCC flaw and also avoid the large crack opening, which typically accompanies bending loading techniques, the tensile loading type setup shown in Figure 2.8(a) was used to produce the flaw in P15. During the cooling process of the restraint weld and fixing frame, a tensile stress was generated due to the difference of shrinkage between restraint weld and fixing frame. The bending loading type setup shown in Figure 2.8(b) was used for P16 and P17, which were planned to fabricate middle and shallow SCC. The process used is depicted as a flowchart in Figure 2.9.

It was decided to have one blank test block, so no flaw was grown in test block P45.

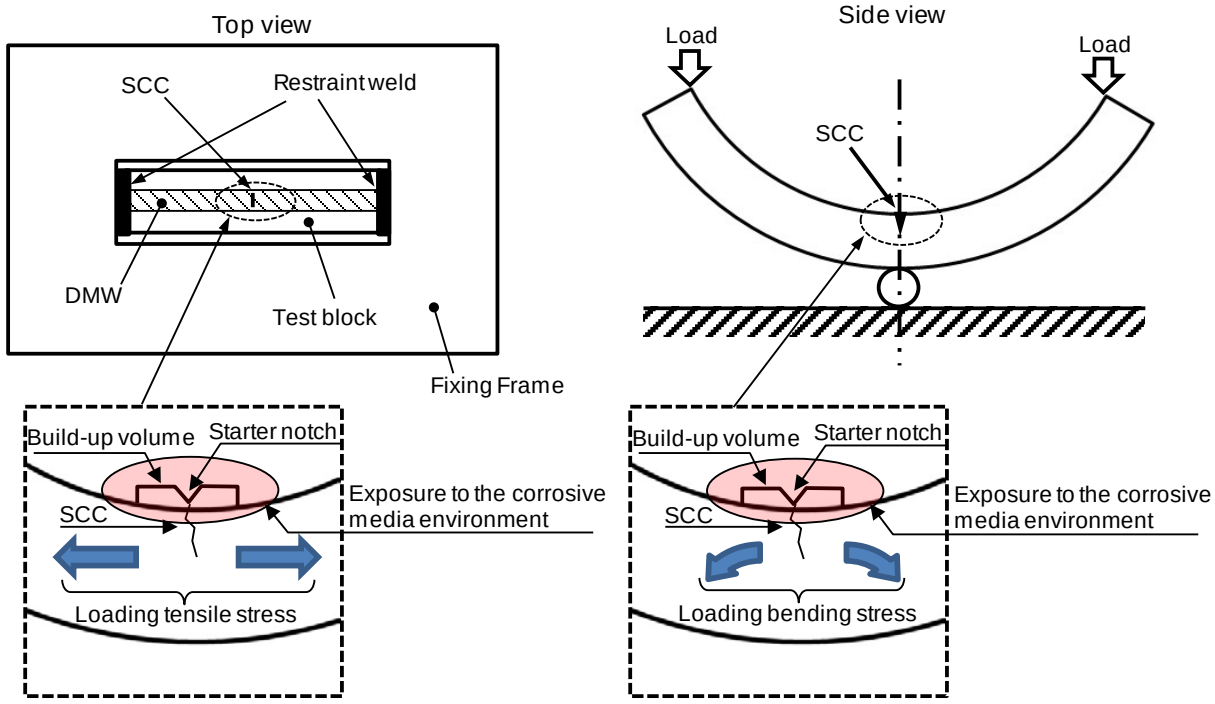

(a) Tensile loading setup for P15 (b) Bending loading setup for P16 and P17

Figure 2.8. Depiction of the Approach Used to Produce a Laboratory-Grown PWSCC/IGSCC

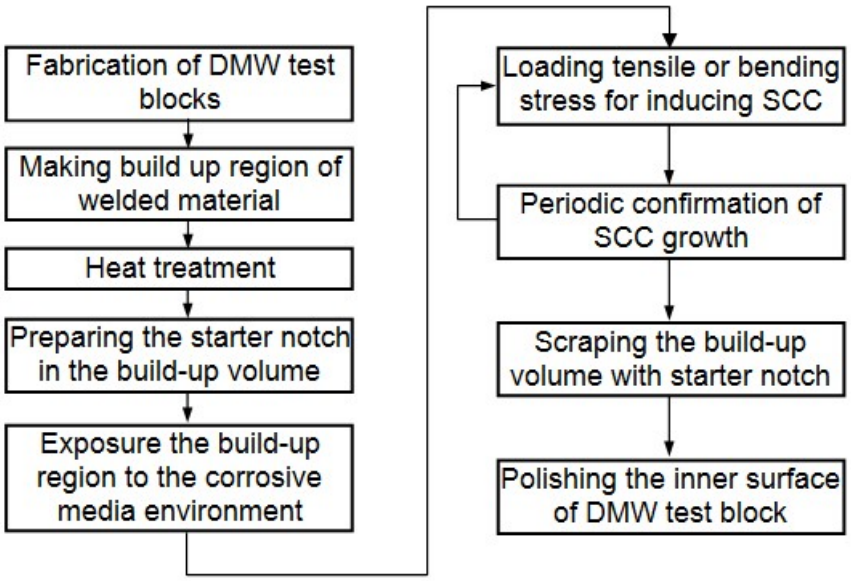

Figure 2.9. Flowchart of the Process Used to Produce a Laboratory-Grown PWSCC/IGSCC

The steps outlined below give a more detailed description of the flaw fabrication process:

1. Fabrication of large-bore DMW test block
   - Large-bore DMW test block is made from the same groove geometry, materials, and welding conditions as the real plant.
   - Welding is performed by PWSCC-susceptible material.
2. Preparing build-up region of welded material
   - The build-up region of welded material that has appropriate thickness is made.
   - The heat treatment is applied on the test blocks.
3. Preparing the starter notch
   - The starter notch is prepared in the build-up region of welded material to induce the initiation of PWSCC in the following loading process.
4. Exposure to the corrosive environment and loading
   - The build-up region on inner surface of large-bore DMW is exposed to corrosive media.
   - The tensile stress or the bending stress is loaded, which induces PWSCC from starter notch.
5. Periodic confirmation of PWSCC initiation and growth
   - PWSCC initiation and growth are checked by non-destructive examination such as conventional ultrasound (UT).

6. Finishing of test block

   - After confirmation that PWSCC depth reaches the designed depth, the build-up volume, which includes the starter notch, is scraped.
   - The inside surface of large-bore DMW test block is polished.

2.4 True-State Flaw Locations and Dimensions as Determined by Destructive Analysis

Quick Blind test blocks P15, P16, and P17 were destructively analyzed. The details of the destructive analysis are provided in Appendix A. The actual flaw locations and dimensions (true-state data) as determined by destructive analysis are provided in Table 2.1.

Table 2.1. Actual (True-State) Flaw Locations and Dimensions[(a)]

Test Block	Flaw Orientation	Flaw Depth (mm)	Flaw Length (mm)	Flaw Width (mm)	X1 (mm)	X2 (mm)	Y1 (mm)	Y2 (mm)	Z1 (mm)	Z2 (mm)
P15	Axial	20.1	21.0	11.7	222.4	234.1	−15.0	6.0	48.1	68.2
P16	Axial	13.6	16.0	24.4	211.7	236.1	−12.0	4.0	54.6	68.2
P17	Axial	2.4	21.0	32.9	211.2	244.1	−15.0	6.0	65.8	68.2
P45	No Flaw	-	-	-	-	-	-	-	-	-

(a) Crack length and width in "mm" is the maximum size of the flaw cluster area (X1,X2,Y1,Y2 represents the maximum limit of the crack area).

It is instructive to review the flaws in Table 2.1 in further detail because each one has a complex form and structure (morphology) in the X, Y, and Z directions. Note that all of the flaws have extensive morphology in the X dimension: ~12 mm for P15, ~24 mm for P16, and ~33 mm for P17. The implanted flaws exhibit a cluster or volumetric nature. A stepwise progression through the items in Appendix A that pertain to P15 will help to facilitate an understanding of the destructive analysis performed on P15 and in particular its morphology in the X dimension. To begin, the figures shown on Page A.0 in Appendix A are duplicated in Figure 2.10 with directional axes added.

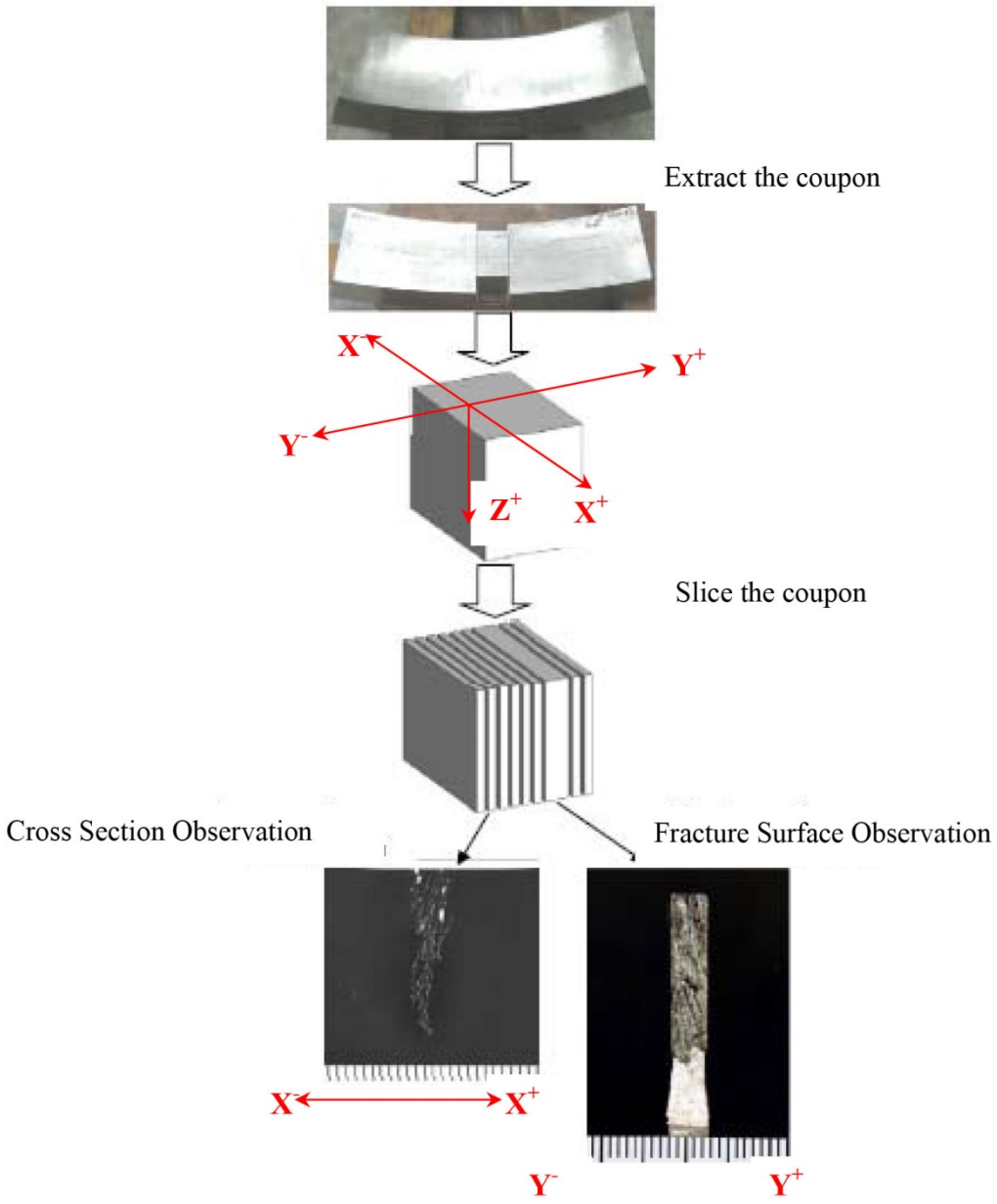

Figure 2.10. Stepwise Depiction of Coupon Extraction for Destructive Analysis

Page A-1 of Appendix A provides a summary of the destructive analysis results for test block P15. A profile graph (2) of the PWSCC, which shows the flaw depth and length, is provided in the upper left portion of the page. For this graph, Y is the horizontal (flaw length) axis and Z is the vertical (flaw depth) axis. The inner diameter surface of the test block is at Z=68.2 mm. The images to the right of the PWSCC profile are cross sections of the flaw taken at Y=−1 and Y=−5. The information in the table (3) provides measured data for Z (flaw depth) and X (flaw width) for multiple cross sections taken between Y=6 and Y=−15. Pages A-1.1 through A-1.16 provide detailed information for each one of these P15 cross sections. Page A-1.5 shows the detailed cross section at Y=2. The photograph of the enlarged cross section (before etching) highlights six indications whose X location and Z (depth) information are summarized in the crack information table beneath it. At this point, the crack is not very deep, but is

showing quite extensive morphology in the X (width) dimension. A review of page A-1.6 at Y=1, page A-1.7 at Y=0, page A-1.8 at Y=−4, page A-1.9 at Y=−5, A-1.10 at Y=−9, A-1.11 at Y=−10, A-1.12 at Y=−11, A-1.13 at Y=−12, and A1.14 at Y=−13 shows that this flaw has a very extensive morphology in all three dimensions. Figure 2.11 shows the enlarged cross section and corresponding crack information table at Y=−11.

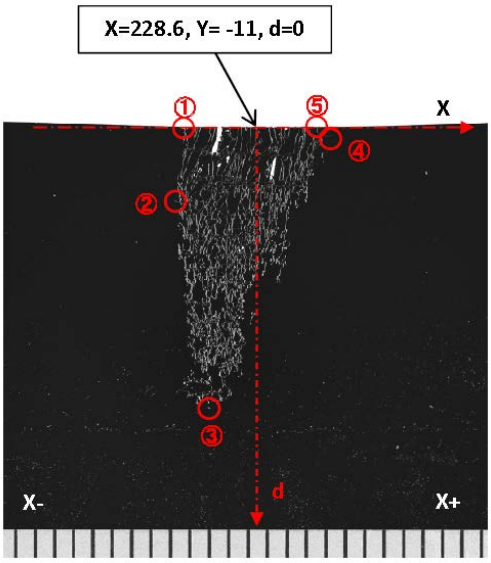

Crack information

Cross section Y (mm)		−11	
Max. crack depth info Z (mm)		53.3	
Crack opening (μm)		<1	
Typical crack information	①	X= 224.0	Z= 68.2
	②	X= 223.5	Z= 64.3
	③	X= 225.7	Z= 53.3
	④	X= 232.9	Z= 67.7
	⑤	X= 232.1	Z= 68.2

Figure 2.11. Cross Section and Crack Information for Test Block P15 at Y=−11

Figure 2.10 shows that a portion of each test block was removed for fracture surface observation. For P15, there were two fracture surface observation segments. The first segment extended as one piece from Y=0 to Y=−4 and the second as one piece from Y=−5 to Y=−9. These two segments are shown on page A-1.17. Figure 2.12 shows the fracture surface for the Y=−5 to Y=−9 segment. The value shown for “d” is the crack depth at the indicated Y value.

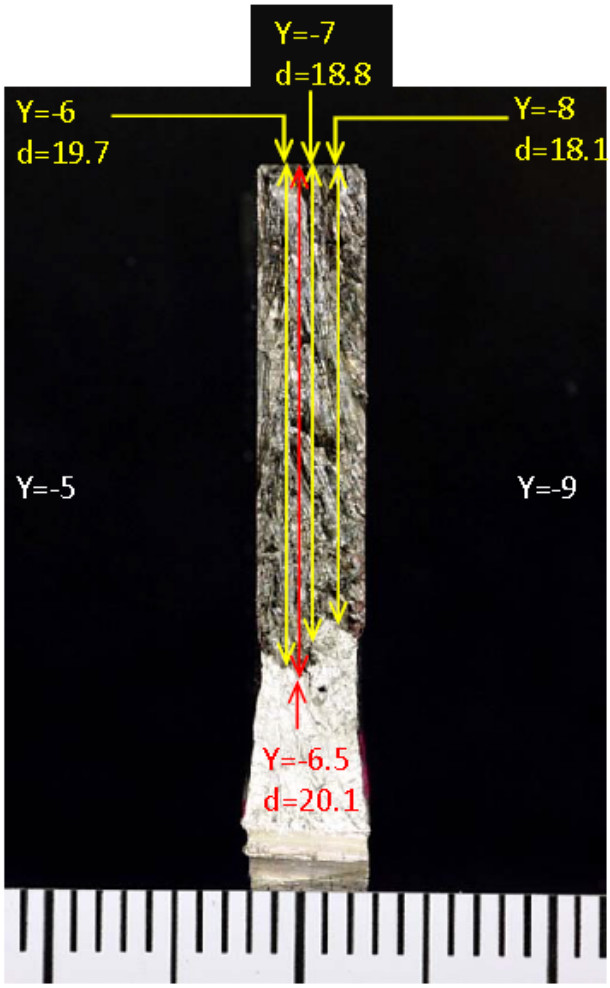

Figure 2.12. Fracture Surface for the Y=−5 to Y=−9 Segment of Test Block P15

Pages A-2 and A-3 of Appendix A are the summary pages for the destructive analysis results of test blocks P16 and P17, respectively. The same information as has been summarized for test block P15 can be found on pages A-2.1 to A-2.15 for P16 and A-3.1 to A-3.19 for P17.

The complex nature of the flaws in the quick blind study are similar to the morphology of stress corrosion cracks detected in dissimilar metal welds of steam generator nozzles in a Japanese nuclear power plant in 2007. The lengths of the two main cracks were approximately 9 mm and 11 mm. Fine cracks were observed to be surrounding the two main cracks. These flaws are shown in Figure 2.13.

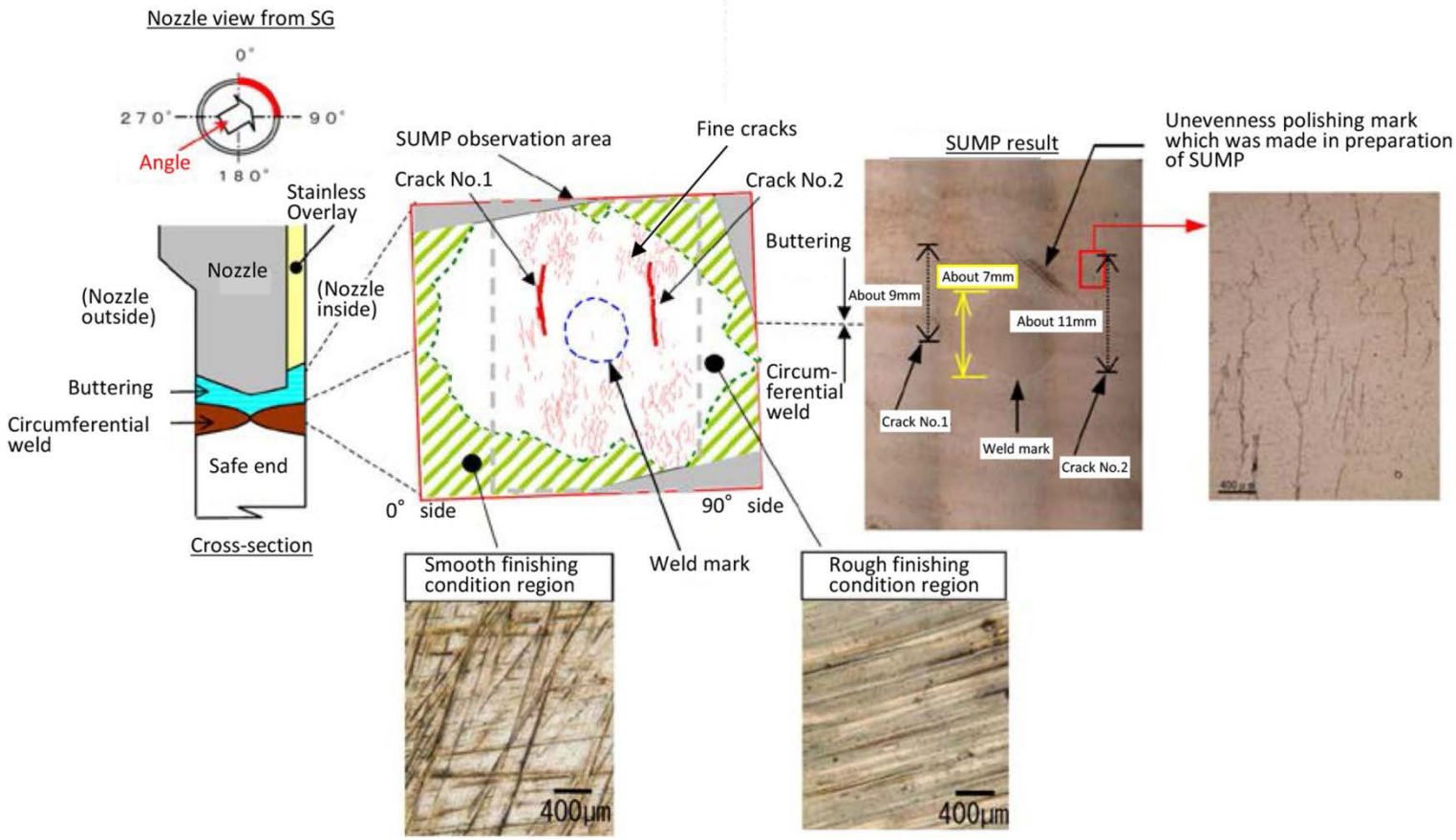

Figure 2.13. Complex Stress Corrosion Crack Morphology of Stress Corrosion Cracks Found During 2007 in Japan in the Dissimilar Metal Weld of a Steam Generator Nozzle

3.0 NDE Teams, Techniques, and Descriptions

Six testing organizations participated in the Quick Blind RRT representing Sweden, Republic of South Korea, Japan, and the USA. This section of the report provides a high-level overview of the NDE techniques applied by each testing team and, where applicable, how multiple techniques were (or were not) combined to arrive at the final flaw detection, location, and sizing data reported.

3.1 Inspection Team and Inspection Procedure Qualifications

The inspection procedures used and the inspection teams that performed the testing were confirmed to have formal nondestructive testing qualifications. The definition of "formal qualifications" for the inspectors and the procedures was left up to the individual invigilators, and is meant to discriminate between NDE professionals and NDE researchers with little or no practical NDE experience. The exact qualifications and/or certifications for each team cannot be given without violating the confidentiality of the inspections. Possible qualifications or certifications for each inspection procedure and personnel include but are not limited to:

Procedures:

- Qualifications given by the SQC Swedish Qualification Centre
- Japan Electric Association JEAC 4207-2008: Ultrasonic Examination for Inservice Inspection of Light Water Cooled Nuclear Power Plant Components
- ASME Code Section XI Appendix VIII

Personnel:

- Japanese Industrial Standard Z 2305:2001, which is consistent with ISO 9712:1999
- ISO-EN 473
- ASNT TC-1A and CP189
- ASME Code Section XI Appendix VIII

3.2 Summary of NDE Techniques Applied by Testing Teams

Table 3.1 summarizes the NDE techniques applied to the Quick Blind test blocks by each of the six test teams. Three types of NDE techniques were used: 1) conventional ultrasonic (shown as Ultrasonic), 2) phased-array ultrasonic (shown as Phased Array UT), and 3) eddy current. The NDE acronyms agreed to by PARENT participants are listed for each technique and include phased-array ultrasound (PA), UT, and eddy current (ECT). The table provides details about whether the technique data collection method was automated or manual, encoded or not, and whether testing was conducted from the inner diameter (ID) or outer diameter (OD) of the test block. A manual examination is one where the inspector uses their own hands to move the probe and records the position of the probes using rulers or other scales. An automated inspection is one where an electronic scanner is used to move the probes and record their positions using encoders. An encoded scan is one where encoders are used to track and record the position of the probe throughout the scan.

To facilitate the analysis and presentation of test results in Section 4 of this report, each NDE technique was assigned a unique Technique identifier. This identifier was developed by concatenating the team number, the NDE acronym, and a sequential number to differentiate between multiple PA or UT techniques used by the same team. The probe frequency, inspection-angle, and skew details are listed for each technique. Probe frequencies for the PA techniques ranged 1.5–5 MHz. Probe frequencies for the UT techniques ranged 1–3 MHz. The single eddy current probe frequency was 200 kHz. All teams used commercially available probes except team 132's PA probes and team 106's ECT probe. The last column of Table 3.1 lists which of the five inspection attributes (detection, characterization, length sizing, depth sizing, and positioning) were addressed by the technique.

3.3 Combining NDE Techniques

Most of the procedures teams applied to the Quick Blind test blocks utilized more than one NDE technique. Some teams that applied multiple techniques combined the information obtained to arrive at the final data reported for flaw indications.

Team 132 used two different automated, encoded 1.5-MHz PA ID examination techniques. Technique 132-PA1 performed flaw detection, characterization, length sizing, and positioning. Technique 132-PA2 provided flaw depth only. The techniques were combined to report the final flaw indication data by adding depth (Z) data from 132-PA2 to the X and Y data from 132-PA1.

Team 108 used manual non-encoded 1-MHz UT and 2-MHz PA techniques 108-UT and 108-PA, respectively. Signals deemed eligible for consideration as reportable flaw indications were made based on several factors including signal-to-noise ratio (S/N) greater than 2, signal walking that exhibited the typical behavior of a flaw, well defined flaw ends, the presence of a definitive tip signal, and so forth. During the process of deciding how to combine techniques, all information from eligible signals was taken into consideration.

Team 134 used a manual non-encoded 1.5-MHz/2-MHz UT technique 134-UT. The technique was used for flaw detection, characterization, length sizing, and positioning. For the three probes used (1.5 MHz/45°, 1.5 MHz/35°, 2 MHz/33°), the probe that produced the sharpest echo-dynamic response was used and reported as the final flaw indication data.

Team 126 used manual encoded 1.5-MHz PA and manual non-encoded 2-MHz UT techniques 126-PA and 126-UT, respectively. While both techniques were used to determine flaw detection, characterization, length sizing, and positioning attributes, phased-array data was the final flaw indication data the team reported.

Table 3.1. NDE Techniques Used for PARENT Quick Blind Round-Robin Testing

Team	NDE Technique	Technique Identifier	Manual Automated	Encoded	NDE Acronym	Exam Surface	Probe Frequency (MHz)/Inspection Angle (Deg.)/ Skew (Deg.)	Probe Availability	Technique Comment
132	Phased Array UT	132-PA1	Automated	Yes	PA	ID	1.5/60–88	Custom	Detection, Characterization, Length, Positioning
	Phased Array UT	132-PA2	Automated	Yes	PA	ID	1.5/40–46 1.5/60–82	Custom	Depth
108	Ultrasonic	108-UT	Manual	No	UT	OD	1.0/45 1.0/60 1.5/35 1.5/45 2.0/33 2.0/45	Commercial Transmit-Receive Longitudinal (TRL) Comp-G	Detection, Characterization, Length, Depth, Positioning
	Phased Array UT	108-PA	Manual	No	PA	OD	2.0/13~45	Commercial	Detection, Characterization, Length, Depth, Positioning
134	Ultrasonic	134-UT	Manual	No	UT	OD	1.5/35 1.5/45 2.0/33	Commercial TRL	Detection, Characterization, Length, Depth, Positioning
126	Ultrasonic	126-UT	Manual	No	UT	OD	2.0/45 2.0/60	Commercial TRL	Detection, Characterization, Length, Depth, Positioning
	Phased Array UT	126-PA	Manual	Yes	PA	OD	1.5/25 1.5/35 1.5/45 1.5/55	Commercial	Detection, Characterization, Length, Depth, Positioning

Team	NDE Technique	Technique Identifier	Manual Automated	Encoded	NDE Acronym	Exam Surface	Probe Frequency (MHz)/Inspection Angle (Deg.)/ Skew (Deg.)	Probe Availability	Technique Comment
106	Ultrasonic	106-UT1	Automated	Yes	UT	ID	2.0/55/0-Skew	Commercial TRL	Detection, Length, Depth, Positioning
	Ultrasonic	106-UT2	Automated	Yes	UT	ID	2.0/55/90-Skew	Commercial TRL	Detection, Length, Depth, Positioning
	Ultrasonic	106-UT3	Automated	Yes	UT	ID	2.0/55/180-Skew	Commercial TRL	Detection, Length, Depth, Positioning
	Ultrasonic	106-UT4	Automated	Yes	UT	ID	2.0/55/270-Skew	Commercial TRL	Detection, Length, Depth, Positioning
	Ultrasonic	106-UT5	Automated	Yes	UT	ID	2.0/45/0-Skew	Commercial TRL	Depth
	Eddy Current	106-ECT	Automated	Yes	ECT	ID	0.2	Custom Driver Pickup Cross Wound Coil	Detection, Characterization, Length, Positioning
113	Ultrasonic	113-UT	Automated	Yes	UT	ID	3/55	Commercial	Detection, Characterization, Positioning
	Phased Array UT	113-PA1	Automated	Yes	PA	ID	2.0/30 2.0/45 2.0/55	Commercial	Detection, Characterization, Positioning, Length & Depth Sizing
	Phased Array UT	113-PA2	Automated	Yes	PA	ID	5.0/35 5.0/40 5.0/45 5.0/50 5.0/55	Commercial	Detection, Characterization, Positioning, Length & Depth Sizing

Team 106 used automated encoded 2-MHz UT and 200-kHz ECT techniques 106-UT and 106-ECT, respectively. Data collection was done with all probes mounted together in one assembly. Detection was determined primarily with ECT, but UT was used as a supplement. ECT was used to confirm whether or not a flaw indication was surface-breaking. Length sizing was performed with both ECT and UT and the greatest length was reported. Depth sizing was performed with UT.

Team 113 used automated encoded 2-MHz PA, 5-MHz PA, and 3-MHz UT techniques 113-PA1, 113-PA2, and 113-UT, respectively. Information obtained from the various techniques was combined using the following scheme:

- All probes were used for detection (S/N > 2 was the minimum criteria) and characterization.
- PA results were used for length and depth sizing. The largest value between the two techniques was reported.

4.0 Analysis of Performance

The data submitted by the Quick Blind testing teams was examined, and scored to determine the effectiveness of the various techniques. This section describes the scoring criteria used to analyze the data and the results. Section 4.1 describes the scoring procedures used in the round-robin tests. Section 4.2 provides an evaluation of detection capability for the NDE techniques and procedures applied. Section 4.3 provides the details of the length and depth sizing results for the round-robin tests.

4.1 Scoring Procedure Used for the PARENT Round-Robin Tests

This section describes how inspection results were compared to the test block true states. Specifically, this section describes (1) the method used to determine whether or not an individual flaw was detected; (2) if the flaw was detected, what depth and length size should be assigned to it; (3) unintended defects (flaws that occurred during the test block fabrication process that were not intended to be part of the test block); and (4) the methodology used to determine false calls (i.e., indications not associated with any known flaw).

Scoring merges the inspection results with the true-state results by associating inspection indications with true-state flaws. The scoring procedure is summarized by the flowchart in Figure 4.1.

The first step of the scoring process consisted of uniquely identifying the flaws in the inspected volume of the weld. For this analysis, a table of flaws was developed for each test specimen. The inspection volume field indicated in the round-robin test data submitted by testing teams was then compared with the flaw table for each specimen to determine which flaws fell within the inspected volume. These flaws were then placed in the inspected flaw table.

The next step of the scoring process compared the entries in the inspected flaw table to the entries in the indication table (the indications that were recorded on inspection data sheets) to determine which flaw cuboids intersected with which indication cuboids.

A tolerance box was defined around each flaw to account for possible location error. Without a tolerance box, location errors might be misclassified as non-detections. Figures 4.2 and 4.3 show the probability of detection (POD) versus size of tolerance for test blocks and test teams, respectively. Three of the six test teams had a POD of 1 over the full scoring box tolerance range and these teams are therefore not readily visible in Figure 4.3. Figures 4.2 and 4.3 both show that there is no improvement in detection for tolerances larger than 10 mm. Therefore, for the analysis used in this report, a tolerance box of 10 mm was used to score the results. This tolerance box size should be roughly equal in magnitude to the maximum position measurement error of the inspection procedures.

Once the tolerance is defined, $\Delta X=10$, $\Delta Y=10$, and $\Delta Z=10$, then the flaw cuboid, X1, X2; Y1, Y2; Z1, Z2, becomes

$$(X1 - \Delta X, X2 + \Delta X, Y1- \Delta Y, Y2 + \Delta Y, Z1 - \Delta Z, Z2 + \Delta Z) \quad (4.1)$$

A list of all indications not intersecting with any flaws was compiled and was termed the false call table. The false call table was compiled after the intersecting flaw-indication cuboids had been identified for each indication.

The scoring process therefore resulted in two outputs—the detection of flaws, including the length and through-wall depth determined for each flaw, and a list of false calls.

Finally, detection and sizing information were appended to all flaws in the inspected flaw table, using the intersection information, to produce the detection and sizing results table.

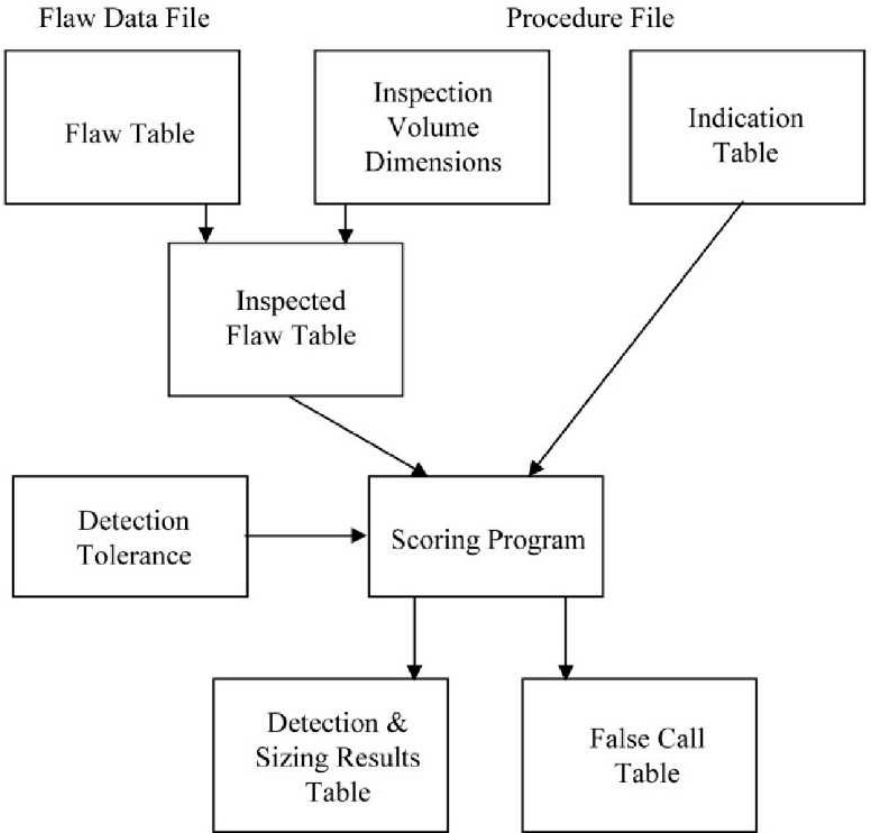

Figure 4.1. Scoring Procedure for PARENT Quick Blind Round-Robin Tests

False call probability (FCP) and probability of detection quantify inspection performance on blank (un-flawed) versus flawed material. The FCP is the probability that an inspector will call a flaw in a blank unit of material, while POD is the probability that an inspector will call a flaw in a flawed unit of material. With these definitions, (FCP, POD) measure the capability for inspection to correctly classify units of material as unflawed or flawed. Another equivalent term for FCP is false positive probability while POD is equivalent to 1 minus false negative probability.

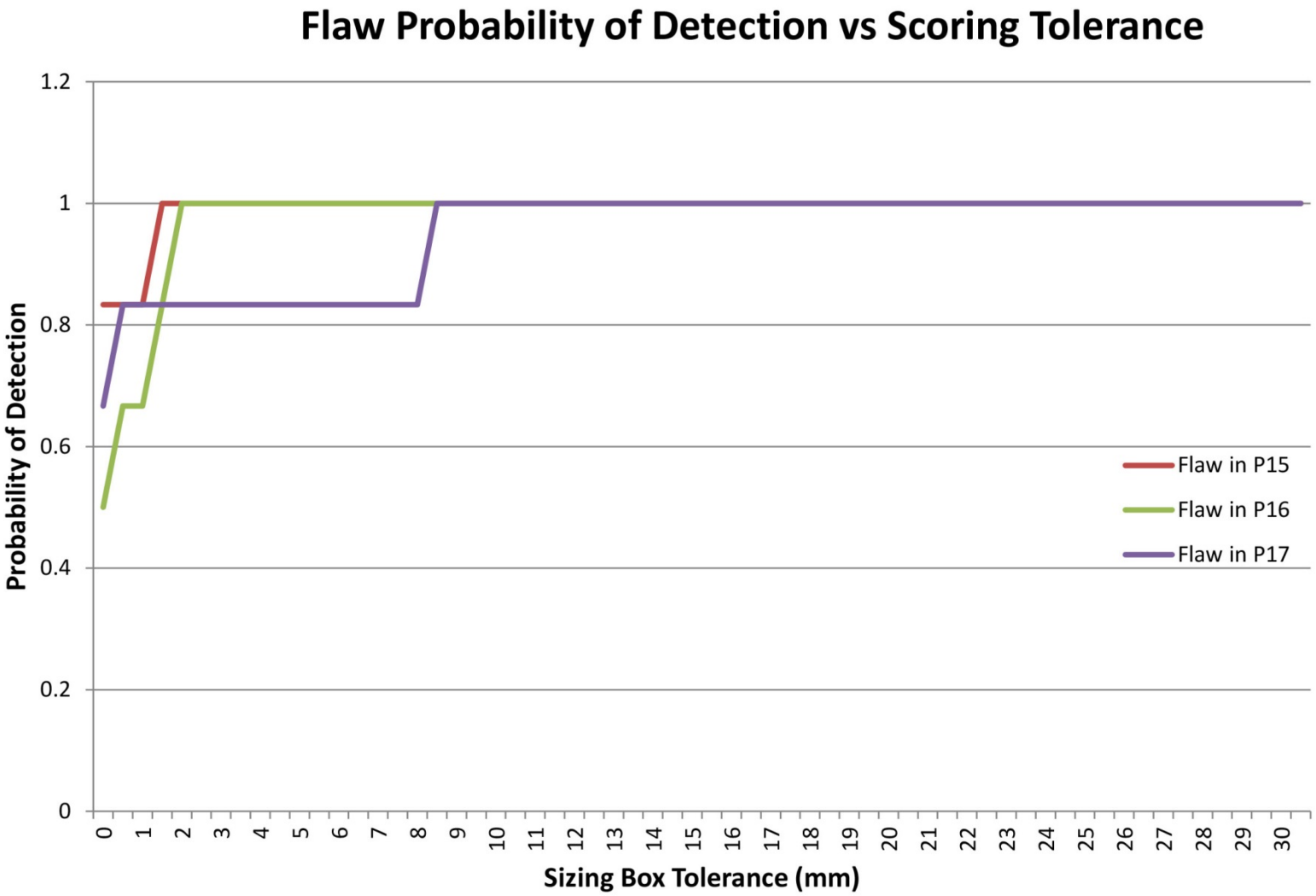

Figure 4.2. Probability of Detection versus Scoring Tolerance for Flaws in Test Blocks

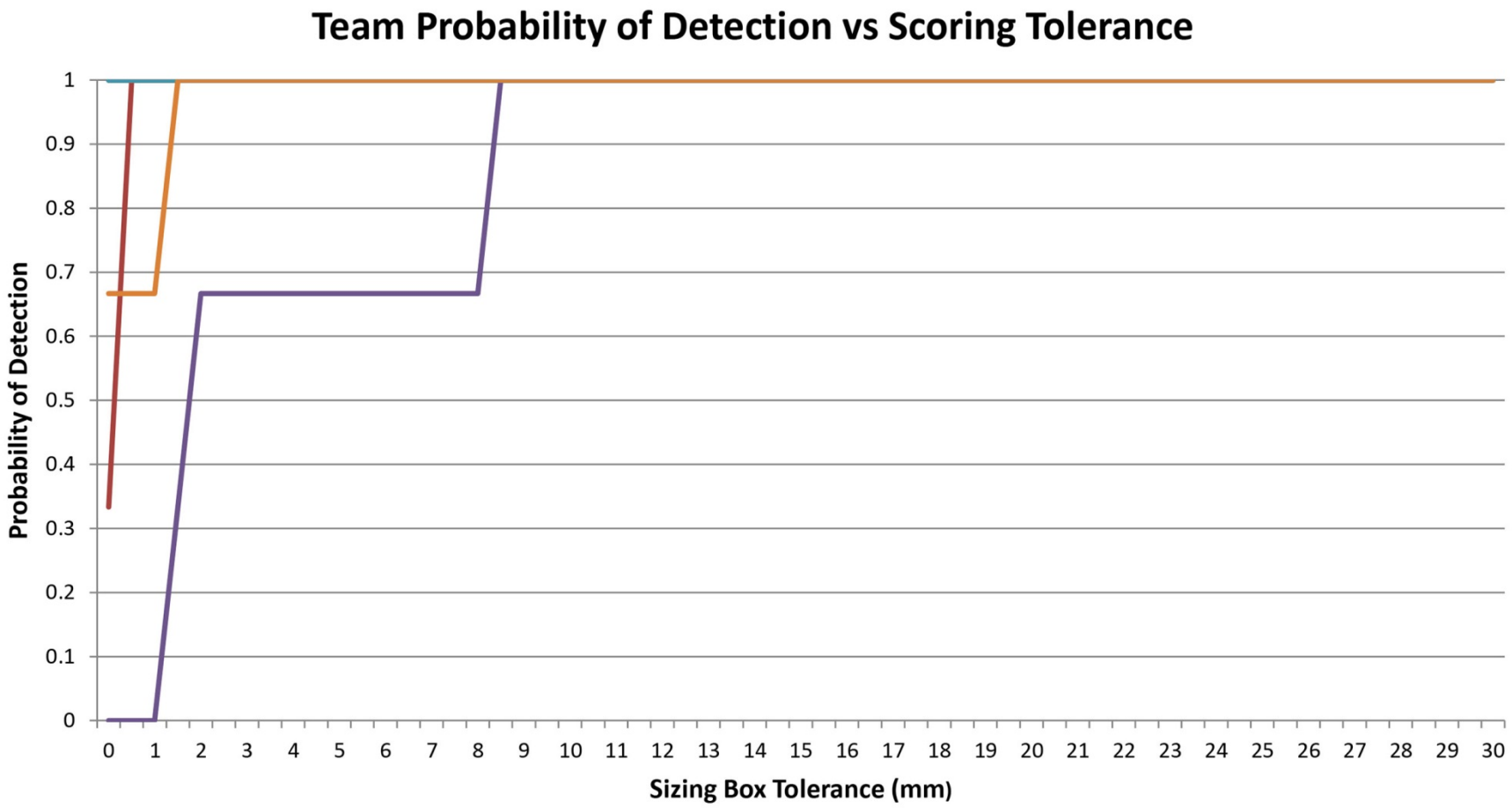

Figure 4.3. Probability of Detection versus Scoring Tolerance for Test Teams

POD is frequently expressed as a function of various flaw, material, or inspection variables that might affect detection performance. For example, in PARENT, POD is considered to be a function of flaw size, so the expression POD(S) is used to represent the probability of calling a detection in a unit of material that contains a flaw of size S.

One would expect POD(S) to be a monotonically increasing function of flaw size S. Also, one should note that using the false call probability as the POD for a flaw of size zero (POD(0) = FCP) follows from the definition of FCP and POD. When the S = 0 point is included on the POD curve, this curve provides the most basic description of inspection efficacy. An inspection that is no more effective than guessing will have a flat POD curve. More specifically, if the POD for flaws of size S is equal to FCP, (POD(S) = FCP) then flaws of this size are not really being detected by the inspection procedure.

To be able to calculate FCP and POD, one has to define the applicable unit of material. We call this unit of material the grading unit; in other words, each grading unit in the round-robin study will generate a detection statistic when inspected. For inspection of dissimilar metal weldments, the ideal grading unit would be an entire weld, but a round-robin test that used whole weldments as the experimental unit would be too costly. Due to cost constraints, the grading unit used is the length of a flaw plus an allowance for sizing error.

To produce unbiased estimates of FCP and POD, the blank and flawed grading units should be identical in all important respects (except that the flawed grading units contain a flaw).

4.1.1 Calculation of False Call Probability

For this study, no attempt was made to create blank grading units that were statistically equivalent to flawed units. To calculate FCP, blank material was divided into 100-mm long units (in the circumferential direction), and FCP was estimated by dividing the number of false calls by the number of blank grading units.

$$\text{FCP} = (\#\ \text{False Calls})/(\#\ \text{Blank Grading Units}) \tag{4.2}$$

Since a 100-mm length produces a blank grading unit that is somewhat larger than the flawed units, the estimated FCP may be somewhat larger than it should be. On the other hand, the location of flaws in these test blocks was visibly discernible by the naked eye and this creates a bias in the other direction.

4.1.2 Logistic Regression Model for POD

Estimates produced by the algorithm are maximum-likelihood estimates. The regression fits included data for flaw size zero (i.e., the FCP estimates described in the last section). Thus, in the regression plots, data points are shown at size=0, which represents false call data.

The confidence bounds presented for the POD curves are “hybrid bounds.” They are 95% maximum-likelihood bound combined with simple binomial bounds (on the aggregated flaw data), with the larger bound being chosen at each flaw size. Use of this hybrid bound was employed because of the few data points available.

4.1.3 Scoring Example

To facilitate an easy understanding of the scoring process, examples of scoring results are presented for test blocks P15, P16, and P45 (blank). These three examples represent each of the three situations that occurred when comparing data reported by test teams to the true state data: 1) detections, 2) false calls, and 3) missed flaws. Because the X-Y plane is the one that is relevant to the scoring definition, scoring is conducted using the X and Y data. Table 4.1 shows data reported by the testing teams for P15, P16, and P45.

Table 4.1. Typical PARENT Inspection Results

Test Block #	Flaw Indication #	X1 (mm)	X2 (mm)	Y1 (mm)	Y2 (mm)	Scoring Result
P15	Not Detected	NA	NA	NA	NA	Missed Flaw
P16	1	192	192	−16.6	−0.6	False Call
	2	238	238	−24.6	3.4	Detection
P45	1	140.3	140.3	−0.6	−20.6	False Call
	2	162.3	162.3	−0.6	−20.6	False Call

NA – Examination conducted, indication data was blank or completed with NA

The scoring results are summarized visually in Figure 4.4. The locations of the indications called by the inspection team are shown as narrow white color-filled rectangles that have flaw indication numbers inside of them. The true-state positions of the flaws are shown by the red boxes, where the 10-mm scoring box tolerance is included in accordance with Eq. (4.1). When a called indication intersects (even partially) with an actual flaw (red), it is classified as detection. Appendix B contains all the scoring plots for all the test teams, test blocks, and NDE techniques applied to the Quick Blind round-robin test blocks (using the 10-mm sized scoring tolerance). The plots at the top of the page contain the X-Y data used for scoring. The plots at the bottom of the page show the depth X-Z data reported by the testing team (this data was not used for scoring and is mentioned here for clarity). Note that while testing teams reported all data obtained by the various NDE techniques, they were selective about which ones to report as the final indication on the inspection summary datasheets. These summary indications can be identified in the scoring plots by the text “Form.type: sum.dmw” located at the center of the inspection sheet. All indications produced by an individual NDE technique have the text “Form.type: tech.dmw” at the center of the inspection sheet. A comparison review was made for each test block of the summary indications reported by all six testing teams. This review shows that there are no unintended or unidentified flaws or reflectors in any of the test blocks. At a minimum, two testing teams would need to have identified the presence of such a flaw at a location other than the location of the main flaw, and there was not one instance of this.

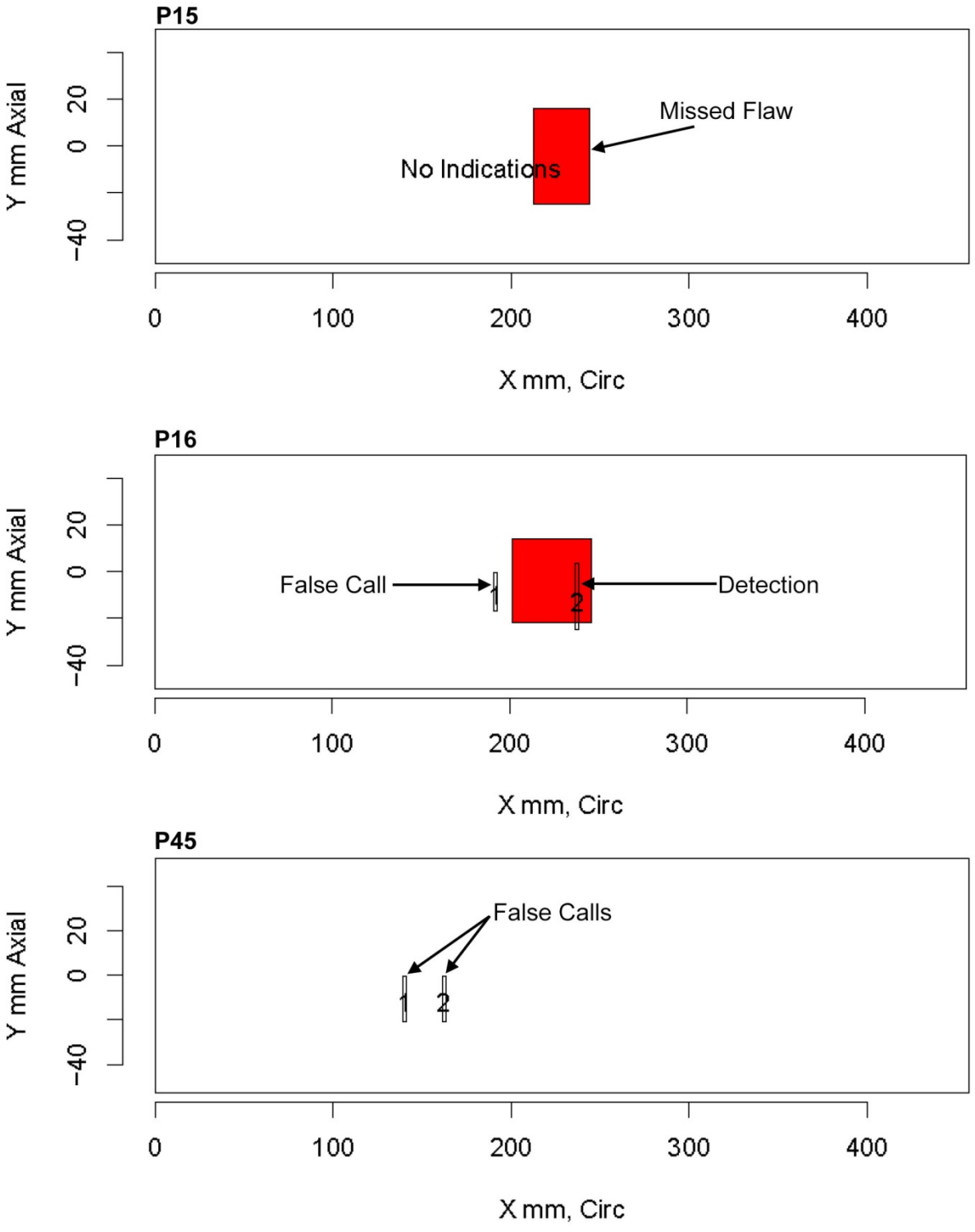

Figure 4.4. Scoring Examples for Test Blocks P15, P16, and P45

4.2 Evaluation of Detection Capability

4.2.1 Probability of Detection Results

Table 4.2 provides a summary of the POD data for each test team using the 10-mm tolerance for scoring. The "No. of Observations" column describes the number of flaws inspected by each team. As there were three flaws (one in each test block), all flaws were inspected by each team. All the teams detected all flaws in all test blocks (POD=1). Team 126 was the only team that made false calls having a false call rate of 2.9 false-calls/m. Table 4.3 provides the POD by flaw and the dimensions of the flaws as determined by the destructive analysis results. All flaws were detected with a POD of 1. Note that all three flaws have a complex morphology and exhibit characteristics of both an axial and a circumferentially oriented flaw. Table 4.4 provides a summary of the false calls by test block.

Table 4.2. Probability of Detection by Team with 10-mm Tolerance

Team Number	No. of Observations	POD	False-Calls per Meter of Weld Inspected
106	3	1.0	0.0
108	3	1.0	0.0
113	3	1.0	0.0
126	3	1.0	2.9
132	3	1.0	0.0
134	3	1.0	0.0

Table 4.3. Probability of Detection by Flaw

Flaw Number	No. of Observations	POD	Flaw Type[(a)]	True Depth (mm)	Through Wall Depth (%)	True Length[(b)] (mm)	True Width[(c)] (mm)
P15.1	6	1.0	C and A	20.1	29	21	11.7
P16.1	6	1.0	C and A	13.6	20	16	24.4
P17.1	6	1.0	C and A	2.4	3.5	21	32.9

(a) C-Circular, A-Axial (flaws exhibit volumetric morphology having significant extent in the X, Y, and Z directions)
(b) Length along the axial direction – Y
(c) Width in the circumferential direction – X

Table 4.4. Summary of False Calls Table

Test Block Number	Number of Flaws	Number of Inspections	Block Length (m)	Number of False Calls	False-Calls per Meter[(a)]
P15	1	6	.457	1	0.40
P16	1	6	.457	1	0.41
P17	1	6	.457	1	0.42
P45	0	6	.457	2	0.76

(a) Number of False Calls/Length of Blank Material Inspected

4.2.2 Probability of Detection Curves for Flaw Depth and Length

Figures 4.5 and 4.6 are POD curves plotted as a function of flaw depth and length. These were developed from the combined detection and false call data of the six test teams. The dashed red lines represent the 95% confidence bounds. The wide confidence interval is a direct function of the limited number of data points available. The black circles near the origin of both figures are representative of the false call probability. The black circles at the top of Figure 4.5 represent the POD data for the 2.4 mm, 13.6 mm, and 20.1 mm deep flaws. The black circles at the top of Figure 4.6 show the POD for the 16 mm and 21 mm long flaws. Conclusions about POD drawn from these curves are presented in Section 5.2.

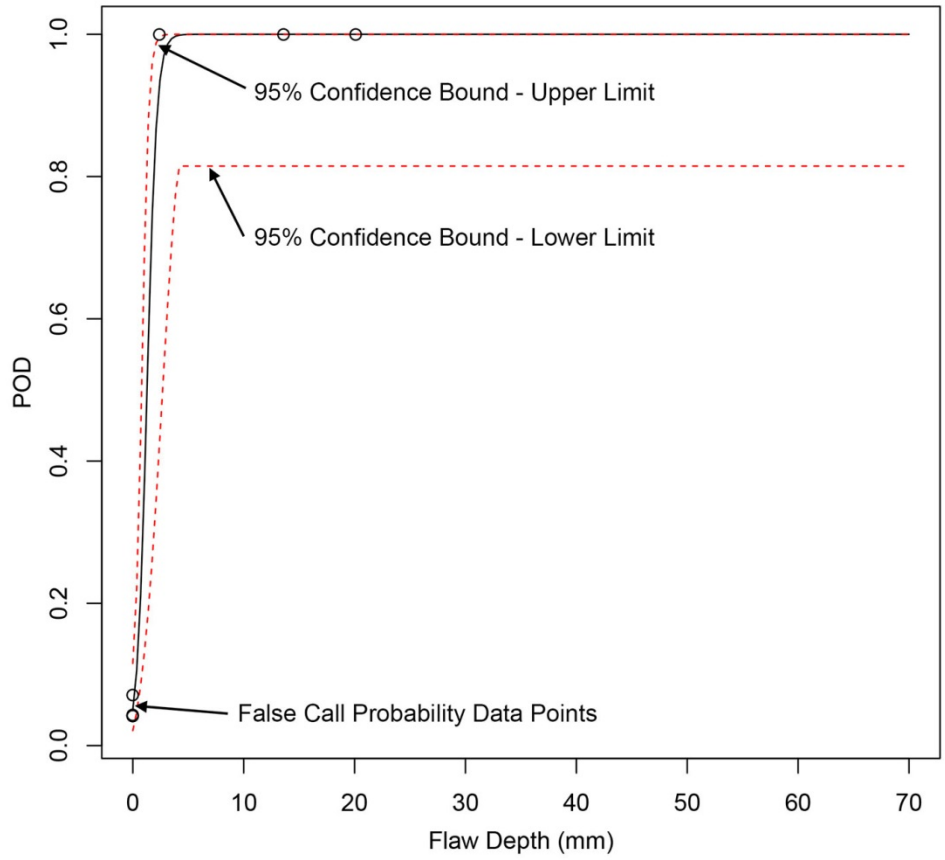

Figure 4.5. Probability of Detection versus Flaw Depth

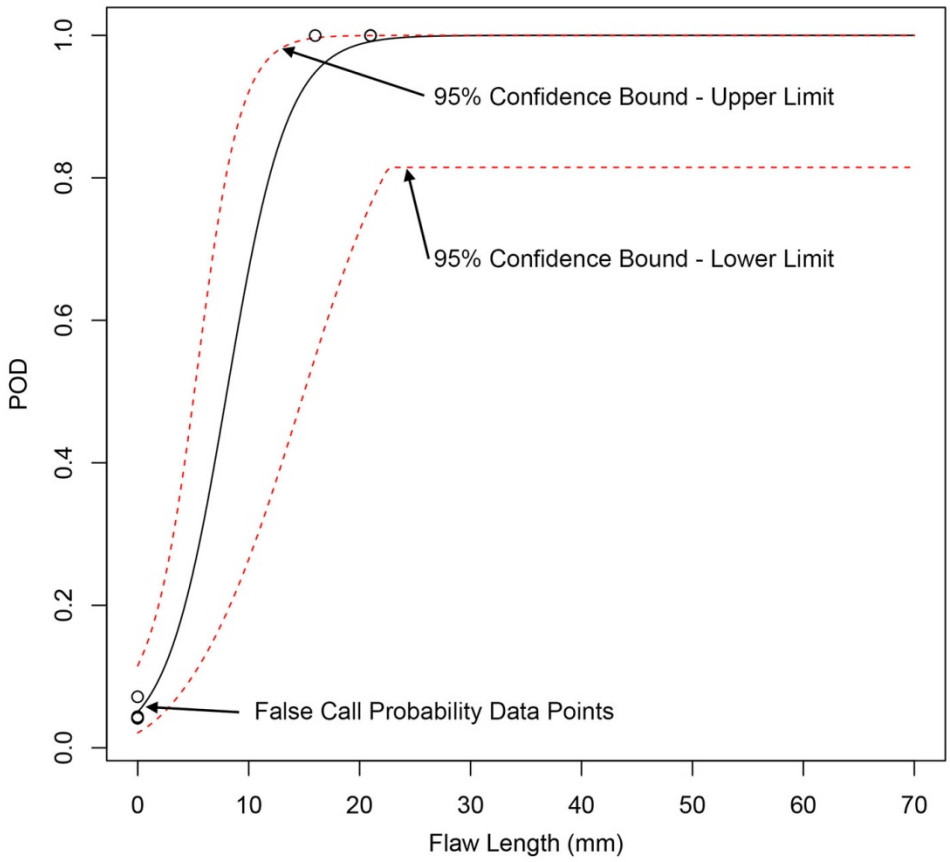

Figure 4.6. Probability of Detection versus Flaw Length

4.3 Flaw Sizing Results

Due to the complex morphology of the flaws, many testing teams reported data showing that the flaw indications had significant extent in the circumferential direction (X) as well as the axial direction (Y). Therefore, in addition to the very important analysis of the depth sizing effectiveness of the NDE techniques applied, the analysis will include a review of axial and circumferential sizing results too.

4.3.1 Evaluation of Sizing Performance

Some statistical analysis of flaw length and depth characterization is provided in this section so that conclusions may be drawn concerning flaw characterization capability. The number of data points available for analysis does not lend itself to performing linear regressions. Therefore, the statistical analysis presented in this report was limited to calculations of the mean error, standard deviation of error, and the root mean square error (RSME). How these quantities were calculated is described below. If M_i and T_i represent the respective measured and true sizes of flaw i, then the measurement error is represented as E_i according to the following formula:

$$E_i = M_i - T_i \tag{4.3}$$

The mean error μ for a sample of n flaws is represented as μ_E and is calculated according to the following formula.

$$\mu_E = \frac{1}{n}\sum_{i=1}^{n} E_i \tag{4.4}$$

The standard deviation σ represents the variability of within a sample of n flaws (± 1σ represents 68.2% of the population, ± 2σ represents 95% of the population), and is calculated according to the following formula.

$$\sigma_E = \sqrt{\frac{1}{n}\sum_{i=1}^{n}\left(E_i - \mu_E\right)^2}, \tag{4.5}$$

The RMSE serves to aggregate the magnitude of the errors described above and is a good measure of accuracy. RMSE is computed according to the formula shown below.

$$RMSE^2 = \sigma_E^2 + \mu_E^2 = \frac{\sum_{i=1}^{n}\left(M_i - T_i\right)^2}{n}. \tag{4.6}$$

4.3.2 Flaw Data

Eighteen inspections were performed by the six test teams on the three test blocks that contained flaws. The flaw size data reported by the test teams is shown in Table 4.5. The flaw length and width data reported by team 132 has flaw lengths and flaw widths that are significantly larger than the true-state data provided in Table 4.3. Table 4.6 shows by test team, test procedure, and ID/OD access a comparison between the reported data for indications and the true-state data. Negative difference values indicate flaw under sizing. Note that data for flaw width differences was not included in Table 4.6 because it is recognized that these flaws were intended to be axially oriented. It is instructive to put the difference values in Table 4.6 into perspective. In the United States, to pass a typical weld qualification examination, the maximum difference between indicated and true-state values for flaw depth and length is 3.18 mm (1/8 inch) and 19.05 mm (3/4 inch), respectively.

Table 4.5. Flaw Size Data Reported by Testing Teams

			Reported Flaw Size (mm)		
Inspection	**Team**	**Test Block**	**Depth**	**Length**	**Width**
1	134	P15	5.60	23.00	2.00
2	134	P16	5.00	10.00	12.00
3	134	P17	6.00	10.00	9.00
4	126	P15	13.50	24.00	0.00
5	126	P16	6.00	28.00	0.00
6	126	P17	6.00	20.00	0.00
7	108	P15	2.80	18.00	2.00
8	108	P16	4.00	15.00	0.00
9	108	P17	2.00	10.00	0.00
10	113	P15	20.00	13.00	0.20
11	113	P16	14.60	13.00	0.30
12	113	P17	4.20	8.00	10.50
13	106	P15	19.70	8.00	14.00
14	106	P16	9.70	10.00	19.00
15	106	P17	6.60	8.00	19.00
16	132	P15	11.23	53.40	118.10
17	132	P16	1.23	38.10	111.25
18	132	P17	1.23	45.72	118.12

Table 4.6. Comparison Between Reported Indication Data and True-State Flaw Sizes

			Difference - Reported Data versus True-State (mm)[a]					
			P15		P16		P17	
Team	**Procedure[b]**	**Access**	**Depth - Z**	**Length - Y**	**Depth - Z**	**Length - Y**	**Depth - Z**	**Length - Y**
134	UT	OD	−14.5	2.0	−8.6	−6.0	3.6	−11.0
132	PA	ID	−8.9	32.3	−12.4	22.1	−1.2	24.7
108	UT+PA	OD	−17.3	−3.0	−9.6	−1.0	−0.4	−11.0
126	UT+PA	OD	−6.6	3.0	−7.6	12.0	3.6	−1.0
113	UT+PA	ID	−0.1	−8.0	1.0	−3.0	1.8	−13.0
106	UT+ECT	ID	−0.4	−13.0	−3.9	−6.0	4.2	−13.0

(a) Negative difference values indicate flaw under sizing
(b) UT – Conventional Ultrasound, PA – Phased Array Ultrasound, ECT – Eddy Current

4.3.3 Depth Sizing Analysis

Figure 4.7 shows the indicated flaw depths plotted against the true-state depths by test team. If all test indications matched the true state, they would fall directly on top of the red line. It is evident from this plot that teams tended to oversize small flaws and undersize larger flaws.

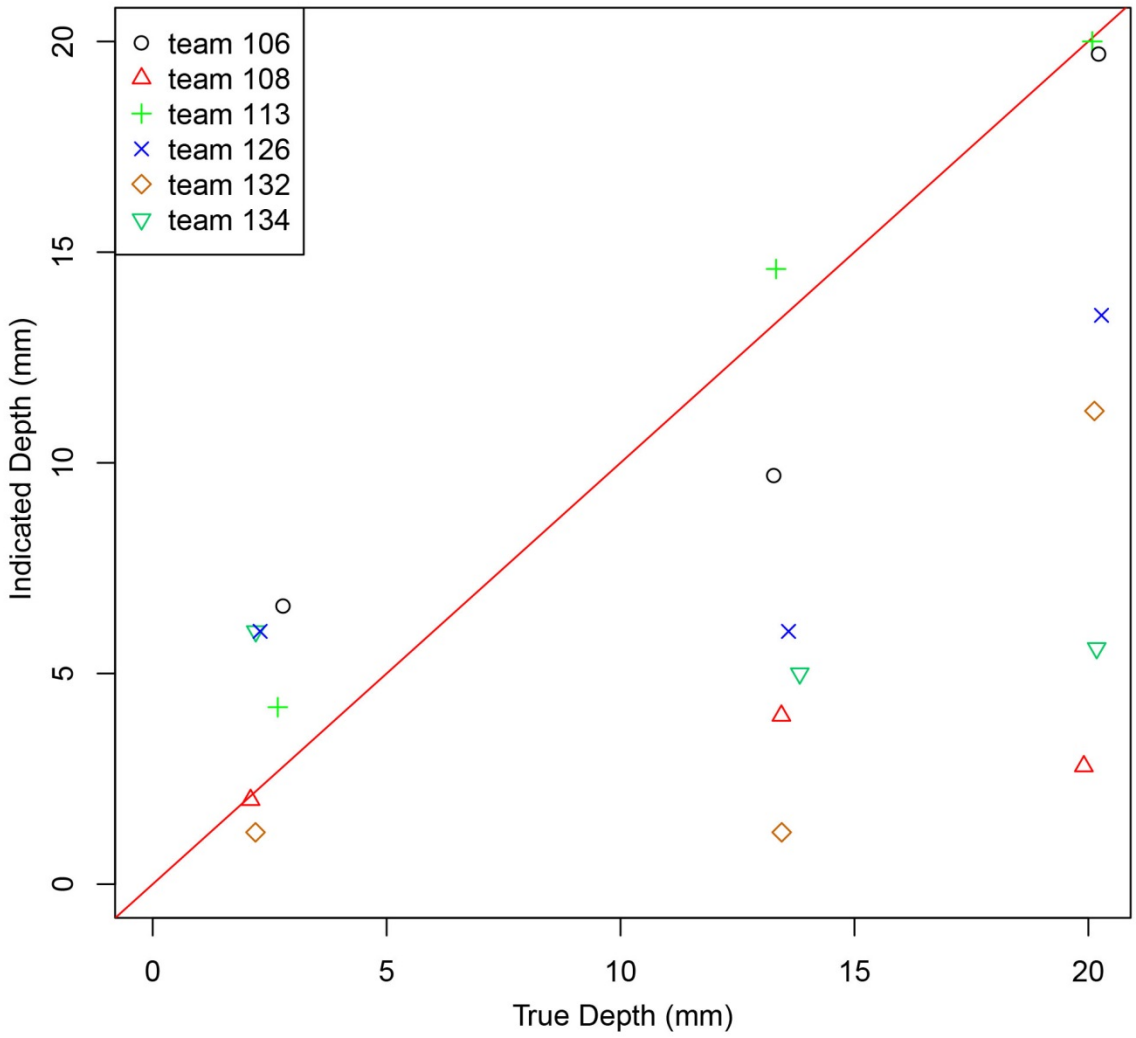

Figure 4.7. Indicated versus True-Flaw Depth by Test Team

Table 4.7 shows the depth sizing error by test team and by ID or OD access for combined data taken on test blocks P15, P16, and P17. Teams 113 and 106 had the lowest root mean square error (RMSE), both having accessed the test block from the ID. Table 4.8 provides a summary of the depth sizing errors for the 18 inspections performed by the six testing teams on P15, P16, and P17. Based on the −4.3 mm sizing error for flaw depth, it can be concluded that overall, teams tended to undersize the depth.

Table 4.7. Flaw Depth Sizing Error by Team

		Depth Sizing Error (mm)		
Team	Access	Mean Depth	Standard Deviation	RMSE
134	OD	−6.5	9.2	11.3
132	ID	−7.5	5.7	9.4
108	OD	−9.1	8.5	12.4
126	OD	−3.5	6.2	7.1
113	ID	0.9	1.0	1.3
106	ID	0.0	4.1	4.1

Table 4.8. Flaw Depth Sizing Error Summary

	Sizing Error		
Flaw Dimension	Mean (mm)	Standard Deviation (mm)	RMSE (mm)
Depth (mm)	−4.3	6.6	7.9

Figure 4.8 shows indicated depth plotted against the true-state depth, further highlighting differences in the data taken by teams that made measurements from the ID or OD of the test blocks. If all test indications matched the true state, they would fall directly on top of the red line. Table 4.9 shows how the depth sizing error differs for ID and OD access. The RSME values for depth sizing error by access corroborate the conclusion one makes from Figure 4.8, that generally those teams whose procedures accessed the test block from the ID outperformed teams that accessed the OD.

Table 4.9. Flaw Depth Sizing Error by ID/OD Access

	Depth Sizing Error		
Access	Mean (mm)	Standard Deviation (mm)	RMSE (mm)
ID	−2.2	5.3	5.8
OD	−6.4	27.7	28.4

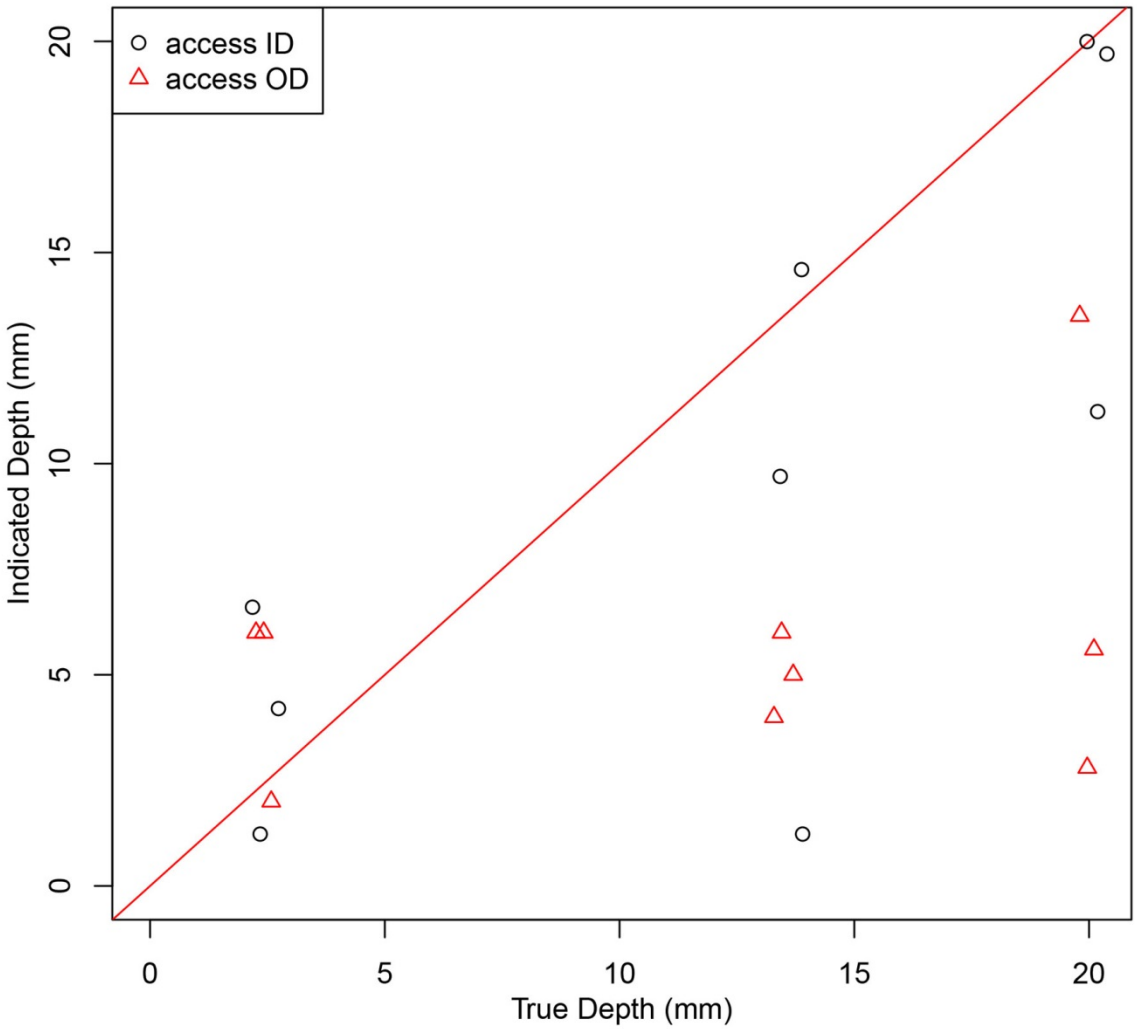

Figure 4.8. Indicated versus True Axial Flaw Depth by Test Team

Figure 4.9 shows indicated flaw depth plotted as a function of true flaw depth for all of the depth sizing techniques applied to the Quick Blind test blocks and for which data was reported on the Technique Datasheets. If all test indications matched the true state, they would fall directly on top of the red line. The definitions for the technique identifiers (shown as Technique Identifier in the legend) were provided in Table 3.1. Note that not all of the data shown in Figure 4.9 was selected by testing teams for inclusion in the Summary Datasheets. This figure provides useful feedback as to how well individual techniques applied performed. Conclusions about depth sizing are summarized in Section 0.

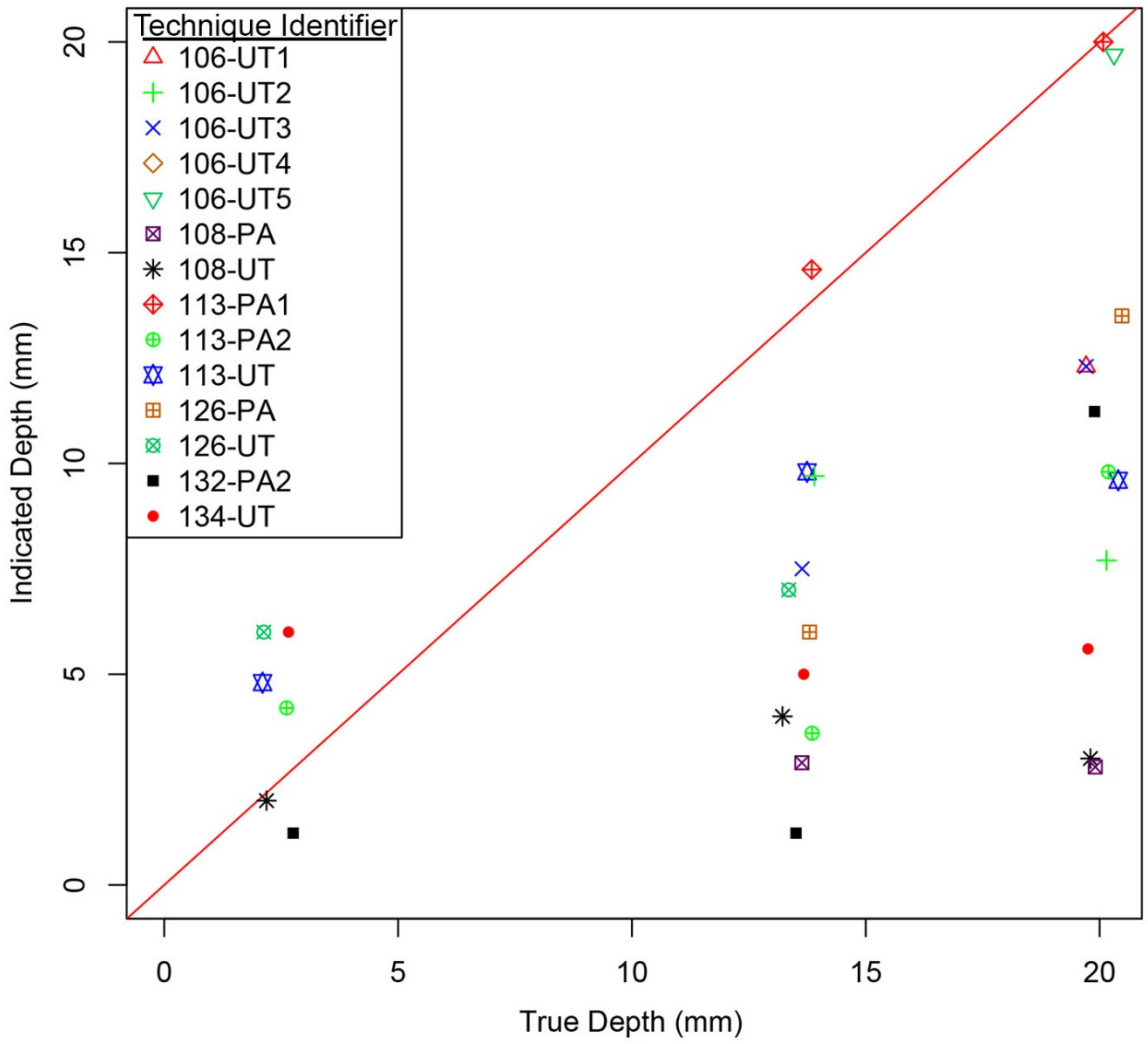

Figure 4.9. Indicated versus True Axial Flaw Depth by NDE Technique

4.3.4 Length Sizing Analysis

Figure 4.10 shows the indicated axial flaw lengths plotted against the true flaw lengths by test team for test blocks P15, P16, and P17. If all test indications matched the true state, they would fall directly on top of the red line. The lengths indicated by team 132 are more than two times the true flaw length. Table 4.10 shows the length sizing error by test team for combined data taken on test blocks P15, P16, and P17. While team 108 had the lowest RMSE, all teams except 132 performed well. Table 4.11 provides a summary of the length sizing errors for the combined 18 inspections performed by the six testing teams on P15, P16, and P17. While the mean error is quite small, the RMSE is quite large and this is a result of the large flaw lengths reported by team 132.

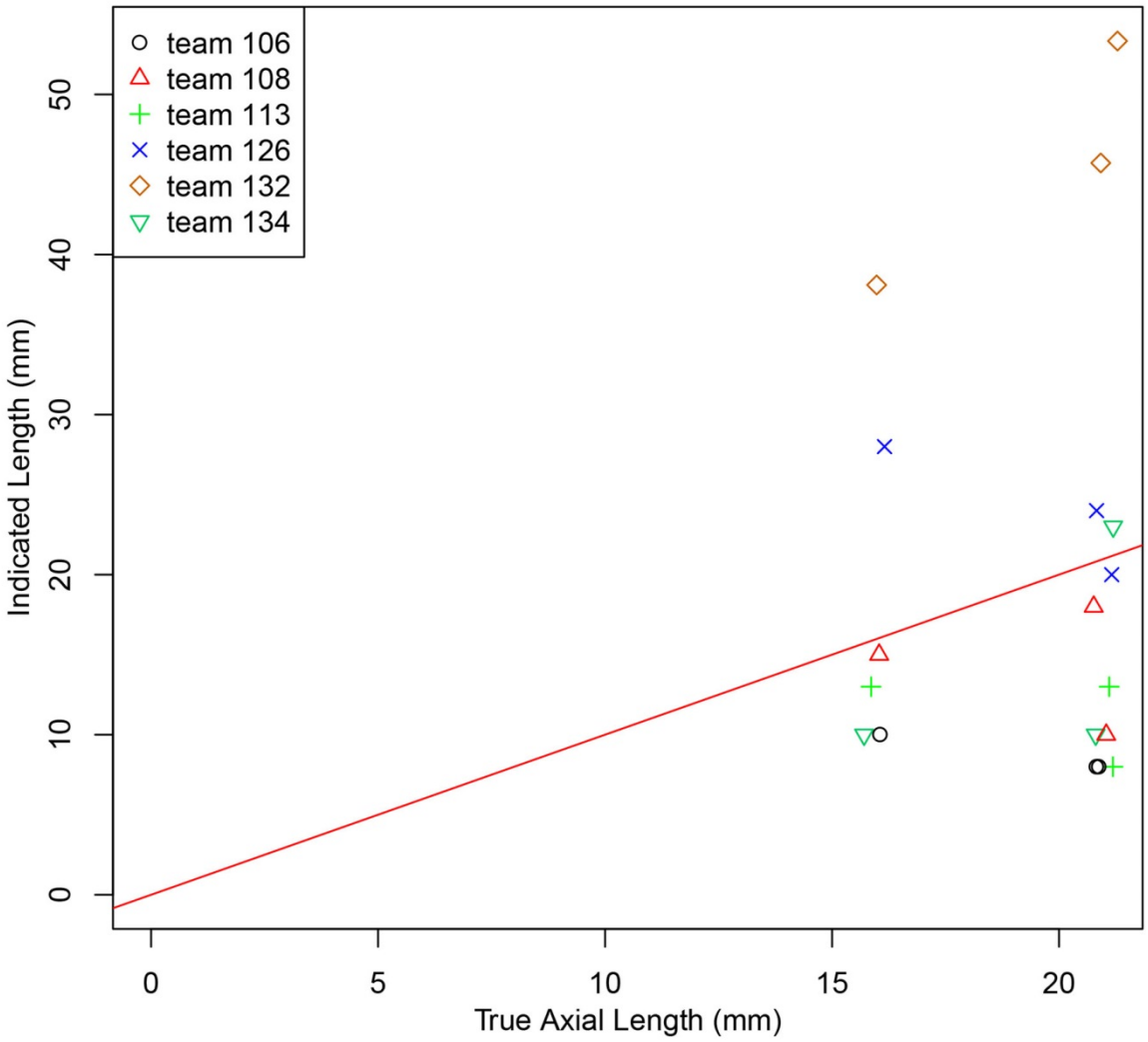

Figure 4.10. Indicated versus True Axial Flaw Length by Test Team

Table 4.10. Flaw Axial Length Sizing Error by Team

	Length Sizing Error (mm)		
Team	**Mean Depth**	**Standard Deviation**	**RMSE**
134	−5.0	6.6	8.2
132	26.4	5.3	26.9
108	−5.0	5.3	7.3
126	4.7	6.7	8.1
113	−8.0	5.0	9.4
106	−10.7	4.0	11.4

Table 4.11. Flaw Axial Length Sizing Errors

Flaw Dimension	Sizing Error		
	Mean (mm)	Standard Deviation (mm)	RMSE (mm)
Length (mm)	0.4	13.7	13.7

Figure 4.11 shows indicated flaw length plotted as a function of true flaw length for all of the length sizing techniques applied to the Quick Blind test blocks and for which data was reported on the Technique Datasheets. If all test indications matched the true state, they would fall directly on top of the red line. The definitions for the technique identifiers (shown as Technique Identifier in the legend) were provided in Table 3.1. Note that not all of the data shown in Figure 4.11 was selected by testing teams for inclusion in the Summary Datasheets. This figure provides useful feedback as to how well individual techniques applied performed. Conclusions about axial length sizing are summarized in Section 5.3.

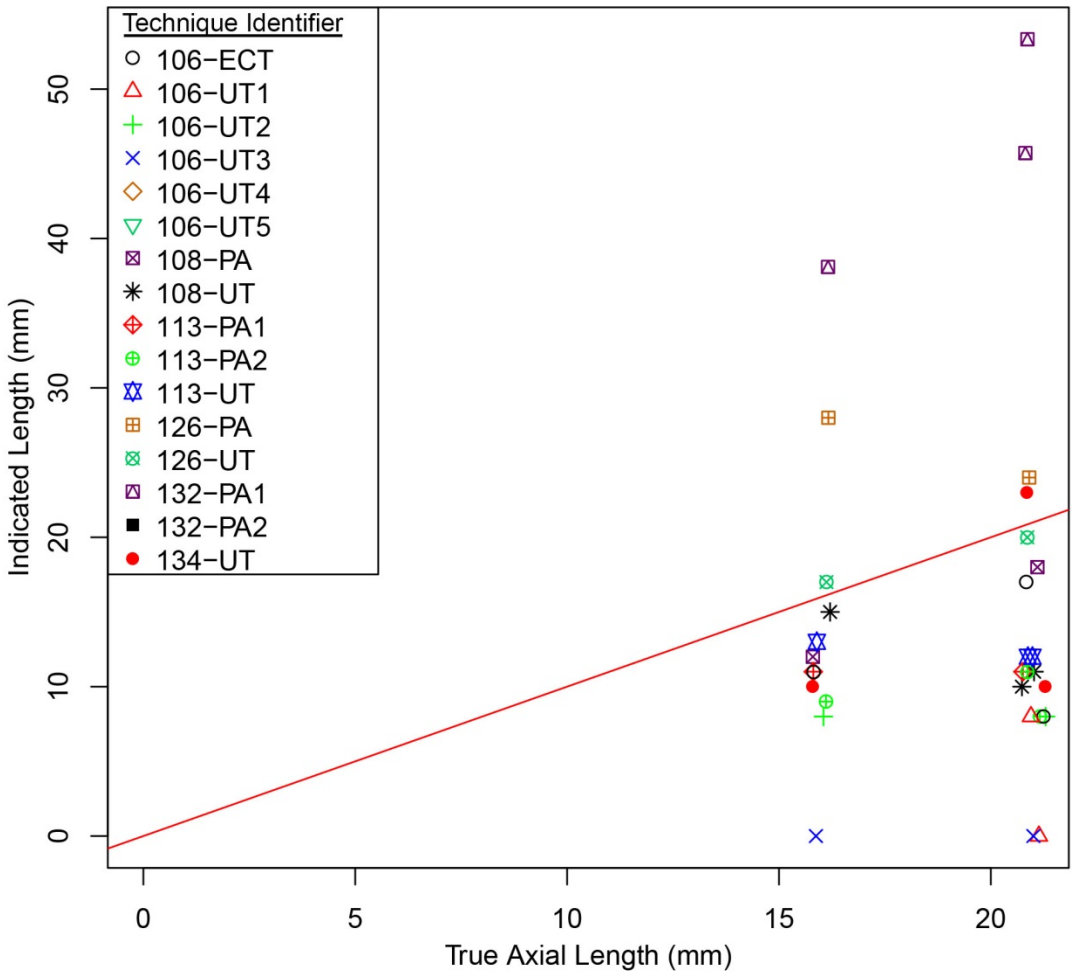

Figure 4.11. Indicated versus True Axial Flaw Length by NDE Technique

Figure 4.12 shows the indicated circumferential flaw lengths (widths) plotted against the true-state lengths by test team for test blocks P15, P16, and P17. If all test indications matched the true state, they would fall directly on top of the red line. Team 132 reported having poor echo dynamics, which took their procedure beyond the operational parameters it was qualified for use under. Because these flaws were intended to be axially oriented and the circumferential (width) characteristic they exhibit has a complex morphology (an unintended outcome of their manufacture), no analysis of sizing error has been performed. In spite of the complex flaw morphology issue, Figure 4.12 shows that team 106 sized the circumferential extent (width) of the flaw width reasonably well.

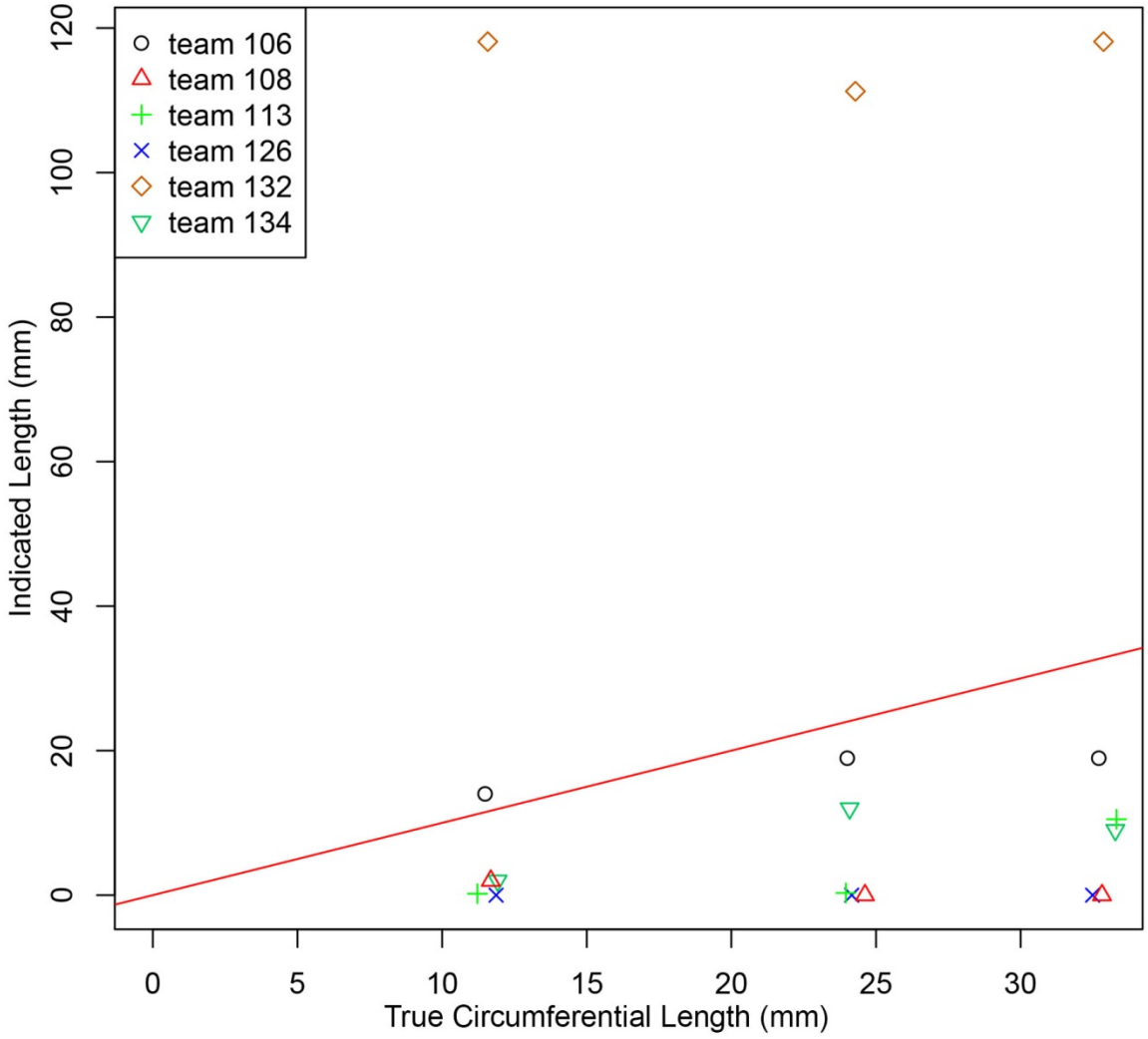

Figure 4.12. Indicated versus True Circumferential Flaw Length by Test Team

5.0 Conclusions

This section summarizes the outcomes of the Quick Blind round-robin tests and destructive analysis.

5.1 Destructive Analysis Results

A destructive analysis of the three test blocks that contained flaws revealed that the flaws exhibited a clustered or volumetric nature. In particular, these axial flaws have significant extent in the circumferential (width) direction—two of them having widths that exceed their lengths by approximately 50%.

5.2 Probability of Detection Performance

For five of the six testing teams, detection results were perfect (i.e., all flaws were detected with no false calls). Team 126 detected all the flaws but made one or more false calls in each of the four test blocks. Probability of detection curves were developed for flaw depth and length, but due to the limited number of data points, the 95% confidence bounds are very wide, having the lower limit at a POD = 0.8. The volumetric nature of these flaws made them easier to detect than those expected to be encountered in the field.

5.3 Depth Sizing Performance

Data was reported for eighteen inspections conducted by the six test teams on the three test blocks that contained flaws. An analysis of this data showed that testing teams tended to oversize the shallow (2.40 mm) flaw and to undersize the deeper flaws (13.6 mm and 20.1 mm). With an RSME of 1.3 mm, team 113 had the best depth sizing performance. For comparison, to pass a typical weld qualification examination in the USA, the maximum difference between indicated and true-state values for flaw depth is 3.18 mm. Team 113 employed a procedure that combined conventional and phased-array ultrasonic techniques. Team 113's good performance is consistent with the conclusion reached in PINC where tests showed that a combination of conventional and phased-array ultrasound techniques provided the best performance for flaw depth sizing. Team 113 reported 3-MHz UT data for the 2.4-mm deep flaw and 2-MHz PA data for the 13.6-mm and 20.1-mm deep flaws. Team 106 was the next best performing team with an RSME of 4.1 mm. Team 106 reported 2-MHz UT data for all the flaws. All teams taken together tended to undersize the depth by an average of 4.3 mm and had a combined depth sizing RSME of 7.9 mm. Generally, teams whose procedures accessed the test block from the inner diameter outperformed teams that accessed from the outer diameter with RSME values of 5.8 mm and 24.8 mm, respectively.

5.4 Length Sizing Performance

The destructive analysis showed that the flaws have extent in both the axial and circumferential directions. While all teams reported data in the axial (Y) direction, not all teams reported circumferential data that would indicate flaw morphology in the circumferential (X) direction. For this reason, and because it was the intention of the test block providers to produce axially oriented flaws, the length sizing

error analysis was performed only on the axially oriented data. With the exception of team 132, the RSME axial length sizing error range (7.3–11.4 mm) for the individual testing teams was reasonable considering that in the USA, to pass a typical weld qualification examination, the maximum difference between indicated and true-state values for flaw length is 19 mm. Team 132 had an RSME axial length sizing error of 26.9 mm. This error value brought the combined RSME error for testing teams to 13.7 mm, whereas without team 132, it would be below 10 mm. Team 108 had the lowest RSME (7.3) and applied a procedure that combined 1–2-MHz conventional and 2-MHz phased-array ultrasonic techniques.

Due to the limited flaw lengths (16 mm and 21 mm), not much more can be concluded from this data regarding the length sizing ability of the techniques applied. Having shorter flaws in the mix would have enhanced the test. This will be remedied by combining this data with that from the Blind round-robin test blocks, as they have several shorter flaws.

6.0 Reference

Cumblidge SE, SR Doctor, PG Heasler, and TT Taylor. 2010. *Results of the Program for the Inspection of Nickel Alloy Components*, NUREG/CR-7019; PNNL-18713, U.S. Nuclear Regulatory Commission, Washington, D.C.

Appendix A

Destructive Analysis of Quick Blind Test Blocks

Appendix A : Destructive Analysis of Quick Blind Test Blocks

The destructive analysis of Quick Blind test blocks were carried out by the following steps.

1. Extract the coupon from SCC induced region.
2. This coupon was sliced by one mm pitch.
3. The cross sections of sliced pieces were polished and observed by the microscope.
   The cross sections were etched and observed by microscope again.
3. Some regions were not sliced. These regions were broken by crack opening force.
   The fracture surfaces were observed by microscope, and the distribution of SCC depth was measured on the photograph of microscope.

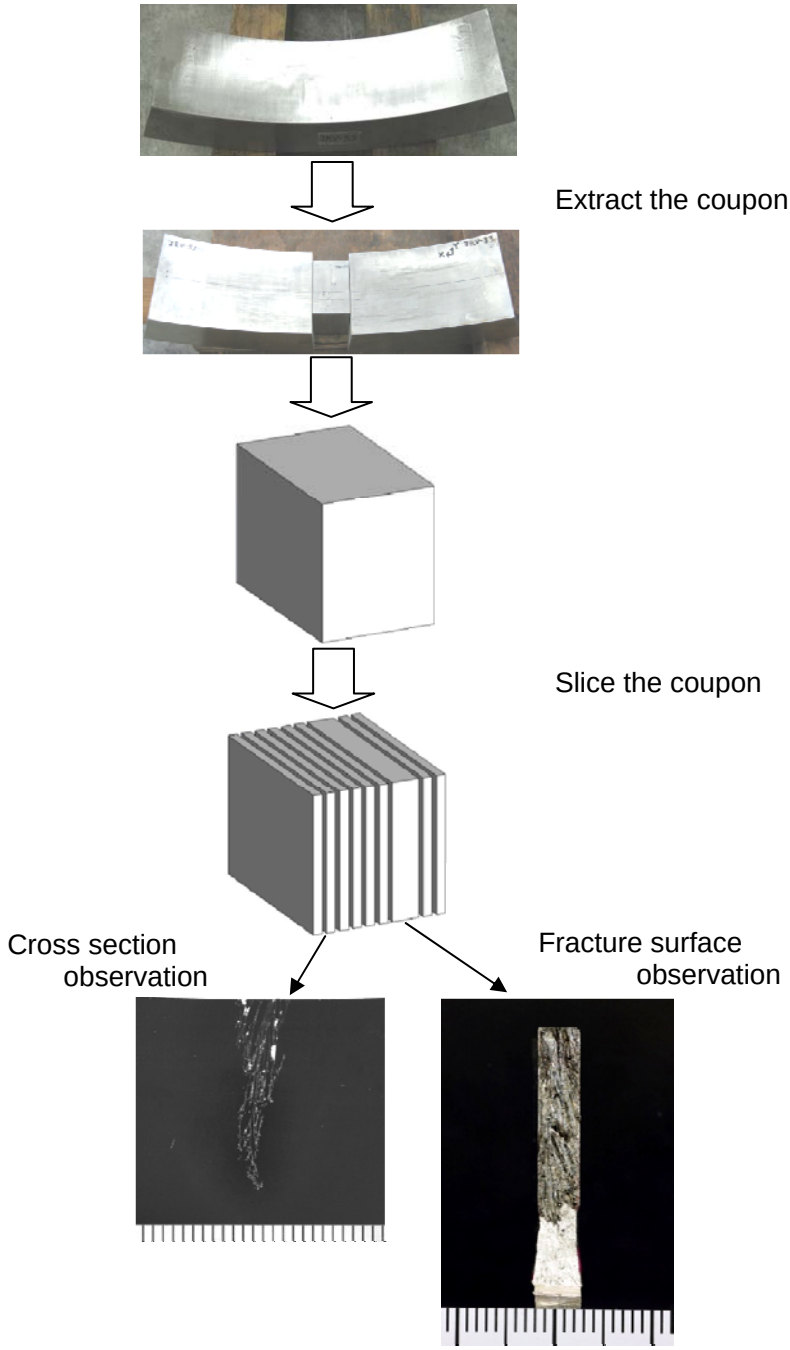

(1) Test brock

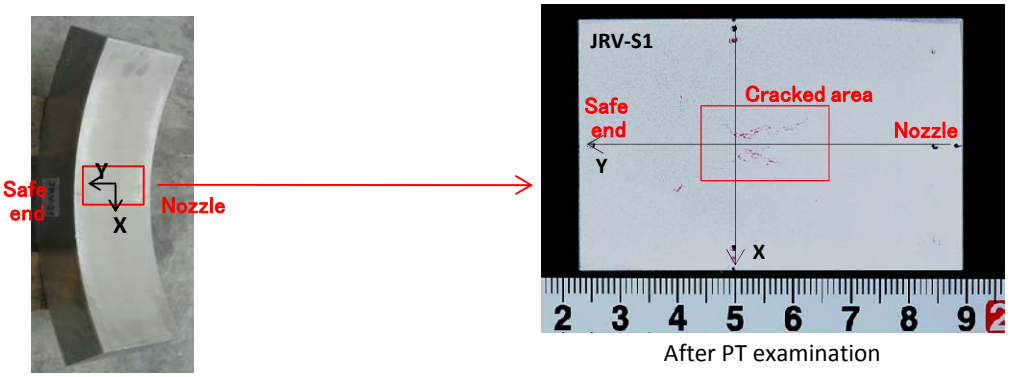

After PT examination

(2) Profile of SCC

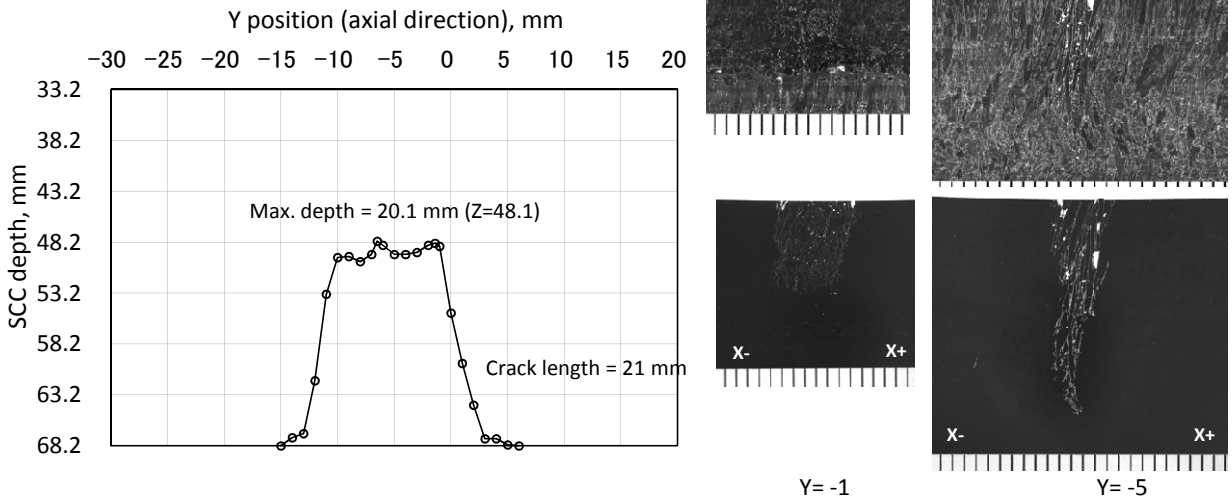

Typical photo of SCC
(Upper:before etching, Lower : after etching)

(3) Measured data of SCC

Measured on sliced cross section

Cross section	Y	mm	6.0	5.0	4.0	3.0	2.0	1.0	0.0	-1.0	-1.4
Depth	Z	mm	68.2	68.1	67.5	67.5	64.2	60.1	55.2	48.6	48.3
X range	Xmin	mm	—	227.6	224.2	224.1	223.6	222.9	223.2		
	Xmax	mm	—	232.1	233.5	232.0	232.8	232.2	232.6		
Typical crack opening		μm	—	<1	5	<1	<1	<1	<1	FS	FS

Cross section	Y	mm	-2.0	-3.0	-4.0	-5.0	-6.0	-6.5	-7.0	-8.0	-9.0
Depth	Z	mm	48.5	49.2	49.4	49.4	48.5	48.1	49.4	50.1	49.6
X range	Xmin	mm			224.1	224.3					223.9
	Xmax	mm			230.5	230.7					232.8
Typical crack opening		μm	FS	FS	<1	5	FS	FS	FS	FS	<1

Cross section	Y	mm	-10.0	-11.0	-12.0	-13.0	-14.0	-15.0
Depth	Z	mm	49.7	53.3	61.8	67.0	67.4	68.2
X range	Xmin	mm	223.9	223.5	224.2	223.5	222.4	—
	Xmax	mm	232.7	232.9	234.1	233.2	233.9	—
Typical crack opening		μm	<1	<1	5	<1	<1	—

FS : Fracture surface

(4) Flaw dimension of test block

X1	X2	Y1	Y2	Z1	Z2
222.4	234.1	-15.0	6.0	48.1	68.2

Fig. A-1 Summarized result of destructive test on P15 (JRV-S1)

(1) Test brock

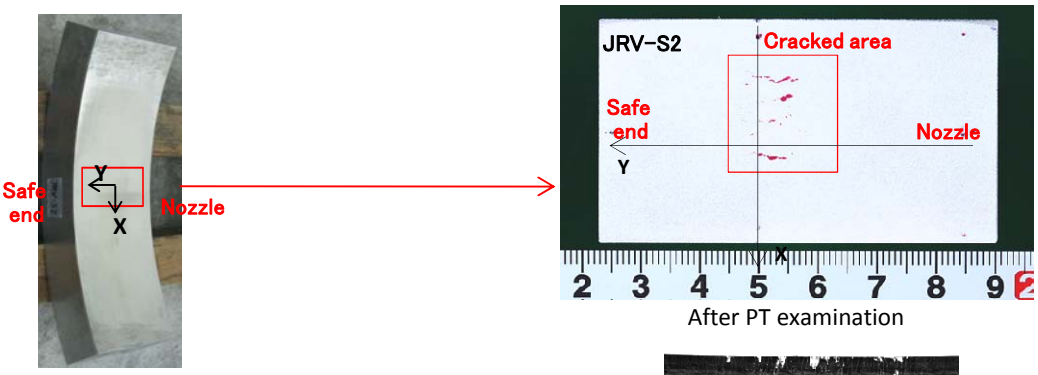

After PT examination

(2) Profile of SCC

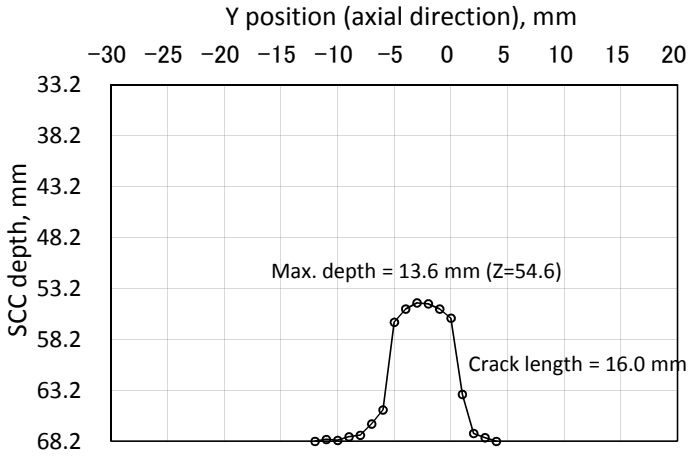

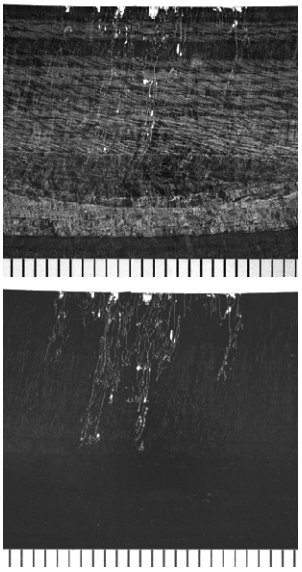

Typical photo of SCC at Y= -2
(Upper:before etching, Lower : after etching)

(3) Measured data of SCC

Measured on sliced cross section

Cross section	Y	mm	4.0	3.0	2.0	1.0	0.0	-1.0	-2.0	-3.0	-4.0
Depth	Z	mm	68.2	67.8	67.4	63.6	56.1	55.2	54.7	54.6	55.2
X range	Xmin	mm	—	216.7	214.2	211.7	214.6	213.9	214.5		
	Xmax	mm	—	234.9	233.9	235.1	233.7	234.4	234.3		
Typical crack opening		µm	—	15	4	5	11	30	5	FS	FS

Cross section	Y	mm	-5.0	-6.0	-7.0	-8.0	-9.0	-10.0	-11.0	-12.0
Depth	Z	mm	56.5	65.1	66.5	67.6	67.8	68.1	68.0	68.2
X range	Xmin	mm		214.0	212.3	224.9	217.2	224.8	224.6	—
	Xmax	mm		233.7	236.1	231.9	231.8	228.2	229.2	—
Typical crack opening		µm	FS	22	<1	<1	24	3	2	—

FS : Fracture surface

(4) Flaw dimension of test block

X1	X2	Y1	Y2	Z1	Z2
211.7	236.1	-12.0	4.0	54.6	68.2

Fig. A-2 Summarized result of destructive test on P16 (JRV-S2)

(1) Test brock

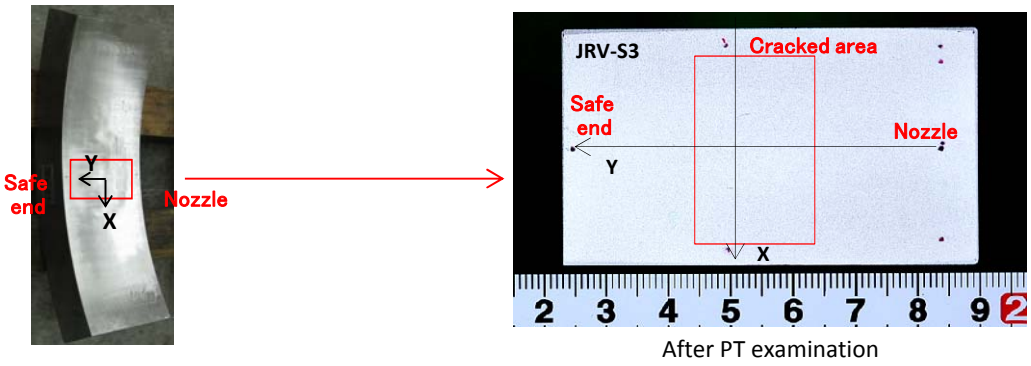

After PT examination

(2) Profile of SCC

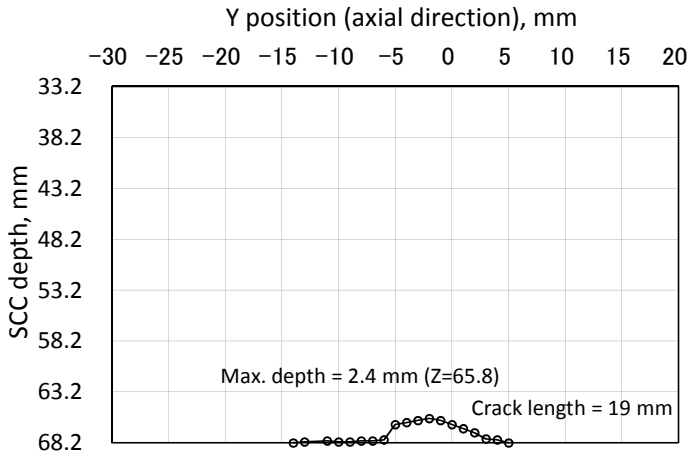

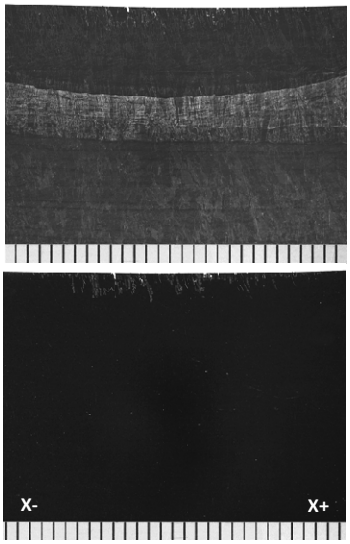

Typical photo of SCC at Y= -2
(Upper:before etching, Lower : after etching)

(3) Measured data of SCC

Measured on sliced cross section

Cross section	Y	mm	5.0	4.0	3.0	2.0	1.0	0.0	-1.0	-2.0	-3.0
Depth	Z	mm	68.2	67.9	67.8	67.2	66.8	66.4	66.0	65.8	66.0
X range	Xmin	mm	—	225.7	216.1	214.5	215.7	211.5	211.2	212.9	213.7
	Xmax	mm	—	226.4	239.8	237.2	235.9	244.0	239.9	244.1	243.6
Typical crack opening		μm	—	<1	<1	<1	5	2	5	<1	<1

Cross section	Y	mm	-4.0	-5.0	-6.0	-7.0	-8.0	-9.0	-10.0	-11.0	-13.0
Depth	Z	mm	66.2	66.4	67.9	68.0	68.0	68.1	68.1	68.0	68.1
X range	Xmin	mm	214.9	214.6	218.8	219.1	219.0	220.7	224.3	225.2	225.2
	Xmax	mm	243.6	241.6	237.8	233.6	233.3	232.5	228.9	230.9	227.9
Typical crack opening		μm	8	6	<1	<1	3	<1	5	5	2

Cross section	Y	mm	-14.0
Depth	Z	mm	68.2
X range	Xmin	mm	—
	Xmax	mm	—
Typical crack opening		μm	—

FS : Fracture surface

(4) Flaw dimension of test block

X1	X2	Y1	Y2	Z1	Z2
211.2	244.1	-15.0	6.0	65.8	68.2

Fig. A-3 Summarized result of destructive test on P17 (JRV-S3)

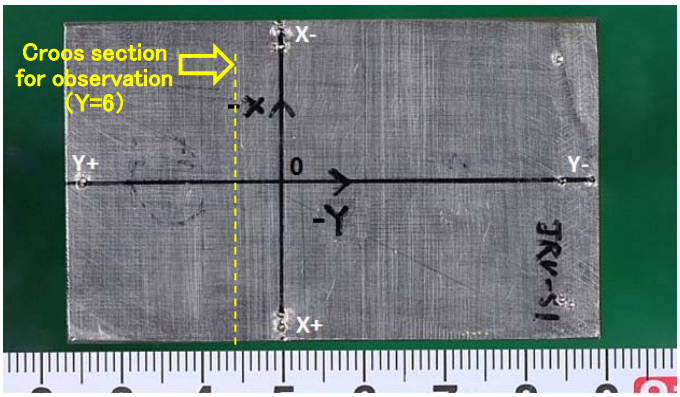

O point :
X=228.6, Y=0

Position of cross section for observation (Y=6)

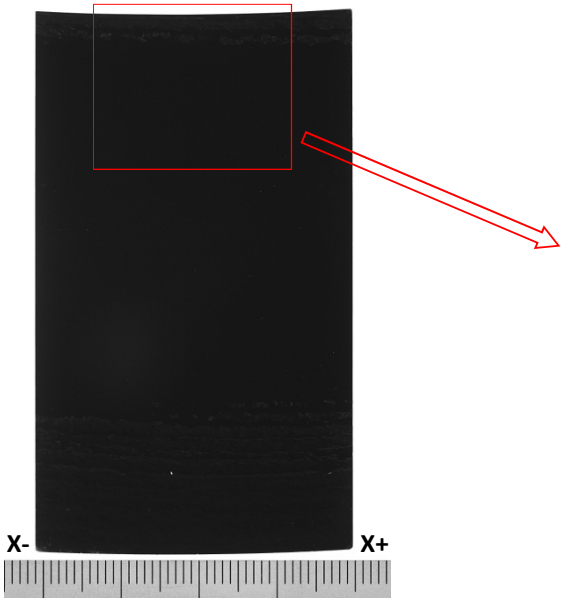

Cross section (before etching)

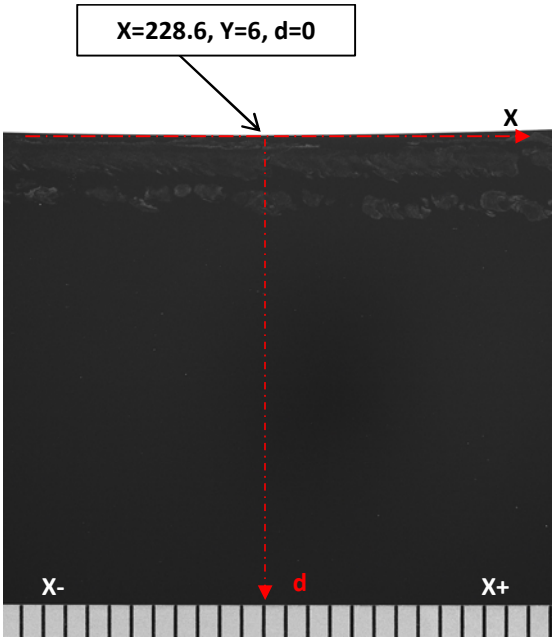

Enlarged cross section (before etching)

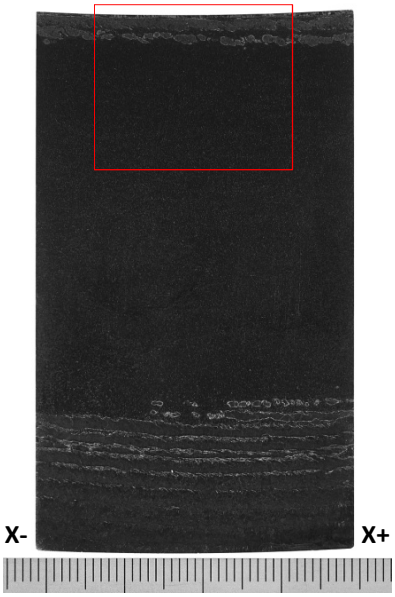

Cross section (after etching)

Crack information

Cross section Y (mm)	6.0
Max. crack depth info Z (mm)	No crack
Crack opening (μ m)	No crack
Typical crack information	No crack

Z = 68.2 - d

Fig. A-1.1 Detailed crack information at Y=6 section in P15 (JRV-S1)

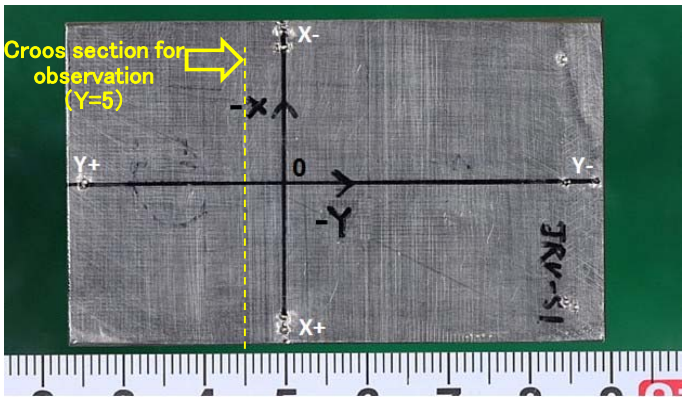

O point :
X=228.6, Y=0

Position of cross section for observation (Y=5)

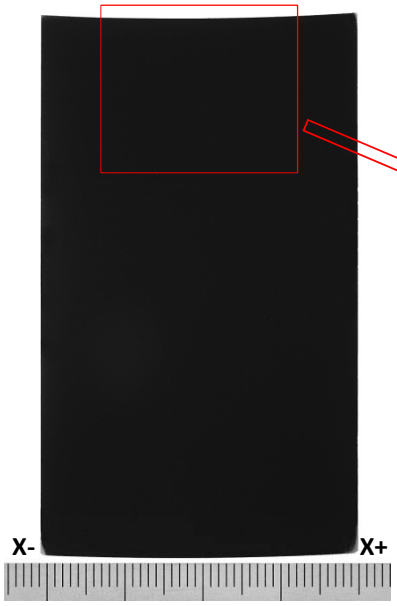

Cross section (before etching)

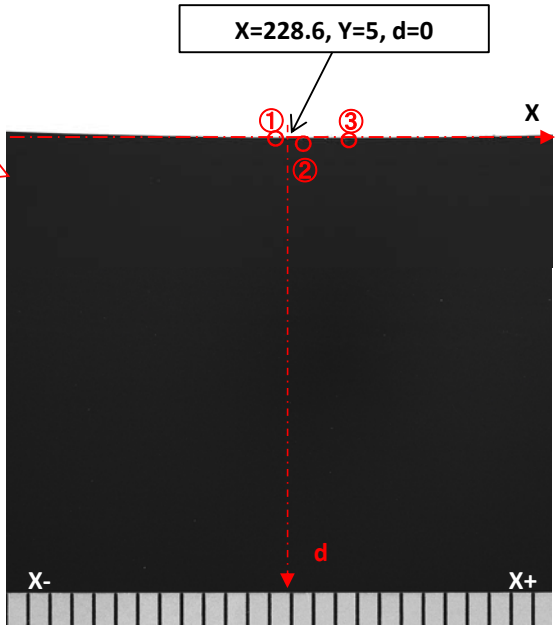

Enlarged cross section (before etching)

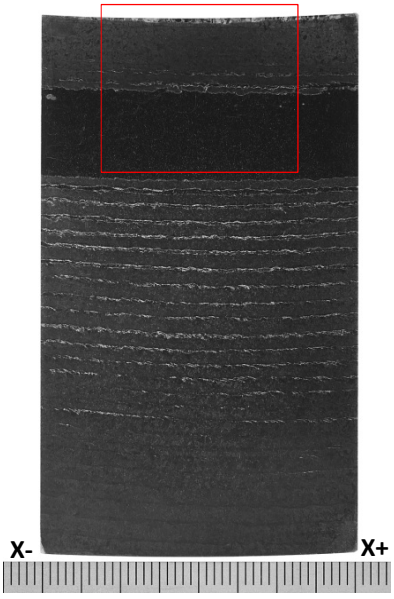

Cross section (after etching)

Crack information

Cross section Y (mm)		5.0
Max. crack depth info Z (mm)		68.1
Crack opening (μ m)		<1
Typical crack information	①	X= 227.6 Z= 68.2
	②	X= 229.5 Z= 68.1
	③	X= 232.1 Z= 68.2

Z = 68.2 - d

Fig. A-1.2 Detailed crack information at Y=5 section in P15 (JRV-S1)

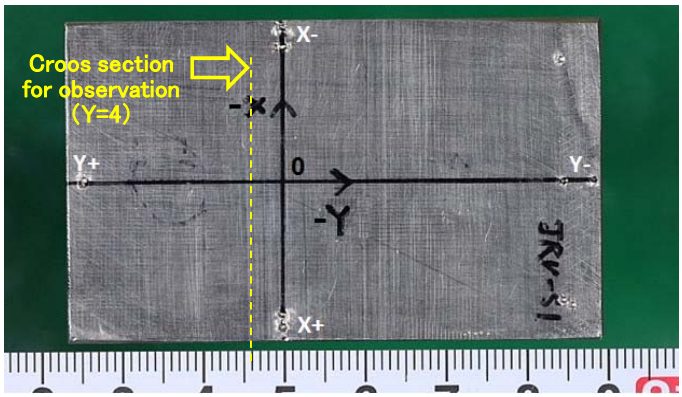

O point :
X=228.6, Y=0

Position of cross section for observation (Y=4)

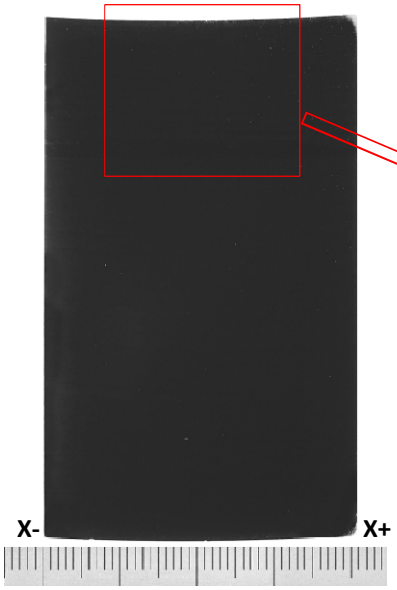

Cross section (before etching)

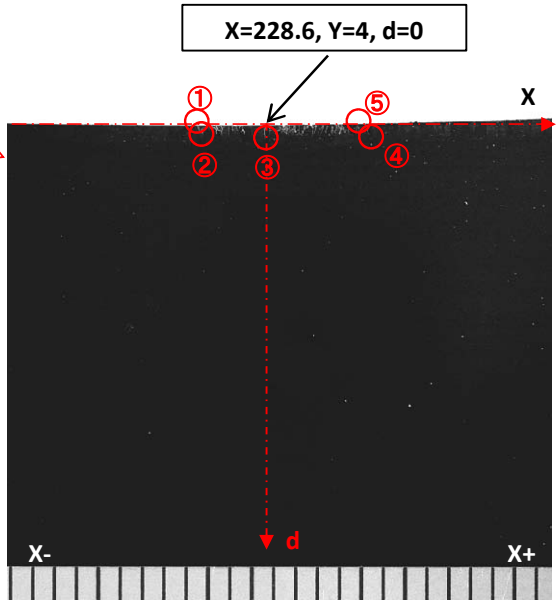

Enlarged cross section (before etching)

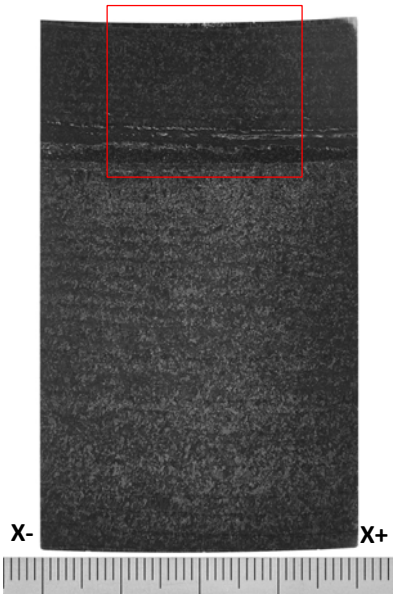

Cross section (after etching)

Crack information

Cross section Y (mm)		4.0
Max. crack depth info Z (mm)		67.5
Crack opening (μ m)		5.0
Typical crack information	①	X= 224.2 Z= 68.2
	②	X= 224.3 Z= 67.8
	③	X= 227.9 Z= 67.5
	④	X= 233.5 Z= 67.8
	⑤	X= 233.3 Z= 68.2

Z = 68.2 - d

Fig. A-1.3 Detailed crack information at Y=4 section in P15 (JRV-S1)

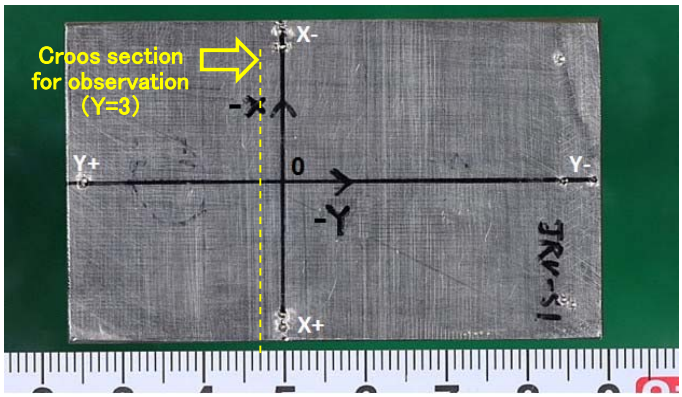

O point :
X=228.6, Y=0

Position of cross section for observation (Y=3)

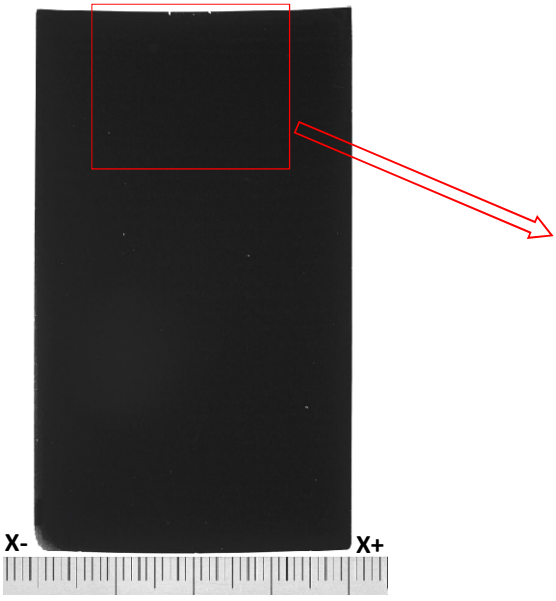

Cross section (before etching)

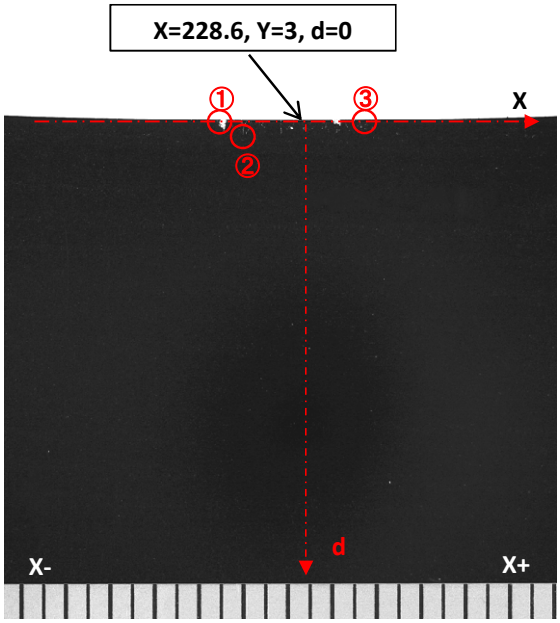

Enlarged cross section (before etching)

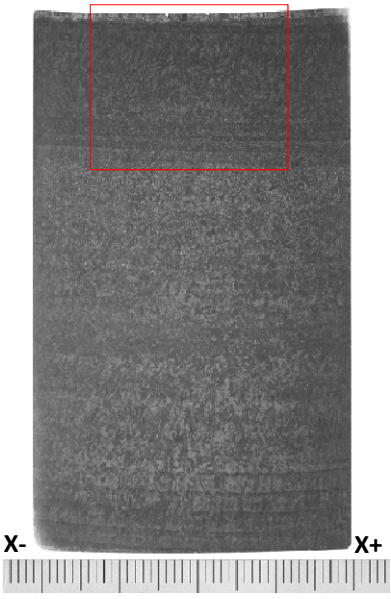

Cross section (after etching)

Crack information

Cross section Y (mm)		3.0
Max. crack depth info Z (mm)		67.5
Crack opening (μ m)		<1
Typical crack information	①	X= 224.1 Z= 68.2
	②	X= 225.1 Z= 67.5
	③	X= 232.0 Z= 68.2

Z = 68.2 - d

Fig. A-1.4 Detailed crack information at Y=3 section in P15 (JRV-S1)

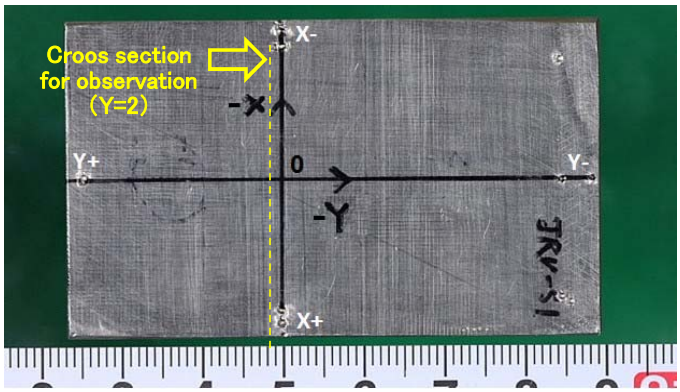

O point :
X=228.6, Y=0

Position of cross section for observation (Y=2)

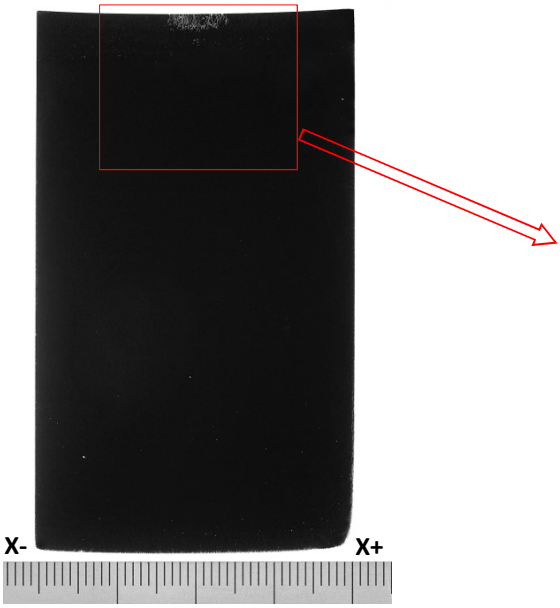

Cross section (before etching)

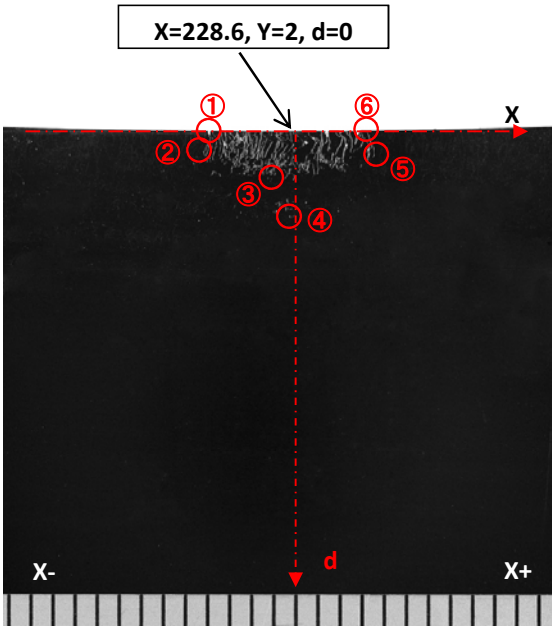

Enlarged cross section (before etching)

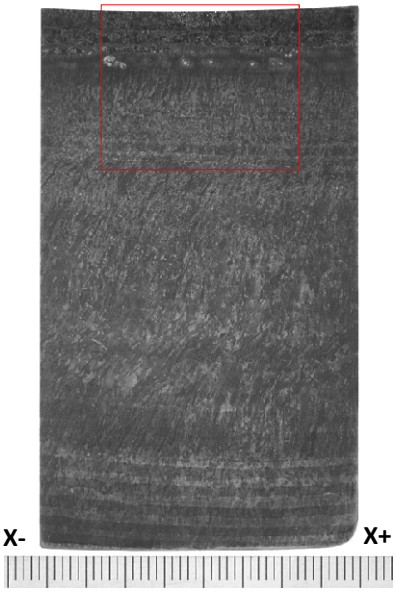

Cross section (after etching)

Crack information

Cross section Y (mm)		2.0
Max. crack depth info Z (mm)		64.2
Crack opening (μ m)		<1
Typical crack information	①	X= 223.8 Z= 68.2
	②	X= 223.6 Z= 67.2
	③	X= 227.2 Z= 65.8
	④	X= 228.3 Z= 64.2
	⑤	X= 232.8 Z= 67.1
	⑥	X= 232.3 Z= 68.2

Z = 68.2 - d

Fig. A-1.5 Detailed crack information at Y=2 section in P15 (JRV-S1)

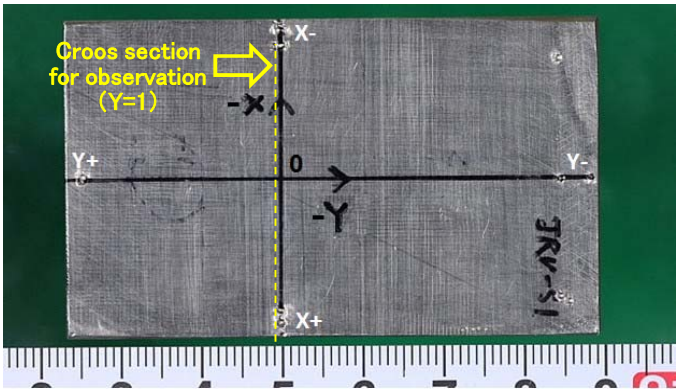

O point :
X=228.6, Y=0

Position of cross section for observation (Y=1)

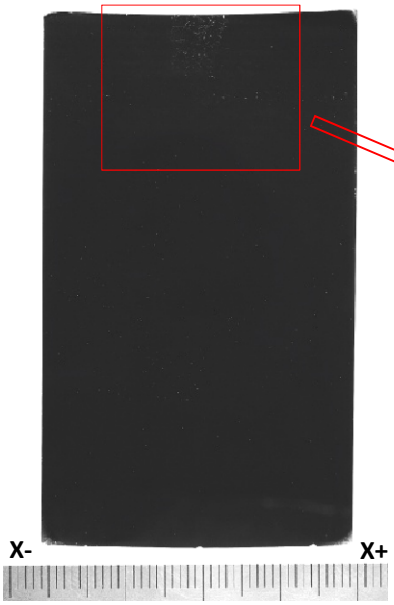

Cross section (before etching)

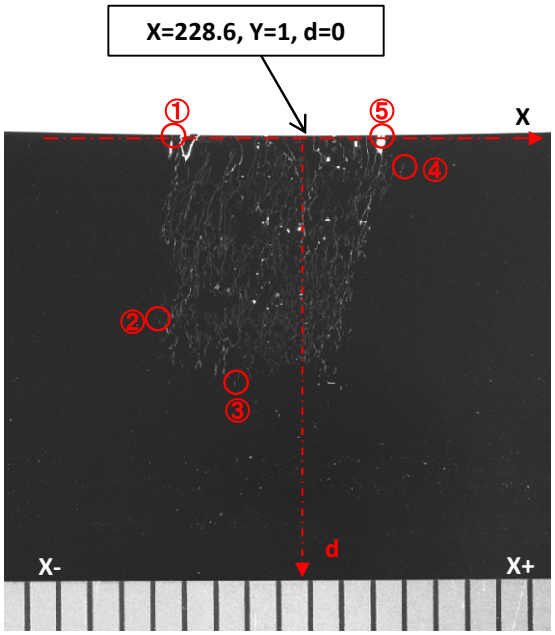

Enlarged cross section (before etching)

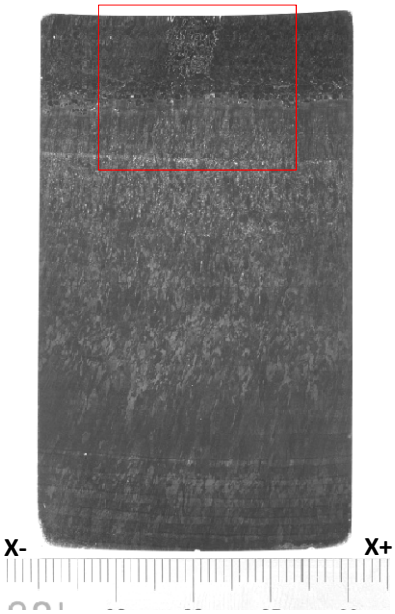

Cross section (after etching)

Crack information

Cross section Y (mm)		1.0
Max. crack depth info Z (mm)		60.1
Crack opening (μ m)		<1
Typical crack information	①	X= 223.5 Z= 68.2
	②	X= 222.9 Z= 62.3
	③	X= 225.9 Z= 60.1
	④	X= 232.2 Z= 67.3
	⑤	X= 231.4 Z= 68.2

Z = 68.2 - d

Fig. A-1.6 Detailed crack information at Y=1 section in P15 (JRV-S1)

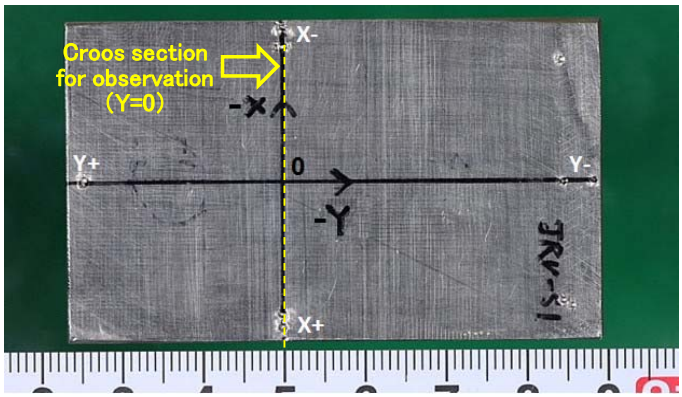

O point :
X=228.6, Y=0

Position of cross section for observation (Y=0)

Cross section (before etching)

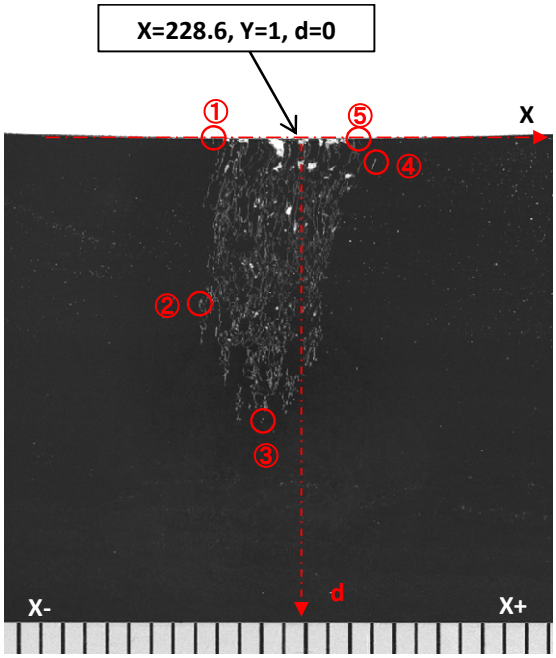

Enlarged cross section (before etching)

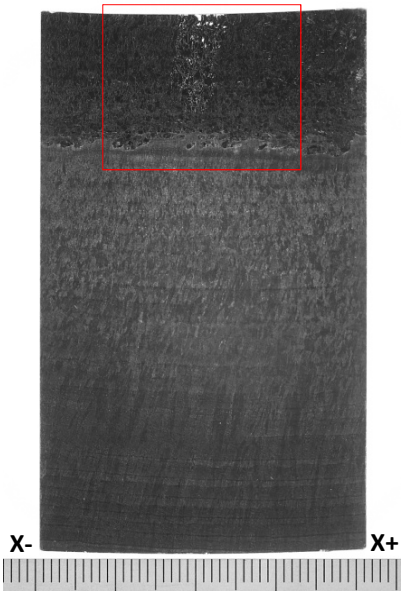

Cross section (after etching)

Crack information

Cross section Y (mm)		0.0
Max. crack depth info Z (mm)		55.2
Crack opening (μ m)		<1
Typical crack information	①	X= 223.9 Z= 68.2
	②	X= 223.2 Z= 60.8
	③	X= 226.7 Z= 55.2
	④	X= 232.6 Z= 67.4
	⑤	X= 231.7 Z= 68.2

Z = 68.2 - d

Fig. A-1.7 Detailed crack information at Y=0 section in P15 (JRV-S1)

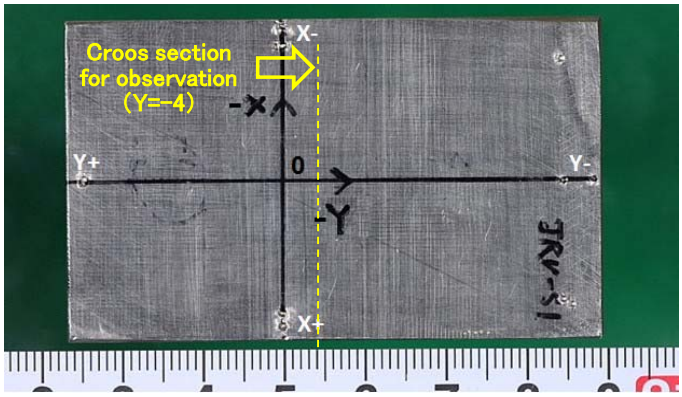

O point :
X=228.6, Y=0

Position of cross section for observation (Y= - 4)

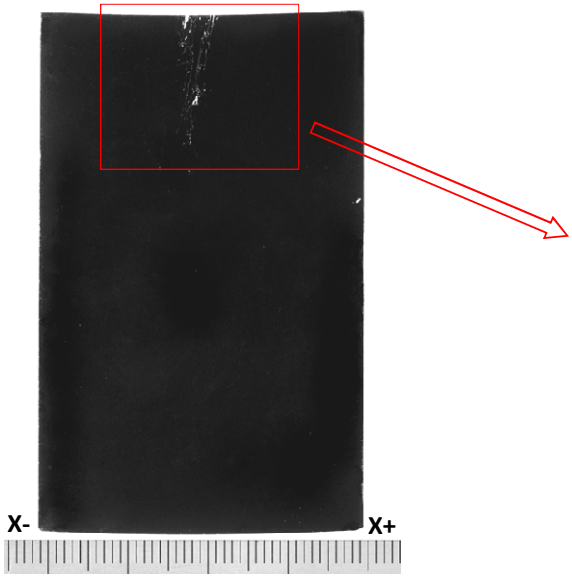

Cross section (before etching)

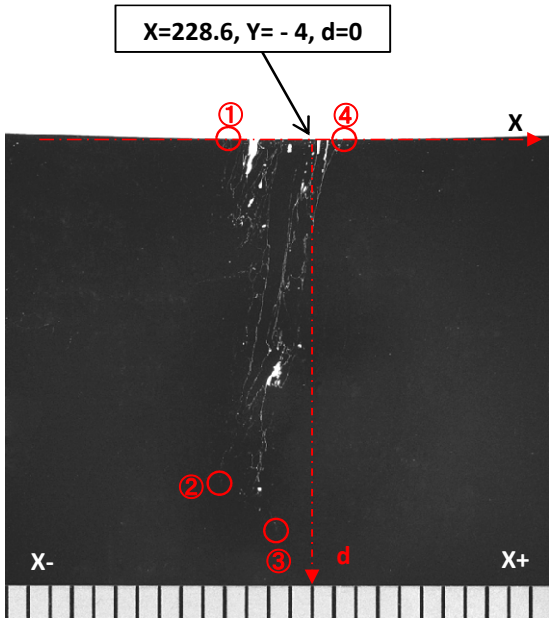

Enlarged cross section (before etching)

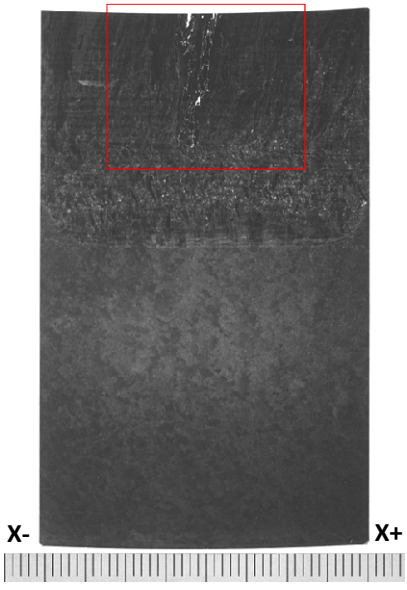

Cross section (after etching)

Crack information

Cross section Y (mm)		-4.0
Max. crack depth info Z (mm)		49.4
Crack opening (μ m)		<1
Typical crack information	①	X= 224.3 Z= 68.2
	②	X= 224.1 Z= 51.9
	③	X= 227.2 Z= 49.4
	④	X= 230.5 Z= 68.2

Z = 68.2 - d

Fig. A-1.8 Detailed crack information at Y= - 4 section in P15 (JRV-S1)

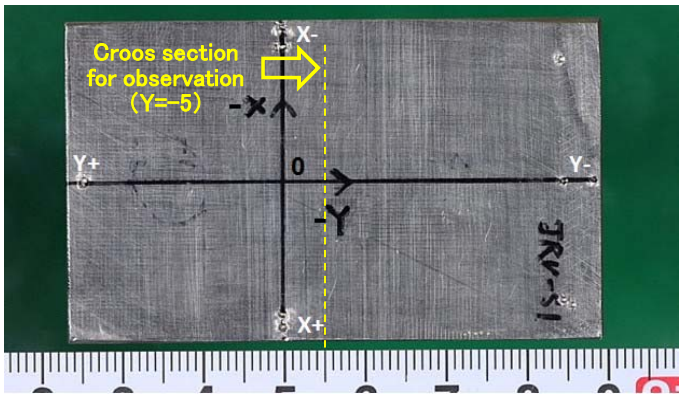

O point :
X=228.6, Y=0

Position of cross section for observation (Y= - 5)

Cross section (before etching)

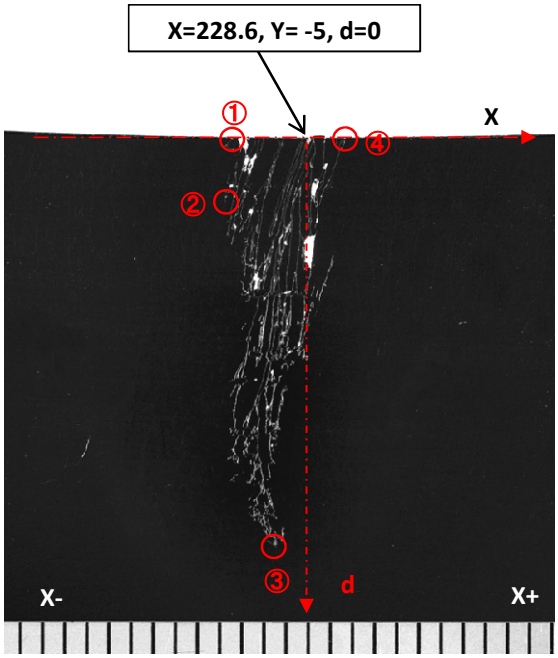

Enlarged cross section (before etching)

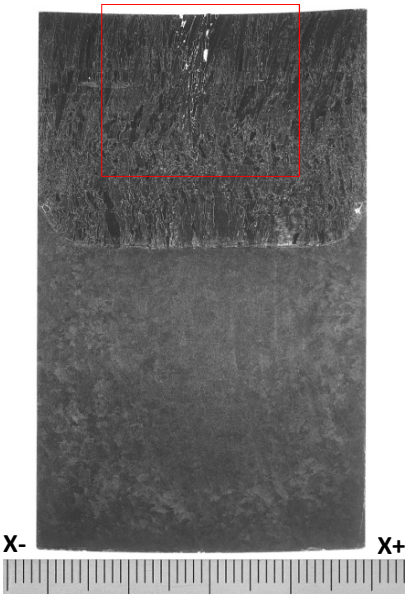

Cross section (after etching)

Crack information

Cross section Y (mm)		−5
Max. crack depth info Z (mm)		49.4
Crack opening (μ m)		5.0
Typical crack information	①	X= 224.7 Z= 68.2
	②	X= 224.3 Z= 65.3
	③	X= 227.1 Z= 49.4
	④	X= 230.7 Z= 68.2

Z = 68.2 - d

Fig. A-1.9 Detailed crack information at Y= - 5 section in P15 (JRV-S1)

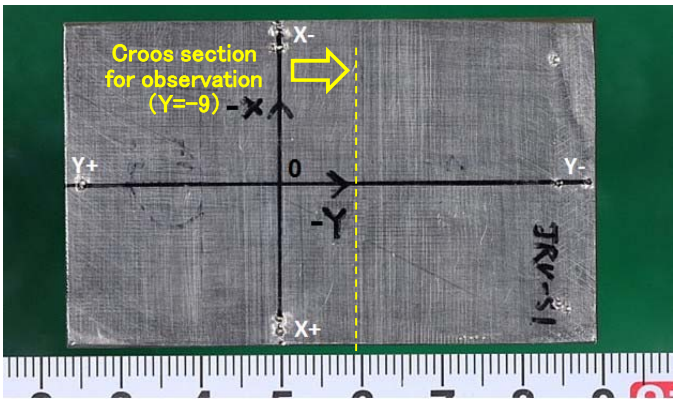

O point :
X=228.6, Y=0

Position of cross section for observation (Y= - 9)

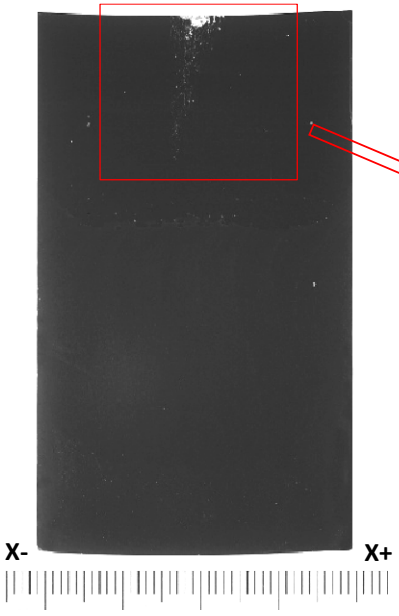

Cross section (before etching)

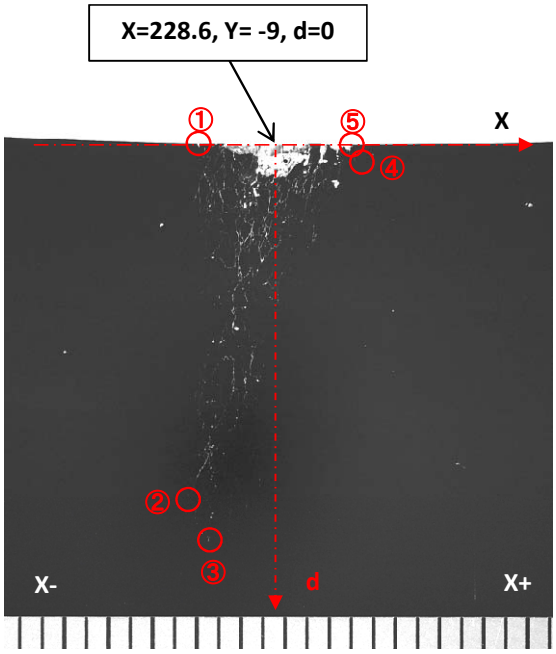

Enlarged cross section (before etching)

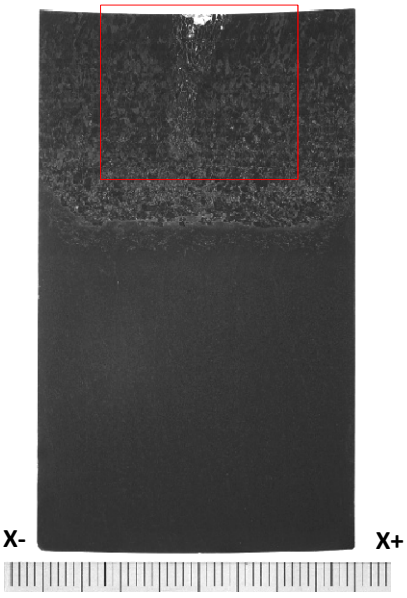

Cross section (after etching)

Crack information

Cross section Y (mm)		-9
Max. crack depth info Z (mm)		49.6
Crack opening (μ m)		<1
Typical crack information	①	X= 224.2 Z= 68.2
	②	X= 223.9 Z= 52.0
	③	X= 225.2 Z= 49.6
	④	X= 232.8 Z= 67.4
	⑤	X= 232.4 Z= 68.2

Z = 68.2 - d

Fig. A-1.10 Detailed crack information at Y= - 9 section in P15 (JRV-S1)

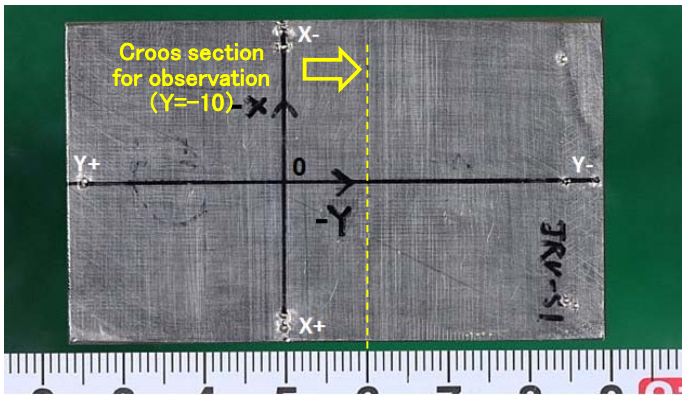

O point :
X=228.6, Y=0

Position of cross section for observation (Y= - 10)

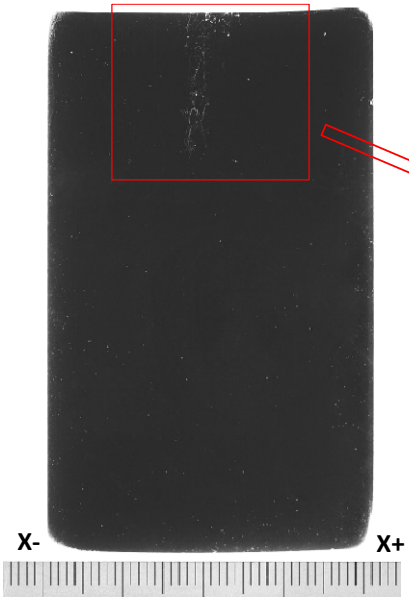

Cross section (before etching)

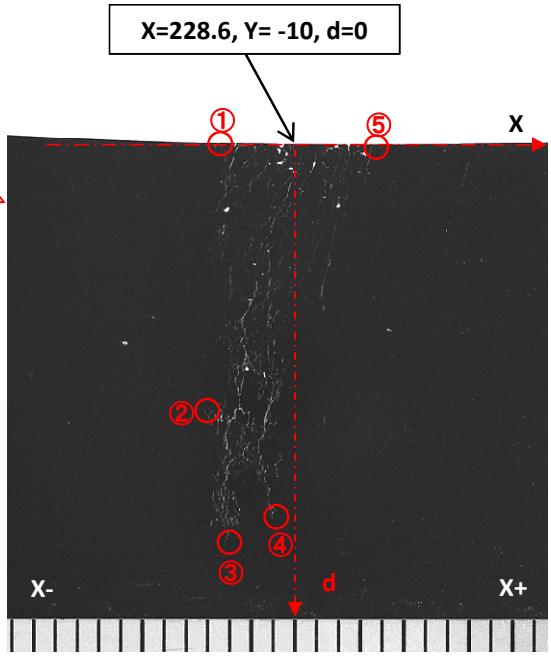

Enlarged cross section (before etching)

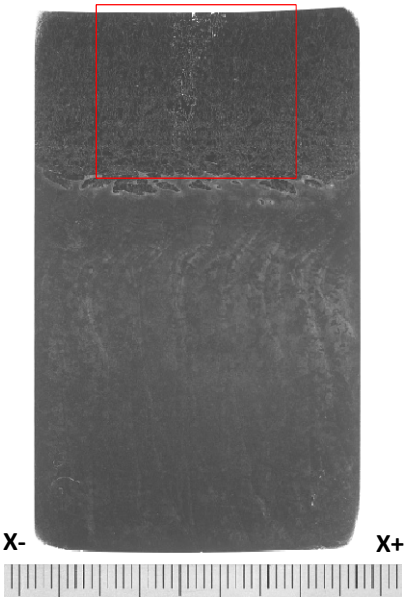

Cross section (after etching)

Crack information

Cross section Y (mm)		−10
Max. crack depth info Z (mm)		49.7
Crack opening (μ m)		<1
Typical crack information	①	X= 224.4 Z= 68.2
	②	X= 223.9 Z= 55.9
	③	X= 225.1 Z= 49.7
	④	X= 227.7 Z= 51.0
	⑤	X= 232.7 Z= 68.2

Z = 68.2 - d

Fig. A-1.11 Detailed crack information at Y= - 10 sectionin P15 (JRV-S1)

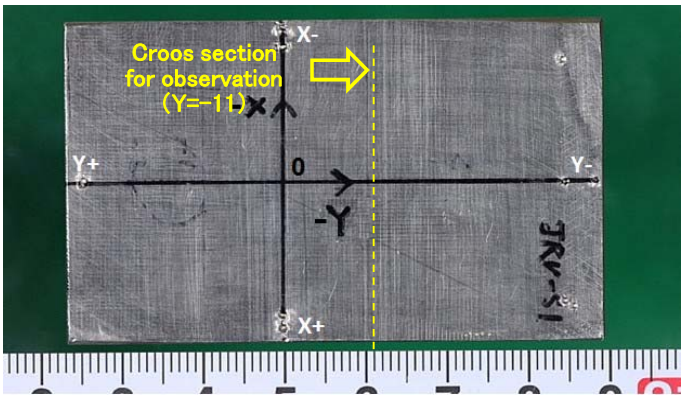

O point :
X=228.6, Y=0

Position of cross section for observation (Y= - 11)

Cross section (before etching)

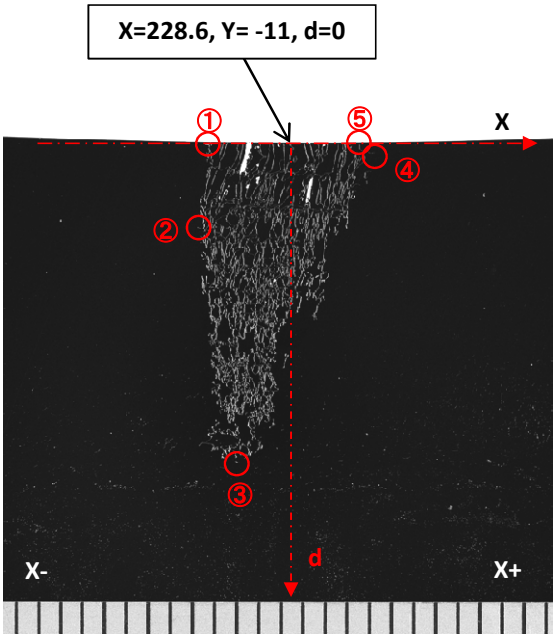

Enlarged cross section (before etching)

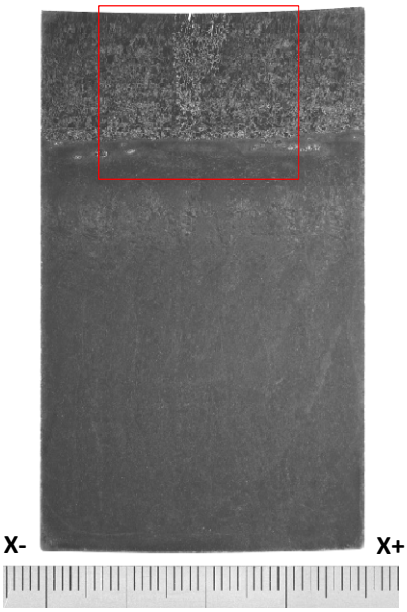

Cross section (after etching)

Crack information

Cross section Y (mm)		−11
Max. crack depth info Z (mm)		53.3
Crack opening (μ m)		<1
Typical crack information	①	X= 224.0 Z= 68.2
	②	X= 223.5 Z= 64.3
	③	X= 225.7 Z= 53.3
	④	X= 232.9 Z= 67.7
	⑤	X= 232.1 Z= 68.2

Z = 68.2 - d

Fig. A-1.12 Detailed crack information at Y= - 11 section in P15 (JRV-S1)

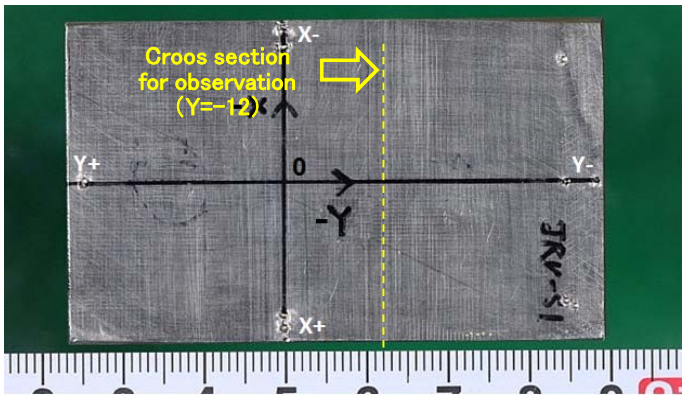

O point :
X=228.6, Y=0

Position of cross section for observation (Y=

Cross section (before etching)

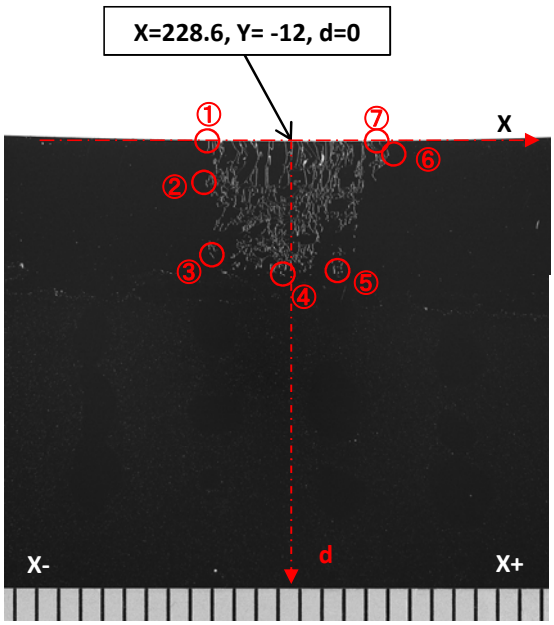

Enlarged cross section (before etching)

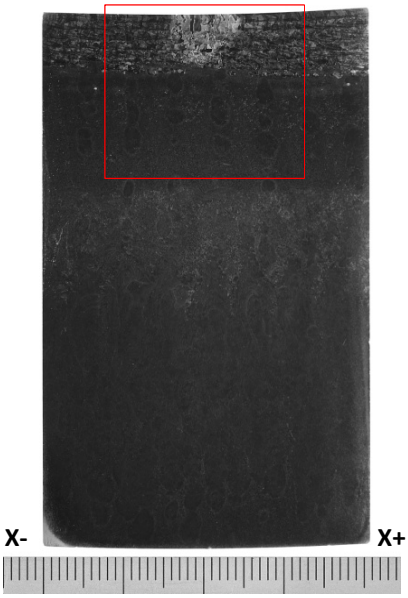

Cross section (after etching)

Crack information

Cross section Y (mm)		−12
Max. crack depth info Z (mm)		61.8
Crack opening (μ m)		5.0
Typical crack information	①	X= 224.3 Z= 68.2
	②	X= 224.2 Z= 66.4
	③	X= 224.7 Z= 62.6
	④	X= 228.5 Z= 61.8
	⑤	X= 231.2 Z= 61.9
	⑥	X= 234.1 Z= 67.6
	⑦	X= 233.6 Z= 68.2

Z = 68.2 - d

Fig. A-1.13 Detailed crack information at Y= - 12 section in P15 (JRV-S1)

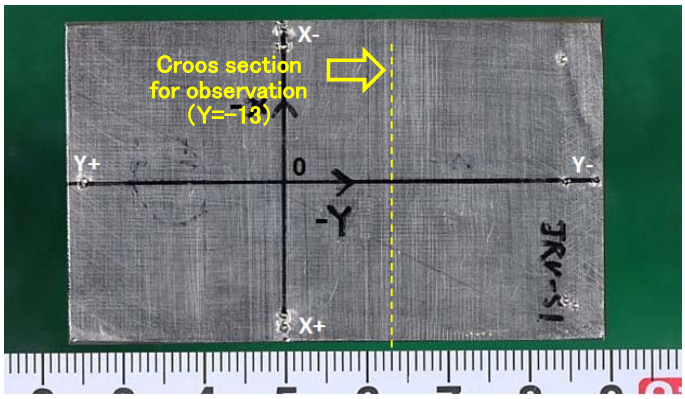

O point :
X=228.6, Y=0

Position of cross section for observation (Y= - 13)

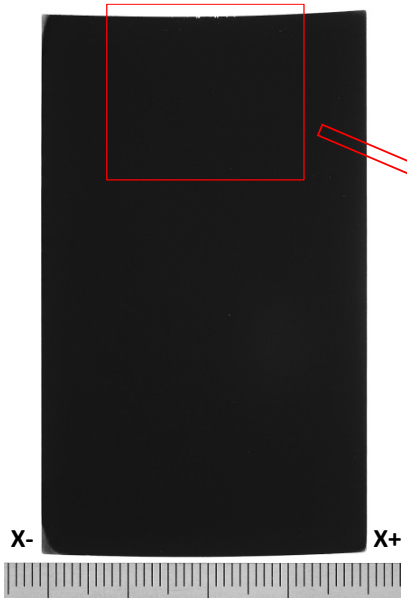

Cross section (before

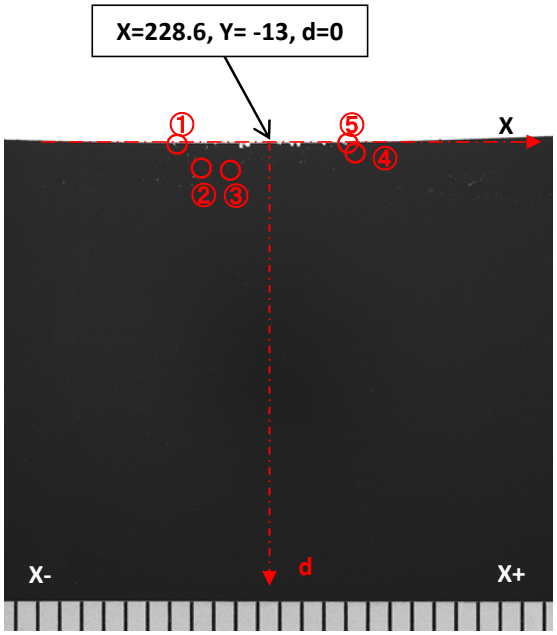

Enlarged cross section (before etching)

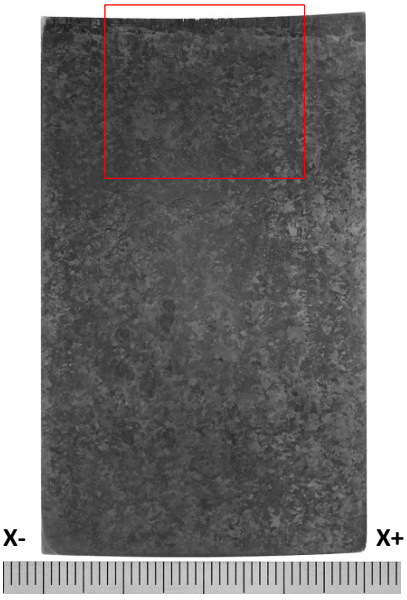

Cross section (after etching)

Crack information

Cross section Y (mm)		-13
Max. crack depth info Z (mm)		67.0
Crack opening (μ m)		<1
Typical crack information	①	X= 223.5 Z= 68.2
	②	X= 224.6 Z= 67.0
	③	X= 226.5 Z= 67.0
	④	X= 233.2 Z= 67.3
	⑤	X= 233.0 Z= 68.2

Z = 68.2 - d

Fig. A-1.14 Detailed crack information at Y= - 13 section in P15 (JRV-S1)

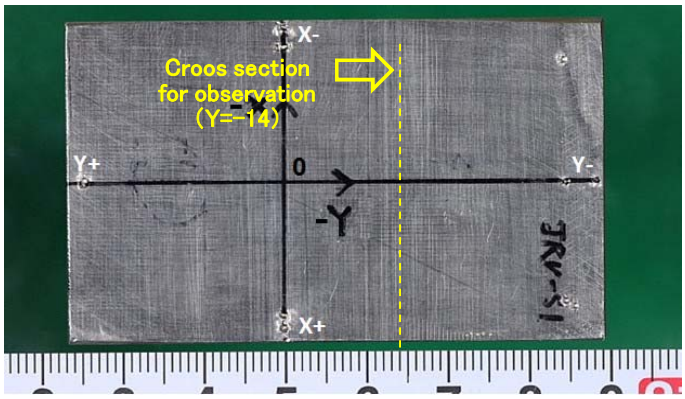

O point :
X=228.6, Y=0

Position of cross section for observation (Y= -

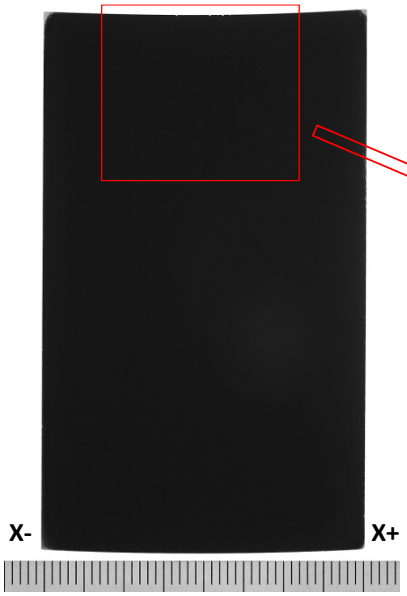

Cross section (before etching)

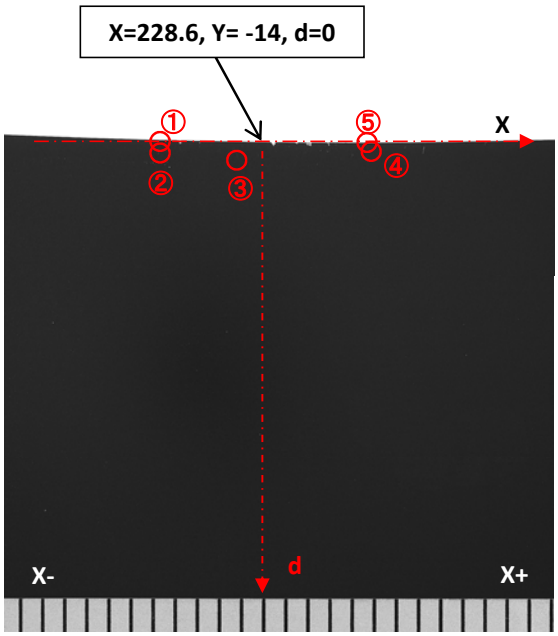

Enlarged cross section (before etching)

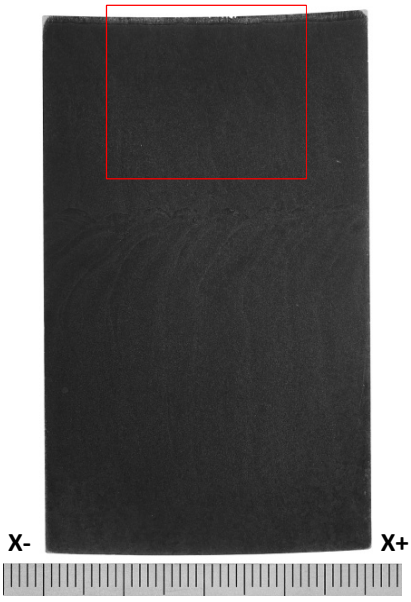

Cross section (after etching)

Crack information

Cross section Y (mm)		-14
Max. crack depth info Z (mm)		67.4
Crack opening (μ m)		<1
Typical crack information	①	X= 222.4 Z= 68.2
	②	X= 222.6 Z= 67.5
	③	X= 225.5 Z= 67.4
	④	X= 233.9 Z= 67.9
	⑤	X= 233.8 Z= 68.2

Z = 68.2 - d

Fig. A-1.15 Detailed crack information at Y= - 14 section in P15 (JRV-S1)

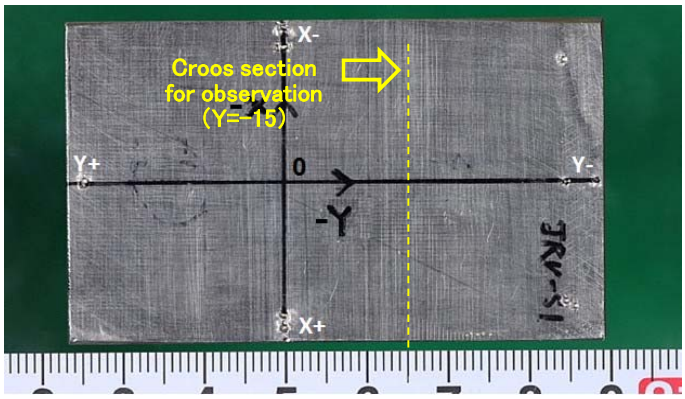

O point :
X=228.6, Y=0

Position of cross section for observation (Y= - 15)

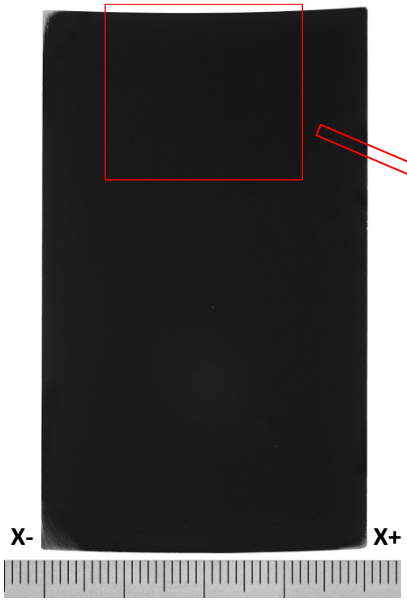

Cross section (before

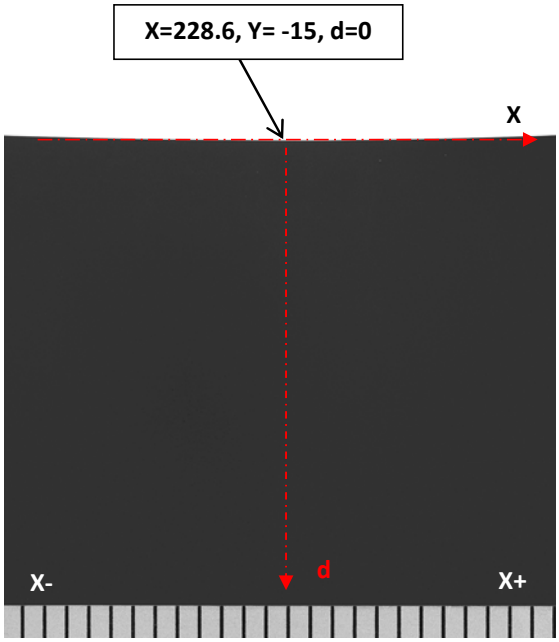

Enlarged cross section (before etching)

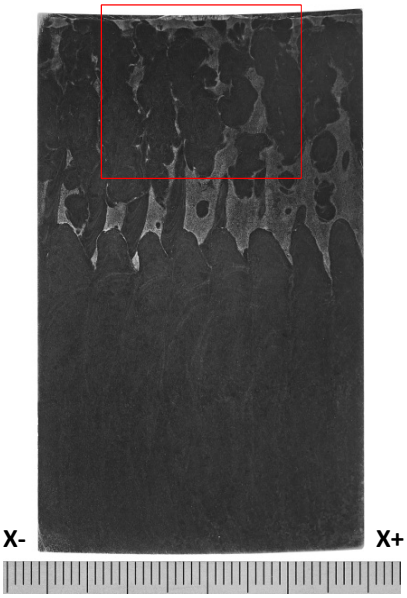

Cross section (after etching)

Crack information

Cross section Y (mm)	−15
Max. crack depth info Z (mm)	No crack
Crack opening (μ m)	No crack
Typical crack information	No crack

Z = 68.2 - d

Fig. A-1.16 Detailed crack information at Y= - 15 section in P15 (JRV-S1)

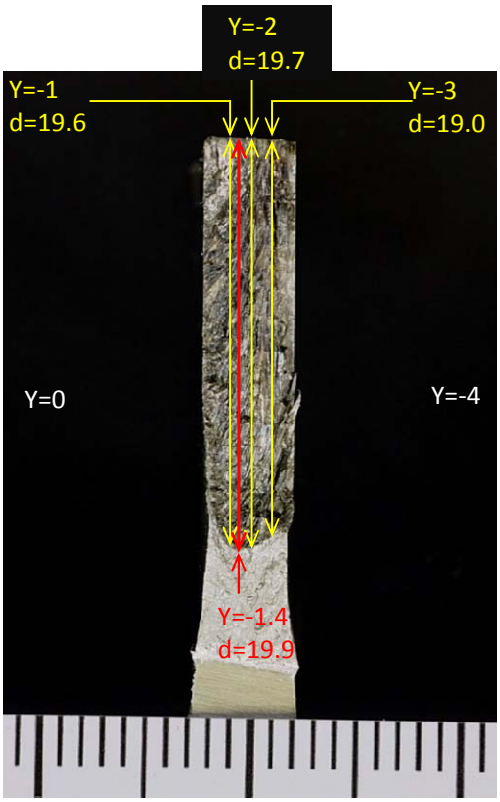

Y=0 to Y= - 4 fracture surface

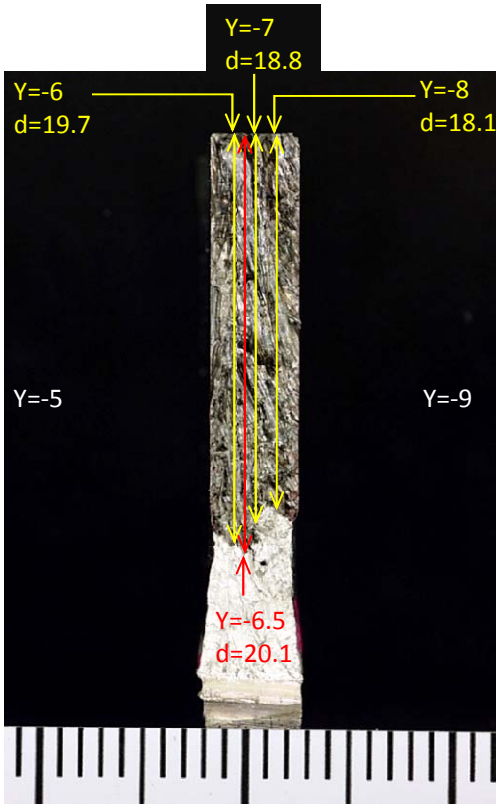

Y= - 5 to Y= - 9 fracture surface

Fig. A-1.17 Detailed crack information at Y= 0 to -4 and Y= -5 to -9 fracture surface in P15 (JRV-S1)

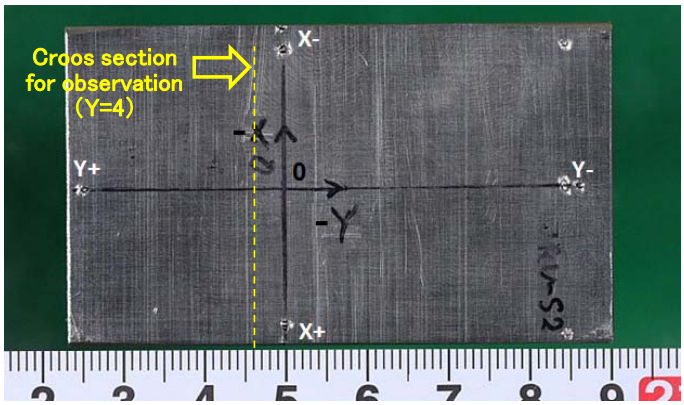

O point :
X=228.6, Y=0

Position of cross section for observation (Y=4)

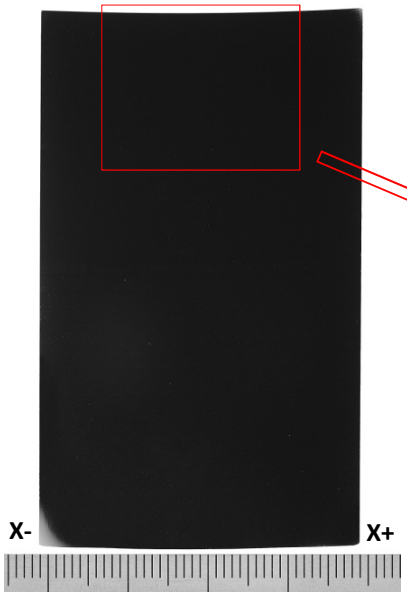

Cross section (before etching)

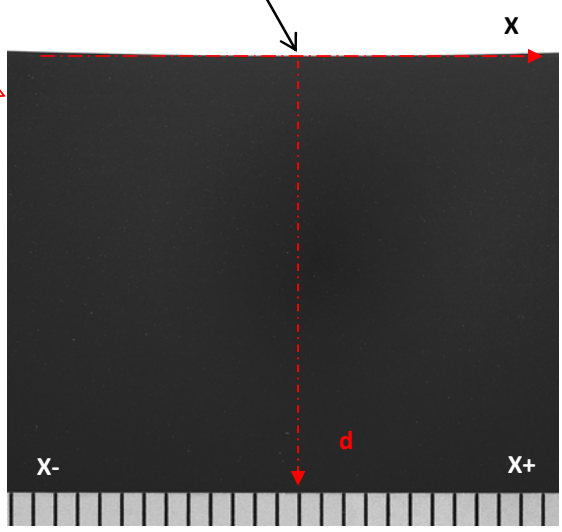

Enlarged cross section (before etching)

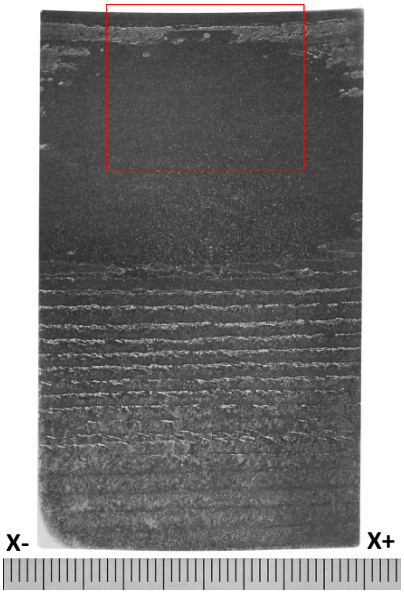

Cross section (after etching)

Crack information

Cross section Y (mm)	4.0
Max. crack depth info Z (mm)	No crack
Crack opening (μ m)	No crack
Typical crack information	No crack

Z = 68.2 - d

Fig. A-2.1 Detailed crack information at Y=4 section in P16 (JRV-S2)

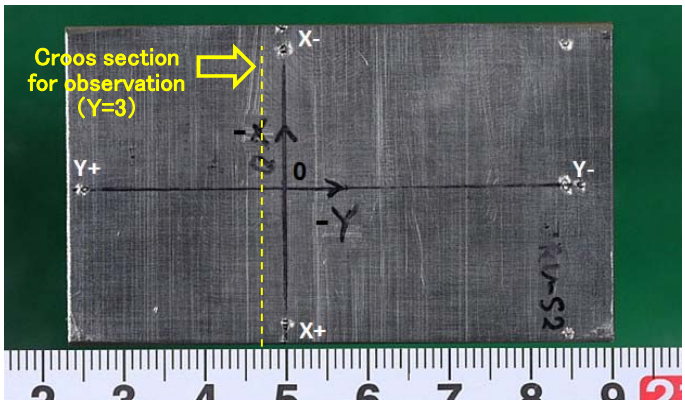

O point :
X=228.6, Y=0

Position of cross section for observation (Y=3)

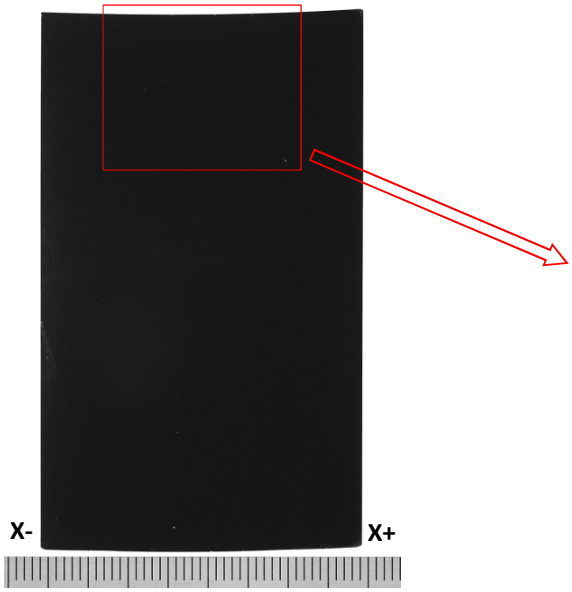

Cross section (before etching)

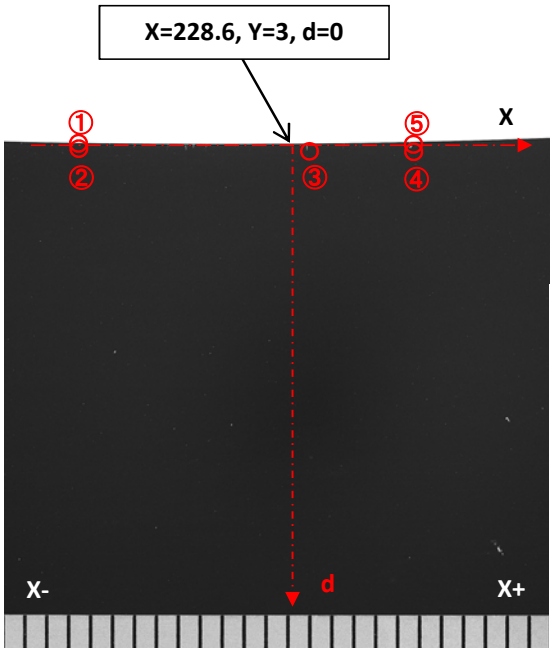

Enlarged cross section (before etching)

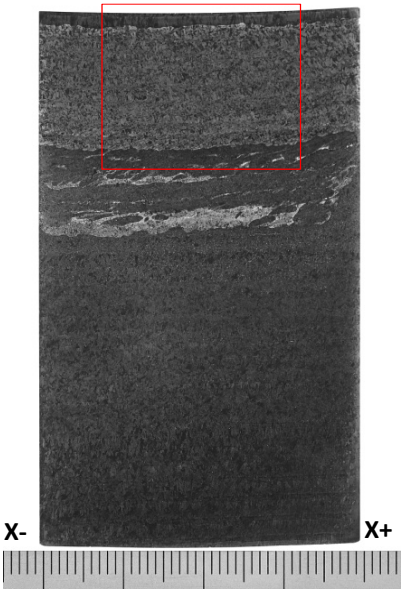

Cross section (after etching)

Crack information

Cross section Y (mm)		3.0
Max. crack depth info Z (mm)		67.8
Crack opening (μ m)		15
Typical crack information	①	X= 216.7 Z= 68.2
	②	X= 216.7 Z= 68.1
	③	X= 229.3 Z= 67.8
	④	X= 234.9 Z= 67.9
	⑤	X= 234.9 Z= 68.2

Z = 68.2 - d

Fig. A-2.2 Detailed crack information at Y=3 section in P16 (JRV-S2)

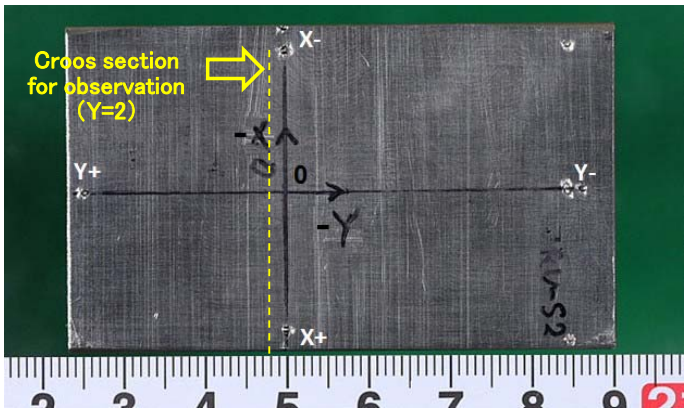

O point :
X=228.6, Y=0

Position of cross section for observation (Y=2)

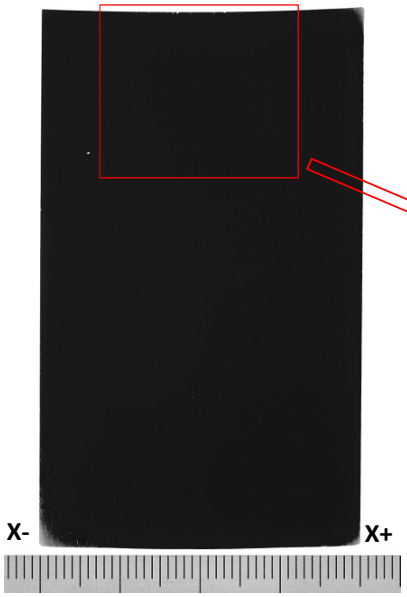

Cross section (before etching)

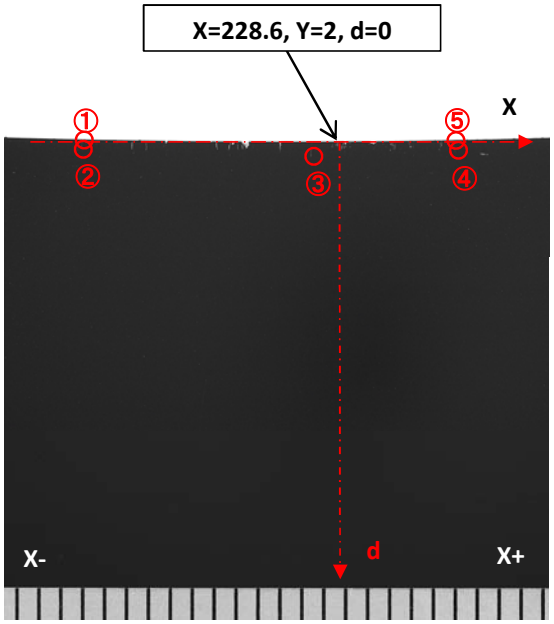

Enlarged cross section (before etching)

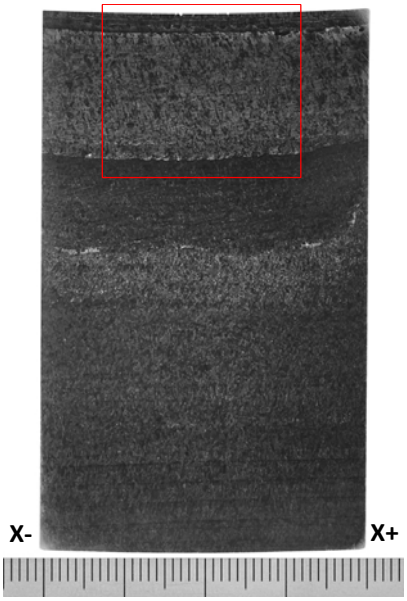

Cross section (after etching)

Crack information

Cross section Y (mm)		2.0
Max. crack depth info Z (mm)		67.4
Crack opening (μ m)		4
Typical crack information	①	X= 214.5 Z= 68.2
	②	X= 214.2 Z= 67.7
	③	X= 226.9 Z= 67.4
	④	X= 233.9 Z= 68.1
	⑤	X= 233.9 Z= 68.2

Z = 68.2 - d

Fig. A-2.3 Detailed crack information at Y=2 section in P16 (JRV-S2)

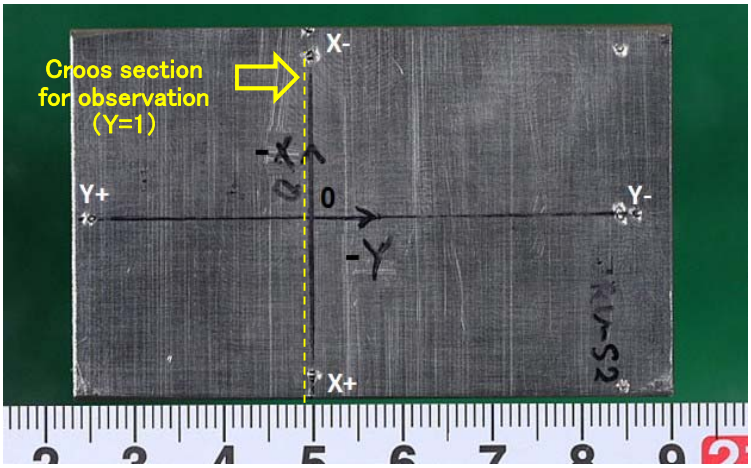

O point :
X=228.6, Y=0

Position of cross section for observation (Y=1)

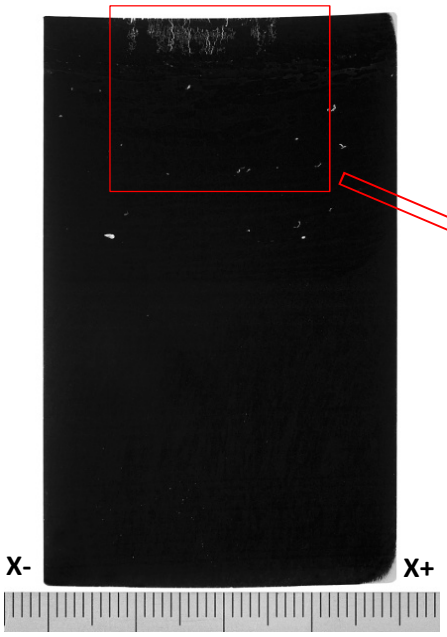

Cross section (before etching)

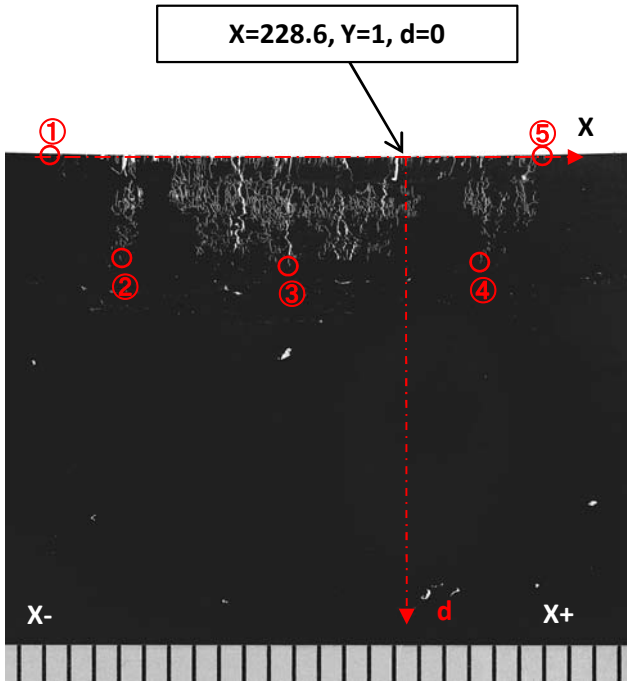

Enlarged cross section (before etching)

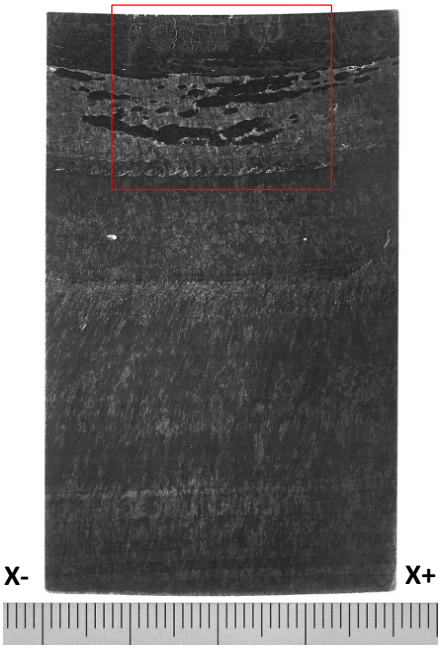

Cross section (after etching)

Crack information

Cross section Y (mm)		1.0	
Max. crack depth info Z (mm)		63.6	
Crack opening (μ m)		5	
Typical crack information	①	X= 211.7	Z= 68.2
	②	X= 215.1	Z= 63.8
	③	X= 223.1	Z= 63.6
	④	X= 232.1	Z= 63.7
	⑤	X= 235.1	Z= 68.2

Z = 68.2 - d

Fig. A-2.4 Detailed crack information at Y=1 section in P16 (JRV-S2)

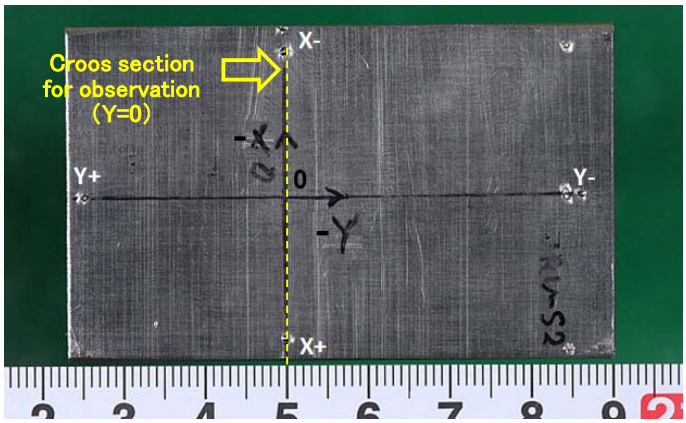

O point :
X=228.6, Y=0

Position of cross section for observation (Y=0)

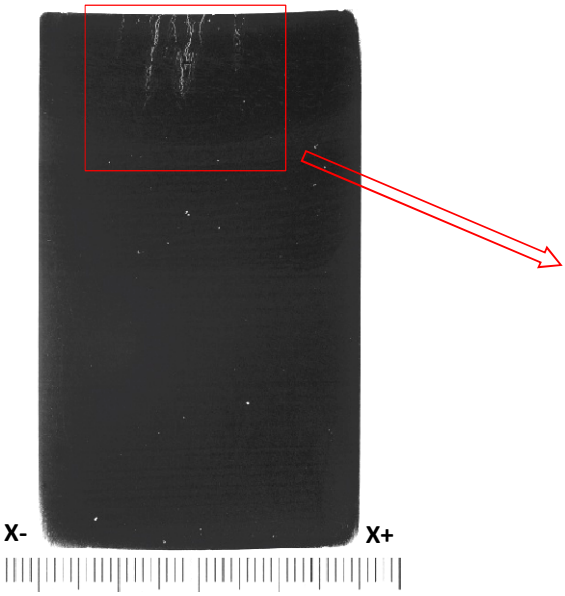

Cross section (before etching)

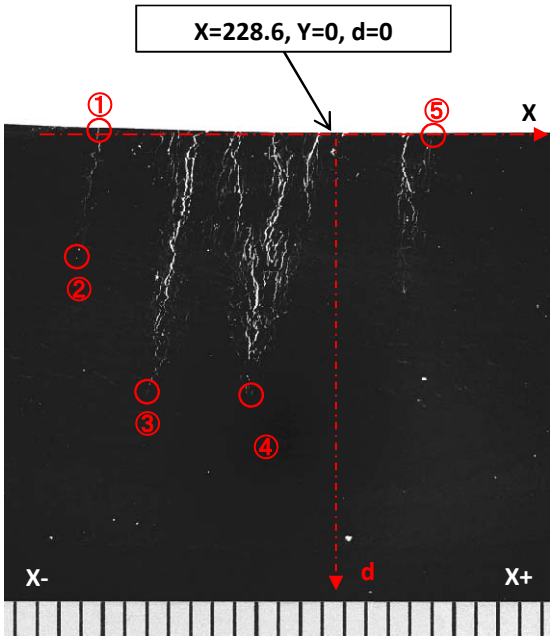

Enlarged cross section (before etching)

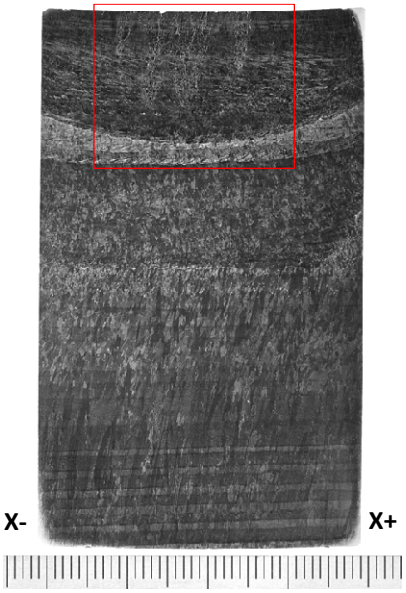

Cross section (after etching)

Crack information

Cross section Y (mm)		0.0
Max. crack depth info Z (mm)		56.1
Crack opening (μ m)		11
Typical crack information	①	X= 215.6 Z= 68.2
	②	X= 214.6 Z= 62.7
	③	X= 218.7 Z= 56.4
	④	X= 224.2 Z= 56.1
	⑤	X= 233.7 Z= 68.2

Z = 68.2 - d

Fig. A-2.5 Detailed crack information at Y=0 section in P16 (JRV-S2)

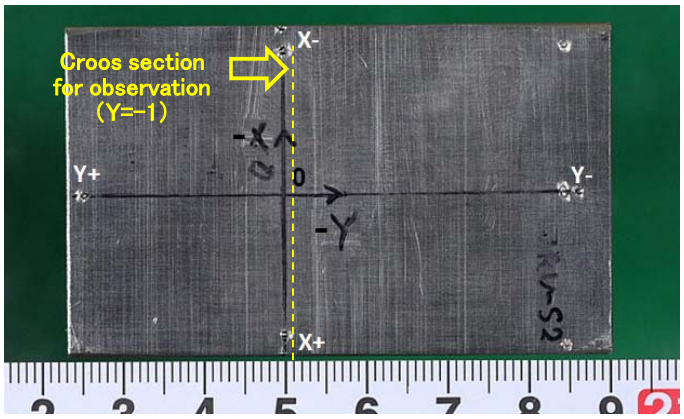

O point :
X=228.6, Y=0

Position of cross section for observation (Y=

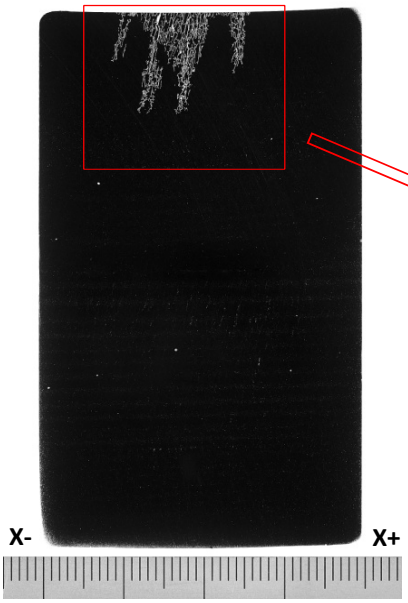

Cross section (before etching)

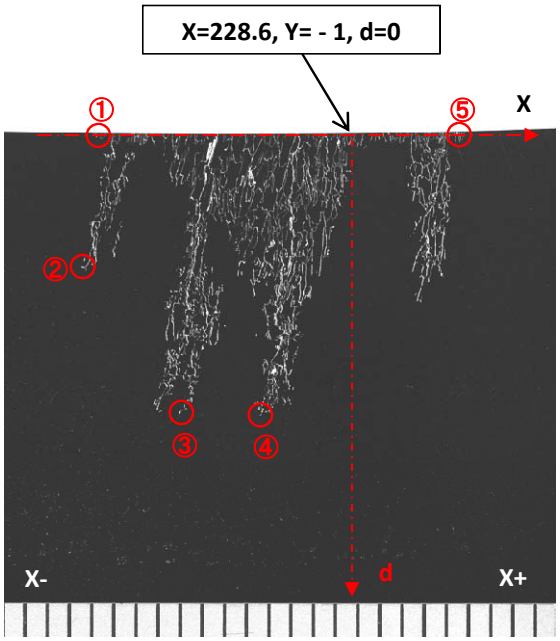

Enlarged cross section (before etching)

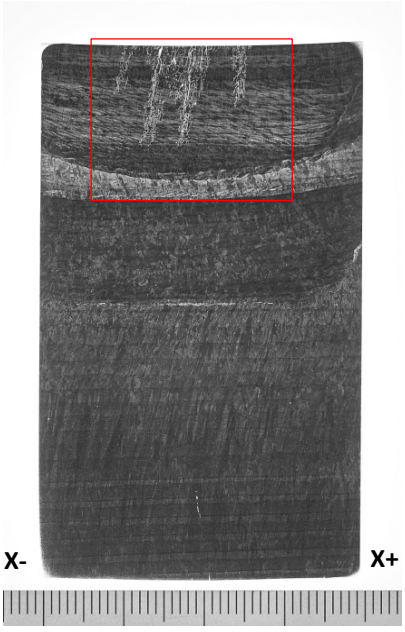

Cross section (after etching)

Crack information

Cross section Y (mm)		-1.0
Max. crack depth info Z (mm)		55.2
Crack opening (μ m)		30
Typical crack information	①	X= 214.5 Z= 68.2
	②	X= 213.9 Z= 62.0
	③	X= 219.2 Z= 55.3
	④	X= 223.5 Z= 55.2
	⑤	X= 234.4 Z= 68.2

Z = 68.2 - d

Fig. A-2.6 Detailed crack information at Y= - 1 section in P16 (JRV-S2)

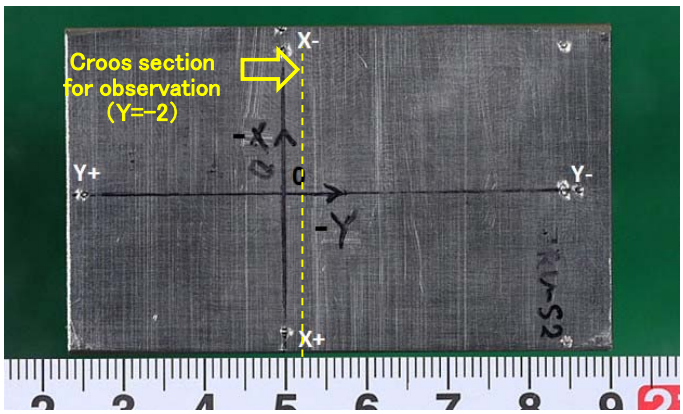

O point :
X=228.6, Y=0

Position of cross section for observation (Y= -

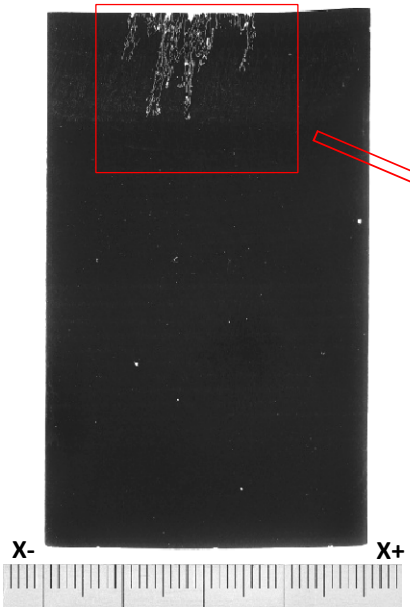

Cross section (before etching)

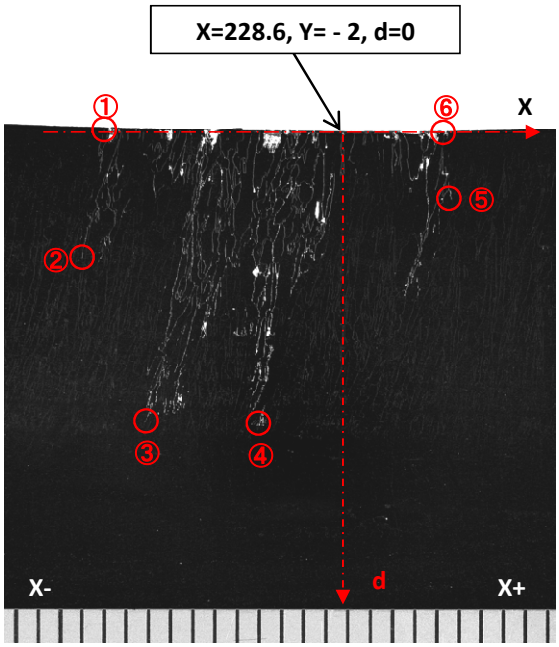

Enlarged cross section (before etching)

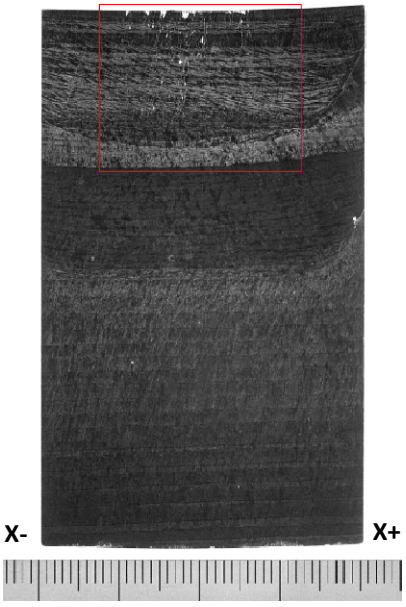

Cross section (after etching)

Crack information

Cross section Y (mm)		-2.0
Max. crack depth info Z (mm)		54.7
Crack opening (μ m)		5.0
Typical crack information	①	X= 215.7 Z= 68.2
	②	X= 214.5 Z= 62.3
	③	X= 218.0 Z= 54.8
	④	X= 224.1 Z= 54.7
	⑤	X= 234.3 Z= 65.2
	⑥	X= 233.9 Z= 68.2

Z = 68.2 - d

Fig. A-2.7 Detailed crack information at Y= - 2 section in P16 (JRV-S2)

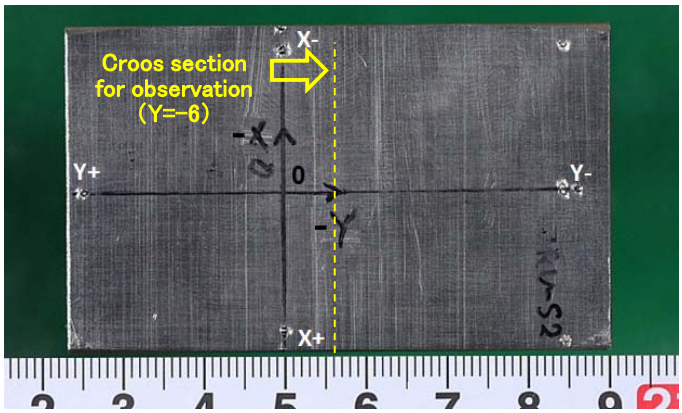

O point :
X=228.6, Y=0

Position of cross section for observation (Y= -

Cross section (before etching)

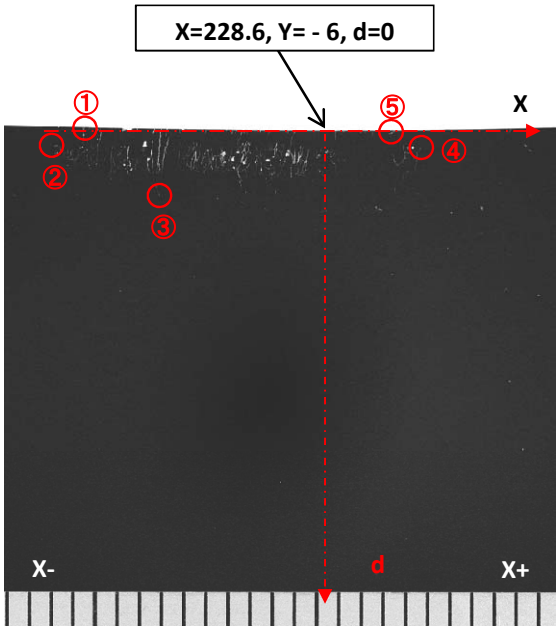

Enlarged cross section (before etching)

Cross section (after etching)

Crack information

Cross section Y (mm)		-6.0
Max. crack depth info Z (mm)		65.1
Crack opening (μ m)		22.0
Typical crack information	①	X= 215.7 Z= 68.2
	②	X= 214.0 Z= 67.3
	③	X= 219.8 Z= 65.1
	④	X= 233.7 Z= 67.5
	⑤	X= 232.2 Z= 68.2

Z = 68.2 - d

Fig. A-2.8 Detailed crack information at Y= - 6 section in P16 (JRV-S2)

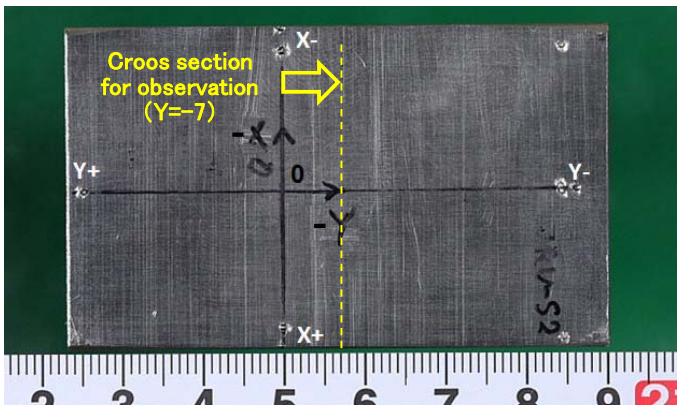

O point :
X=228.6, Y=0

Position of cross section for observation (Y= - 7)

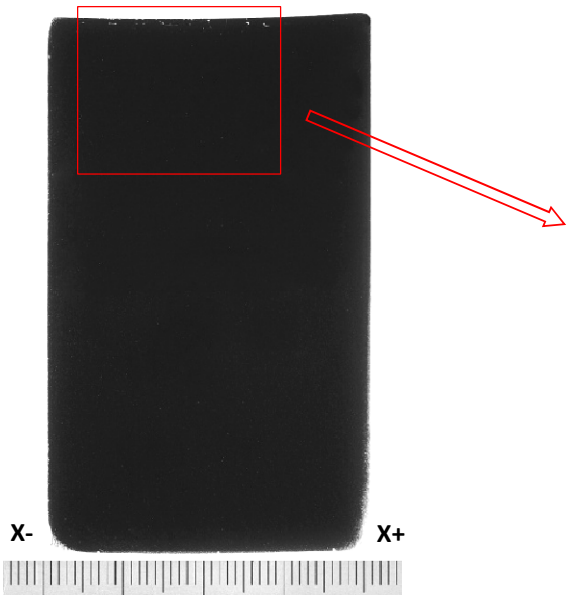

Cross section (before etching)

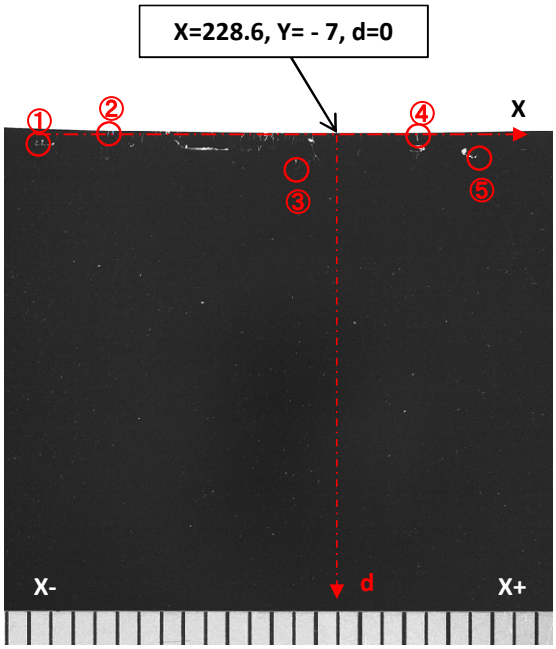

Enlarged cross section (before etching)

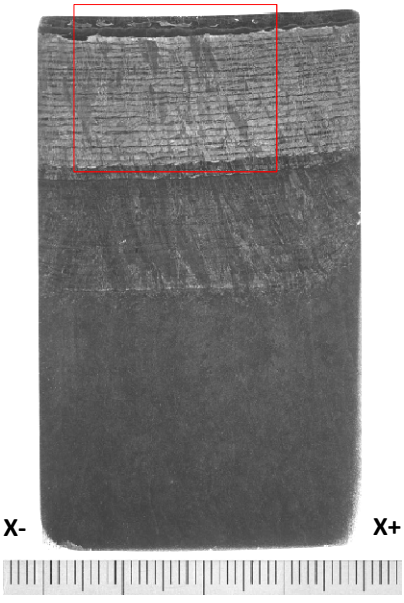

Cross section (after etching)

Crack information

Cross section Y (mm)		−7.0
Max. crack depth info Z (mm)		66.5
Crack opening (μ m)		<1
Typical crack information	①	X= 212.3 Z= 67.5
	②	X= 216.3 Z= 68.2
	③	X= 226.4 Z= 66.5
	④	X= 232.8 Z= 68.2
	⑤	X= 236.1 Z= 67.2

Z = 68.2 - d

Fig. A-2.9 Detailed crack information at Y= - 7 section in P16 (JRV-S2)

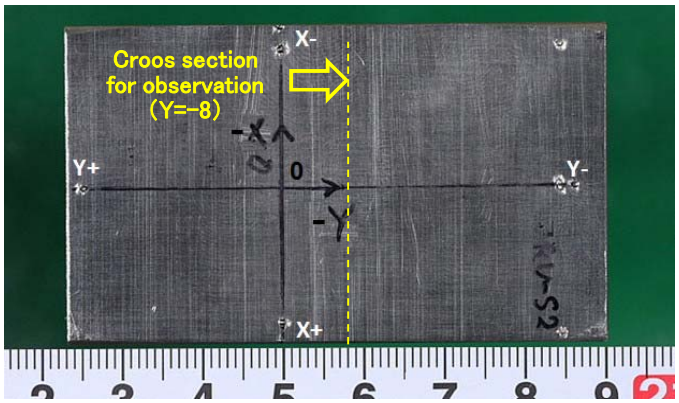

O point :
X=228.6, Y=0

Position of cross section for observation (Y= - 8)

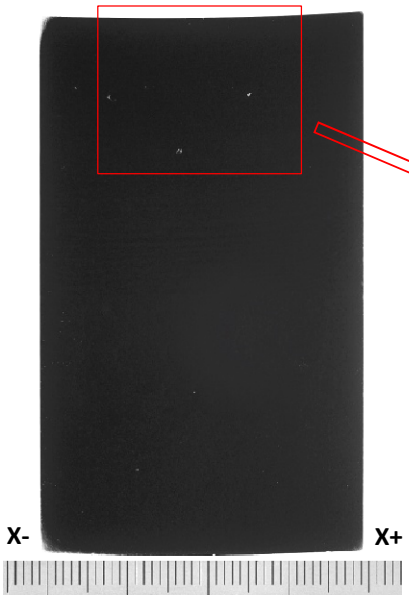

Cross section (before etching)

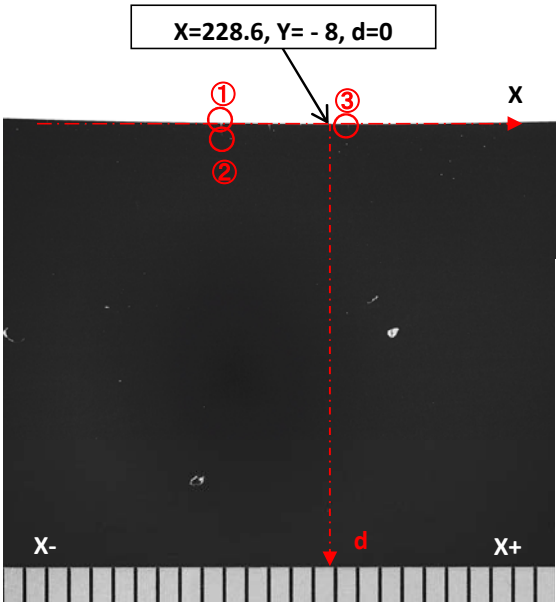

Enlarged cross section (before etching)

Cross section (after etching)

Crack information

Cross section Y (mm)		-8.0
Max. crack depth info Z (mm)		67.6
Crack opening (μ m)		<1
Typical crack information	①	X= 224.9 Z= 68.2
	②	X= 224.9 Z= 67.6
	③	X= 231.9 Z= 68.2

Z = 68.2 - d

Fig. A-2.10 Detailed crack information at Y= - 8 section in P16 (JRV-S2)

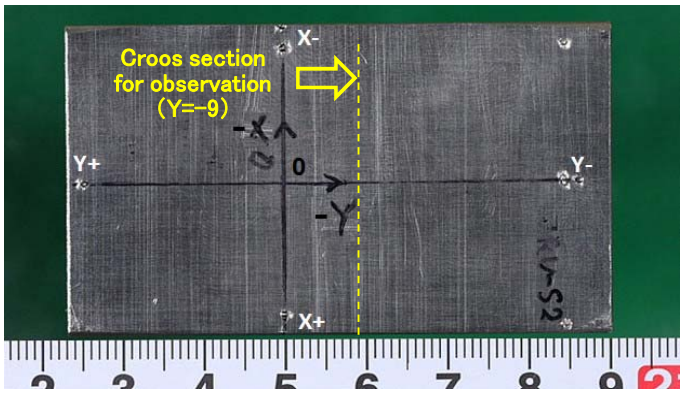

O point :
X=228.6, Y=0

Position of cross section for observation (Y= - 9)

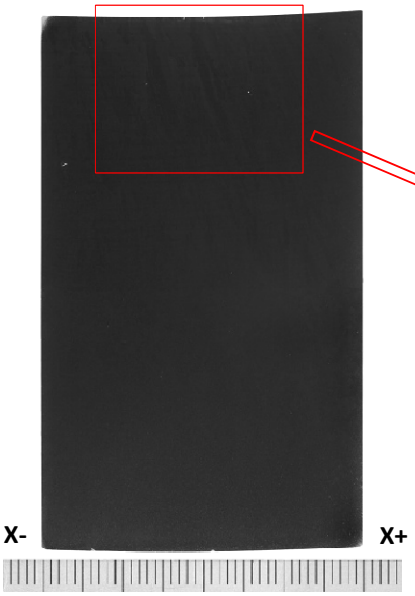

Cross section (before etching)

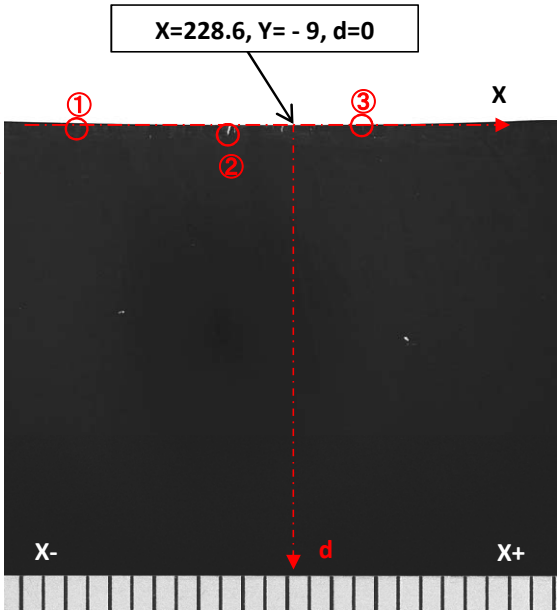

Enlarged cross section (before etching)

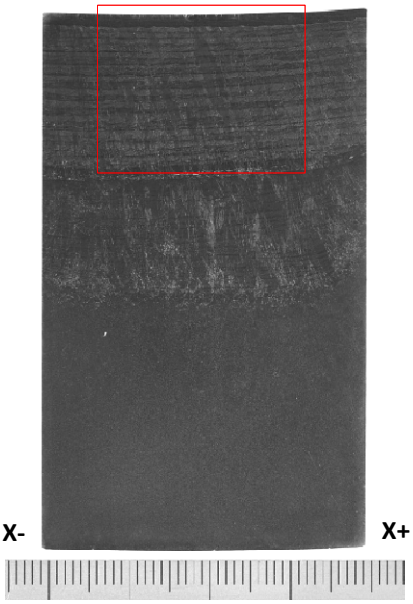

Cross section (after etching)

Crack information

Cross section Y (mm)		-9.0
Max. crack depth info Z (mm)		67.8
Crack opening (μ m)		24.0
Typical crack information	①	X= 217.2 Z= 68.2
	②	X= 224.6 Z= 67.8
	③	X= 231.8 Z= 68.2

Z = 68.2 - d

Fig. A-2.11 Detailed crack information at Y= - 9 section in P16 (JRV-S2)

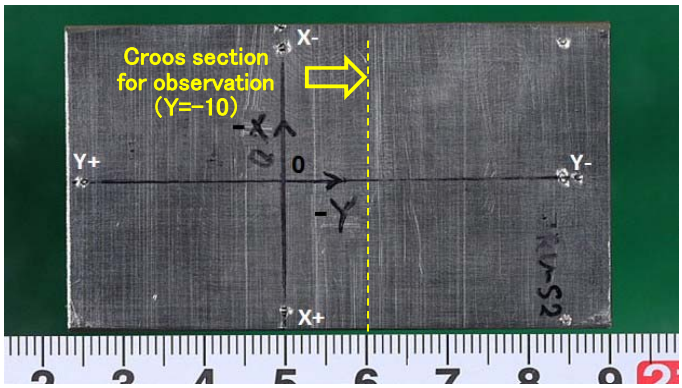

O point :
X=228.6, Y=0

Position of cross section for observation (Y= - 10)

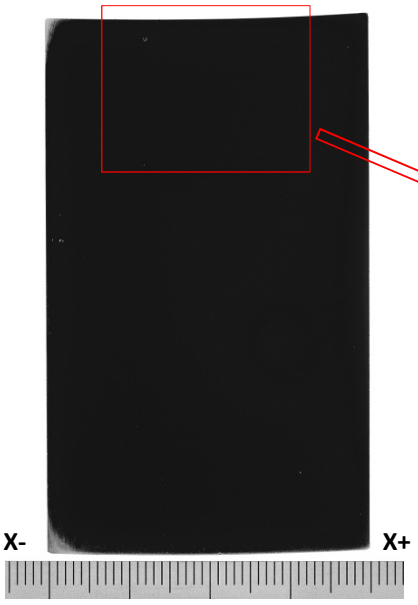

Cross section (before etching)

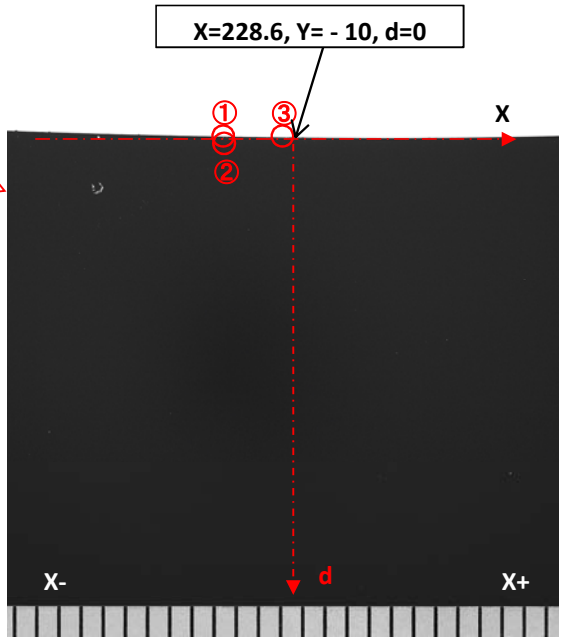

Enlarged cross section (before etching)

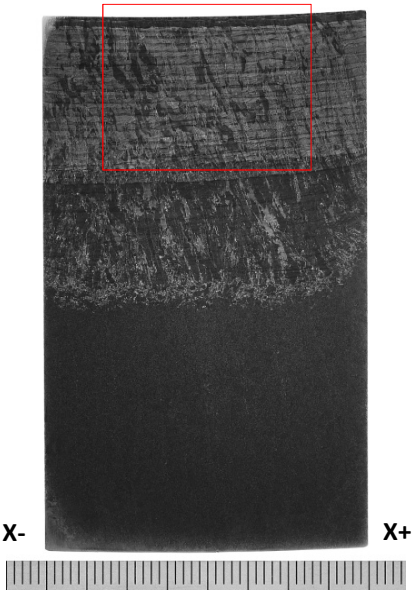

Cross section (after etching)

Crack information

Cross section Y (mm)		-10.0
Max. crack depth info Z (mm)		68.1
Crack opening (μ m)		3.0
Typical crack information	①	X= 224.8 Z= 68.2
	②	X= 224.8 Z= 68.1
	③	X= 228.2 Z= 68.2

Z = 68.2 - d

Fig. A-2.12 Detailed crack information at Y= - 10 section in P16 (JRV-S2)

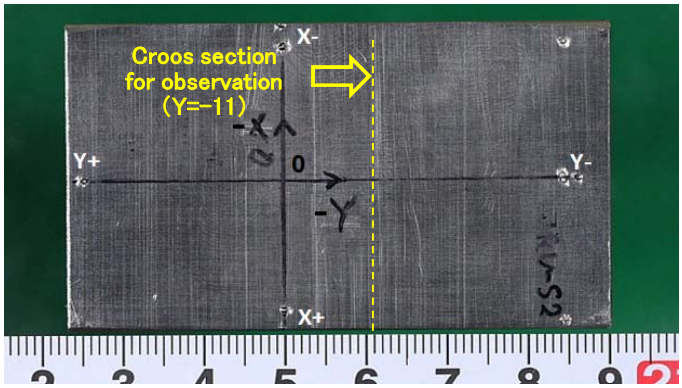

O point :
X=228.6, Y=0

Position of cross section for observation (Y= - 11)

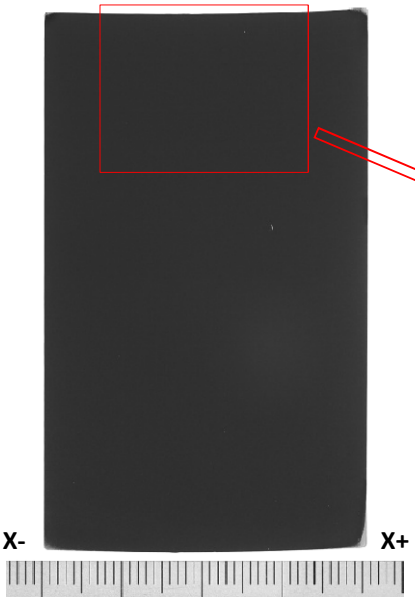

Cross section (before etching)

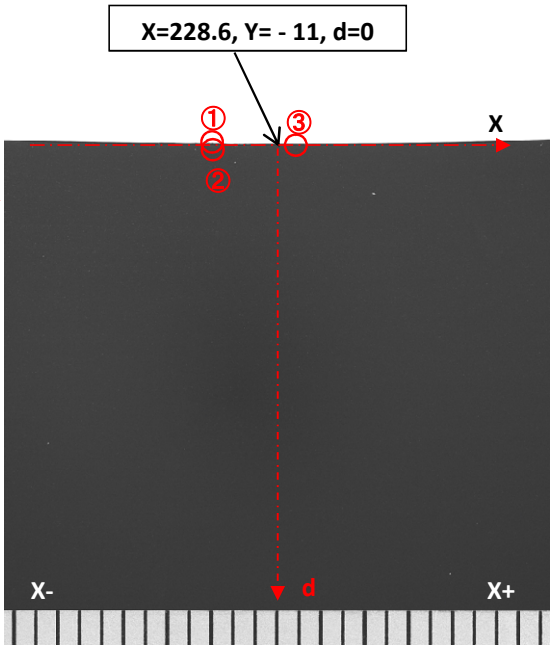

Enlarged cross section (before etching)

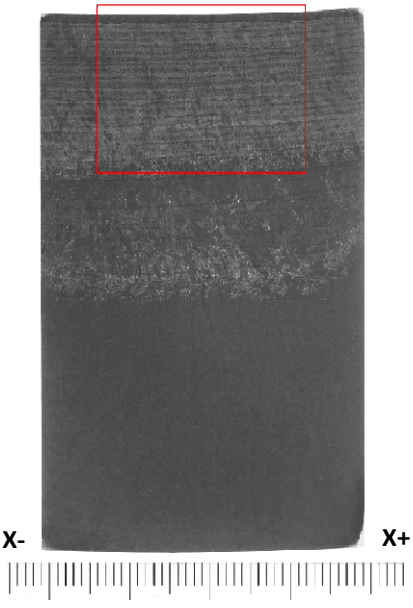

Cross section (after etching)

Crack information

Cross section Y (mm)		−11.0
Max. crack depth info Z (mm)		68.0
Crack opening (μ m)		2.0
Typical crack information	①	X= 224.6 Z= 68.2
	②	X= 224.6 Z= 68.0
	③	X= 229.2 Z= 68.2

Z = 68.2 - d

Fig. A-2.13 Detailed crack information at Y= - 11 section in P16 (JRV-S2)

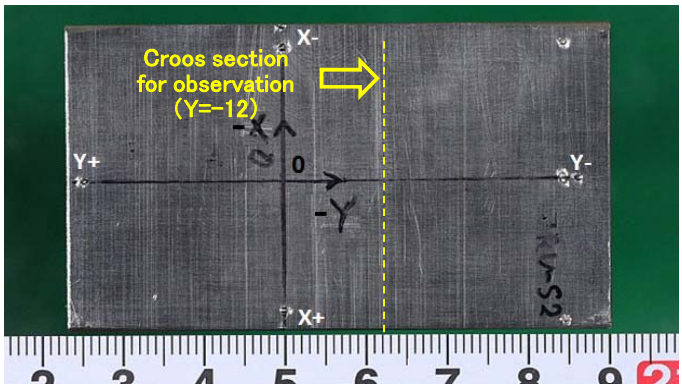

O point :
X=228.6, Y=0

Position of cross section for observation (Y= - 12)

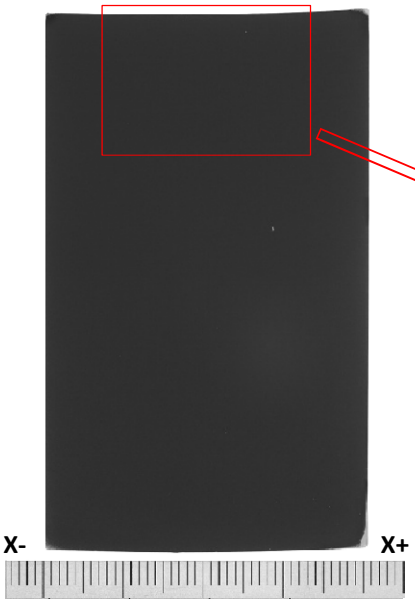

Cross section (before etching)

X=228.6, Y= - 12, d=0

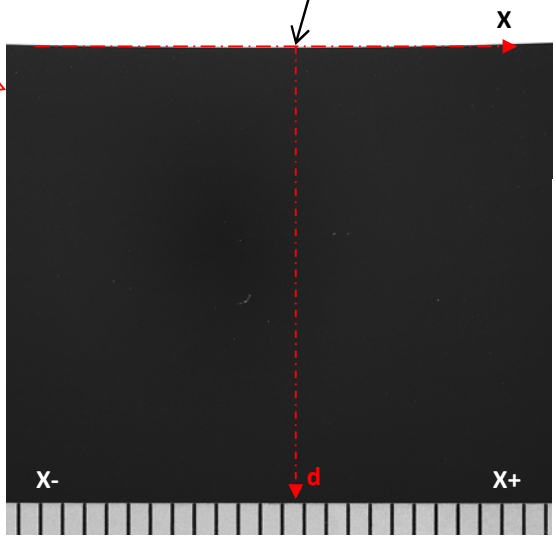

Enlarged cross section (before etching)

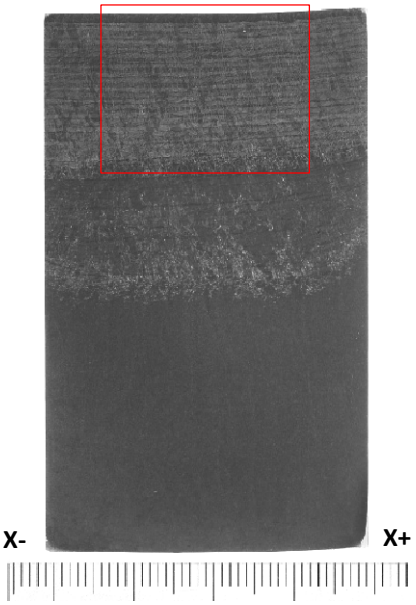

Cross section (after etching)

Crack information

Cross section Y (mm)	−12.0
Max. crack depth info Z (mm)	No crack
Crack opening (μ m)	No crack
Typical crack information	No crack

Fig. A-2.14 Detailed crack information at Y= - 12 section in P16 (JRV-S2)

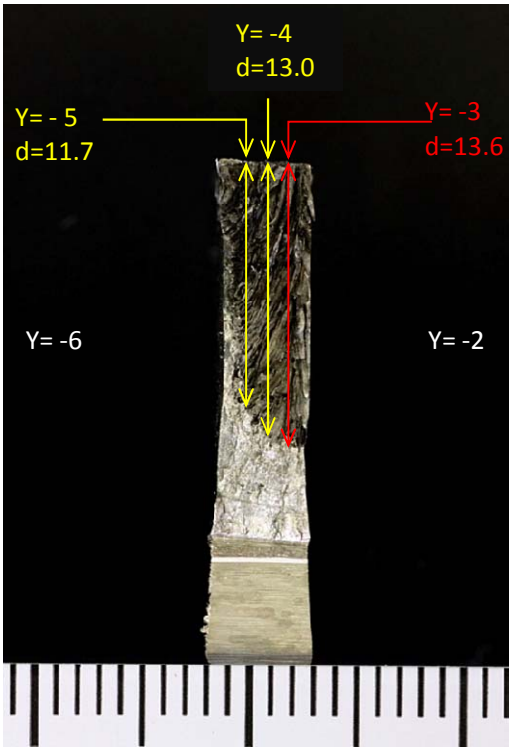

Y= - 2 to Y= - 6 fracture surface

Fig. A-2.15 Detailed crack information at Y= - 2 to - 6 fracture surface in P16 (JRV-S2)

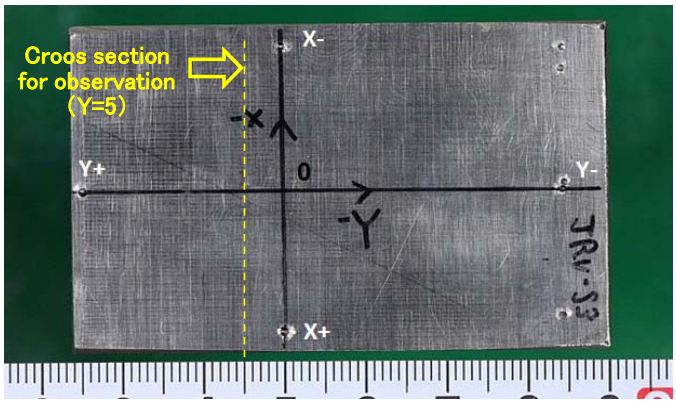

O point :
X=228.6, Y=0

Position of cross section for observation (Y=5)

Cross section (before

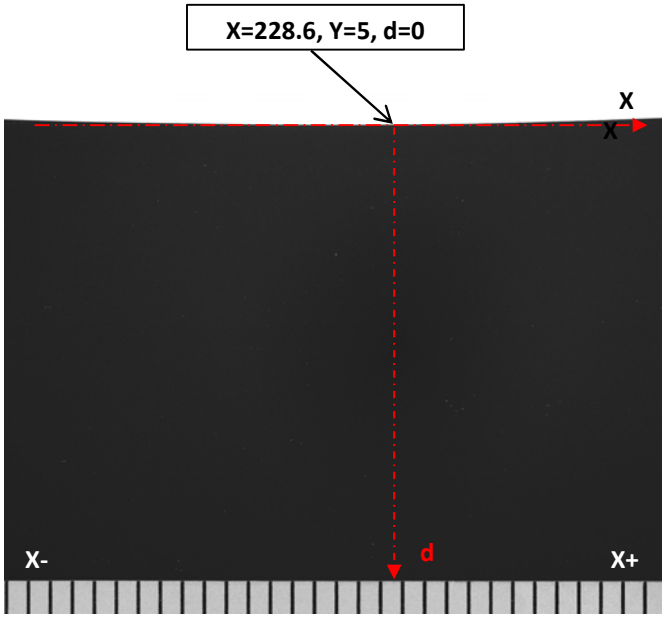

Enlarged cross section (before etching)

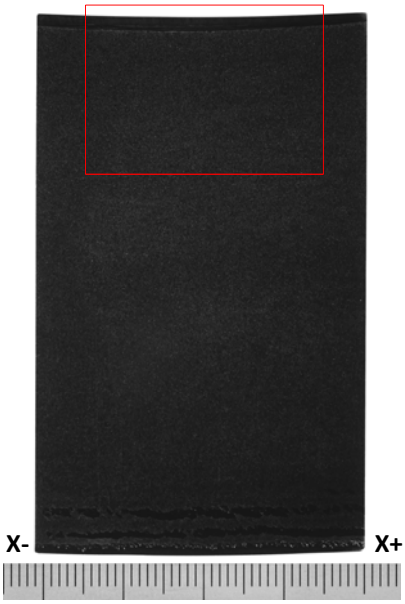

Cross section (after etching)

Crack information

Cross section Y (mm)	5.0
Max. crack depth info Z (mm)	No crack
Crack opening (μ m)	No crack
Typical crack information	No crack

Z = 68.2 - d

Fig. A-3.1 Detailed crack information at Y=5 section in P17 (JRV-S3)

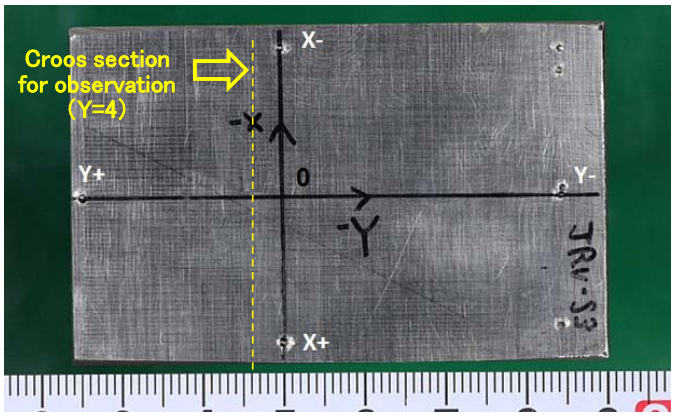

O point :
X=228.6, Y=0

Position of cross section for observation (Y=4)

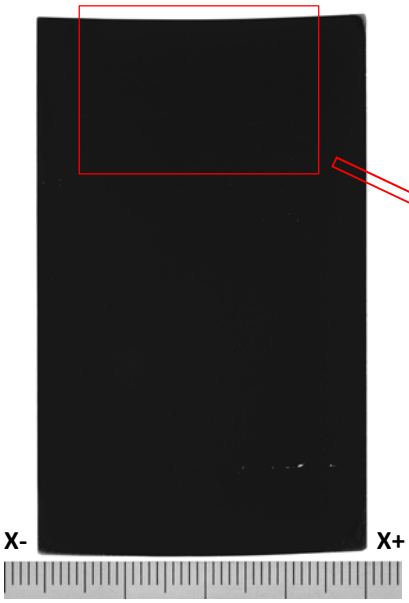

Cross section (before etching)

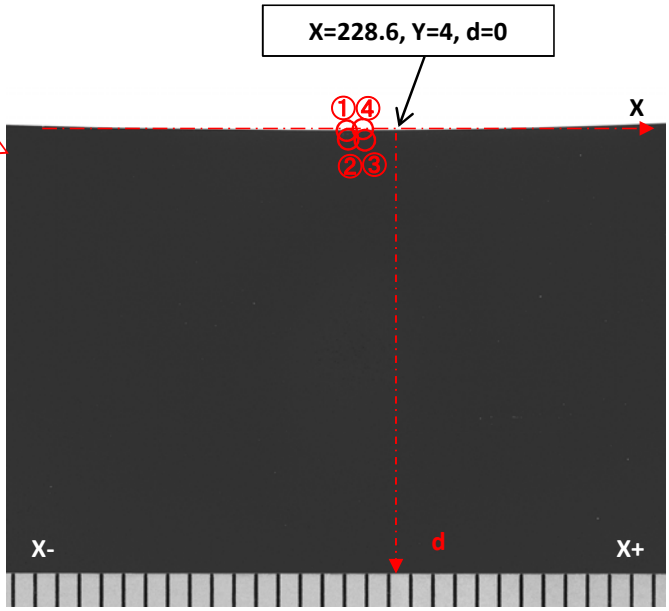

Enlarged cross section (before etching)

Cross section (after etching)

Crack information

Cross section Y (mm)		4.0
Max. crack depth info Z (mm)		67.9
Crack opening (μ m)		<1
Typical crack information	①	X= 225.7 Z= 68.2
	②	X= 225.8 Z= 67.9
	③	X= 226.4 Z= 68.0
	④	X= 226.3 Z= 68.2

Z = 68.2 - d

Fig. A-3.2 Detailed crack information at Y=4 section in P17 (JRV-S3)

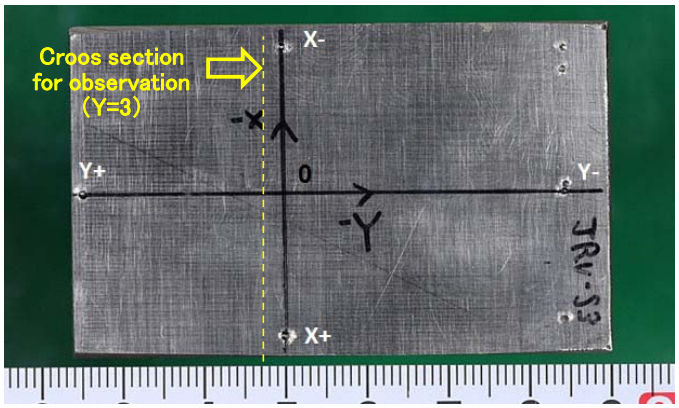

O point :
X=228.6, Y=0

Position of cross section for observation (Y=3)

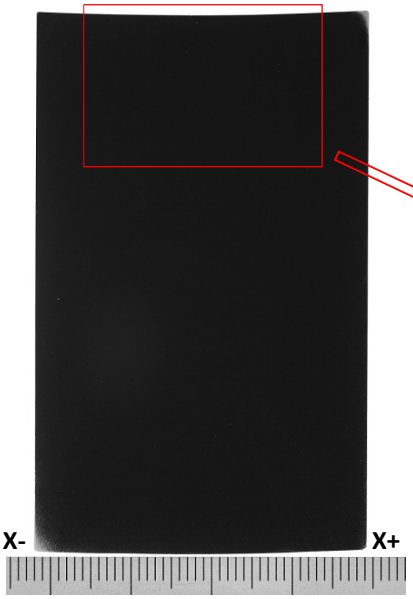

Cross section (before etching)

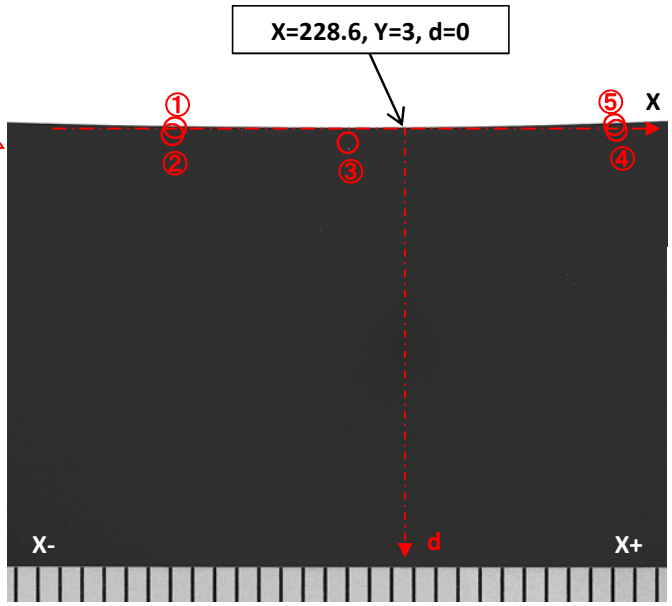

Enlarged cross section (before etching)

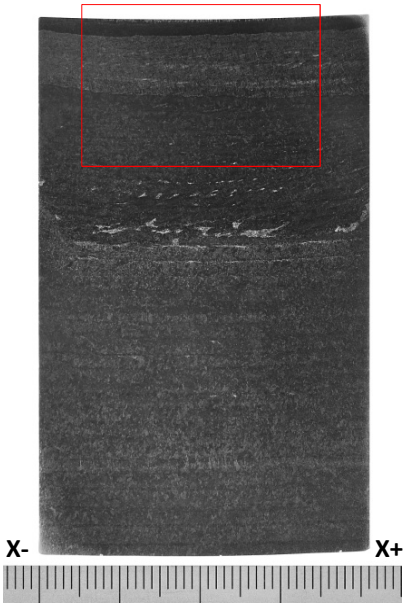

Cross section (after etching)

Crack information

Cross section Y (mm)		3.0
Max. crack depth info Z (mm)		67.8
Crack opening (μ m)		<1
Typical crack information	①	X= 216.3 Z= 68.2
	②	X= 216.1 Z= 68.2
	③	X= 225.4 Z= 67.8
	④	X= 239.8 Z= 68.1
	⑤	X= 239.8 Z= 68.2

Z = 68.2 - d

Fig. A-3.3 Detailed crack information at Y=3 section in P17 (JRV-S3)

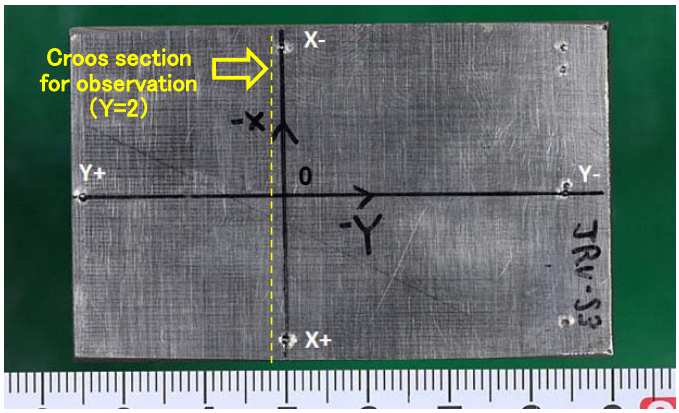

O point :
X=228.6, Y=0

Position of cross section for observation (Y=2)

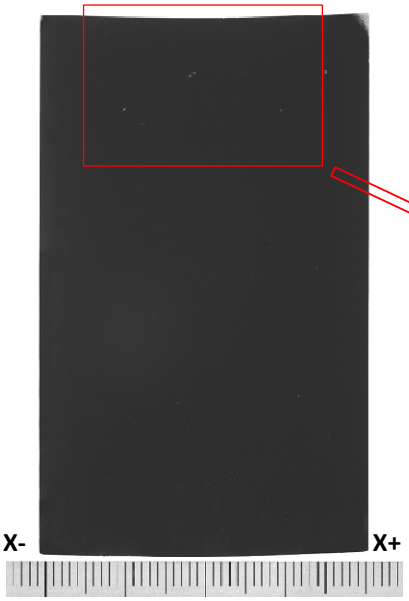

Cross section (before etching)

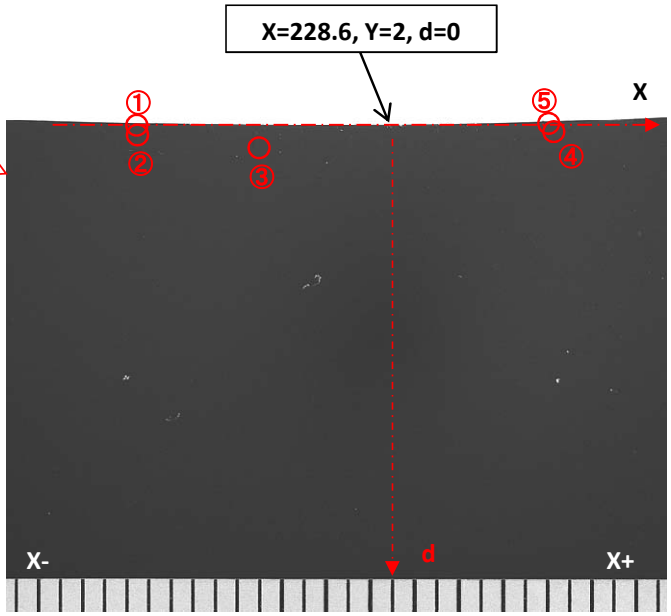

Enlarged cross section (before etching)

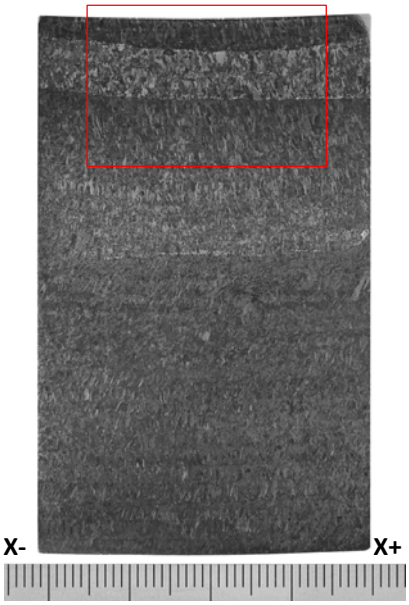

Cross section (after etching)

Crack information

Cross section Y (mm)		2.0
Max. crack depth info Z (mm)		67.2
Crack opening (μ m)		<1
Typical crack information	①	X= 214.6 Z= 68.2
	②	X= 214.5 Z= 68.2
	③	X= 221.3 Z= 67.2
	④	X= 237.2 Z= 68.2
	⑤	X= 237.1 Z= 68.2

Z = 68.2 - d

Fig. A-3.4 Detailed crack information at Y=2 section in P17 (JRV-S3)

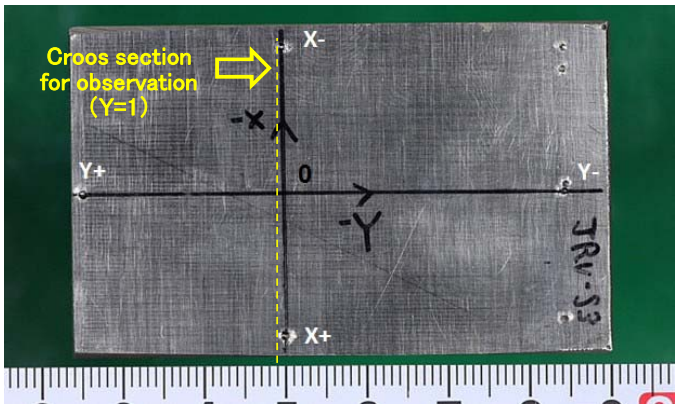

O point :
X=228.6, Y=0

Position of cross section for observation (Y=1)

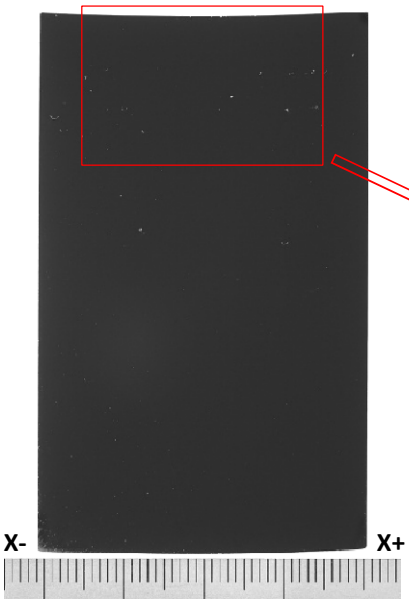

Cross section (before etching)

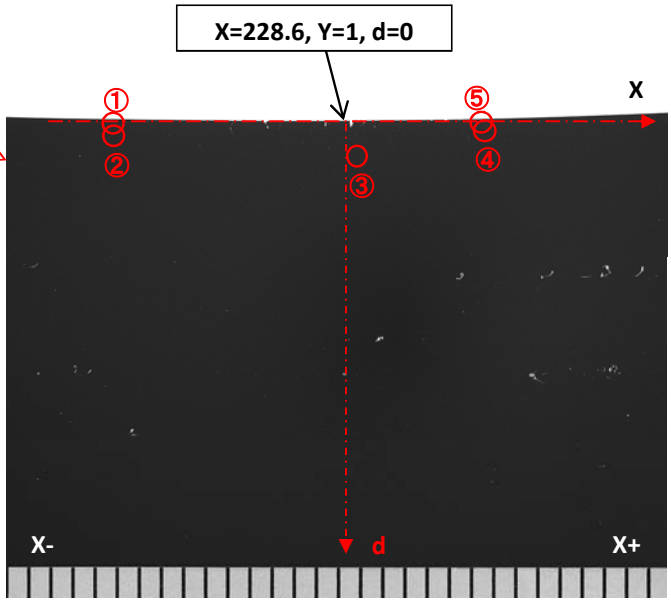

Enlarged cross section (before etching)

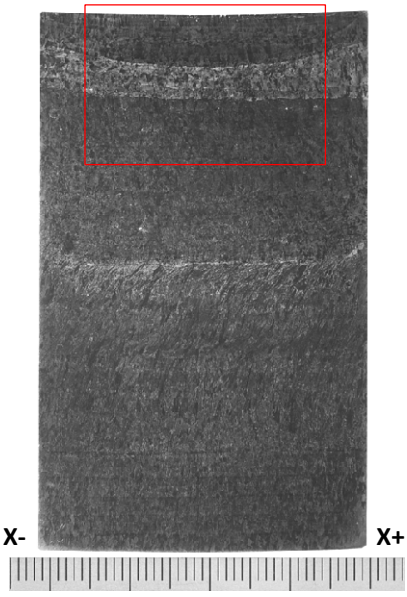

Cross section (after etching)

Crack information

Cross section Y (mm)		1.0
Max. crack depth info Z (mm)		66.8
Crack opening (μ m)		<1
Typical crack information	①	X= 215.7 Z= 68.2
	②	X= 215.7 Z= 68.2
	③	X= 229.1 Z= 66.8
	④	X= 235.9 Z= 68.1
	⑤	X= 235.9 Z= 68.2

Z = 68.2 - d

Fig. A-3.5 Detailed crack information at Y=1 section in P17 (JRV-S3)

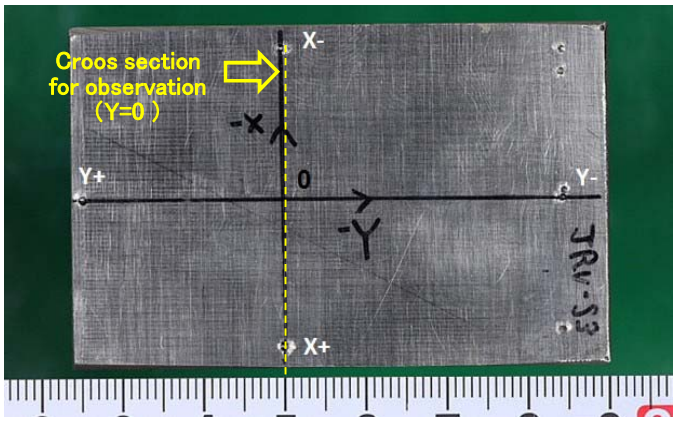

O point :
X=228.6, Y=0

Position of cross section for observation (Y=0)

Cross section (before etching)

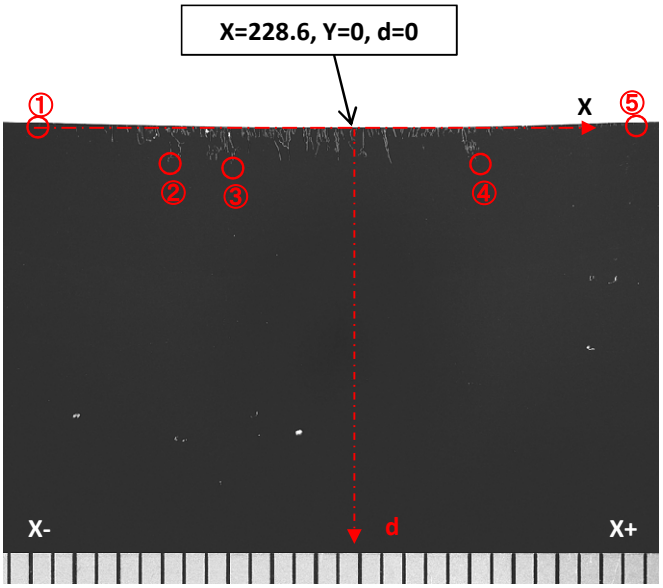

Enlarged cross section (before etching)

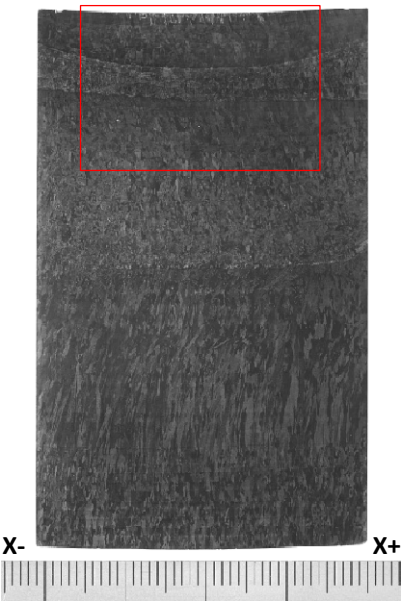

Cross section (after etching)

Crack information

Cross section Y (mm)		0.0
Max. crack depth info Z (mm)		66.4
Crack opening (μ m)		<1
Typical crack information	①	X= 211.5 Z= 68.2
	②	X= 218.5 Z= 66.5
	③	X= 221.9 Z= 66.4
	④	X= 235.2 Z= 66.7
	⑤	X= 244.0 Z= 68.2

Z = 68.2 - d

Fig. A-3.6 Detailed crack information at Y=0 section in P17 (JRV-S3)

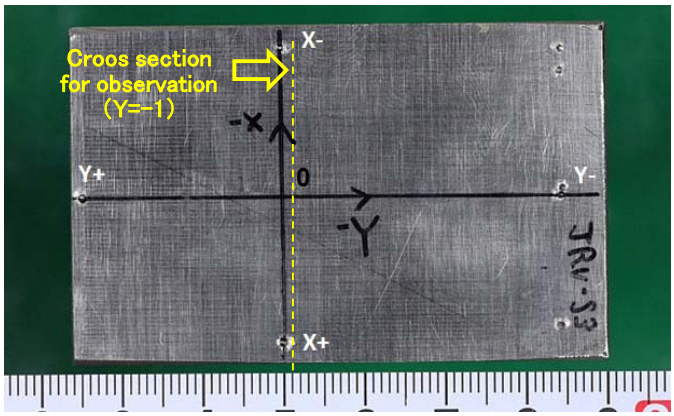

O point :
X=228.6, Y=0

Position of cross section for observation (Y= - 1)

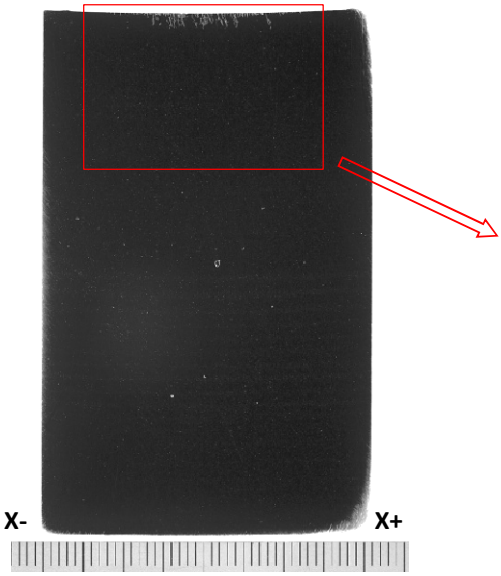

Cross section (before etching)

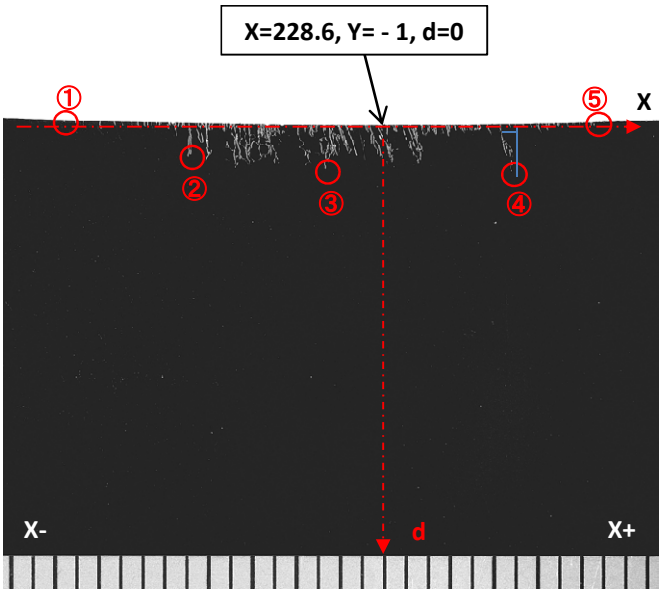

Enlarged cross section (before etching)

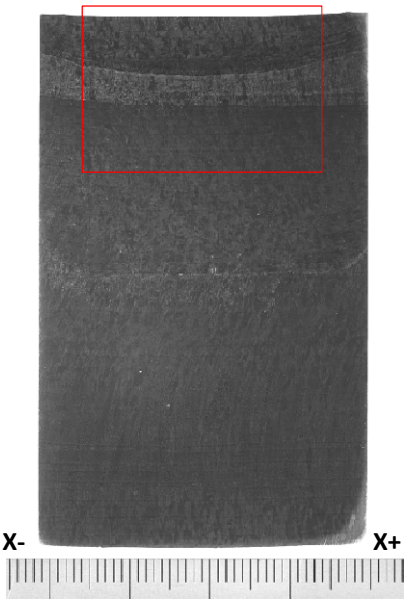

Cross section (after etching)

Crack information

Cross section Y (mm)		−1.0
Max. crack depth info Z (mm)		66.0
Crack opening (μ m)		<1
Typical crack information	①	X= 211.2 Z= 68.2
	②	X= 218.0 Z= 66.6
	③	X= 225.4 Z= 66.1
	④	X= 235.4 Z= 66.0
	⑤	X= 239.9 Z= 68.2

Z = 68.2 - d

Fig. A-3.7 Detailed crack information at Y= - 1 section in P17 (JRV-S3)

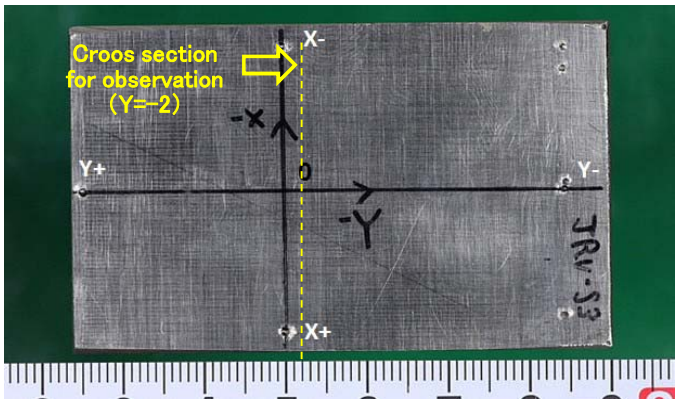

O point :
X=228.6, Y=0

Position of cross section for observation (Y= - 2)

Cross section (before etching)

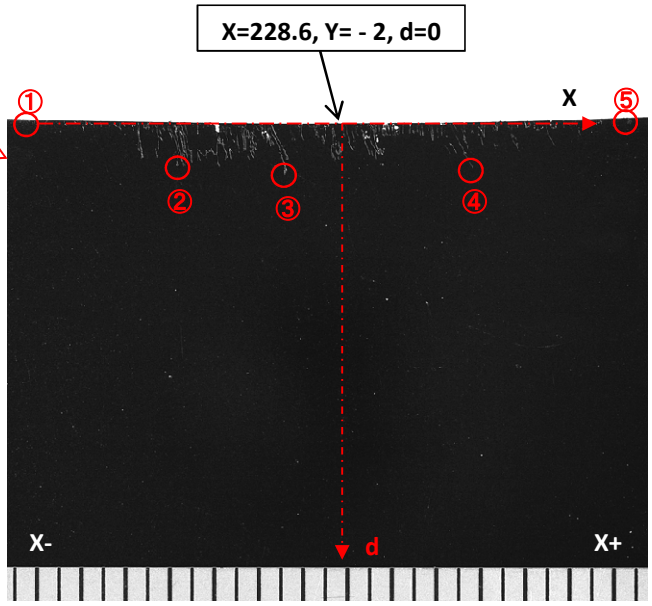

Enlarged cross section (before etching)

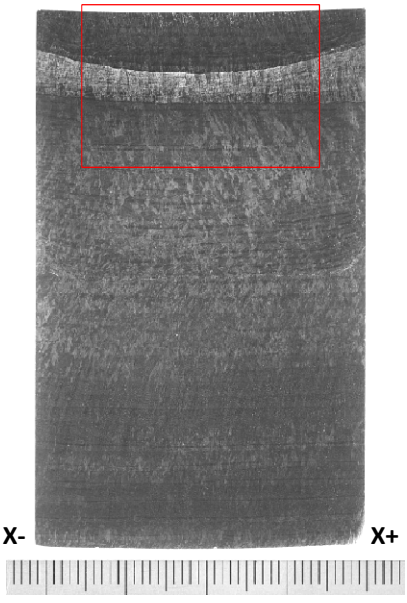

Cross section (after etching)

Crack information

Cross section Y (mm)		−2.0
Max. crack depth info Z (mm)		65.8
Crack opening (μ m)		<1
Typical crack information	①	X= 212.9 Z= 68.2
	②	X= 220.0 Z= 66.1
	③	X= 225.7 Z= 65.8
	④	X= 235.7 Z= 66.1
	⑤	X= 244.1 Z= 68.2

Z = 68.2 - d

Fig. A-3.8 Detailed crack information at Y= - 2 section in P17 (JRV-S3)

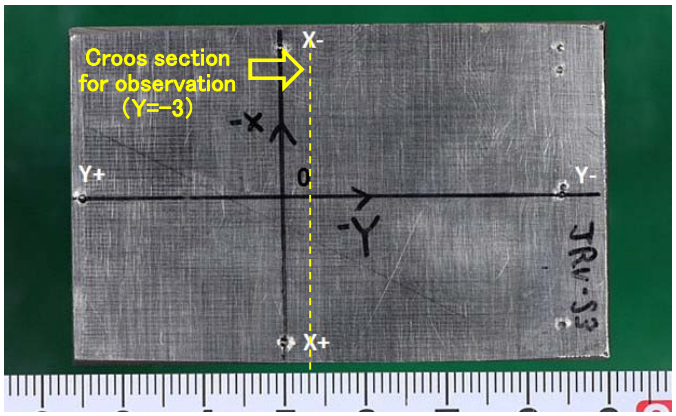

O point :
X=228.6, Y=0

Position of cross section for observation (Y= - 3)

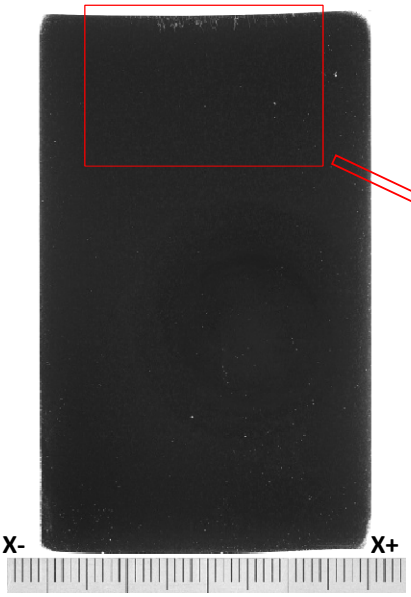

Cross section (before etching)

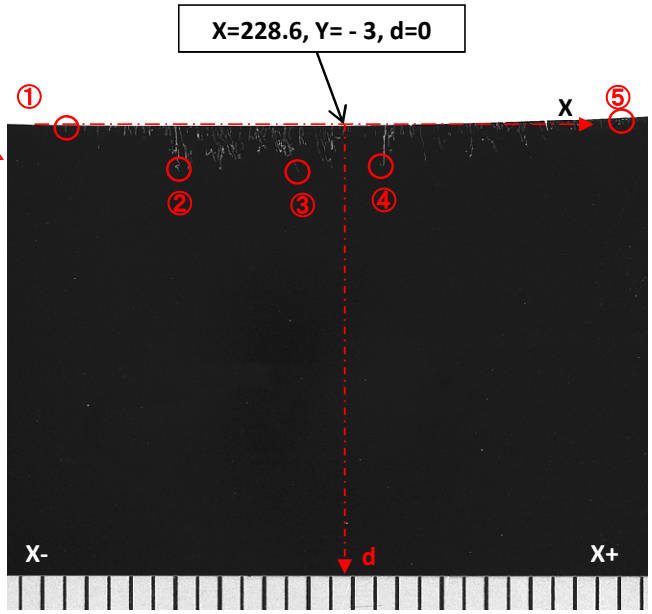

Enlarged cross section (before etching)

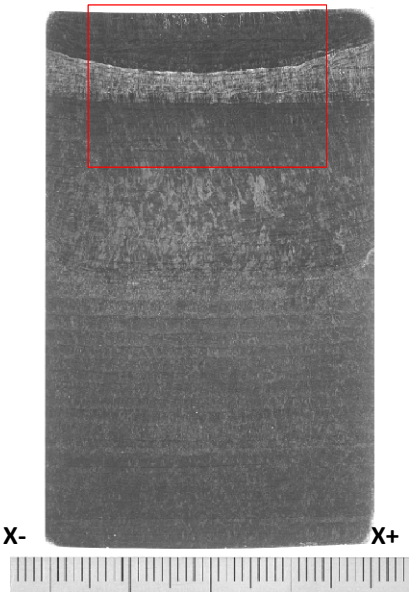

Cross section (after etching)

Crack information

Cross section Y (mm)		-3.0
Max. crack depth info Z (mm)		66.0
Crack opening (μ m)		<1
Typical crack information	①	X= 213.7 Z= 68.2
	②	X= 219.7 Z= 66.1
	③	X= 226.1 Z= 66.0
	④	X= 230.5 Z= 66.3
	⑤	X= 243.6 Z= 68.2

Z = 68.2 - d

Fig. A-3.9 Detailed crack information at Y= - 3 section in P17 (JRV-S3)

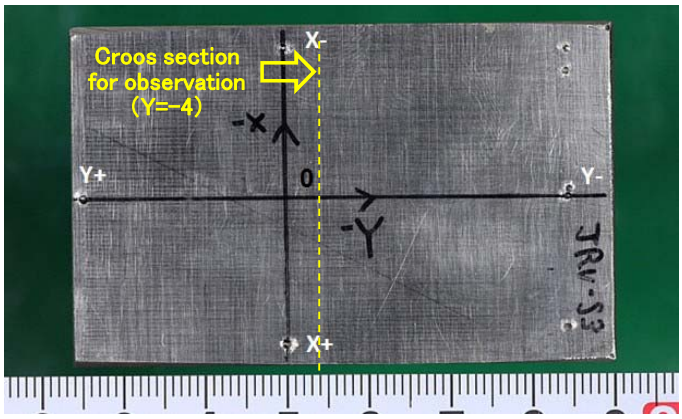

O point :
X=228.6, Y=0

Position of cross section for observation (Y= - 4)

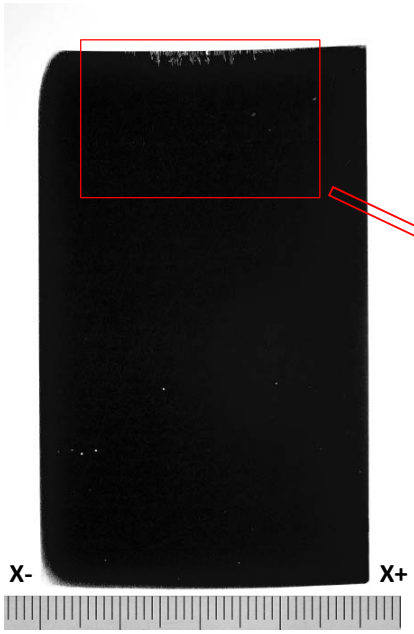

Cross section (before etching)

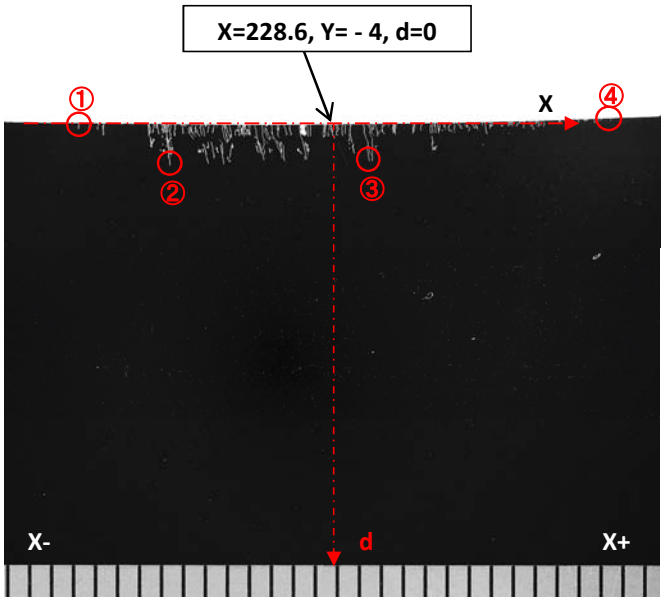

Enlarged cross section (before etching)

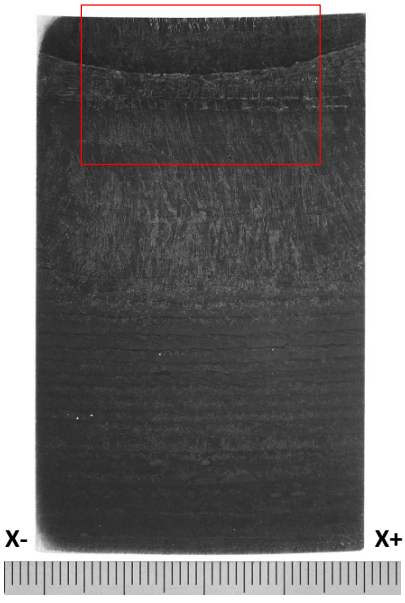

Cross section (after etching)

Crack information

Cross section Y (mm)		-4.0
Max. crack depth info Z (mm)		66.2
Crack opening (μ m)		<1
Typical crack information	①	X= 214.9 Z= 68.2
	②	X= 219.8 Z= 66.2
	③	X= 230.7 Z= 66.4
	④	X= 243.6 Z= 68.5

Z = 68.2 - d

Fig. A-3.10 Detailed crack information at Y= - 4 section in P17 (JRV-S3)

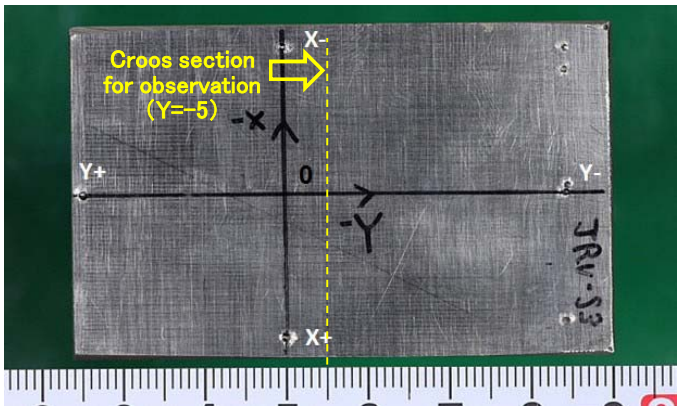

O point :
X=228.6, Y=0

Position of cross section for observation (Y= - 5)

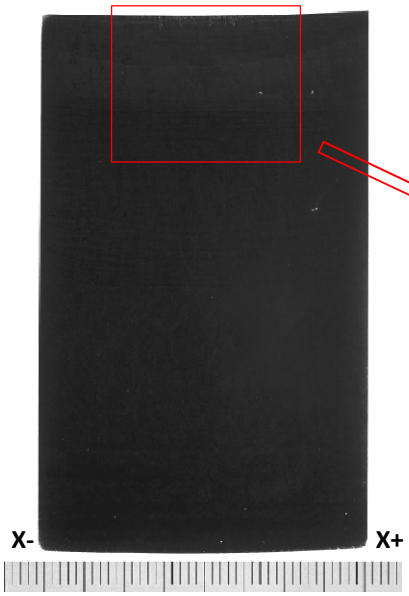

Cross section (before etching)

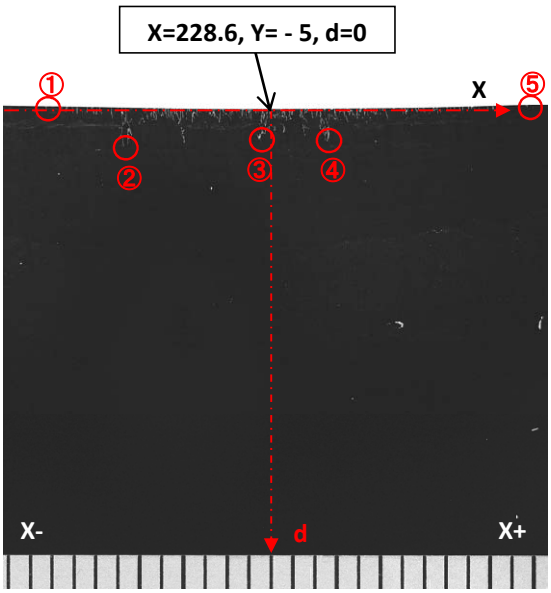

Enlarged cross section (before etching)

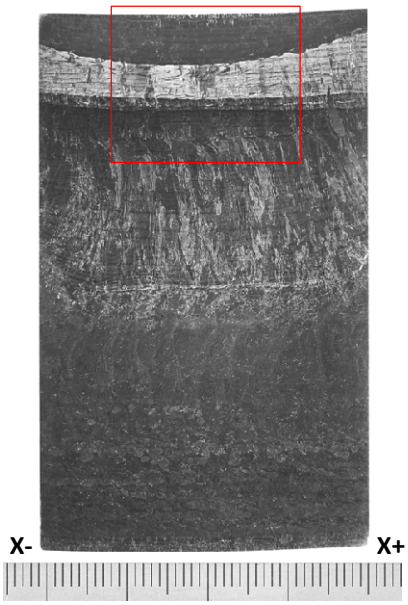

Cross section (after

Crack information

Cross section Y (mm)		-5.0
Max. crack depth info Z (mm)		66.4
Crack opening (μ m)		<1
Typical crack information	①	X= 214.6 Z= 68.2
	②	X= 219.5 Z= 66.4
	③	X= 226.9 Z= 66.6
	④	X= 230.5 Z= 66.7
	⑤	X= 241.6 Z= 68.2

Z = 68.2 - d

Fig. A-3.11 Detailed crack information at Y= - 5 section in P17 (JRV-S3)

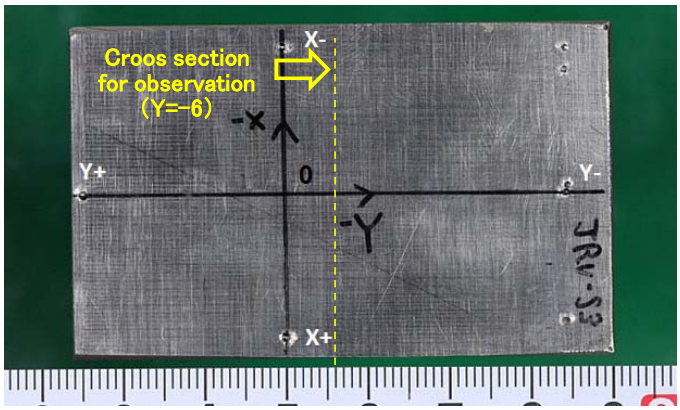

O point :
X=228.6, Y=0

Position of cross section for observation (Y= - 6)

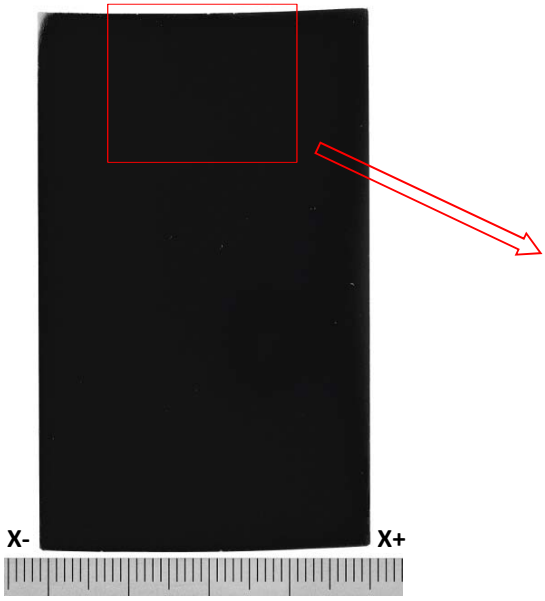

Cross section (before etching)

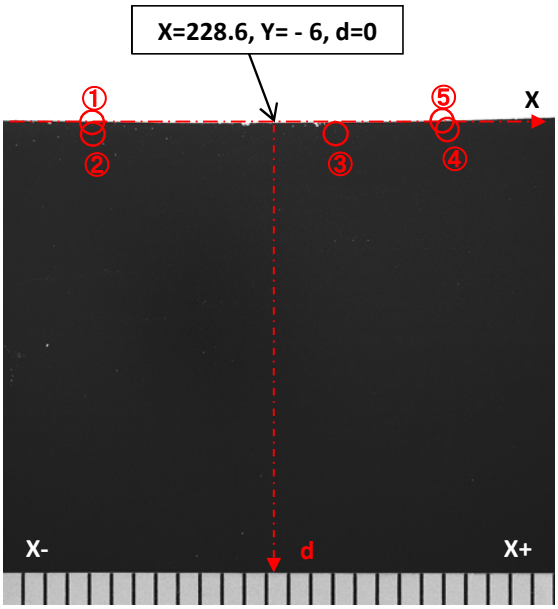

Enlarged cross section (before etching)

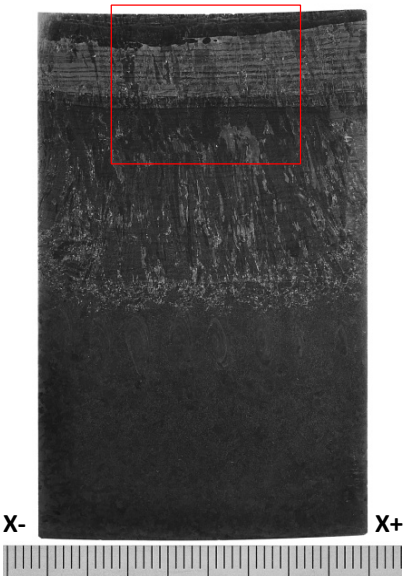

Cross section (after etching)

Crack information

Cross section Y (mm)		−6.0
Max. crack depth info Z (mm)		67.9
Crack opening (μ m)		<1
Typical crack information	①	X= 218.8 Z= 68.2
	②	X= 218.7 Z= 68.1
	③	X= 231.8 Z= 67.9
	④	X= 237.8 Z= 68.1
	⑤	X= 237.8 Z= 68.2

Z = 68.2 - d

Fig. A-3.12 Detailed crack information at Y= - 6 section in P17 (JRV-S3)

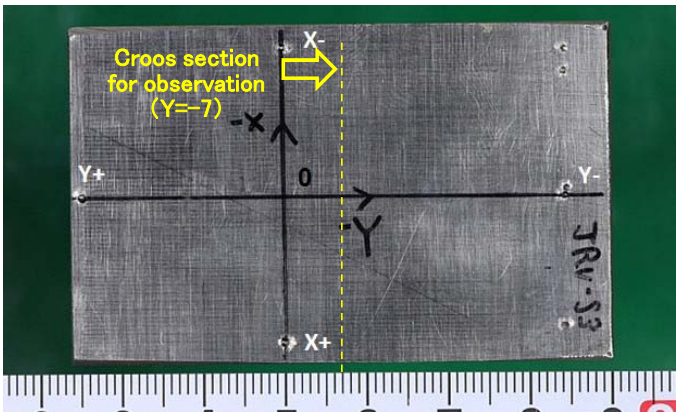

O point :
X=228.6, Y=0

Position of cross section for observation (Y= - 7)

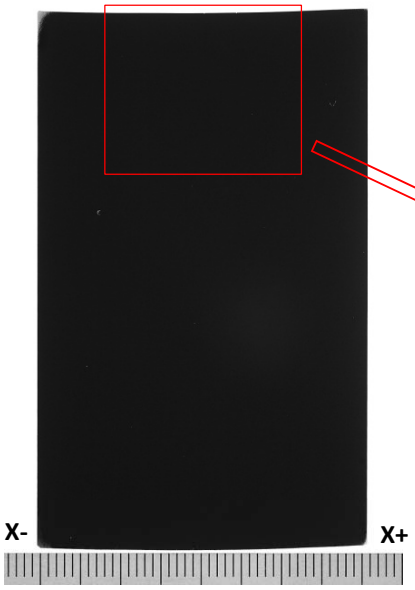

Cross section (before etching)

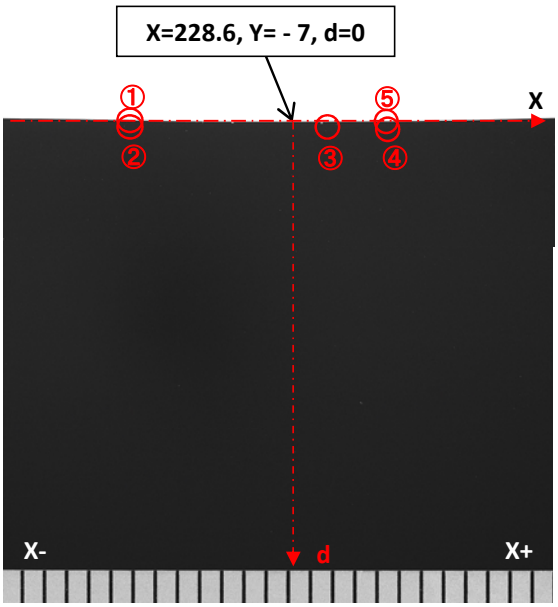

Enlarged cross section (before etching)

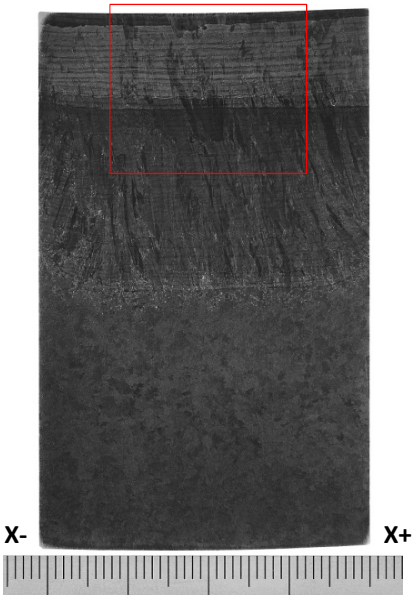

Cross section (after etching)

Crack information

Cross section Y (mm)		-7.0
Max. crack depth info Z (mm)		68.0
Crack opening (μ m)		<1
Typical crack information	①	X= 219.1 Z= 68.2
	②	X= 219.1 Z= 68.2
	③	X= 230.5 Z= 68.0
	④	X= 233.6 Z= 68.1
	⑤	X= 233.6 Z= 68.2

Z = 68.2 - d

Fig. A-3.13 Detailed crack information at Y= - 7 section in P17 (JRV-S3)

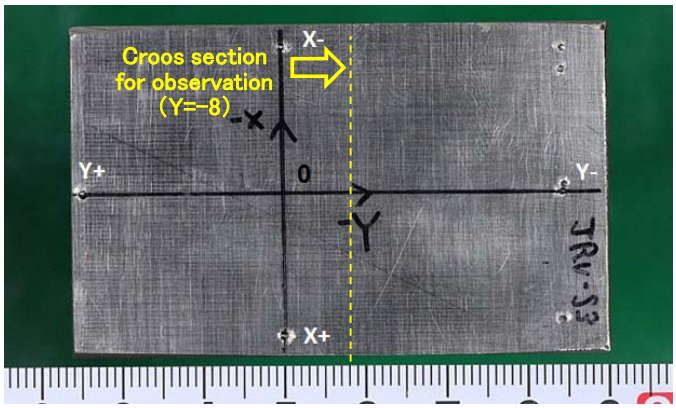

O point :
X=228.6, Y=0

Position of cross section for observation (Y= - 8)

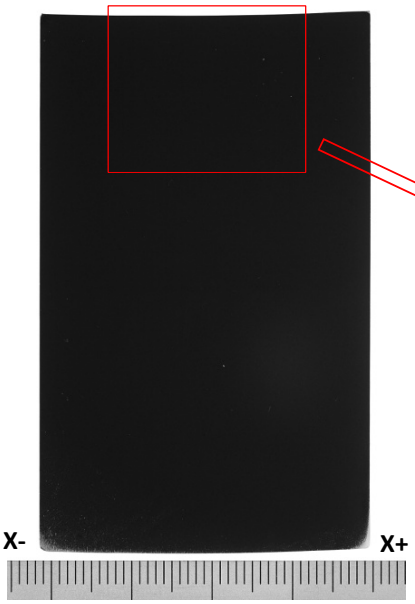

Cross section (before etching)

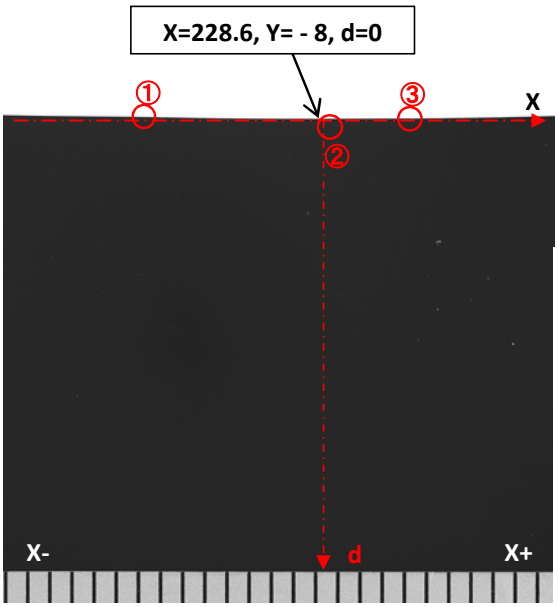

Enlarged cross section (before etching)

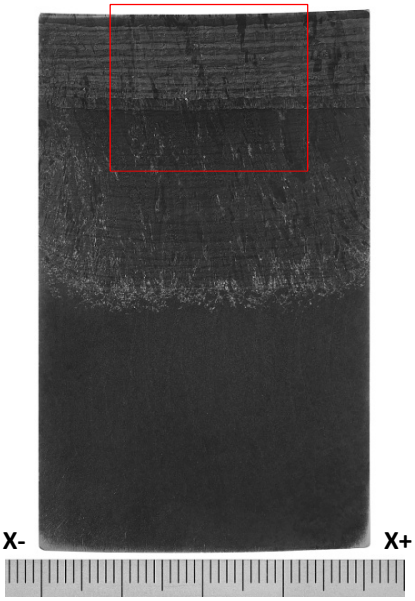

Cross section (after etching)

Crack information

Cross section Y (mm)		-8.0
Max. crack depth info Z (mm)		68.0
Crack opening (μ m)		<1
Typical crack information	①	X= 219.0 Z= 68.2
	②	X= 228.9 Z= 68.0
	③	X= 233.3 Z= 68.2

Z = 68.2 - d

Fig. A-3.14 Detailed crack information at Y= - 8 section in P17 (JRV-S3)

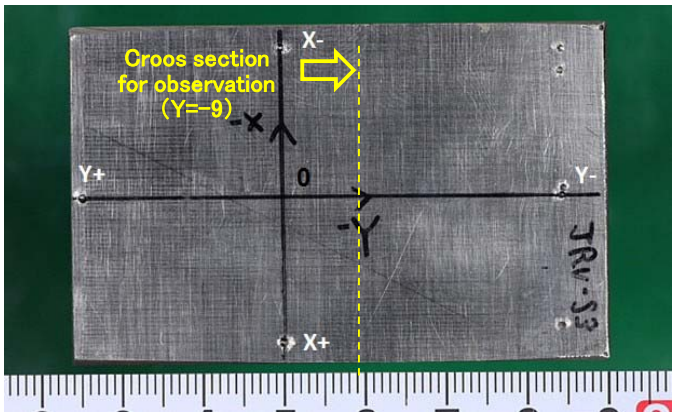

O point :
X=228.6, Y=0

Position of cross section for observation (Y= - 9)

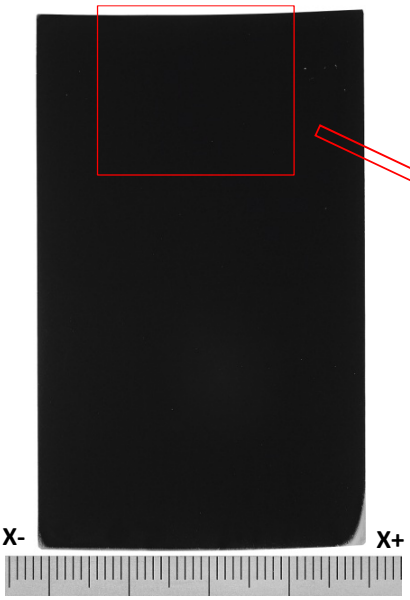

Cross section (before etching)

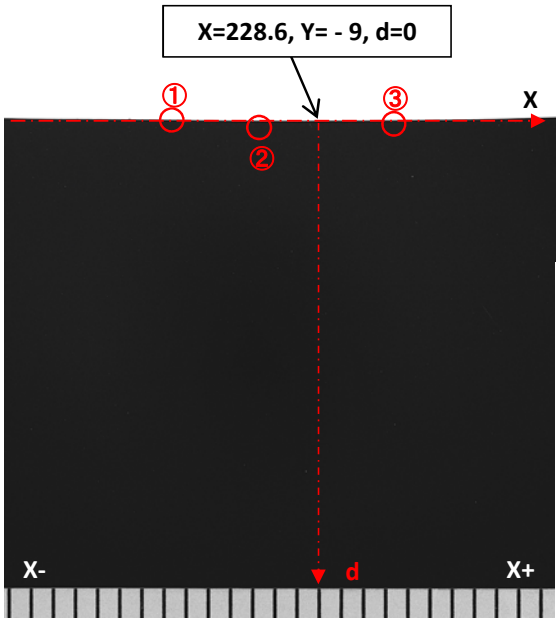

Enlarged cross section (before etching)

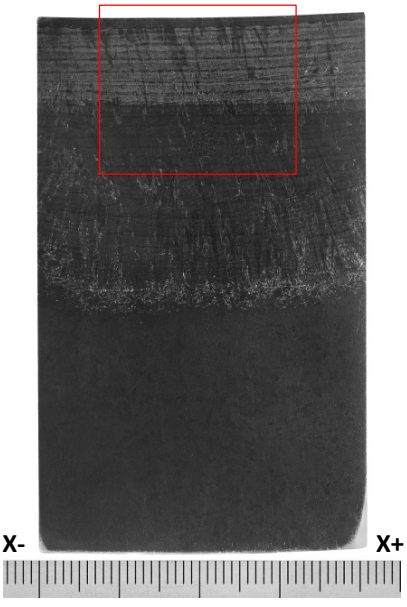

Cross section (after etching)

Crack information

Cross section Y (mm)		-9.0
Max. crack depth info Z (mm)		68.1
Crack opening (μ m)		<1
Typical crack information	①	X= 220.7 Z= 68.2
	②	X= 225.4 Z= 68.1
	③	X= 232.5 Z= 68.2

Z = 68.2 - d

Fig. A-3.15 Detailed crack information at Y= - 9 section in P17 (JRV-S3)

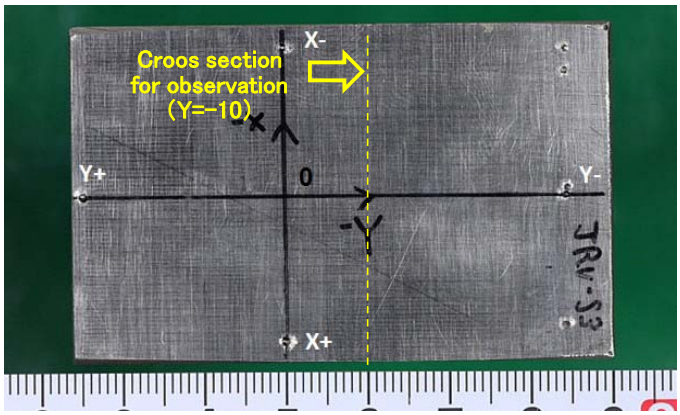

O point :
X=228.6, Y=0

Position of cross section for observation (Y= - 10)

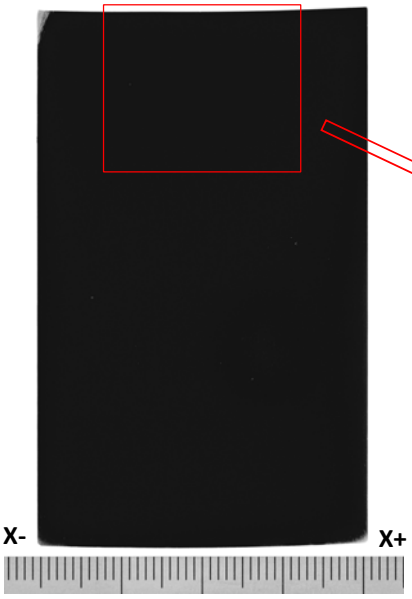

Cross section (before etching)

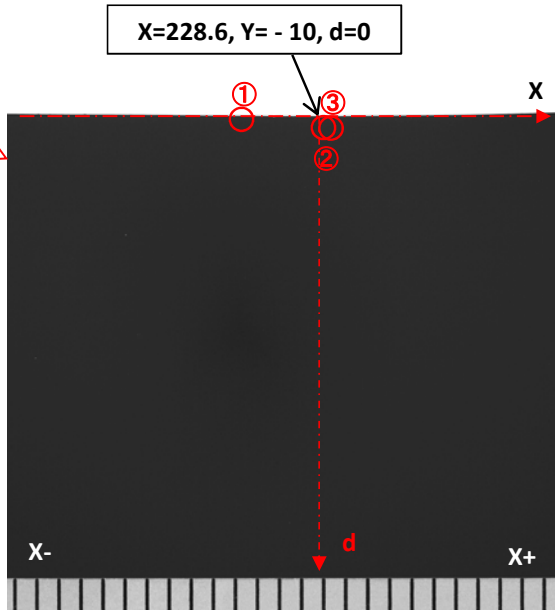

Enlarged cross section (before etching)

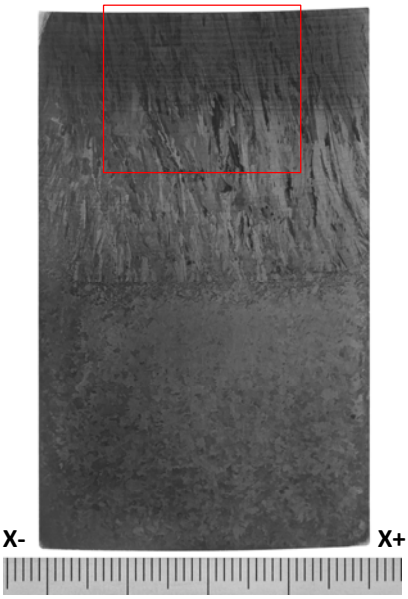

Cross section (after etching)

Crack information

Cross section Y (mm)		−10.0
Max. crack depth info Z (mm)		68.1
Crack opening (μ m)		<1
Typical crack information	①	X= 224.3 Z= 68.2
	②	X= 228.6 Z= 68.1
	③	X= 228.9 Z= 68.2

Z = 68.2 - d

Fig. A-3.16 Detailed crack information at Y= - 10 section in P17 (JRV-S3)

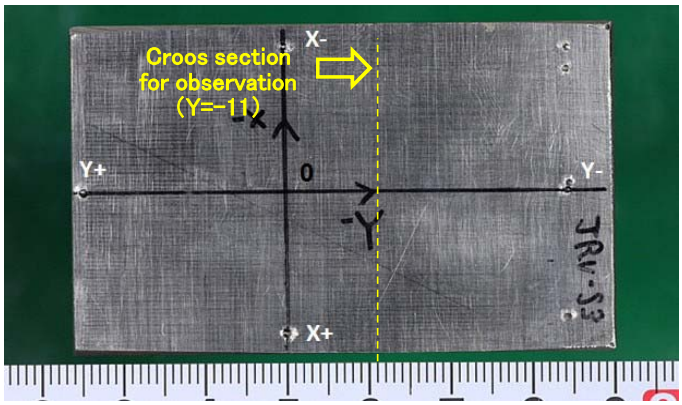

O point :
X=228.6, Y=0

Position of cross section for observation (Y= - 11)

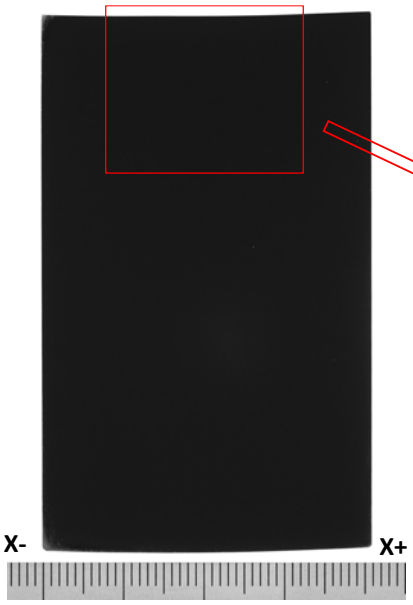

Cross section (before etching)

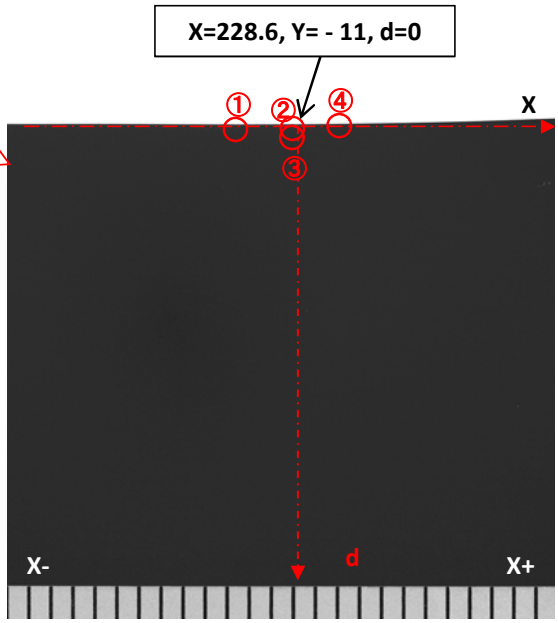

Enlarged cross section (before etching)

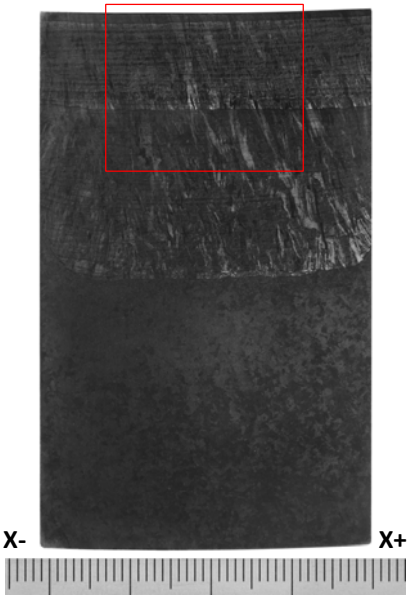

Cross section (after etching)

Crack information

Cross section Y (mm)		−11.0
Max. crack depth info Z (mm)		68.0
Crack opening (μ m)		<1
Typical crack information	①	X= 225.2 Z= 68.2
	②	X= 228.2 Z= 68.2
	③	X= 228.2 Z= 68.0
	④	X= 230.9 Z= 68.2

Z = 68.2 - d

Fig. A-3.17 Detailed crack information at Y= - 11 section in P17 (JRV-S3)

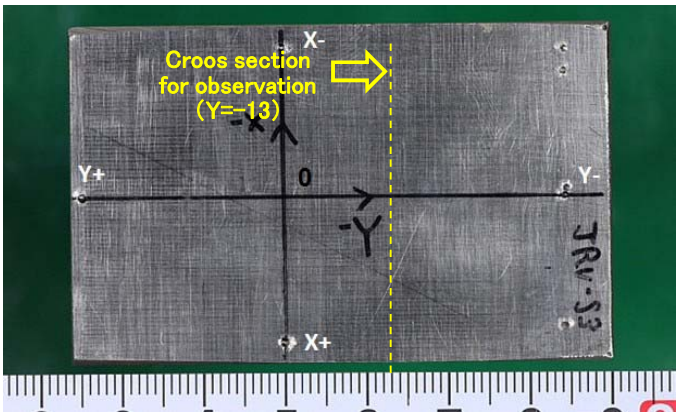

O point :
X=228.6, Y=0

Position of cross section for observation (Y= - 13)

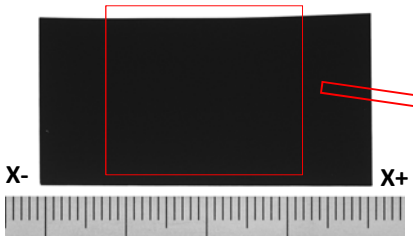

Cross section (before etching)

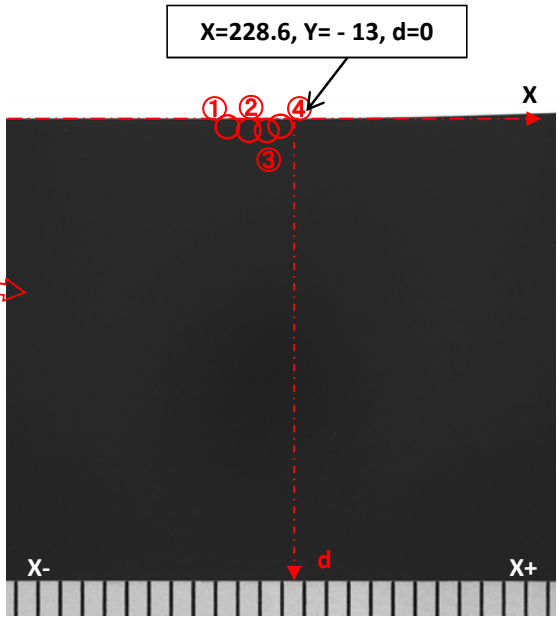

Enlarged cross section (before etching)

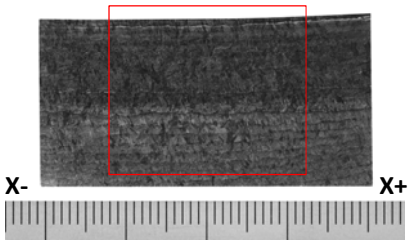

Cross section (after etching)

Crack information

Cross section Y (mm)		−13.0
Max. crack depth info Z (mm)		68.1
Crack opening (μ m)		<1
Typical crack information	①	X= 225.2 Z= 68.2
	②	X= 226.3 Z= 68.1
	③	X= 227.2 Z= 68.1
	④	X= 227.9 Z= 68.2

Z = 68.2 - d

Fig. A-3.18 Detailed crack information at Y= - 13 section in P17 (JRV-S3)

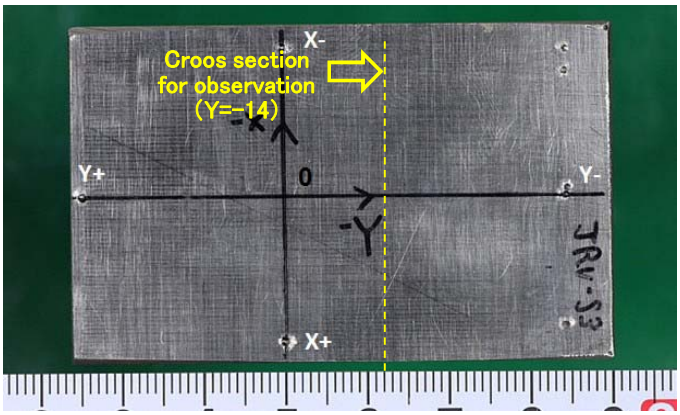

O point :
X=228.6, Y=0

Position of cross section for observation (Y= - 14)

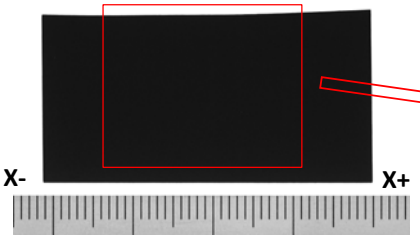

Cross section (before etching)

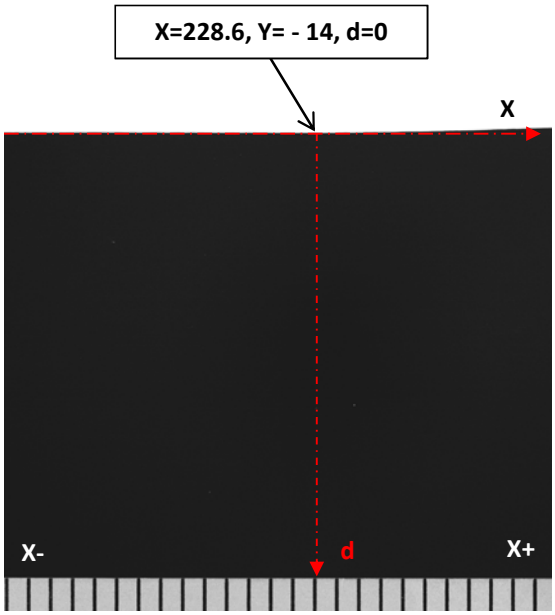

Enlarged cross section (before etching)

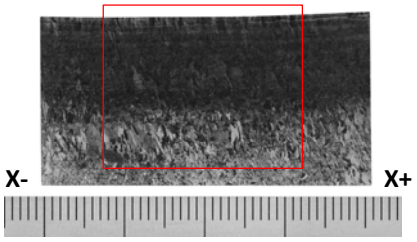

Cross section (after etching)

Crack information

Cross section Y (mm)	−14.0
Max. crack depth info Z (mm)	No crack
Crack opening (μ m)	No crack
Typical crack information	No crack

Z = 68.2 - d

Fig. A-3.19 Detailed crack information at Y= - 14 section in P17 (JRV-S3)

Appendix B

Inspection Plots of Quick Blind Test Blocks

Appendix B

Inspection Plots of Quick Blind Test Blocks

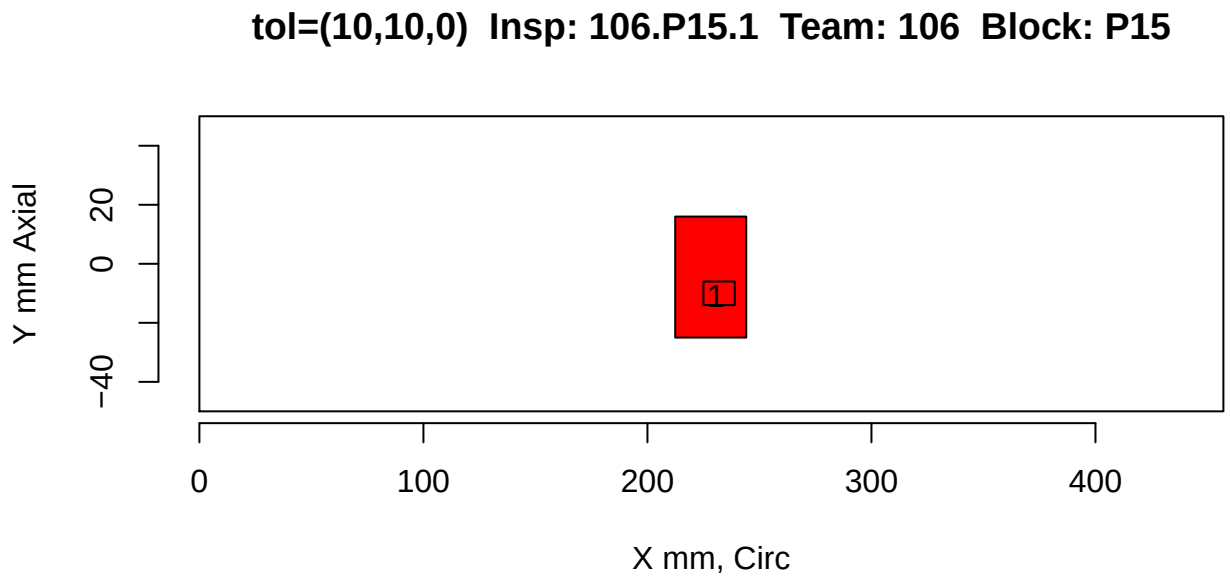

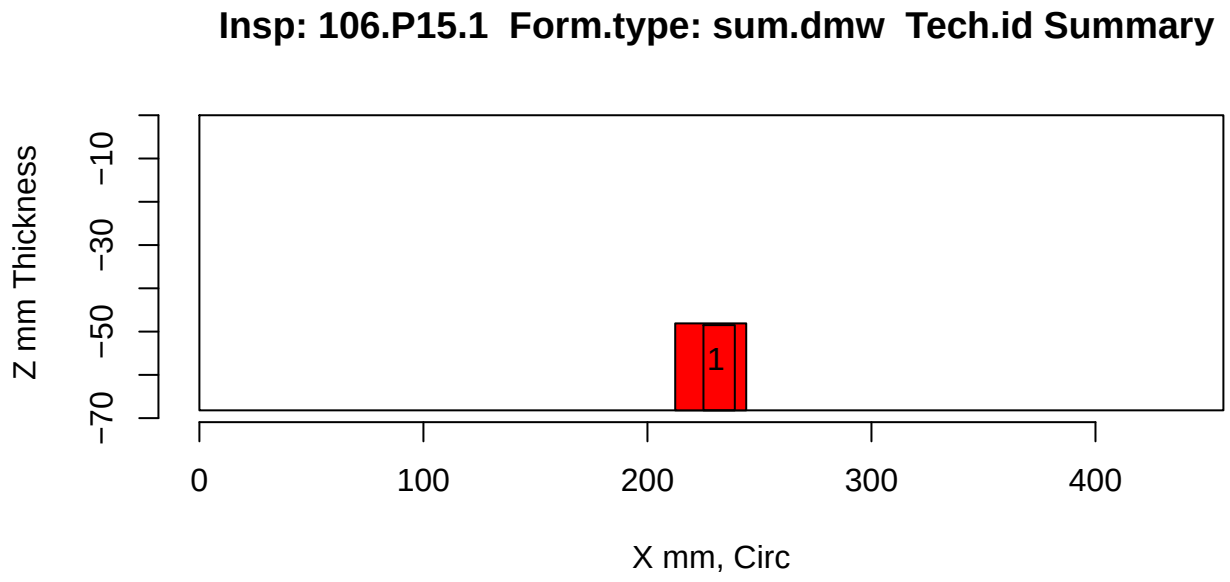

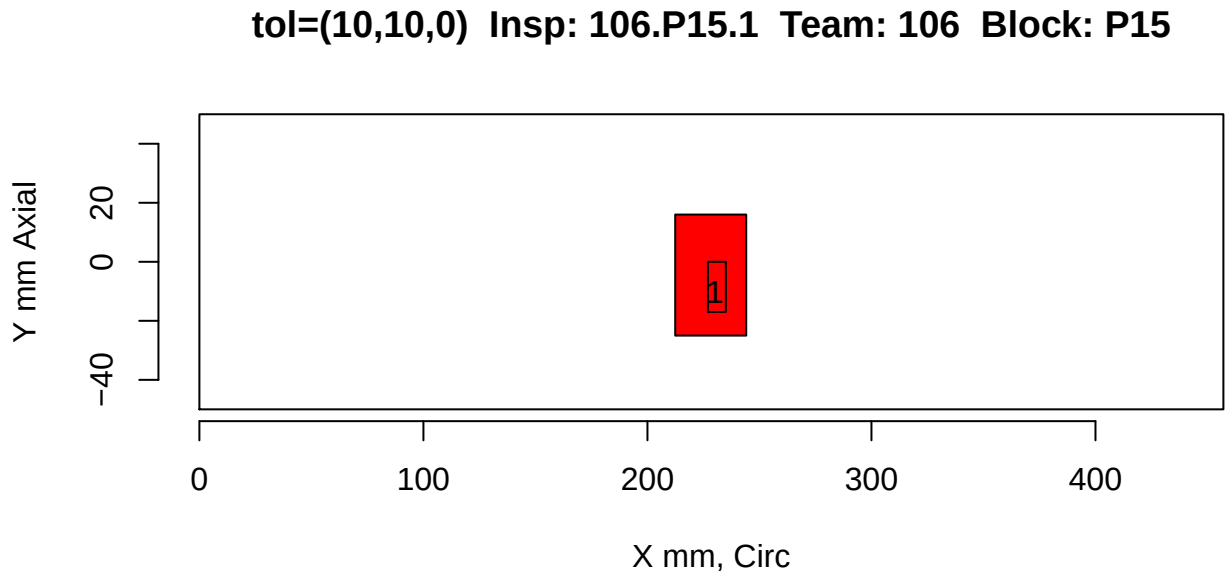
tol=(10,10,0) Insp: 106.P15.1 Team: 106 Block: P15
Y mm Axial
20
0
−40
1
0
100
200
300
400
X mm, Circ

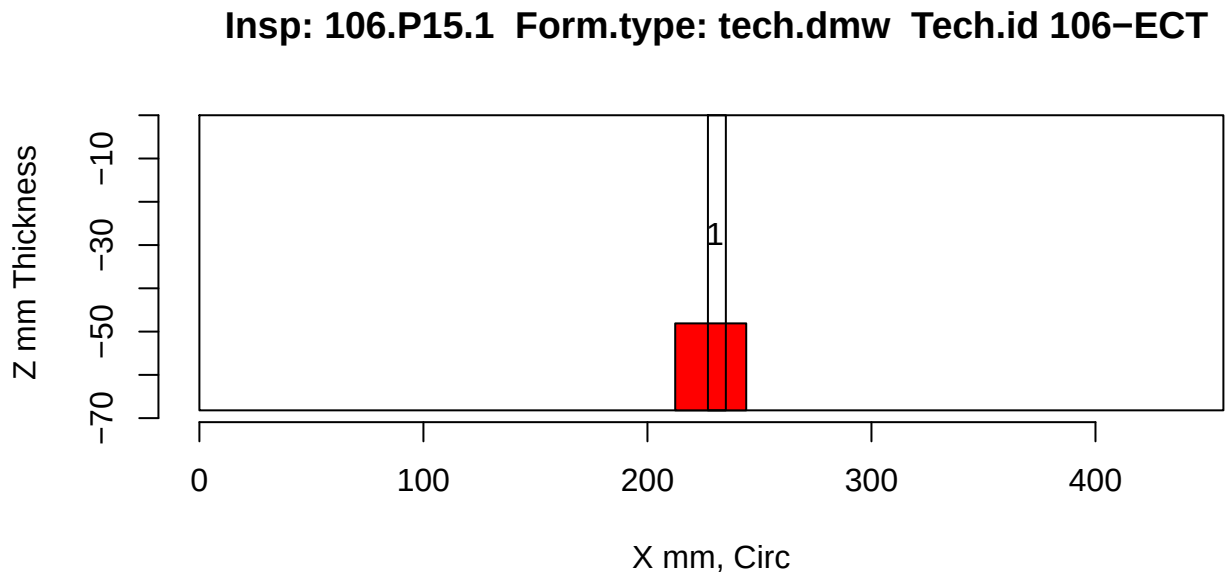
Insp: 106.P15.1 Form.type: tech.dmw Tech.id 106−ECT
Z mm Thickness
−10
−30
−50
−70
1
0
100
200
300
400
X mm, Circ

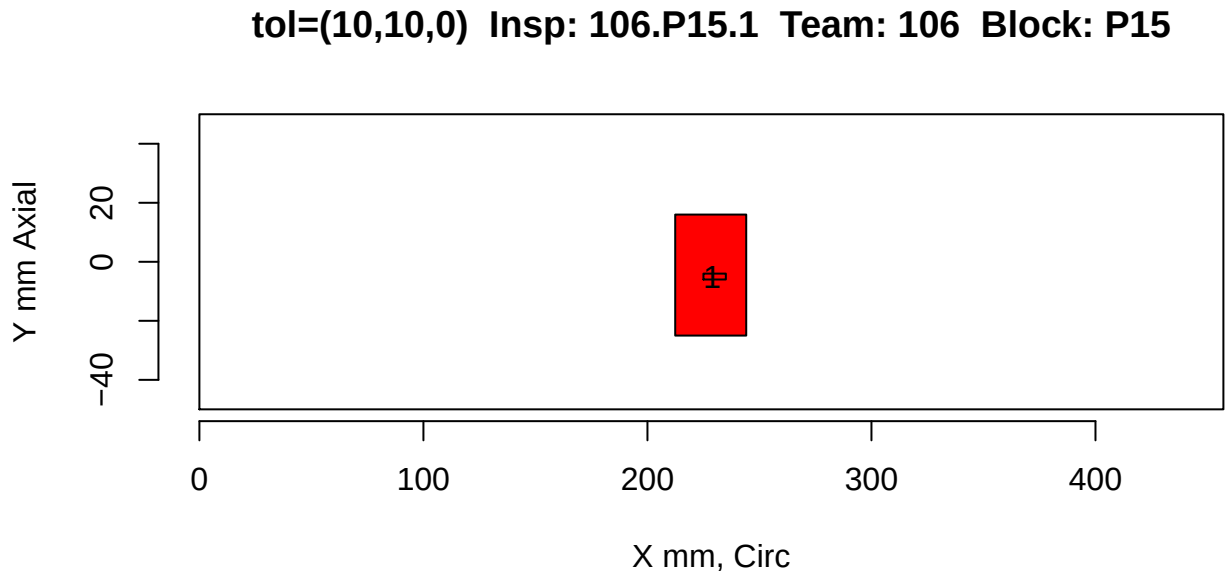
tol=(10,10,0) Insp: 106.P15.1 Team: 106 Block: P15
Y mm Axial
20
0
−40
4
0
100
200
300
400
X mm, Circ

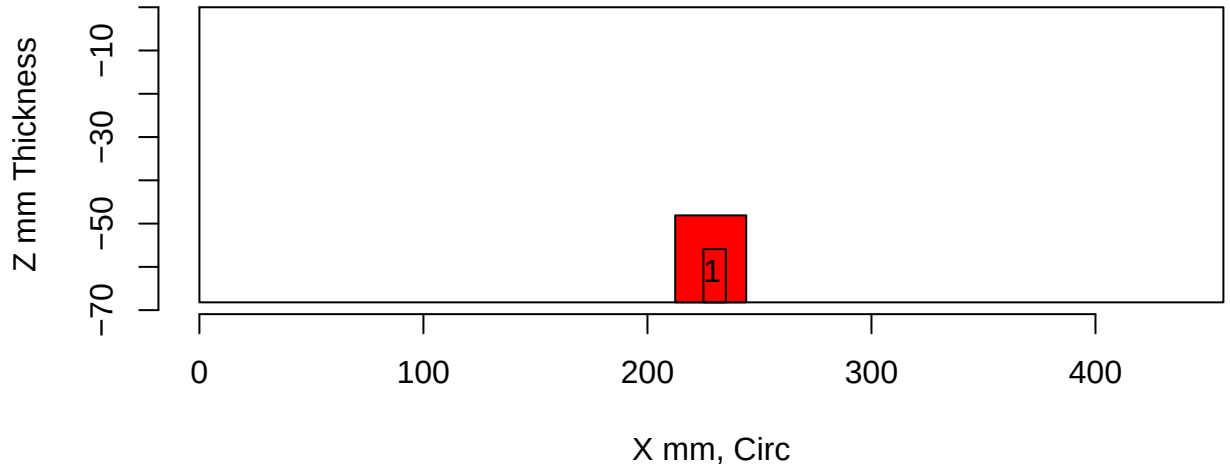
Insp: 106.P15.1 Form.type: tech.dmw Tech.id 106−UT1
Z mm Thickness
−10
−30
−50
−70
1
0
100
200
300
400
X mm, Circ

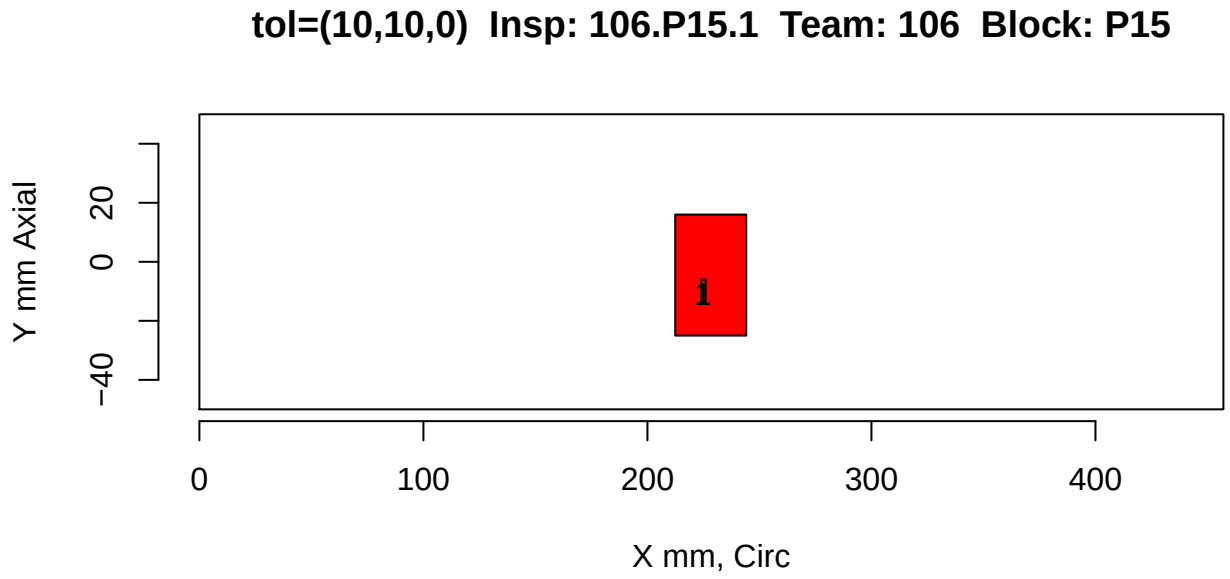
tol=(10,10,0) Insp: 106.P15.1 Team: 106 Block: P15
Y mm Axial
20
0
−40
1
0
100
200
300
400
X mm, Circ

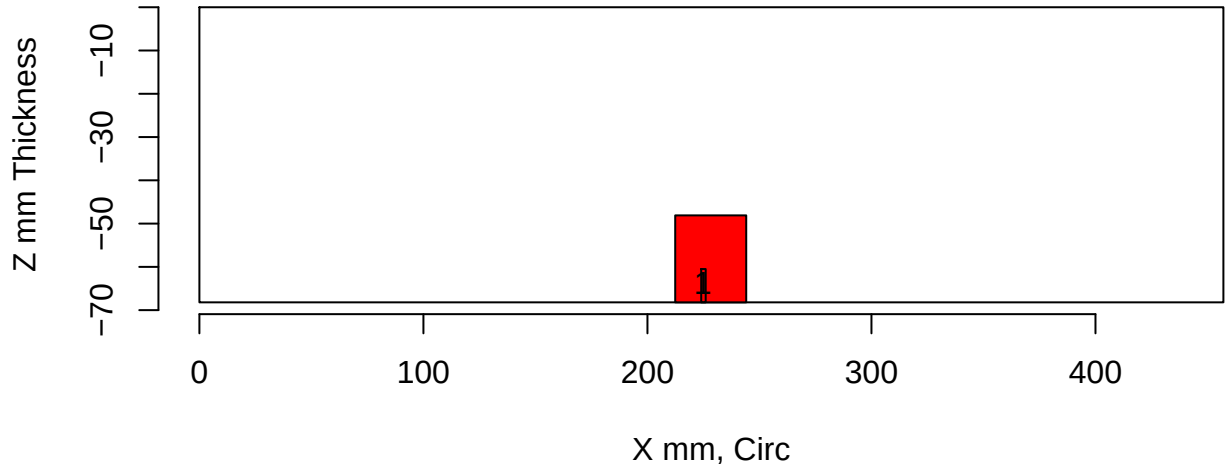
Insp: 106.P15.1 Form.type: tech.dmw Tech.id 106−UT2
Z mm Thickness
−10
−30
−50
−70
1
0
100
200
300
400
X mm, Circ

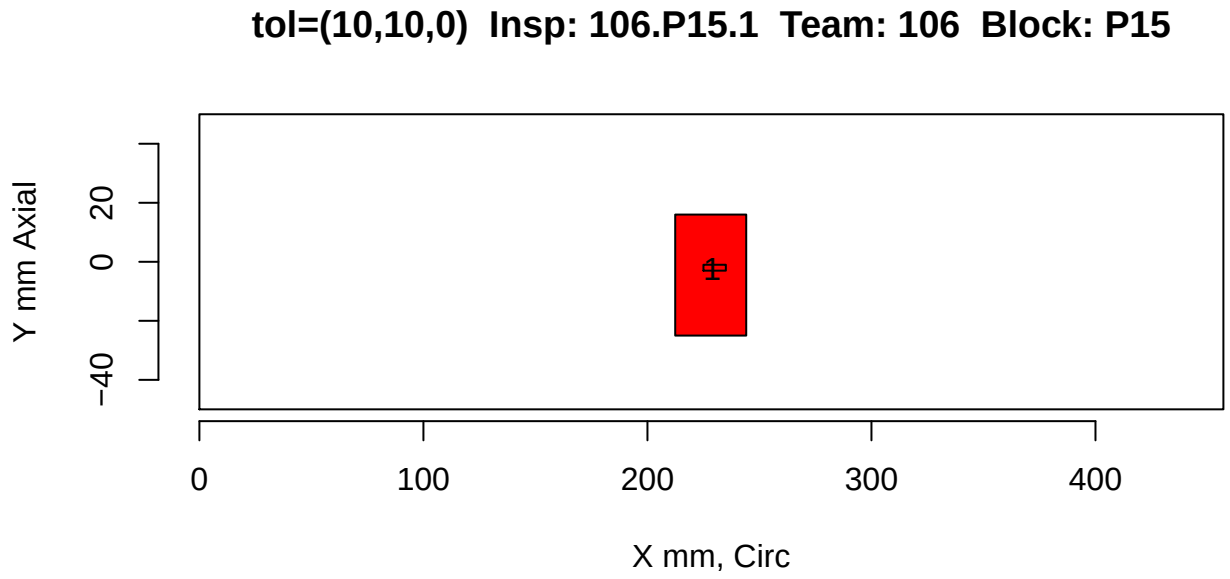
tol=(10,10,0) Insp: 106.P15.1 Team: 106 Block: P15
Y mm Axial
20
0
−40
0
100
200
300
400
X mm, Circ

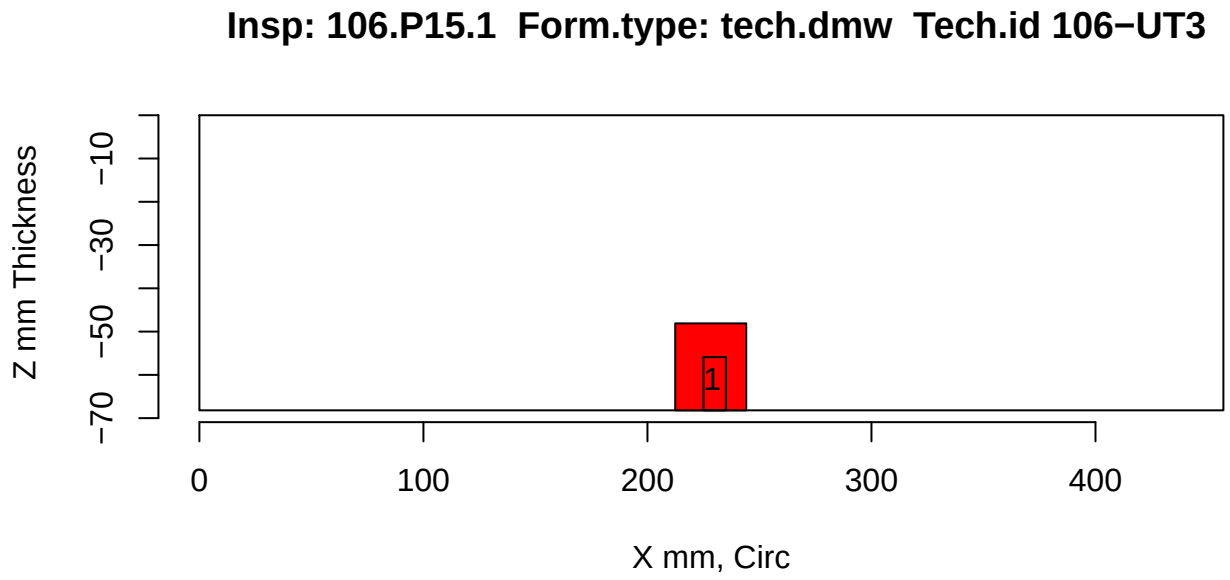
Insp: 106.P15.1 Form.type: tech.dmw Tech.id 106−UT3
Z mm Thickness
−10
−30
−50
−70
1
0
100
200
300
400
X mm, Circ

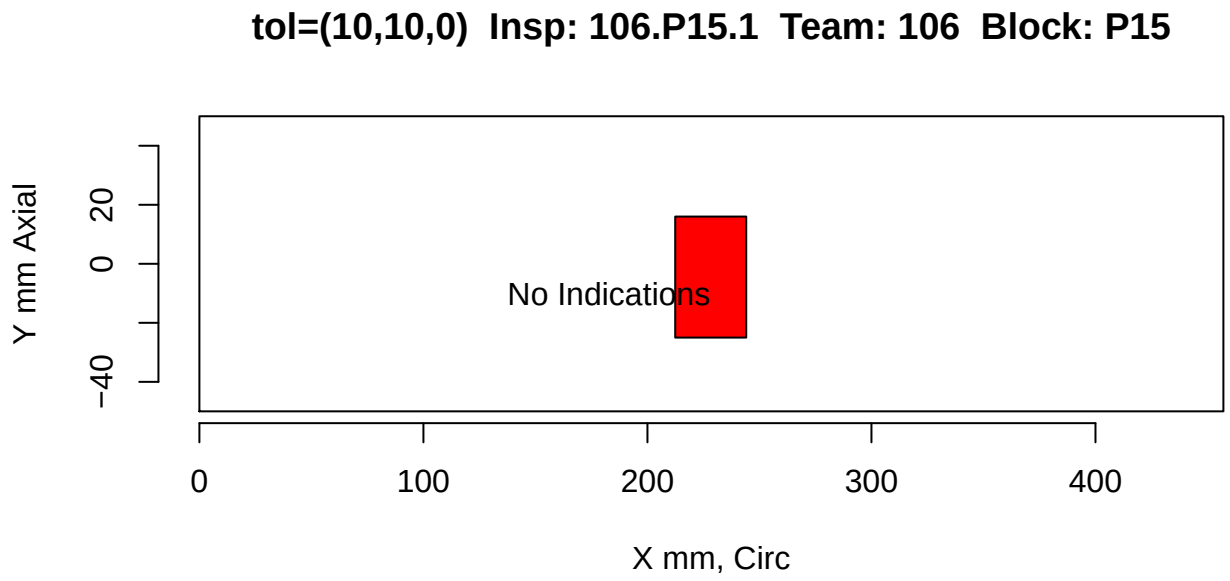
tol=(10,10,0) Insp: 106.P15.1 Team: 106 Block: P15
Y mm Axial
20
0
−40
No Indications
0
100
200
300
400
X mm, Circ

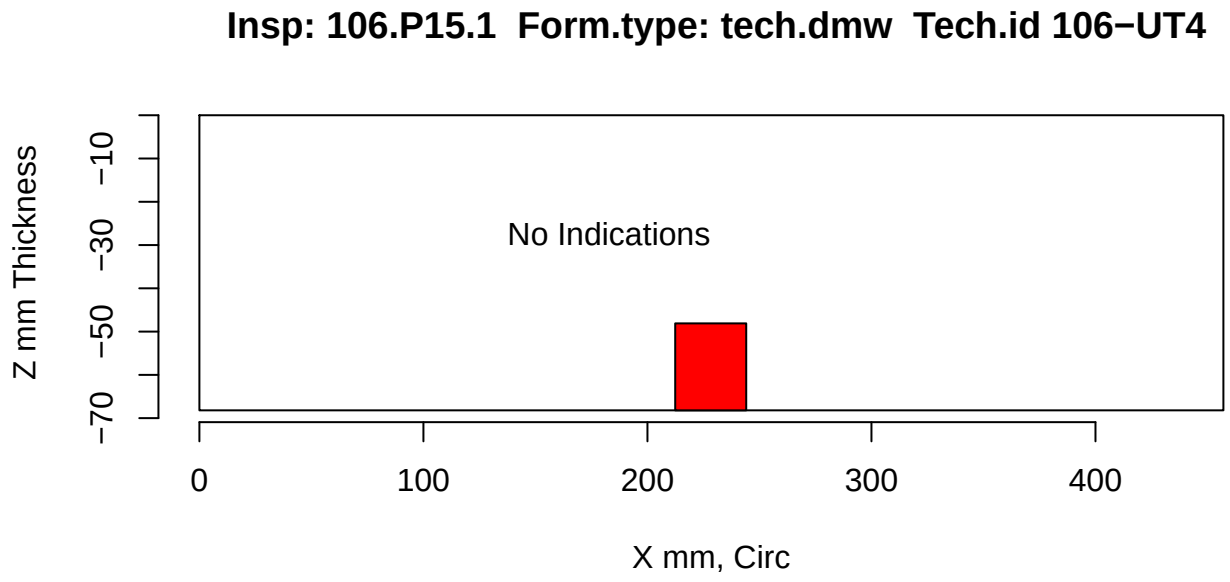
Insp: 106.P15.1 Form.type: tech.dmw Tech.id 106−UT4
Z mm Thickness
−10
−30
−50
−70
No Indications
0
100
200
300
400
X mm, Circ

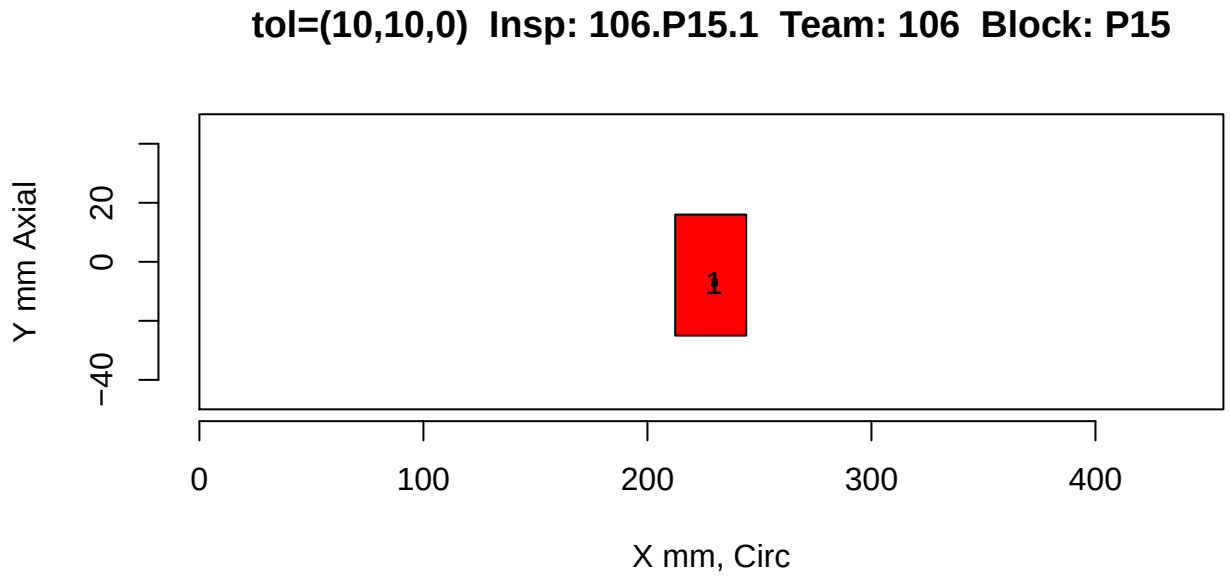
tol=(10,10,0) Insp: 106.P15.1 Team: 106 Block: P15
Y mm Axial
20
0
−40
1
0
100
200
300
400
X mm, Circ

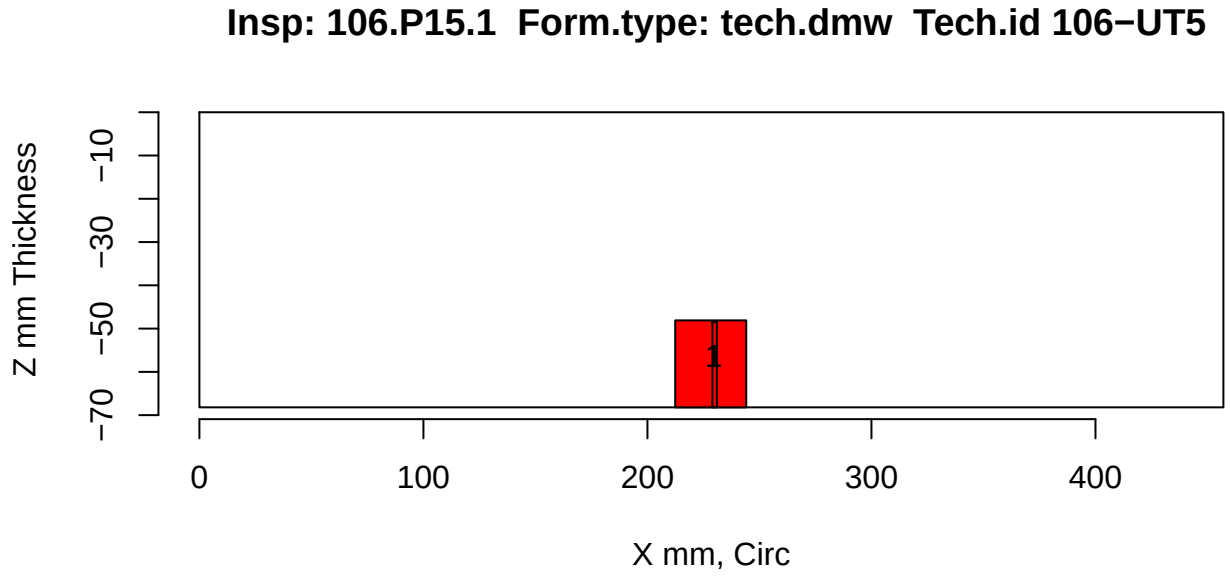
Insp: 106.P15.1 Form.type: tech.dmw Tech.id 106−UT5
Z mm Thickness
−10
−30
−50
−70
1
0
100
200
300
400
X mm, Circ

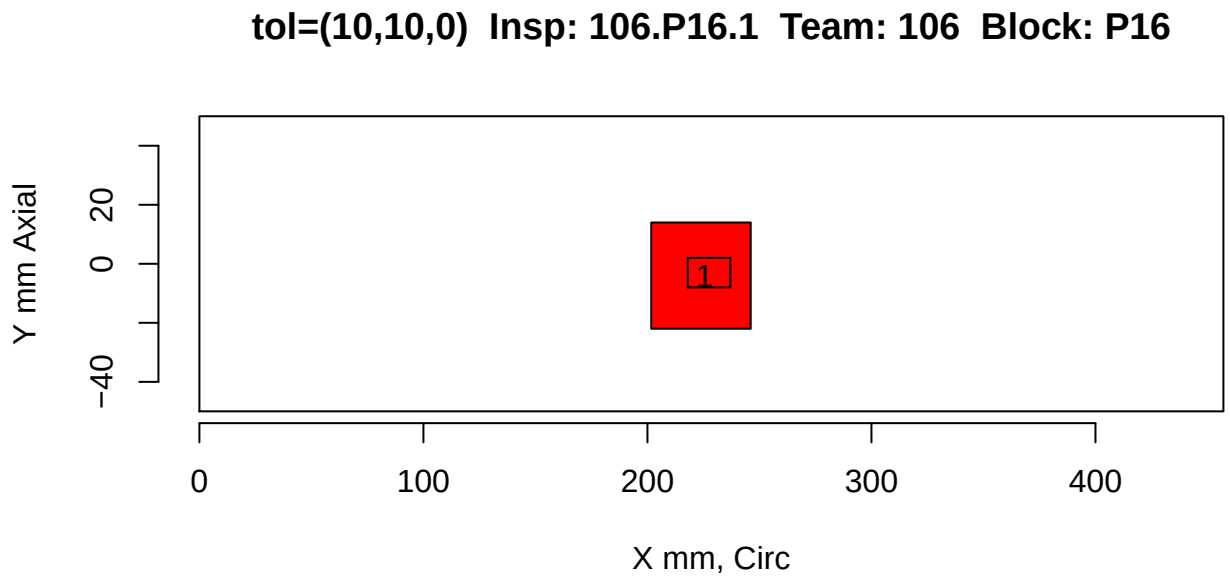
tol=(10,10,0) Insp: 106.P16.1 Team: 106 Block: P16
Y mm Axial
20
0
−40
1
0
100
200
300
400
X mm, Circ

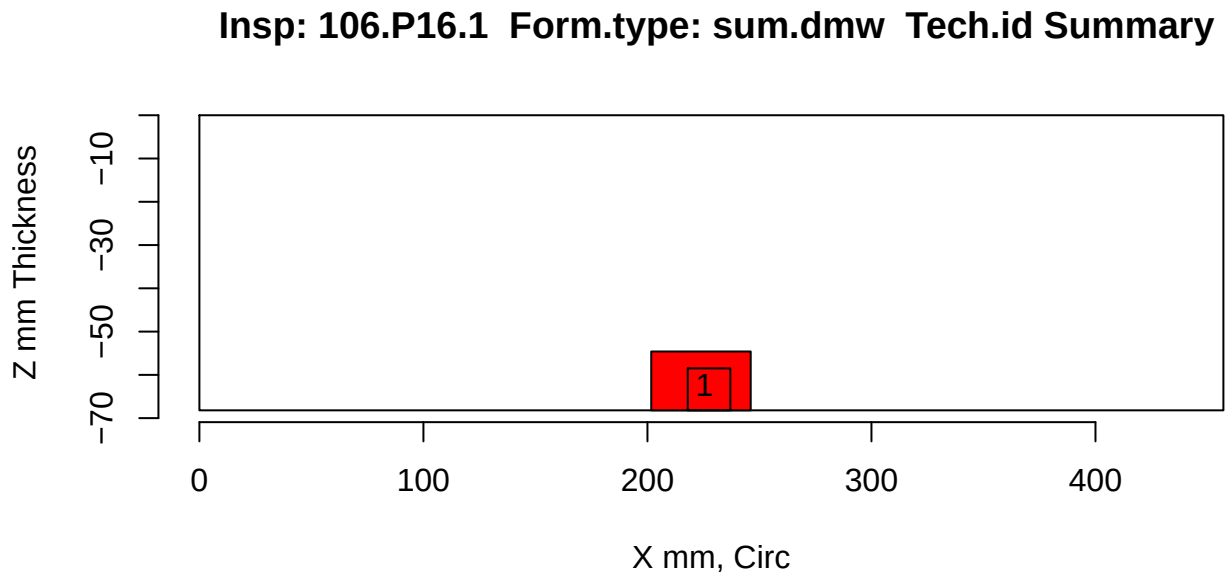
Insp: 106.P16.1 Form.type: sum.dmw Tech.id Summary
Z mm Thickness
−10
−30
−50
−70
1
0
100
200
300
400
X mm, Circ

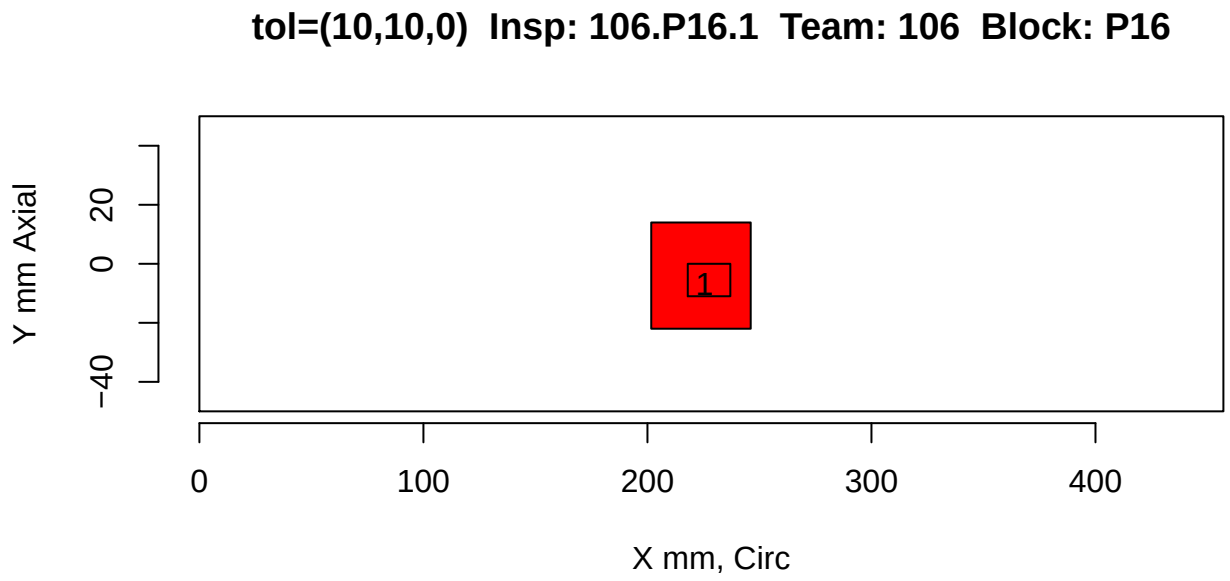
tol=(10,10,0) Insp: 106.P16.1 Team: 106 Block: P16
Y mm Axial
20
0
−40
1
0
100
200
300
400
X mm, Circ

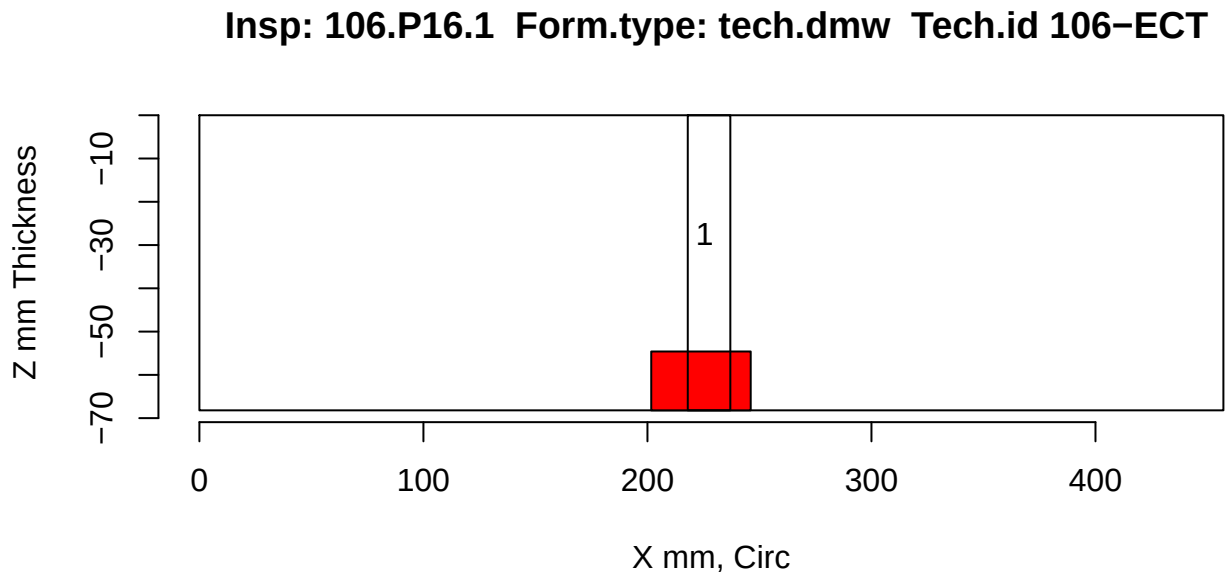
Insp: 106.P16.1 Form.type: tech.dmw Tech.id 106−ECT
Z mm Thickness
−10
−30
−50
−70
1
0
100
200
300
400
X mm, Circ

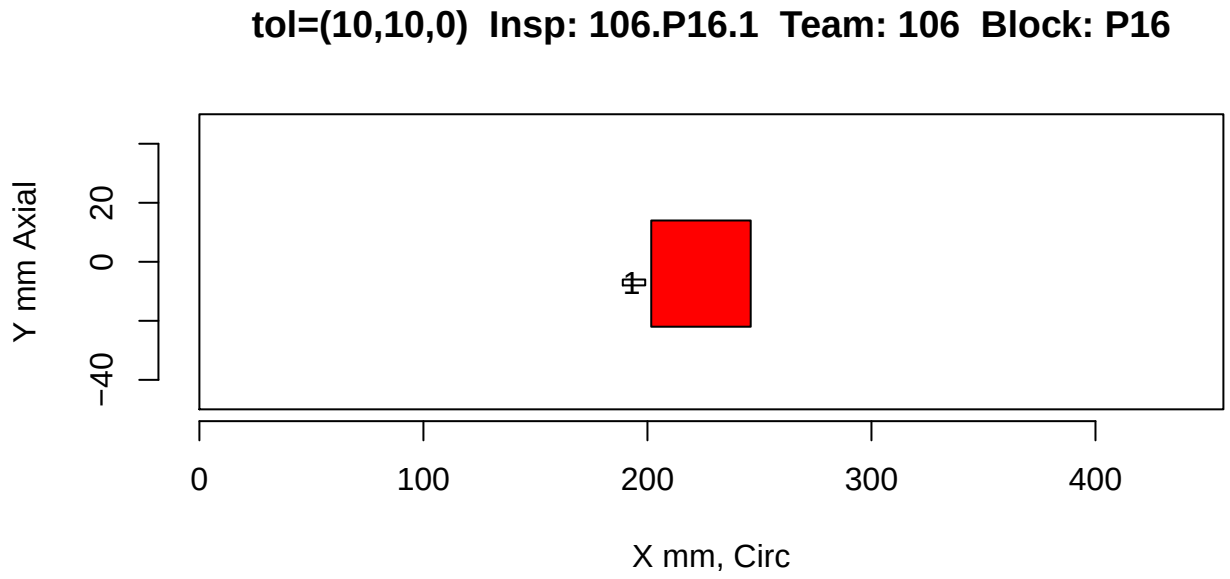
tol=(10,10,0) Insp: 106.P16.1 Team: 106 Block: P16
Y mm Axial
20
0
−40
1
0
100
200
300
400
X mm, Circ

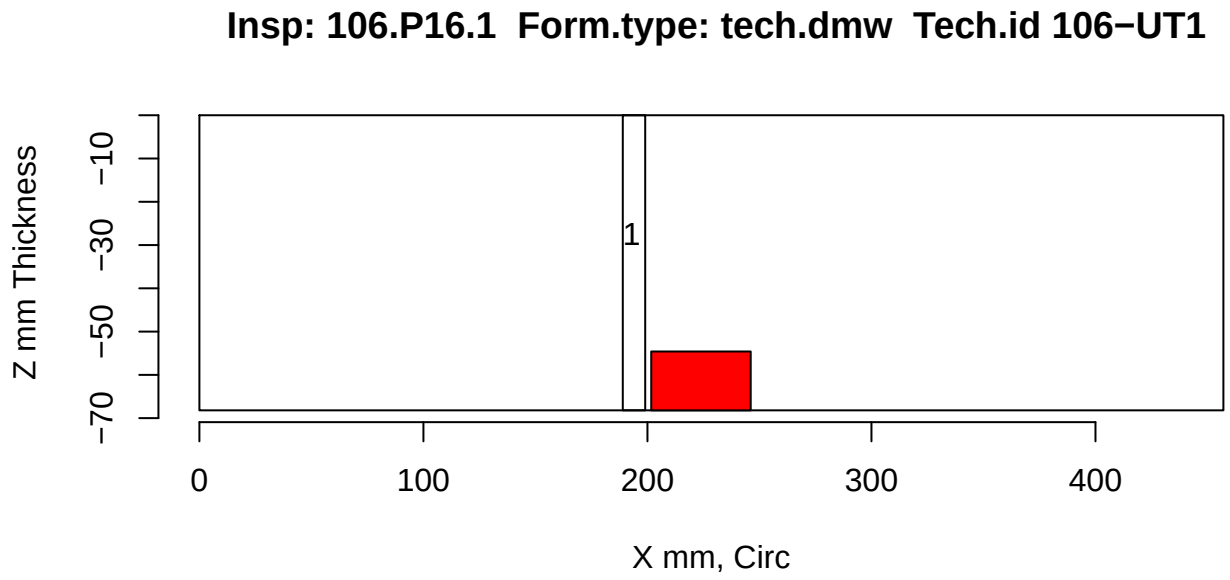
Insp: 106.P16.1 Form.type: tech.dmw Tech.id 106−UT1
Z mm Thickness
−10
−30
−50
−70
1
0
100
200
300
400
X mm, Circ

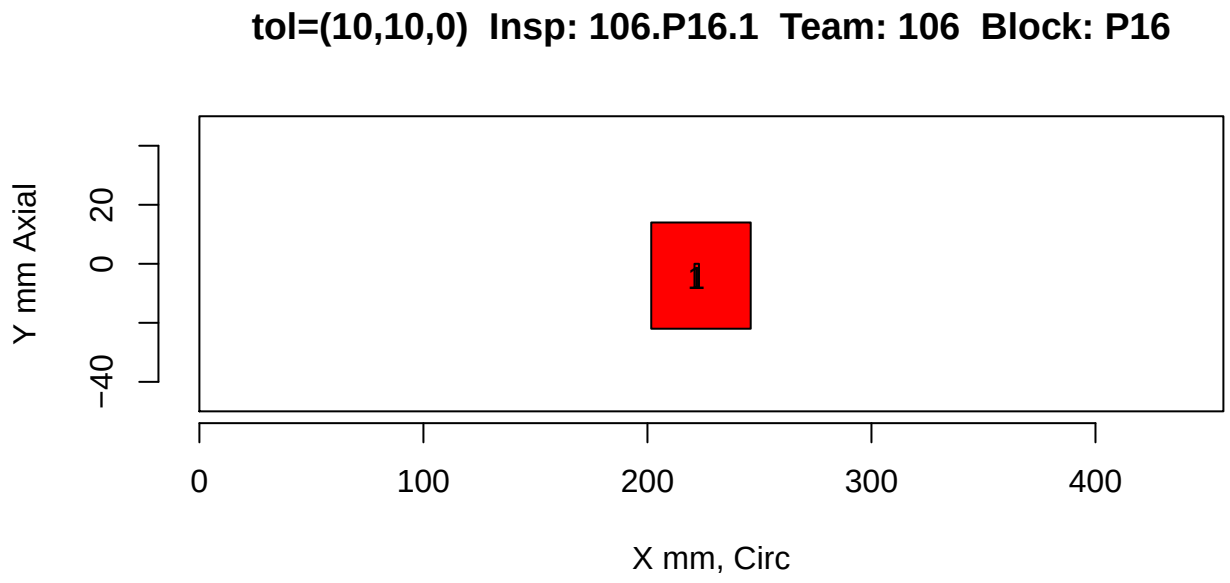
tol=(10,10,0) Insp: 106.P16.1 Team: 106 Block: P16
Y mm Axial
20
0
−40
1
0
100
200
300
400
X mm, Circ

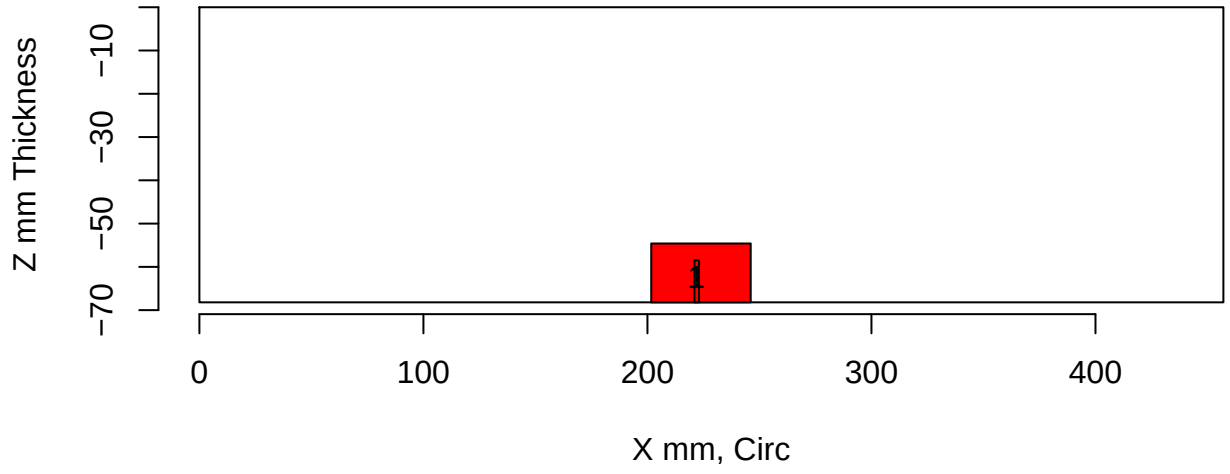
Insp: 106.P16.1 Form.type: tech.dmw Tech.id 106−UT2
Z mm Thickness
−10
−30
−50
−70
1
0
100
200
300
400
X mm, Circ

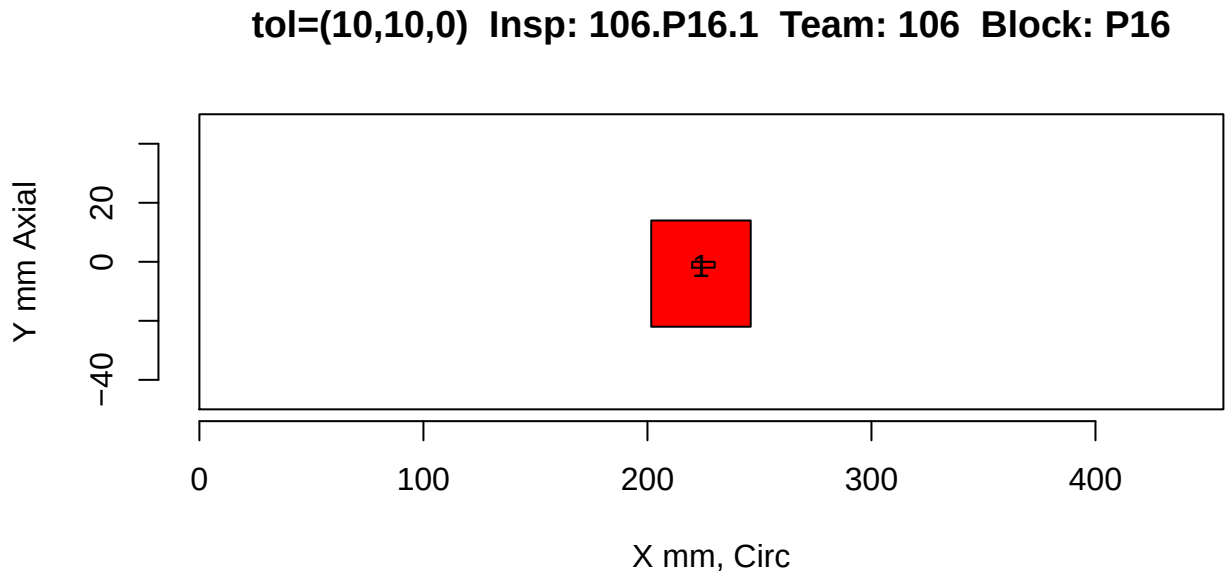
tol=(10,10,0) Insp: 106.P16.1 Team: 106 Block: P16
Y mm Axial
20
0
−40
1
0
100
200
300
400
X mm, Circ

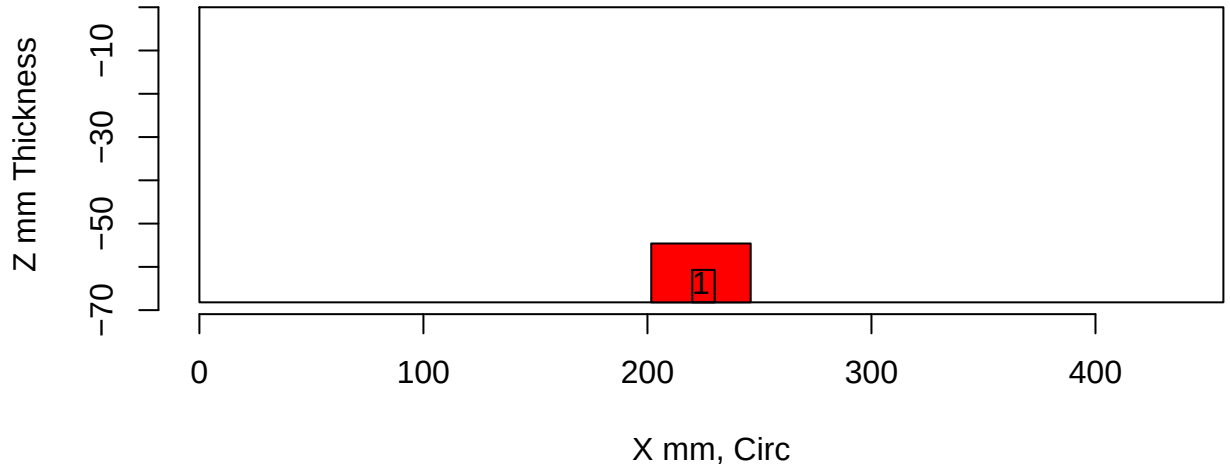
Insp: 106.P16.1 Form.type: tech.dmw Tech.id 106−UT3
Z mm Thickness
−10
−30
−50
−70
1
0
100
200
300
400
X mm, Circ

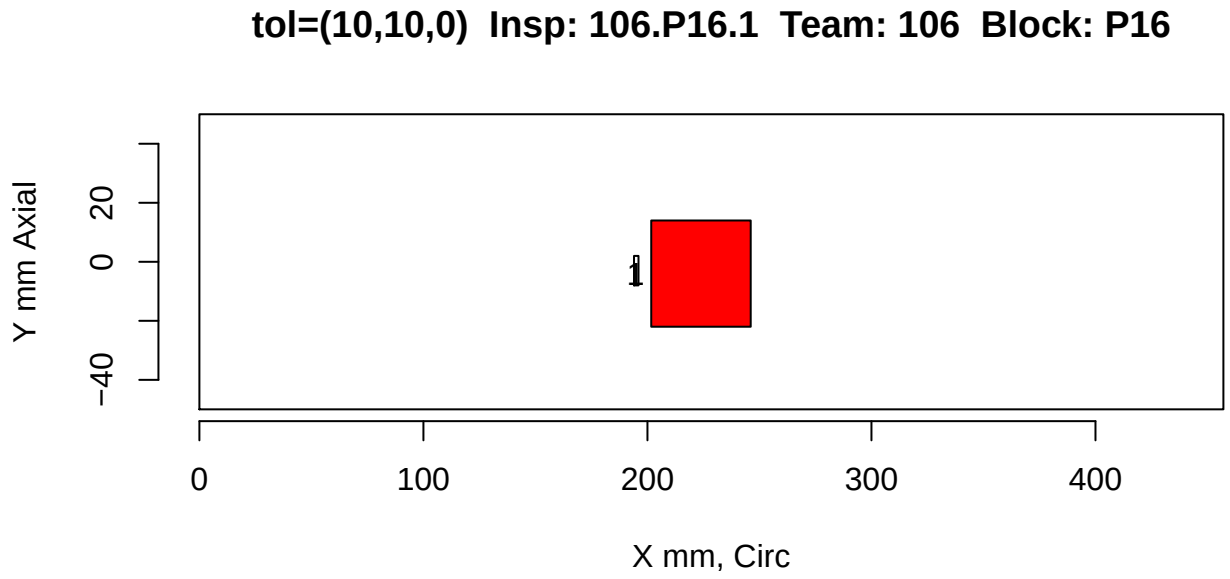
tol=(10,10,0) Insp: 106.P16.1 Team: 106 Block: P16
Y mm Axial
20
0
−40
1
0
100
200
300
400
X mm, Circ

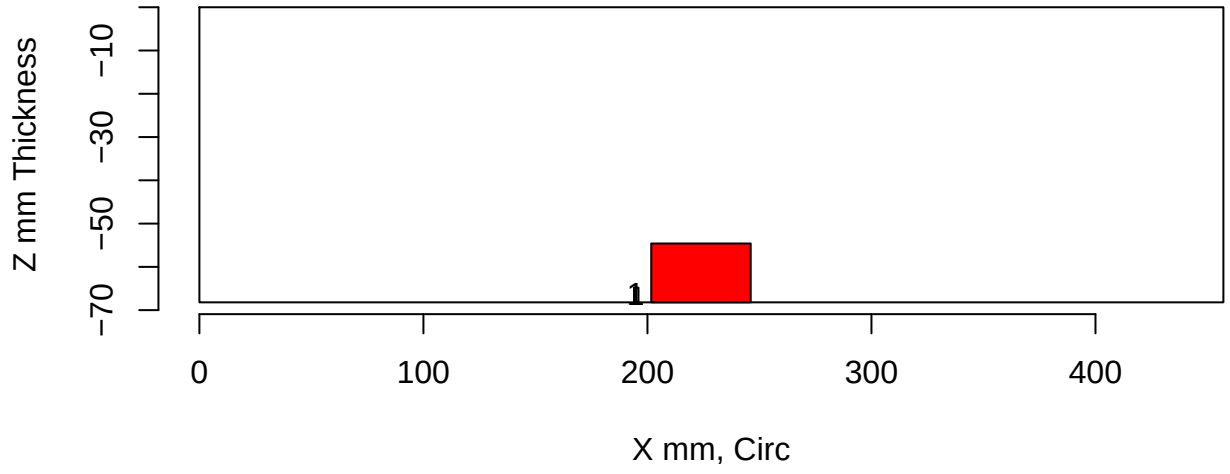
Insp: 106.P16.1 Form.type: tech.dmw Tech.id 106−UT4
Z mm Thickness
−10
−30
−50
−70
1
0
100
200
300
400
X mm, Circ

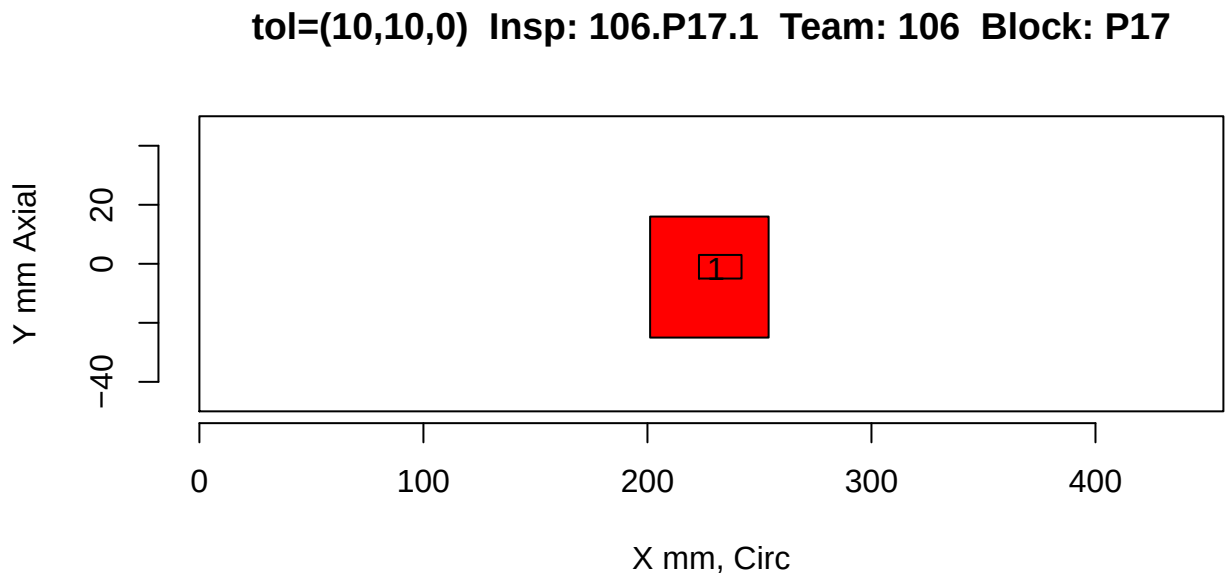
tol=(10,10,0) Insp: 106.P17.1 Team: 106 Block: P17
Y mm Axial
20
0
−40
1
0
100
200
300
400
X mm, Circ

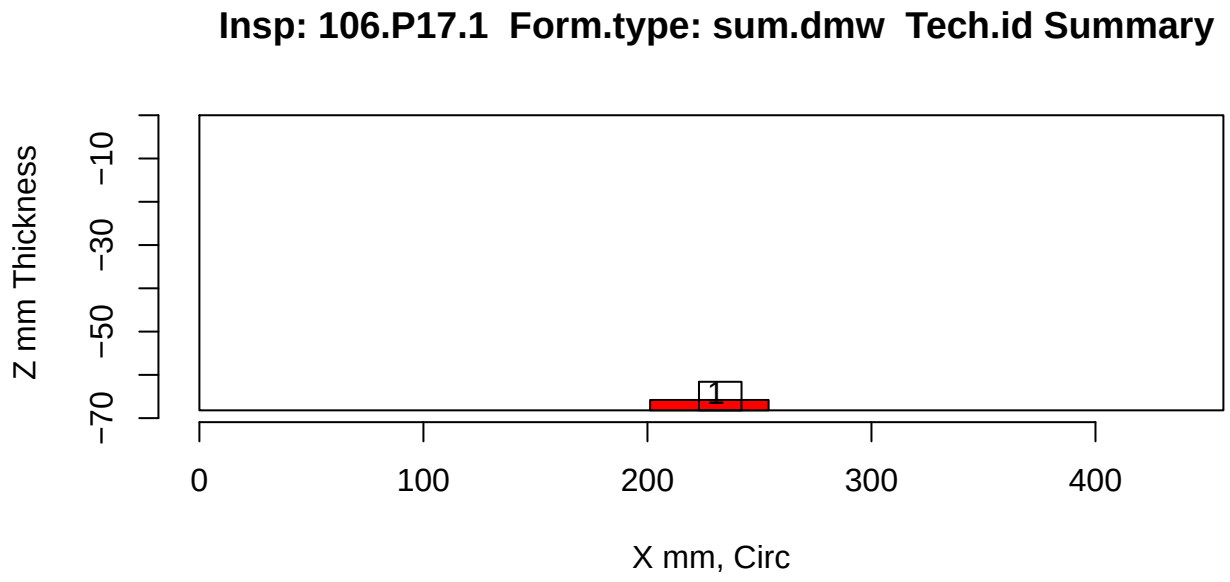
Insp: 106.P17.1 Form.type: sum.dmw Tech.id Summary
Z mm Thickness
−10
−30
−50
−70
1
0
100
200
300
400
X mm, Circ

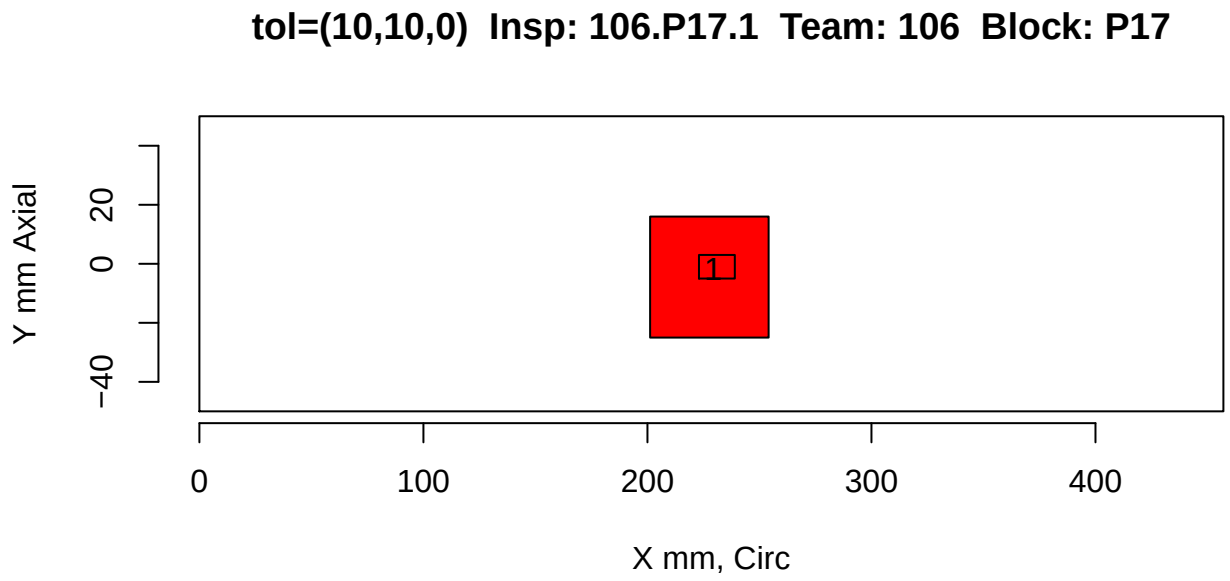
tol=(10,10,0) Insp: 106.P17.1 Team: 106 Block: P17
Y mm Axial
20
0
−40
1
0
100
200
300
400
X mm, Circ

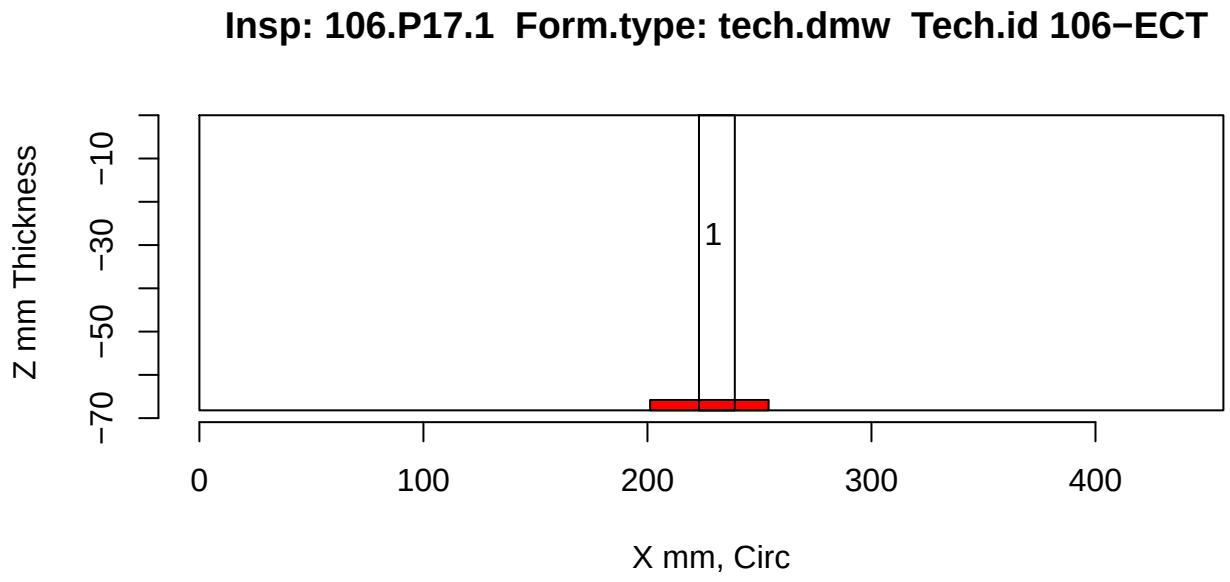
Insp: 106.P17.1 Form.type: tech.dmw Tech.id 106−ECT
Z mm Thickness
−10
−30
−50
−70
1
0
100
200
300
400
X mm, Circ

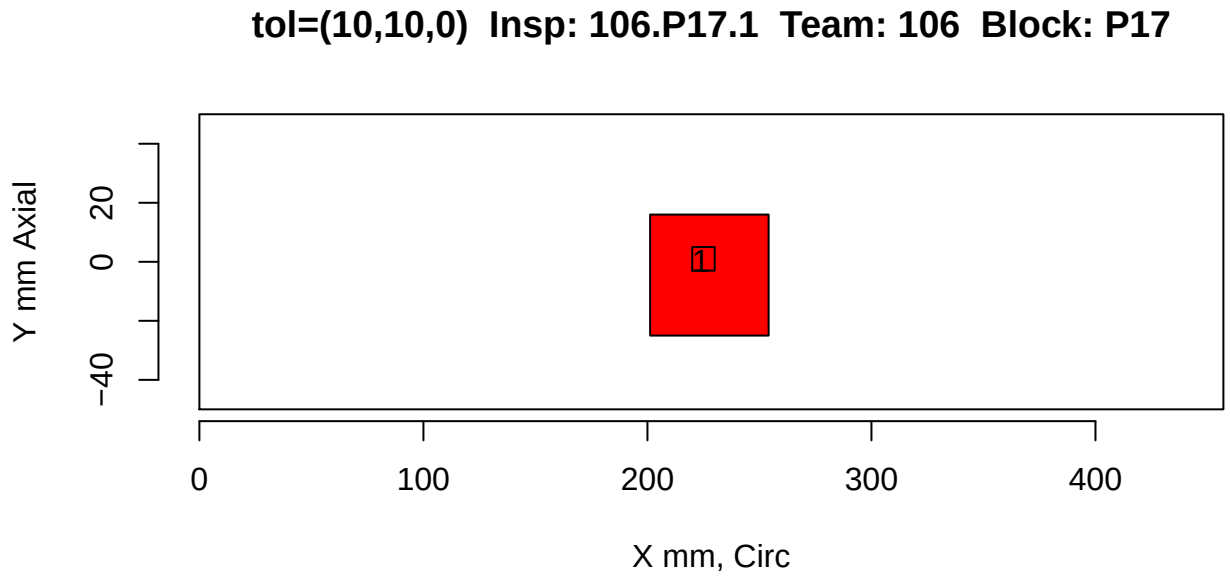
tol=(10,10,0) Insp: 106.P17.1 Team: 106 Block: P17
Y mm Axial
20
0
−40
1
0
100
200
300
400
X mm, Circ

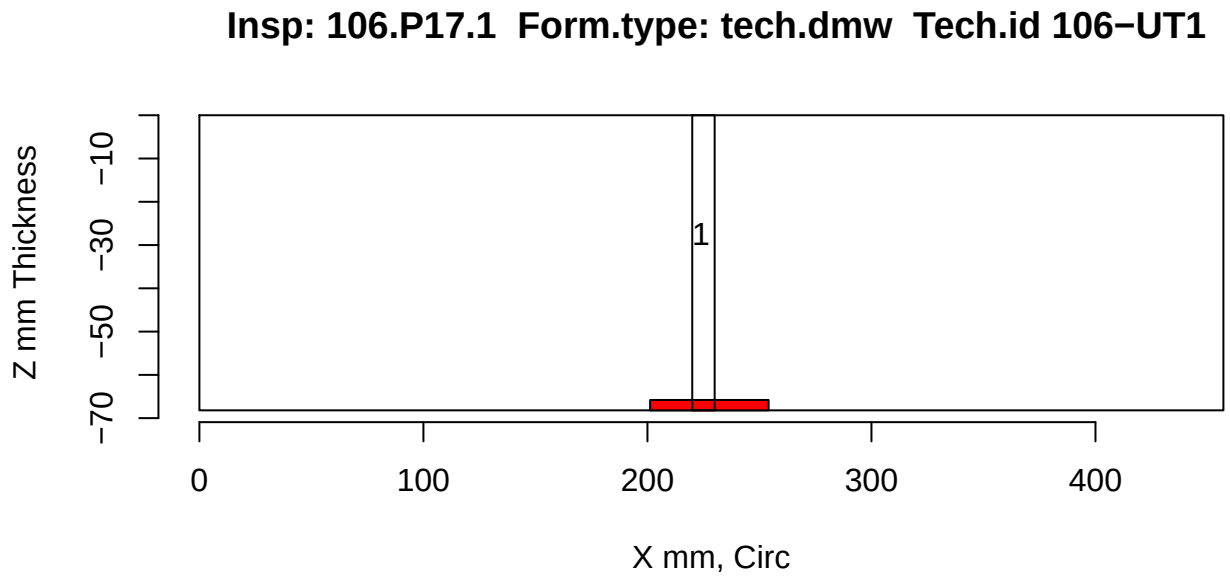
Insp: 106.P17.1 Form.type: tech.dmw Tech.id 106−UT1
Z mm Thickness
−10
−30
−50
−70
1
0
100
200
300
400
X mm, Circ

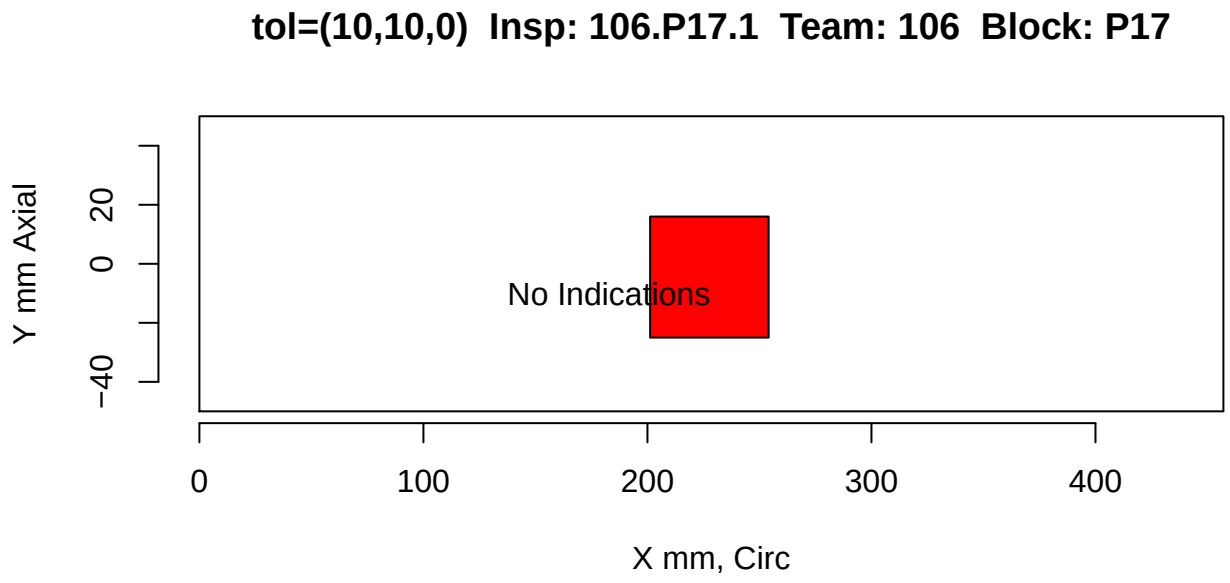
tol=(10,10,0) Insp: 106.P17.1 Team: 106 Block: P17
Y mm Axial
20
0
−40
No Indications
0
100
200
300
400
X mm, Circ

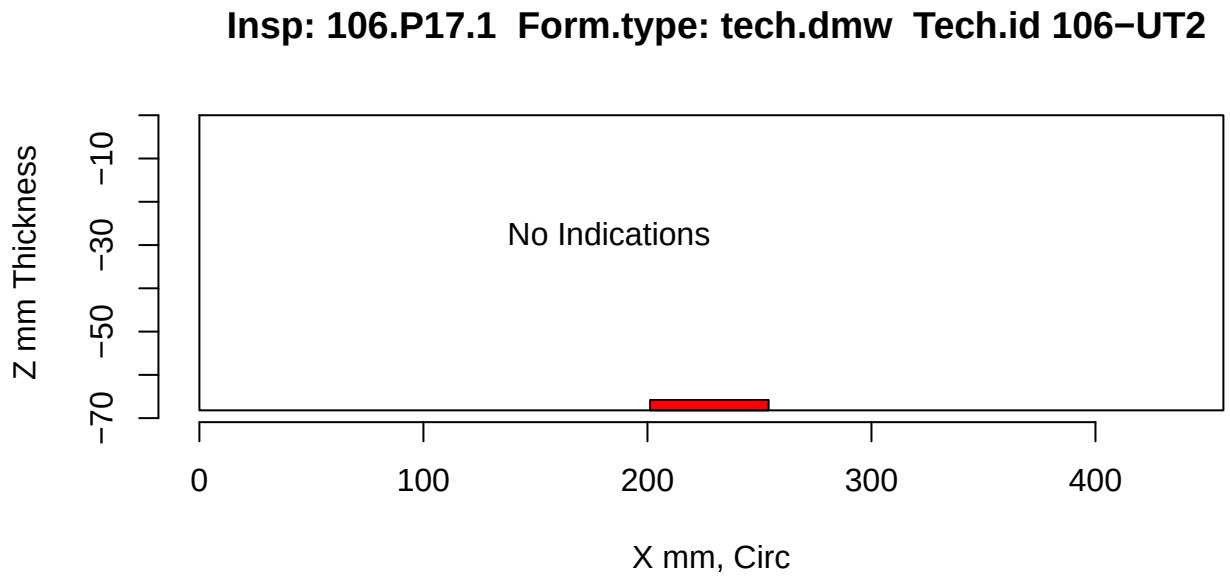
Insp: 106.P17.1 Form.type: tech.dmw Tech.id 106−UT2
Z mm Thickness
−10
−30
−50
−70
No Indications
0
100
200
300
400
X mm, Circ

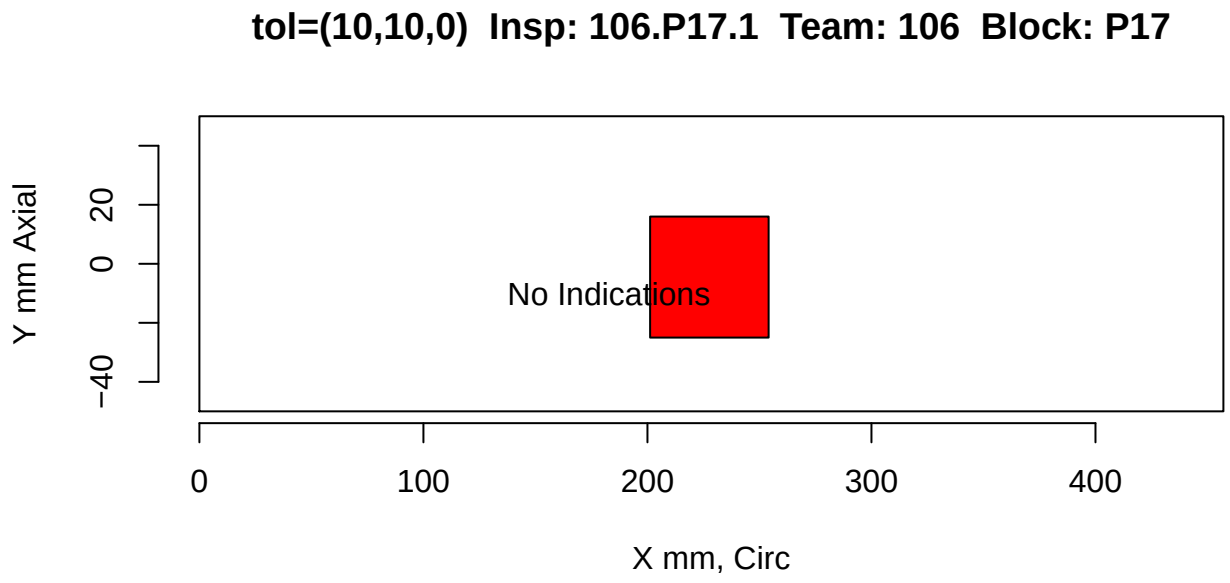
tol=(10,10,0) Insp: 106.P17.1 Team: 106 Block: P17
Y mm Axial
20
0
−40
No Indications
0
100
200
300
400
X mm, Circ

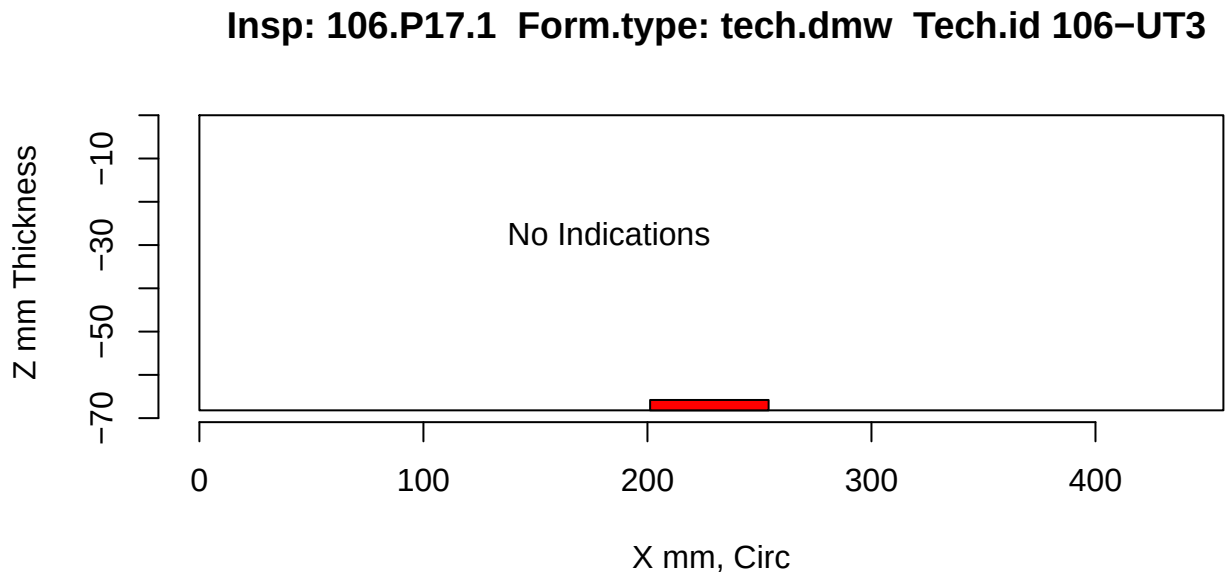
Insp: 106.P17.1 Form.type: tech.dmw Tech.id 106−UT3
Z mm Thickness
−10
−30
−50
−70
No Indications
0
100
200
300
400
X mm, Circ

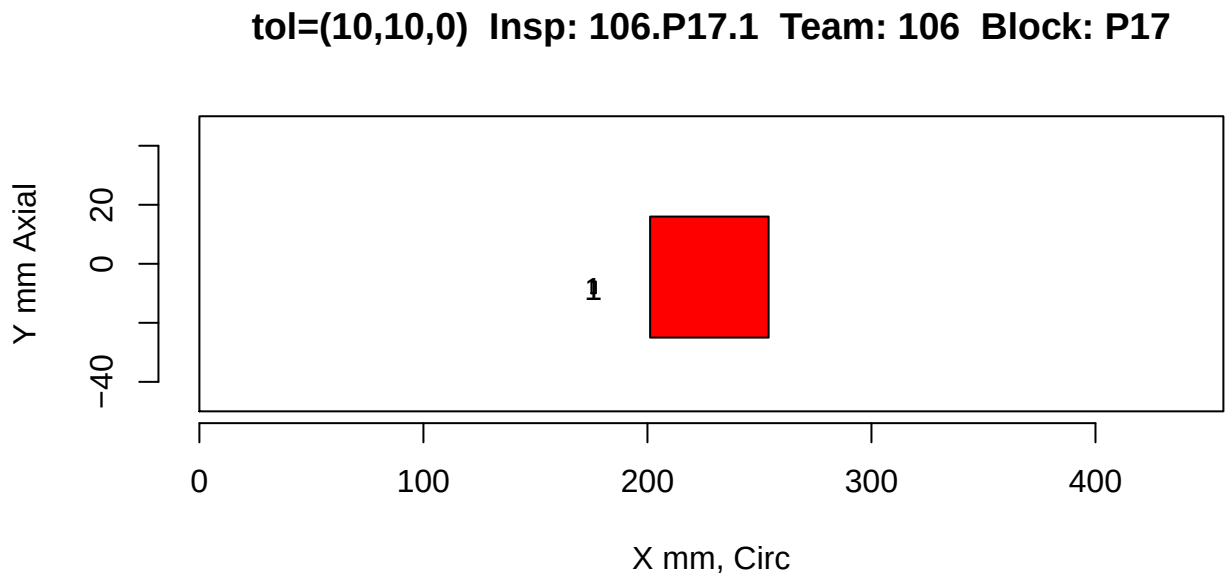
tol=(10,10,0) Insp: 106.P17.1 Team: 106 Block: P17
Y mm Axial
20
0
−40
1
0
100
200
300
400
X mm, Circ

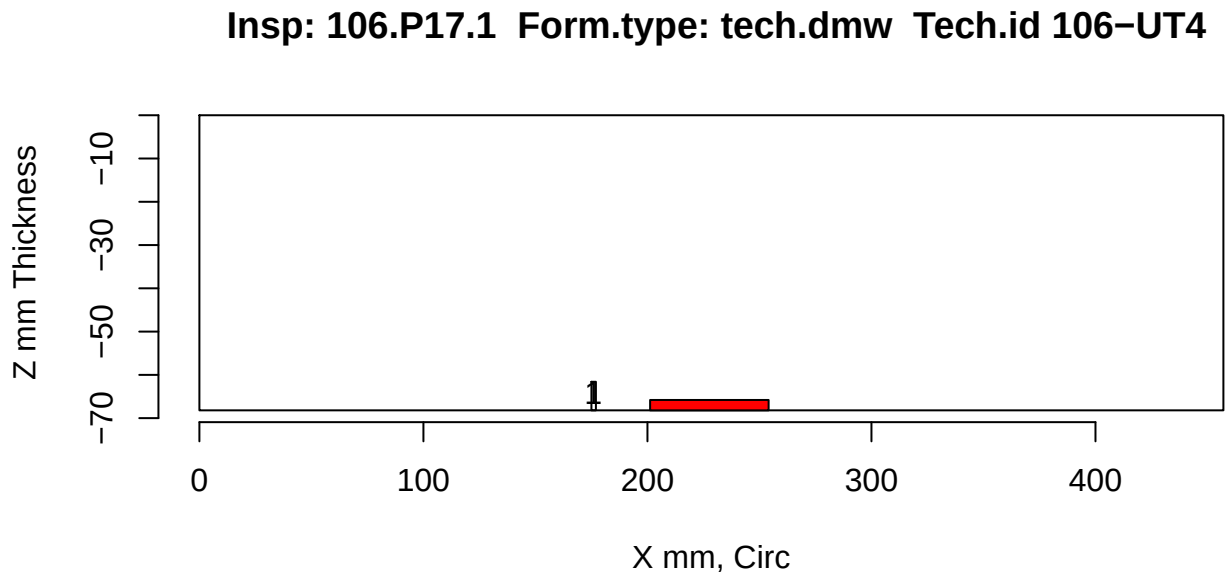
Insp: 106.P17.1 Form.type: tech.dmw Tech.id 106−UT4
Z mm Thickness
−10
−30
−50
−70
1
0
100
200
300
400
X mm, Circ

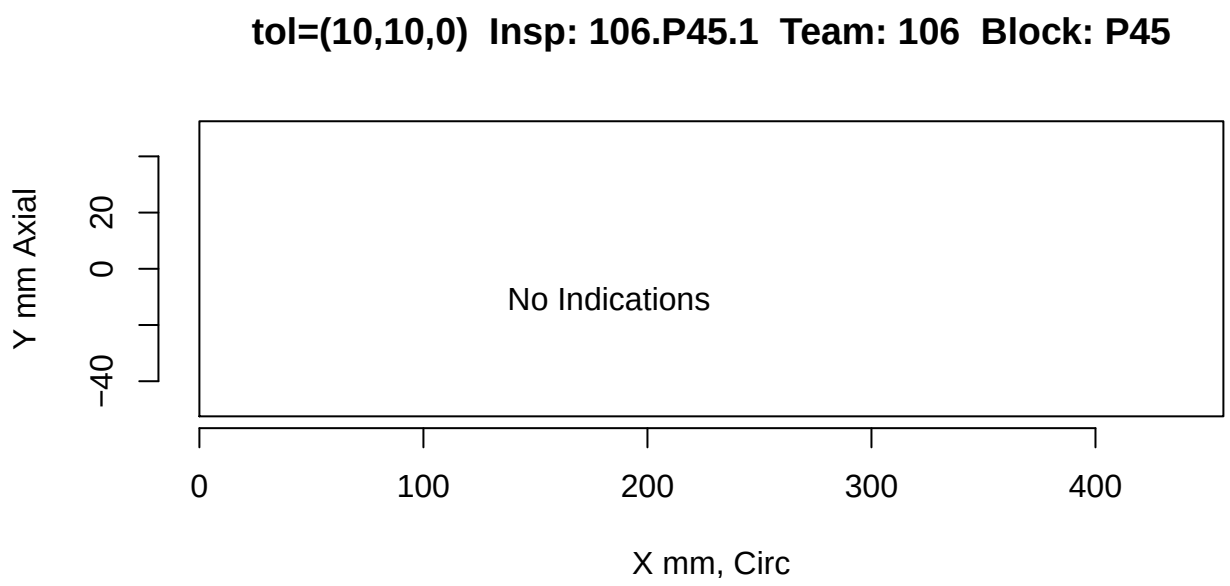
tol=(10,10,0) Insp: 106.P45.1 Team: 106 Block: P45
Y mm Axial
20
0
−40
No Indications
0
100
200
300
400
X mm, Circ

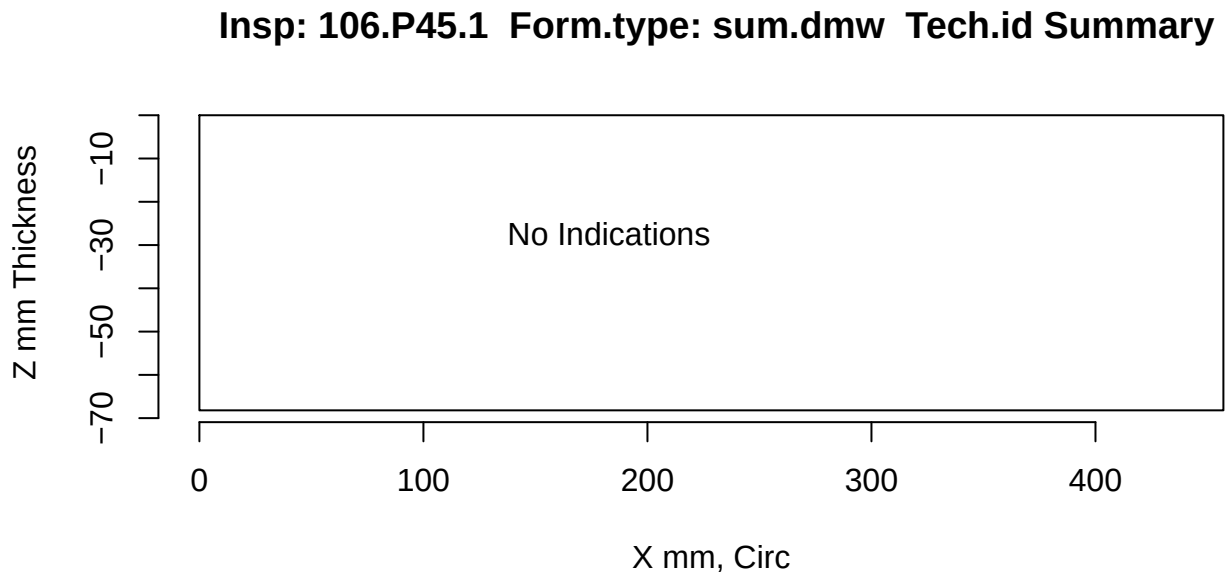
Insp: 106.P45.1 Form.type: sum.dmw Tech.id Summary
Z mm Thickness
−10
−30
−50
−70
No Indications
0
100
200
300
400
X mm, Circ

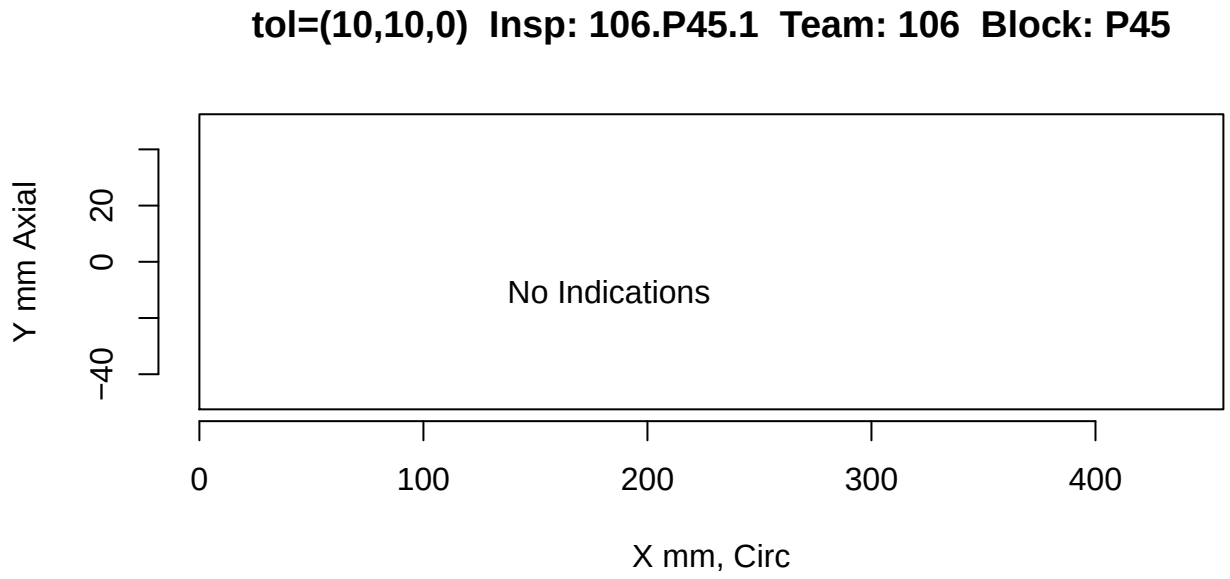
tol=(10,10,0) Insp: 106.P45.1 Team: 106 Block: P45
Y mm Axial
20
0
−40
No Indications
0
100
200
300
400
X mm, Circ

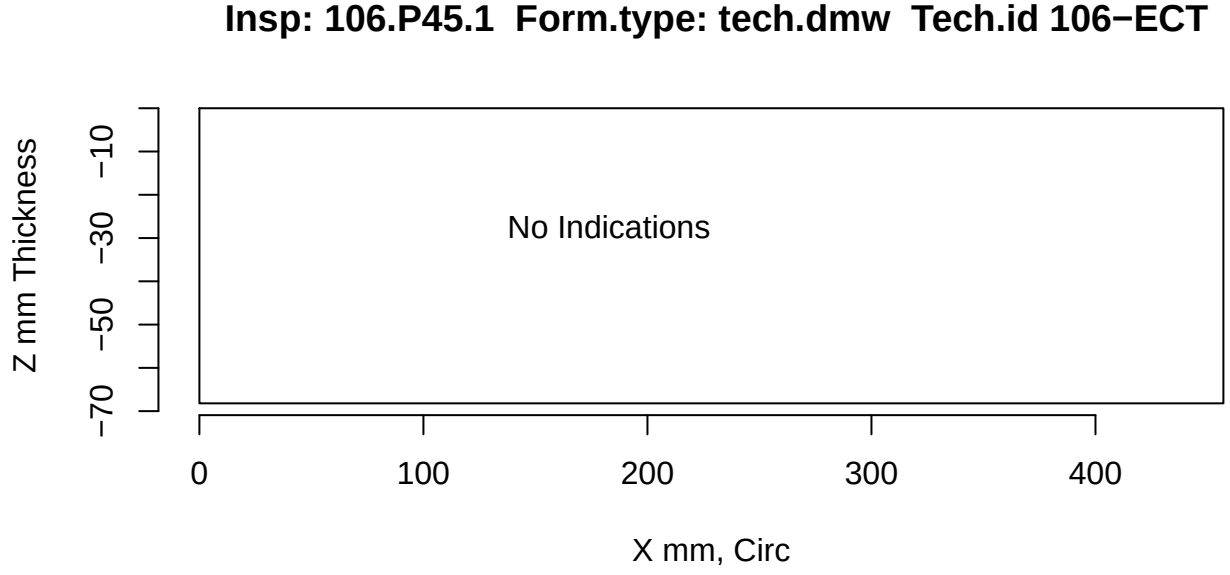
Insp: 106.P45.1 Form.type: tech.dmw Tech.id 106−ECT
Z mm Thickness
−10
−30
−50
−70
No Indications
0
100
200
300
400
X mm, Circ

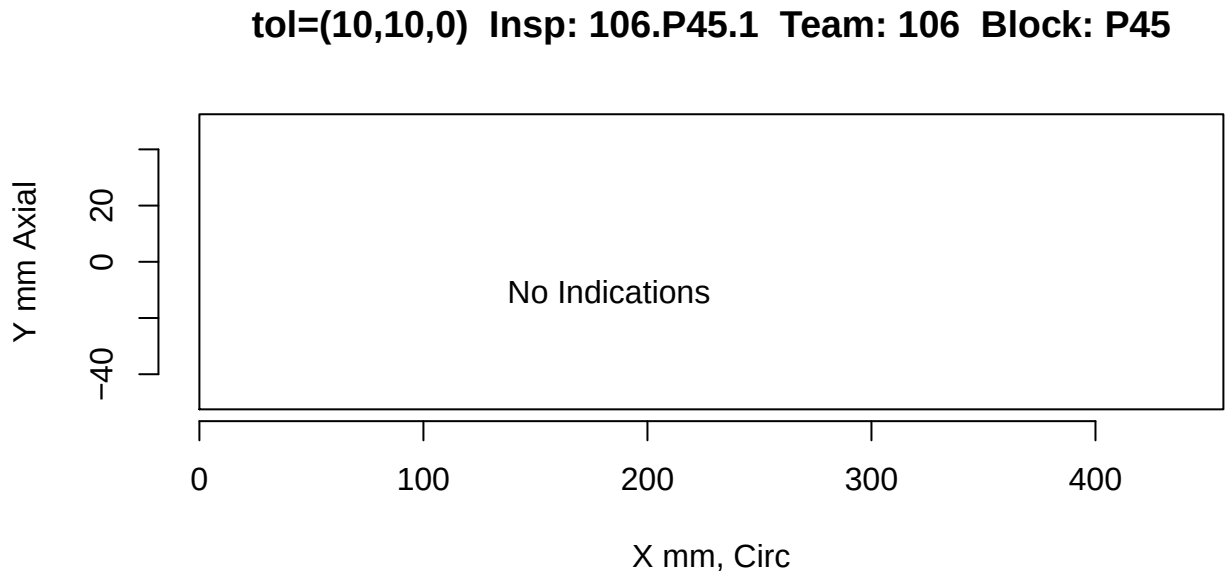
tol=(10,10,0) Insp: 106.P45.1 Team: 106 Block: P45
Y mm Axial
20
0
−40
No Indications
0
100
200
300
400
X mm, Circ

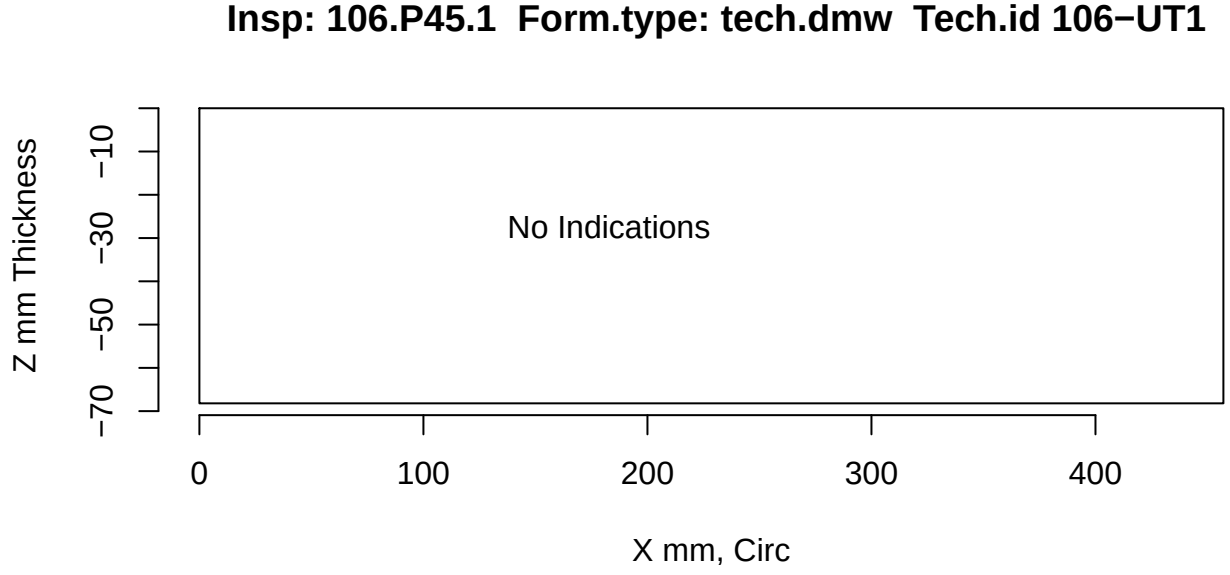
Insp: 106.P45.1 Form.type: tech.dmw Tech.id 106−UT1
Z mm Thickness
−10
−30
−50
−70
No Indications
0
100
200
300
400
X mm, Circ

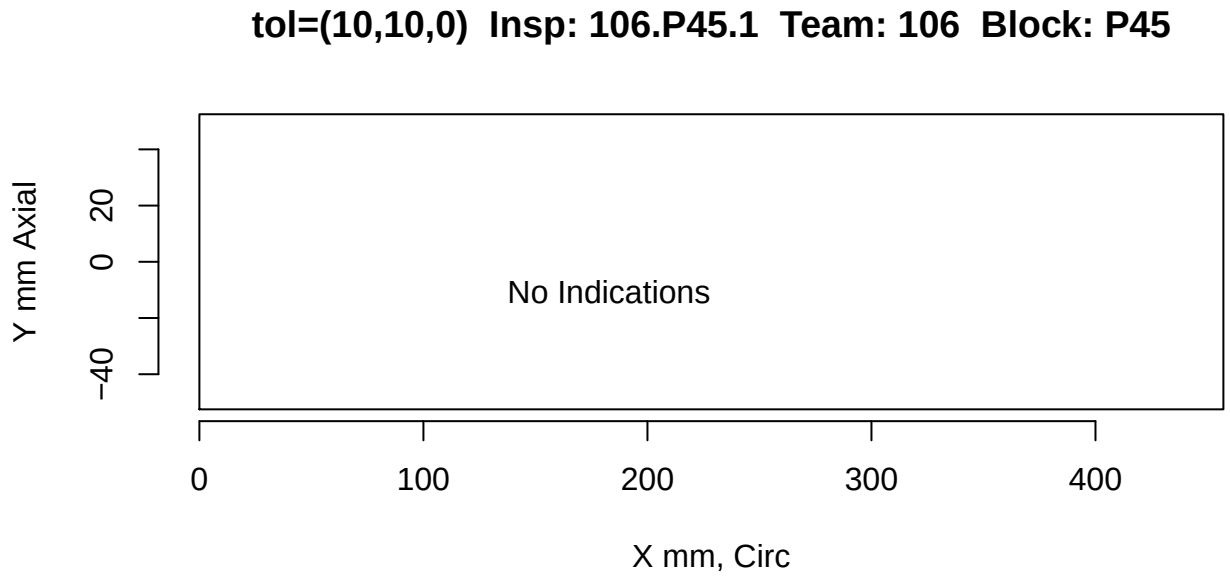
tol=(10,10,0) Insp: 106.P45.1 Team: 106 Block: P45
Y mm Axial
20
0
−40
No Indications
0
100
200
300
400
X mm, Circ

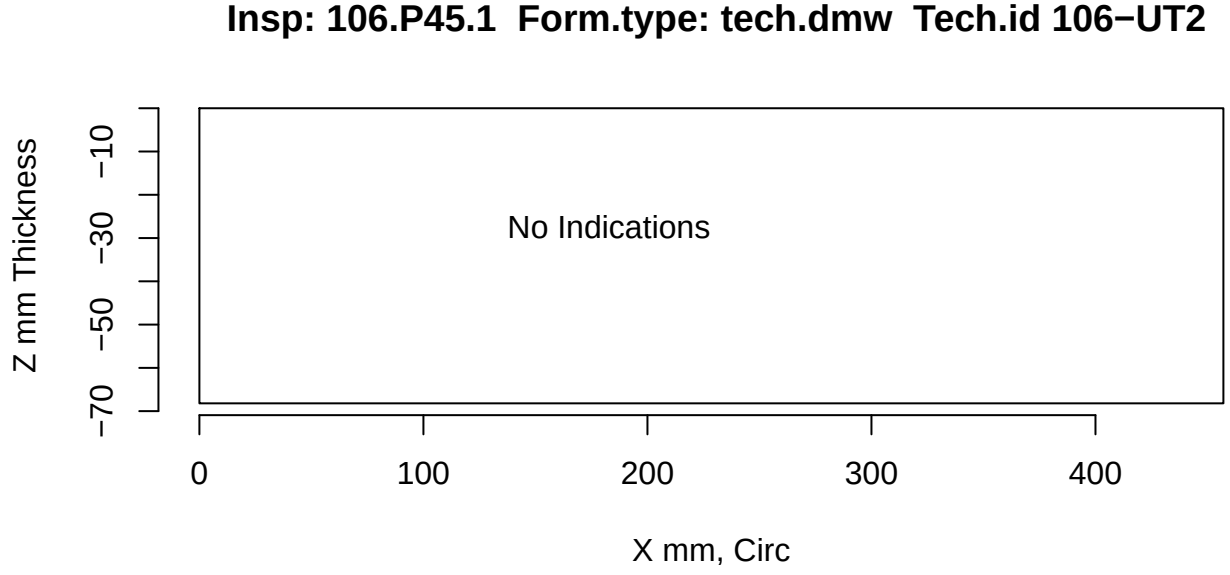
Insp: 106.P45.1 Form.type: tech.dmw Tech.id 106−UT2
Z mm Thickness
−10
−30
−50
−70
No Indications
0
100
200
300
400
X mm, Circ

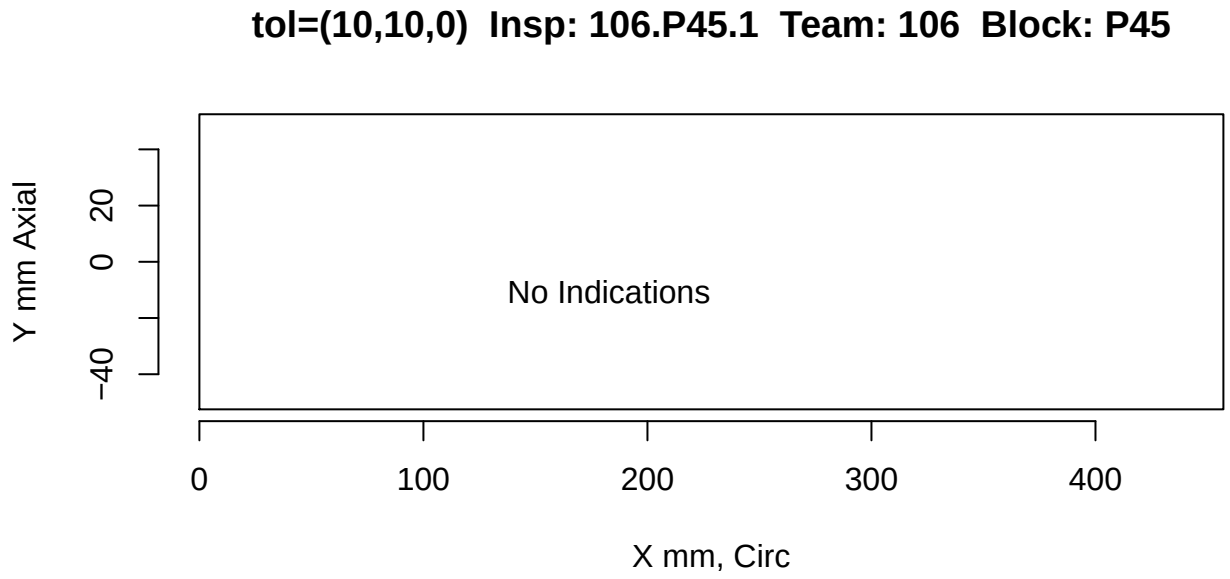
tol=(10,10,0) Insp: 106.P45.1 Team: 106 Block: P45
Y mm Axial
20
0
−40
No Indications
0
100
200
300
400
X mm, Circ

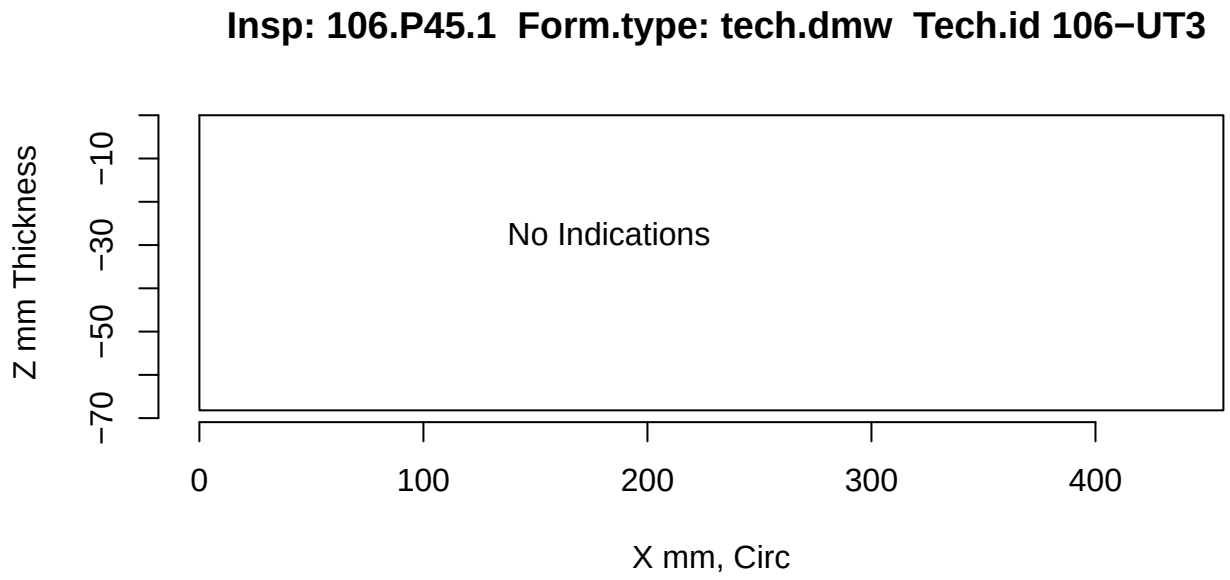
Insp: 106.P45.1 Form.type: tech.dmw Tech.id 106−UT3
Z mm Thickness
−10
−30
−50
−70
No Indications
0
100
200
300
400
X mm, Circ

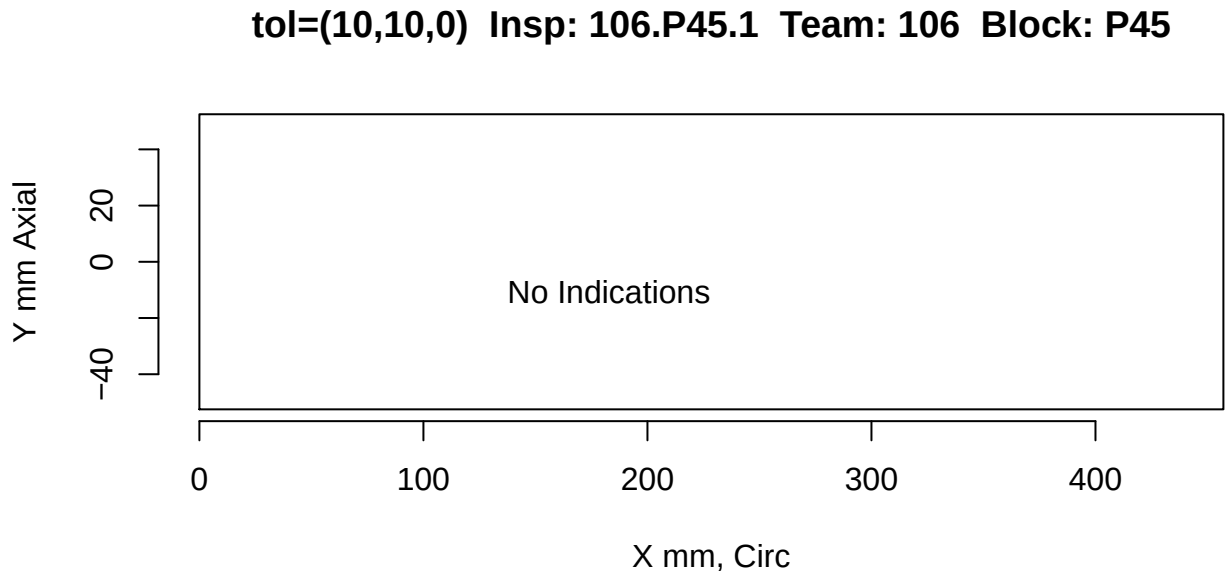
tol=(10,10,0) Insp: 106.P45.1 Team: 106 Block: P45
Y mm Axial
20
0
−40
No Indications
0
100
200
300
400
X mm, Circ

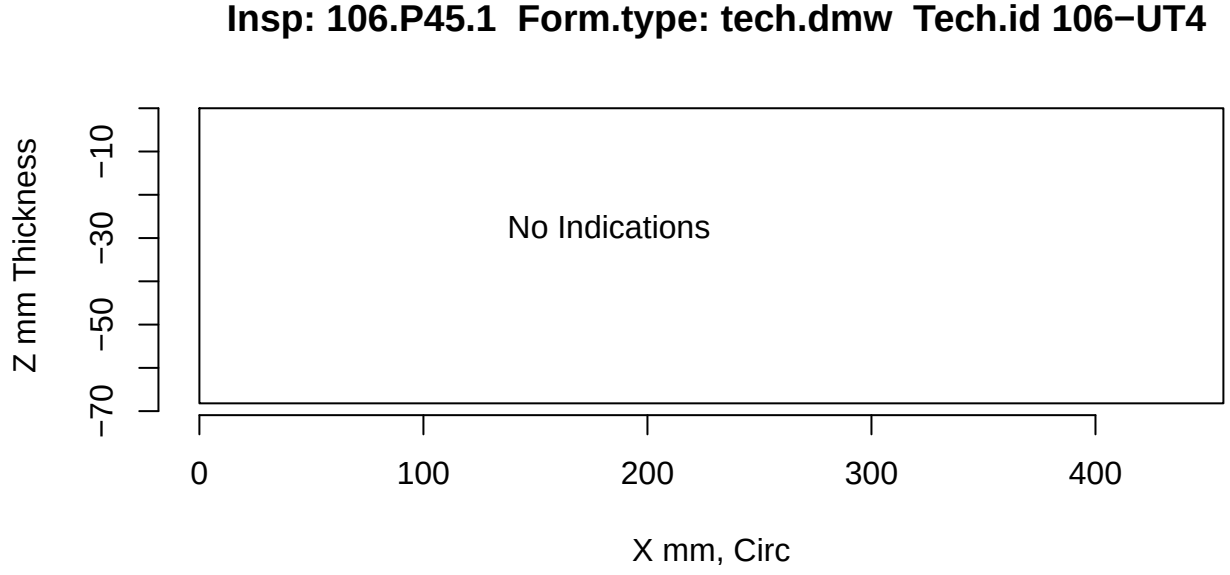
Insp: 106.P45.1 Form.type: tech.dmw Tech.id 106−UT4
Z mm Thickness
−10
−30
−50
−70
No Indications
0
100
200
300
400
X mm, Circ

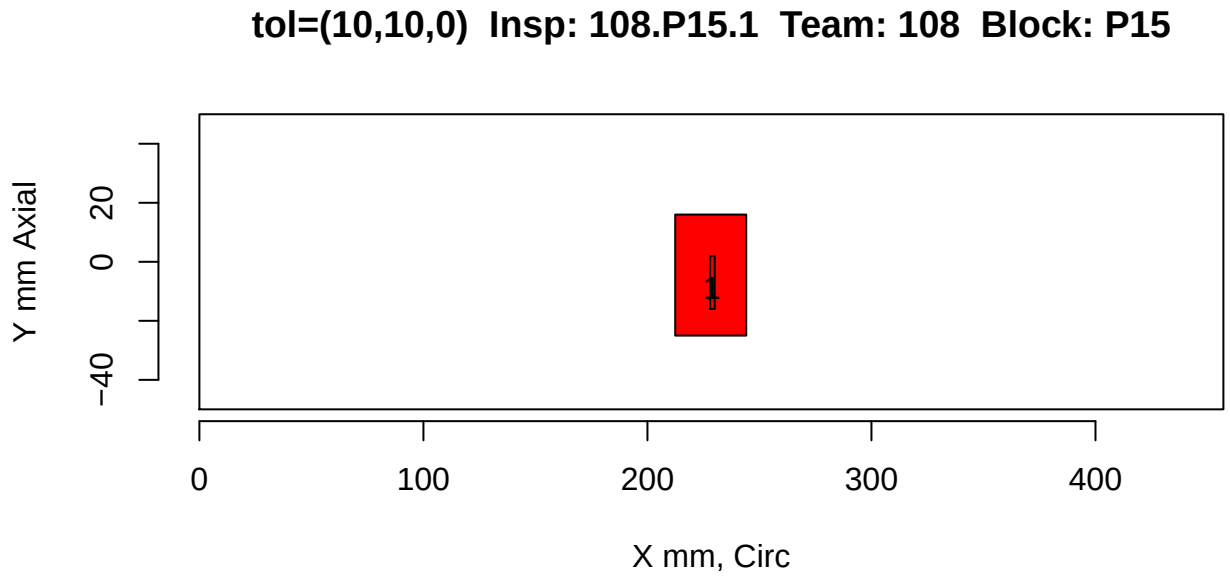
tol=(10,10,0) Insp: 108.P15.1 Team: 108 Block: P15
Y mm Axial
20
0
−40
1
0
100
200
300
400
X mm, Circ

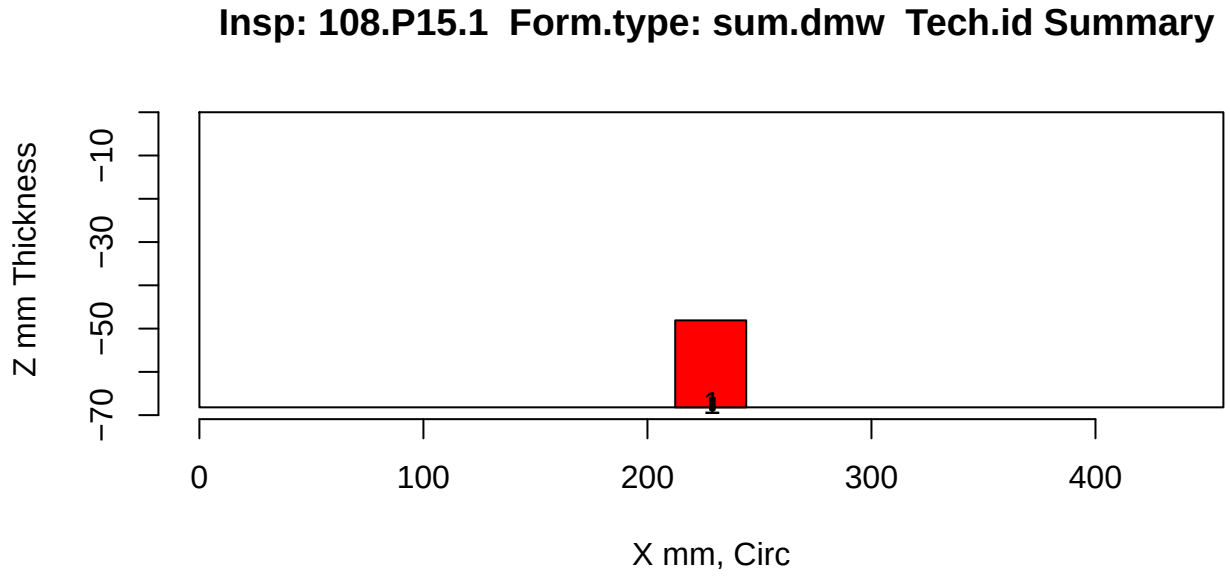
Insp: 108.P15.1 Form.type: sum.dmw Tech.id Summary
Z mm Thickness
−10
−30
−50
−70
1
0
100
200
300
400
X mm, Circ

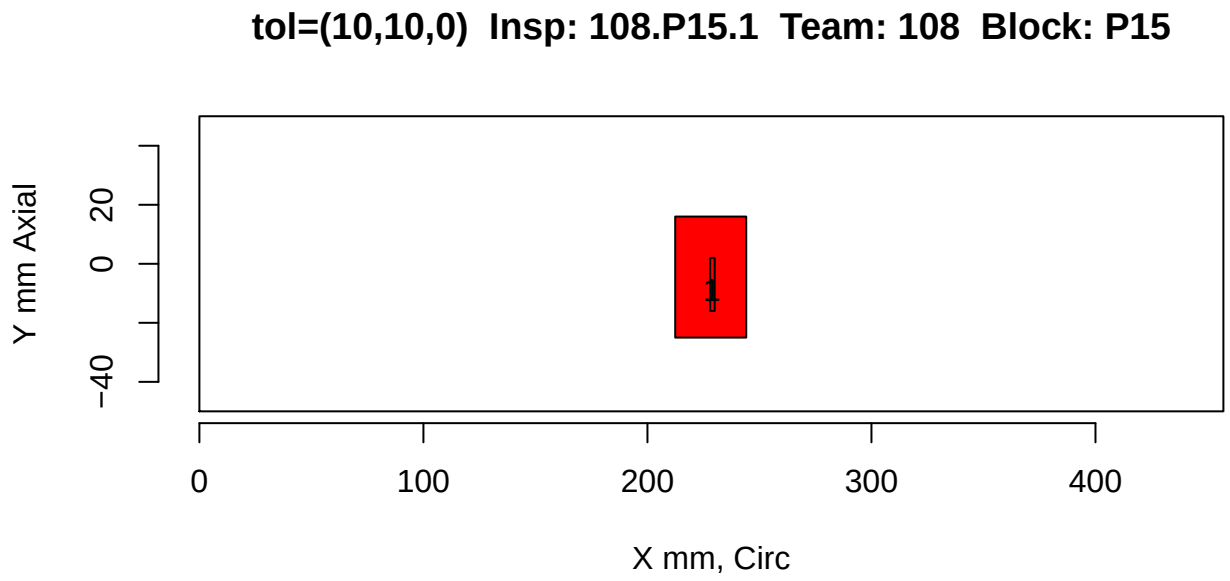
tol=(10,10,0) Insp: 108.P15.1 Team: 108 Block: P15
Y mm Axial
−40
0
20
1
0
100
200
300
400
X mm, Circ

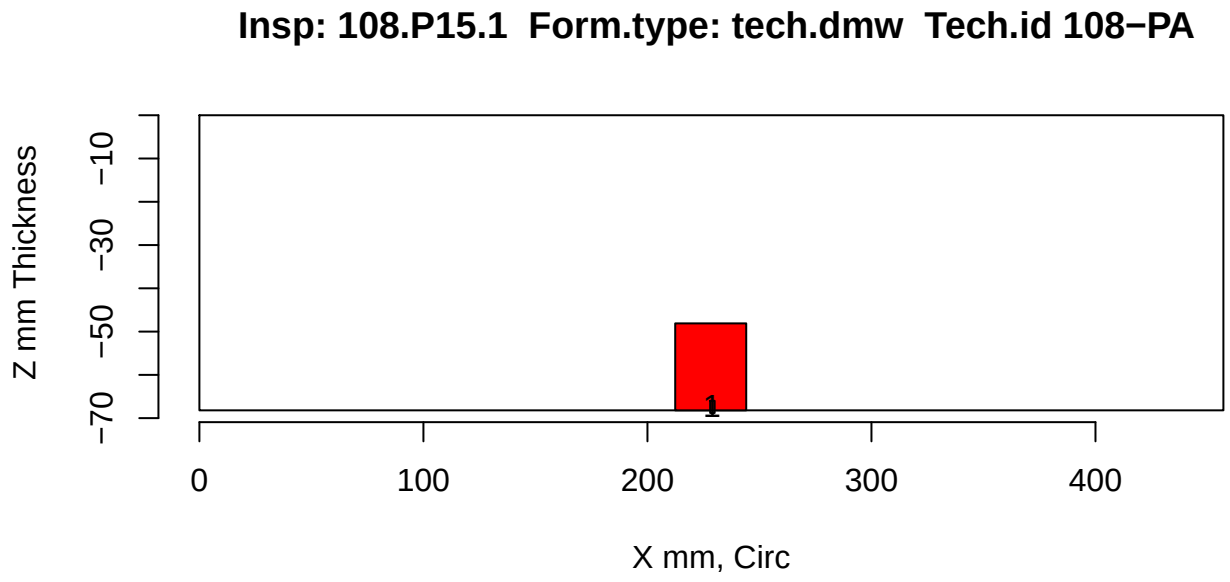
Insp: 108.P15.1 Form.type: tech.dmw Tech.id 108−PA
Z mm Thickness
−70
−50
−30
−10
1
0
100
200
300
400
X mm, Circ

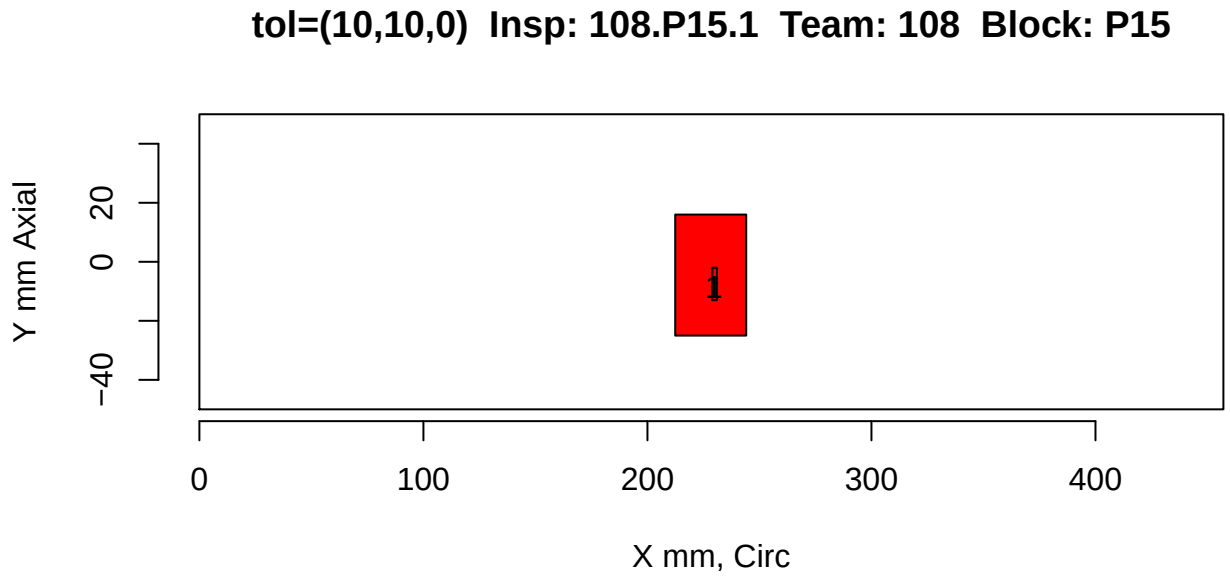
tol=(10,10,0) Insp: 108.P15.1 Team: 108 Block: P15
Y mm Axial
20
0
−40
1
0
100
200
300
400
X mm, Circ

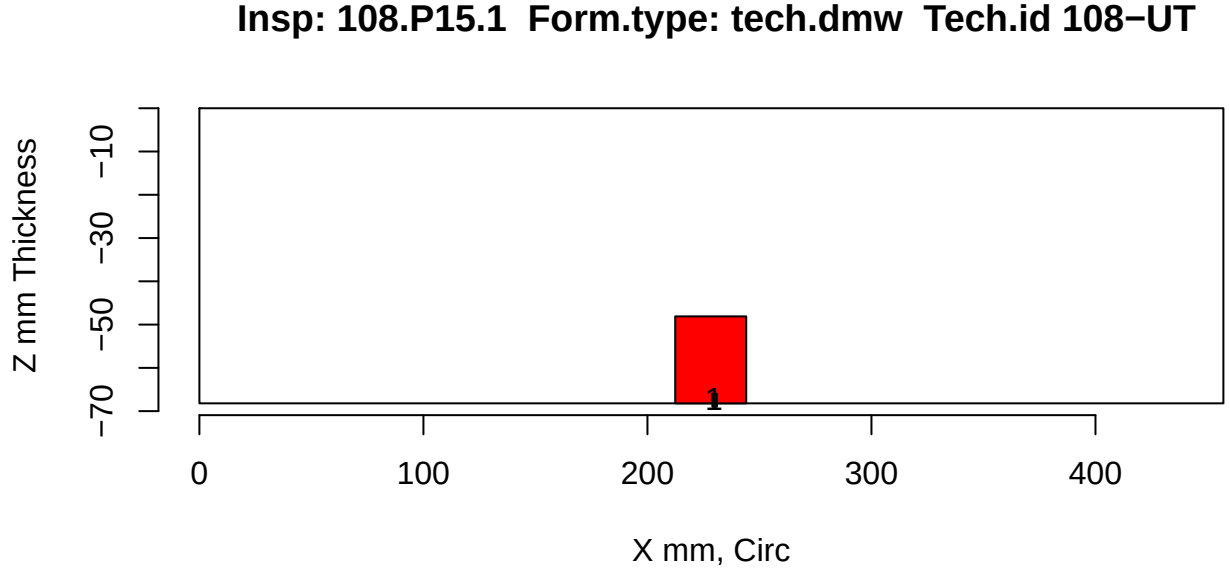
Insp: 108.P15.1 Form.type: tech.dmw Tech.id 108−UT
Z mm Thickness
−10
−30
−50
−70
1
0
100
200
300
400
X mm, Circ

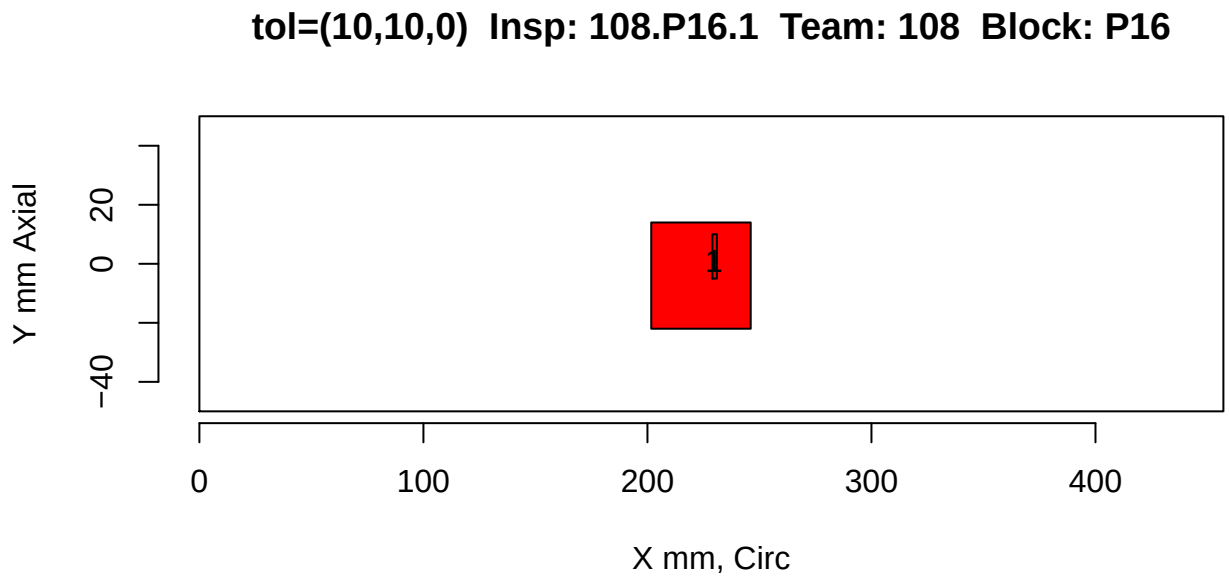
tol=(10,10,0) Insp: 108.P16.1 Team: 108 Block: P16
Y mm Axial
−40
0
20
1
0
100
200
300
400
X mm, Circ

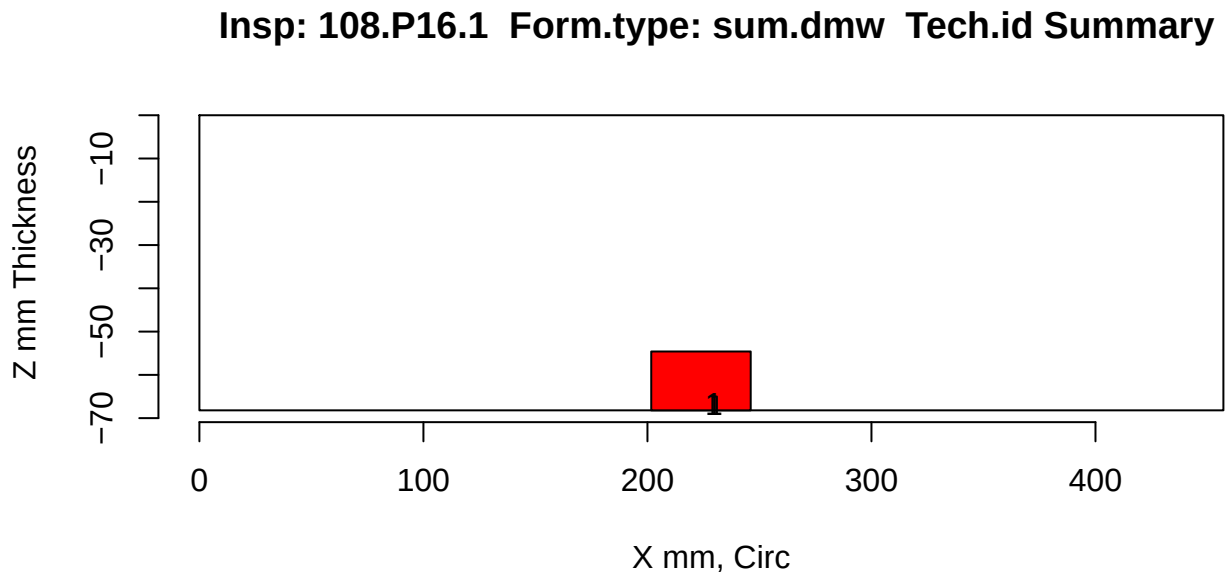
Insp: 108.P16.1 Form.type: sum.dmw Tech.id Summary
Z mm Thickness
−70
−50
−30
−10
1
0
100
200
300
400
X mm, Circ

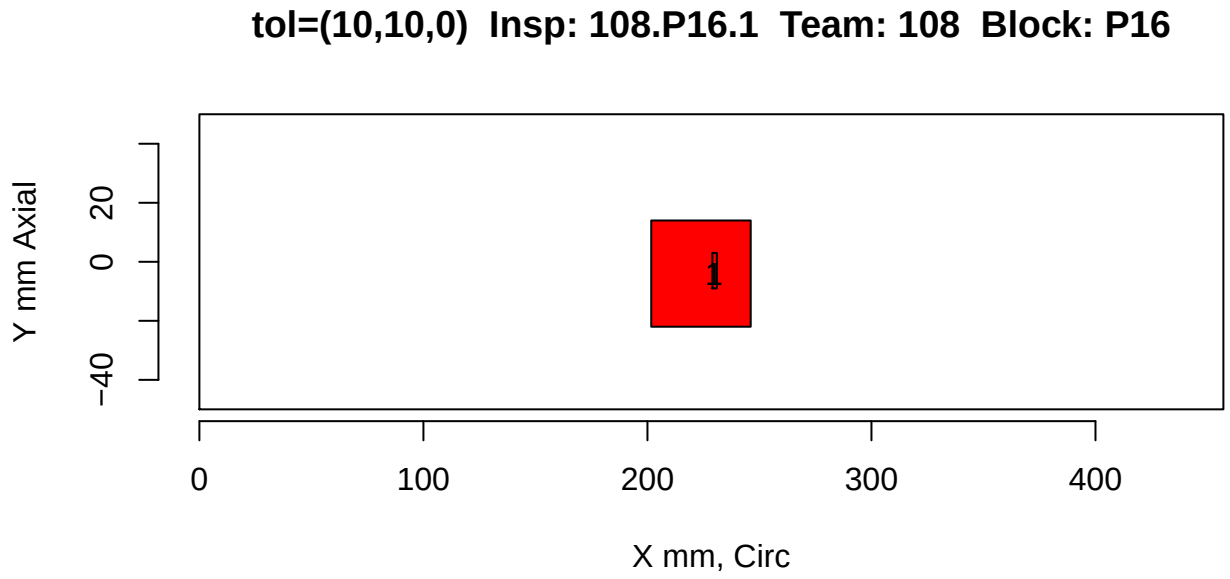
tol=(10,10,0) Insp: 108.P16.1 Team: 108 Block: P16
Y mm Axial
20
0
−40
1
0
100
200
300
400
X mm, Circ

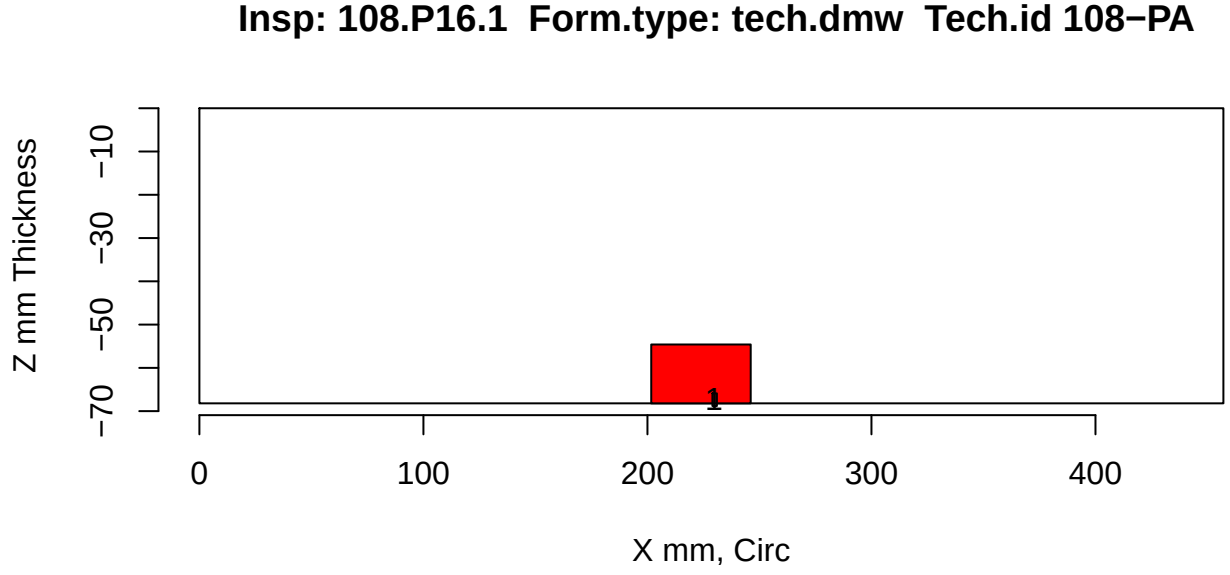
Insp: 108.P16.1 Form.type: tech.dmw Tech.id 108−PA
Z mm Thickness
−10
−30
−50
−70
1
0
100
200
300
400
X mm, Circ

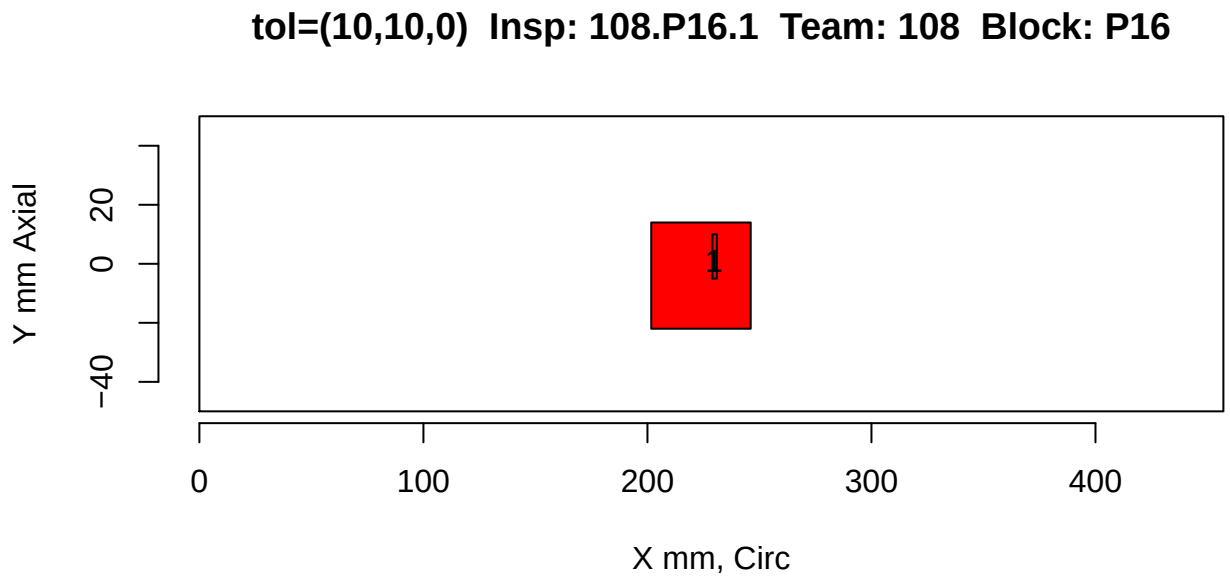
tol=(10,10,0) Insp: 108.P16.1 Team: 108 Block: P16
Y mm Axial
20
0
−40
1
0
100
200
300
400
X mm, Circ

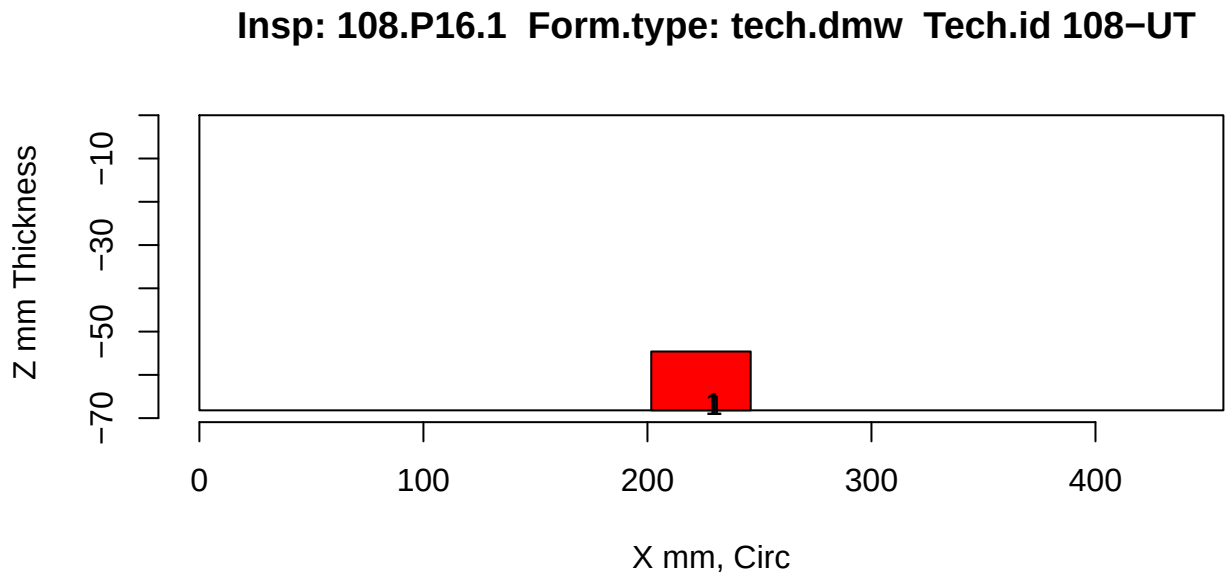
Insp: 108.P16.1 Form.type: tech.dmw Tech.id 108−UT
Z mm Thickness
−10
−30
−50
−70
1
0
100
200
300
400
X mm, Circ

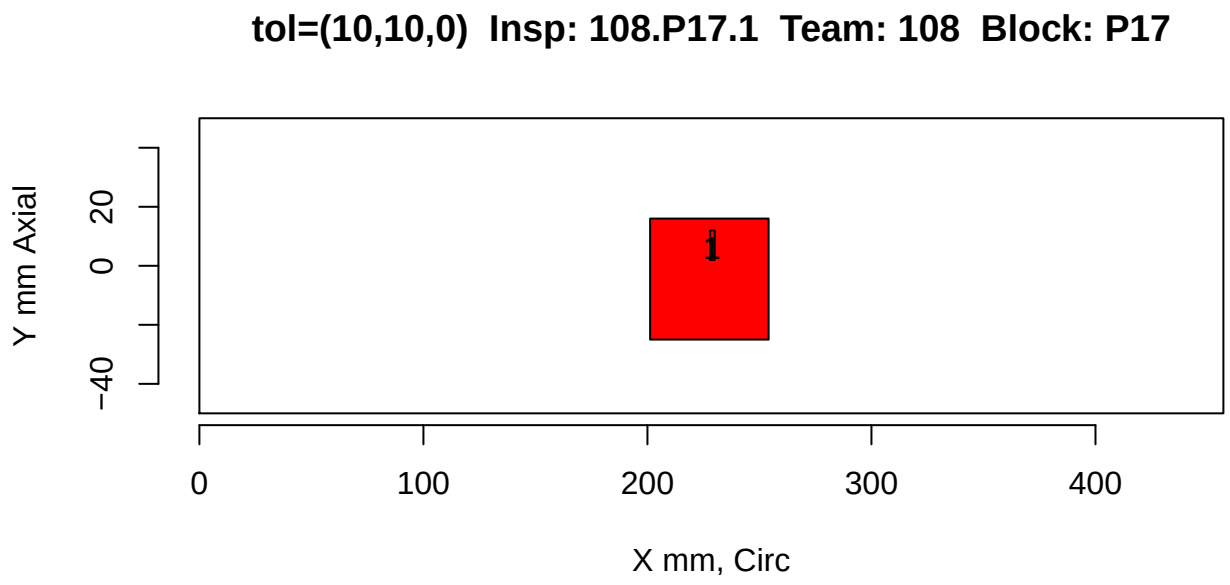
tol=(10,10,0) Insp: 108.P17.1 Team: 108 Block: P17
Y mm Axial
20
0
−40
1
0
100
200
300
400
X mm, Circ

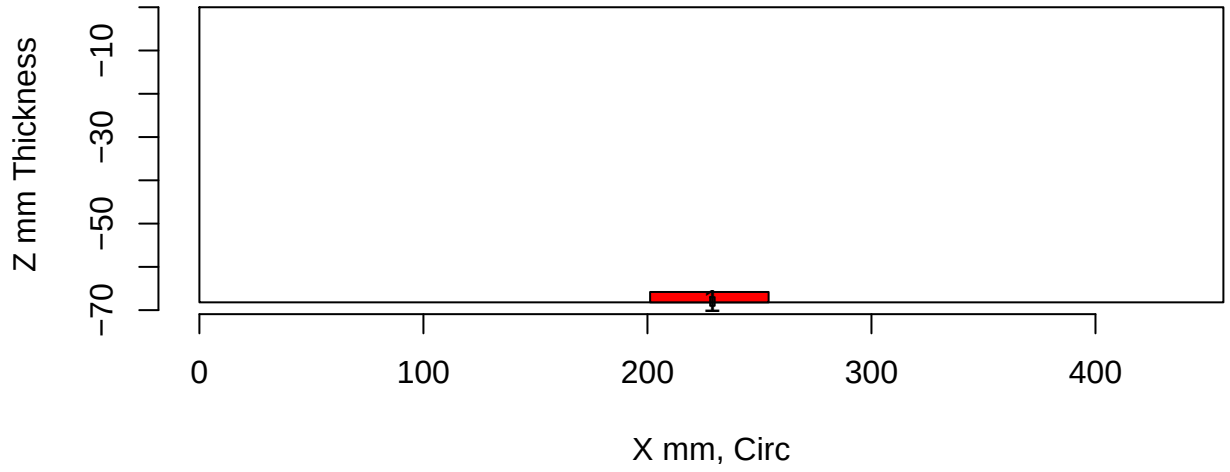
Insp: 108.P17.1 Form.type: sum.dmw Tech.id Summary
Z mm Thickness
−10
−30
−50
−70
1
0
100
200
300
400
X mm, Circ

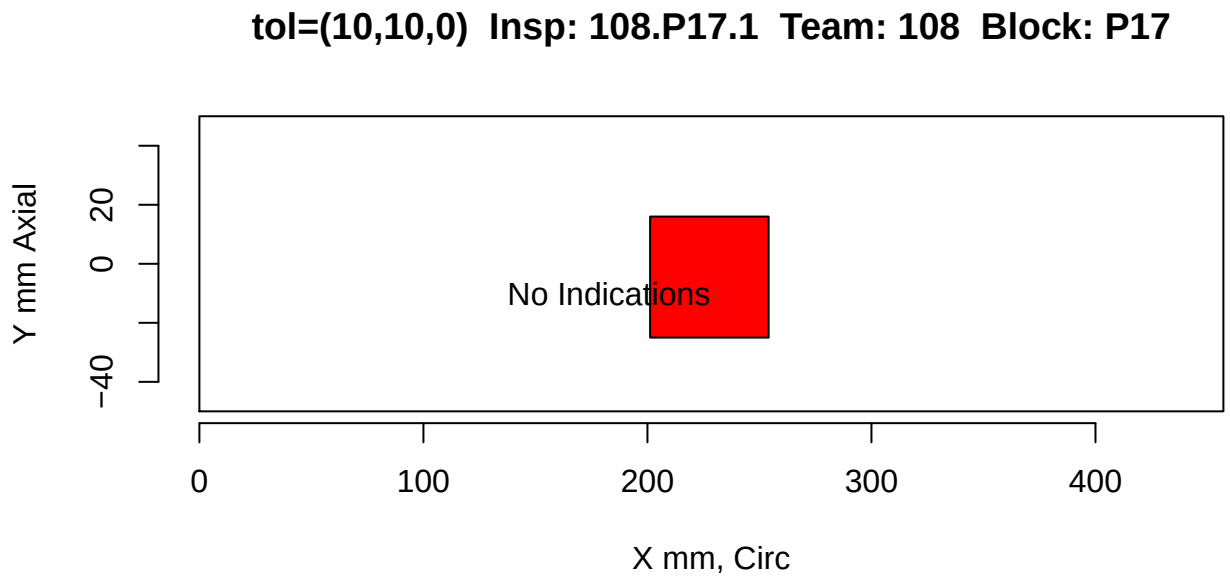
tol=(10,10,0) Insp: 108.P17.1 Team: 108 Block: P17
Y mm Axial
20
0
−40
No Indications
0
100
200
300
400
X mm, Circ

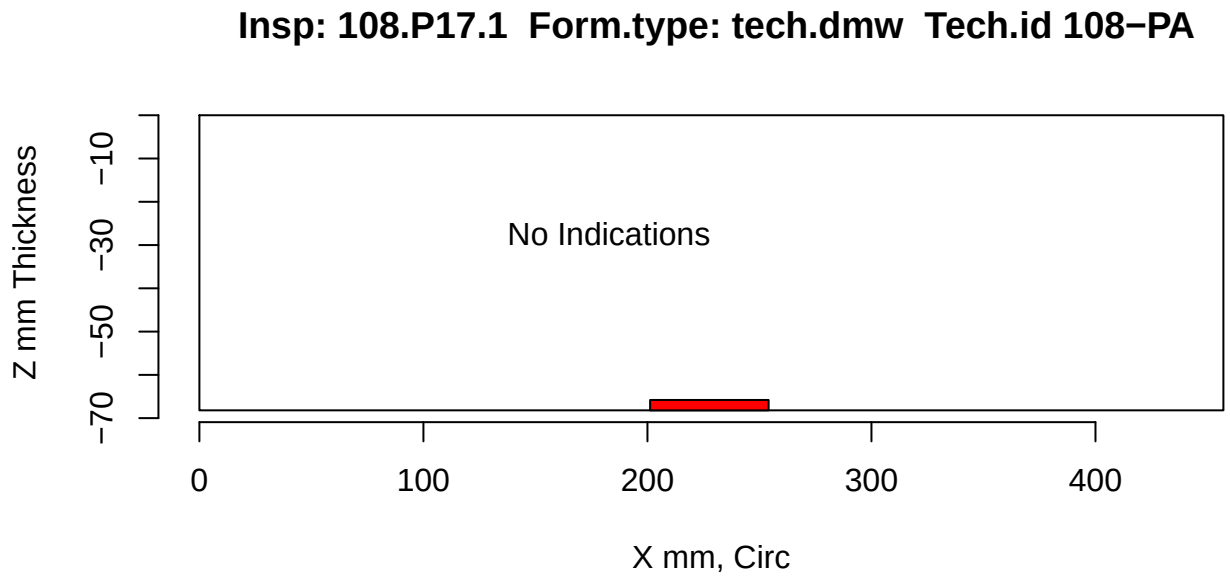
Insp: 108.P17.1 Form.type: tech.dmw Tech.id 108−PA
Z mm Thickness
−10
−30
−50
−70
No Indications
0
100
200
300
400
X mm, Circ

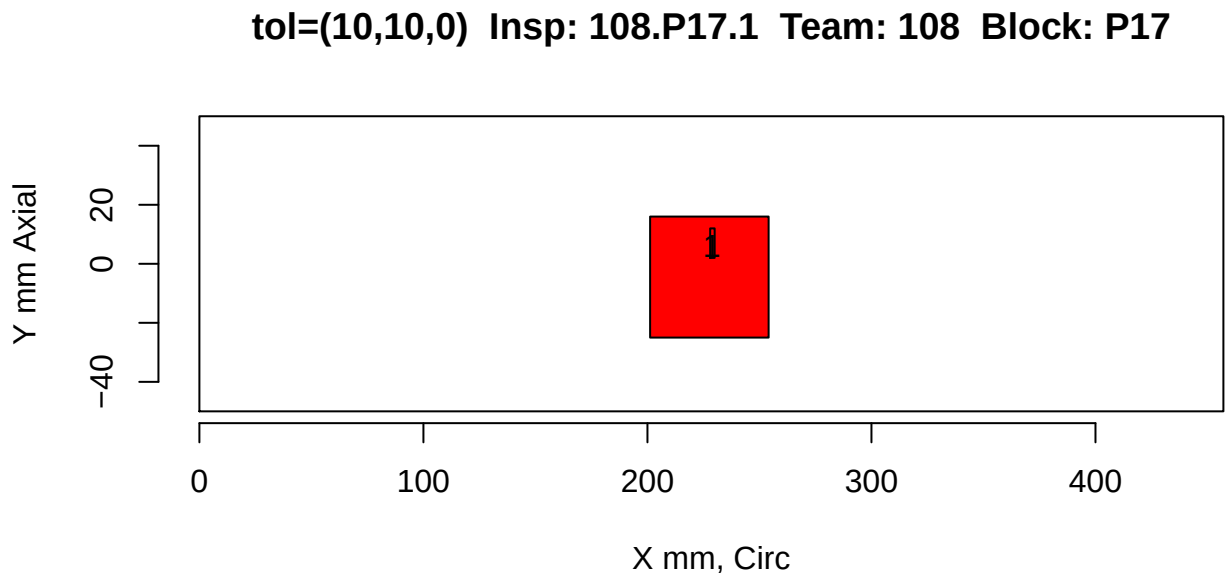
tol=(10,10,0) Insp: 108.P17.1 Team: 108 Block: P17
Y mm Axial
20
0
−40
1
0
100
200
300
400
X mm, Circ

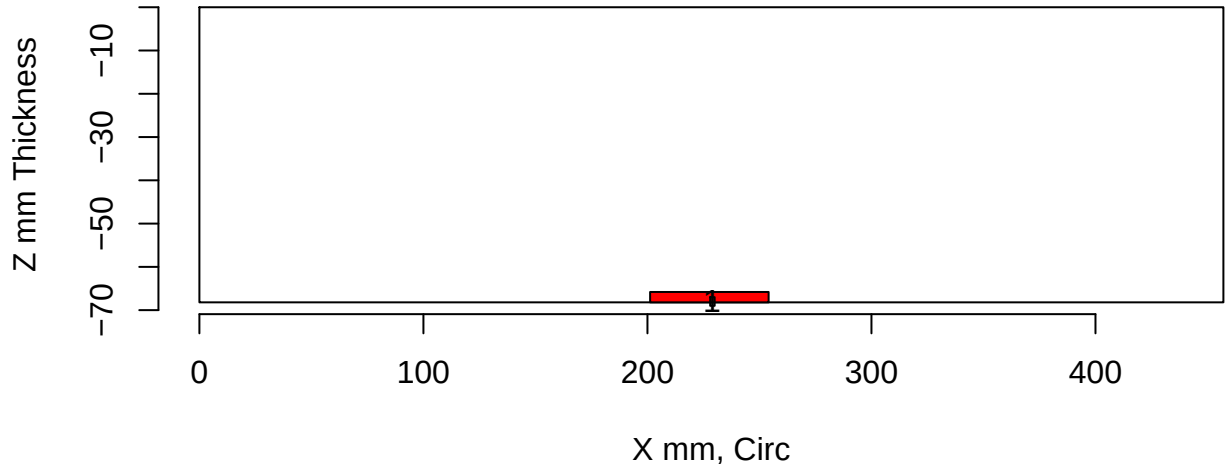
Insp: 108.P17.1 Form.type: tech.dmw Tech.id 108−UT
Z mm Thickness
−10
−30
−50
−70
1
0
100
200
300
400
X mm, Circ

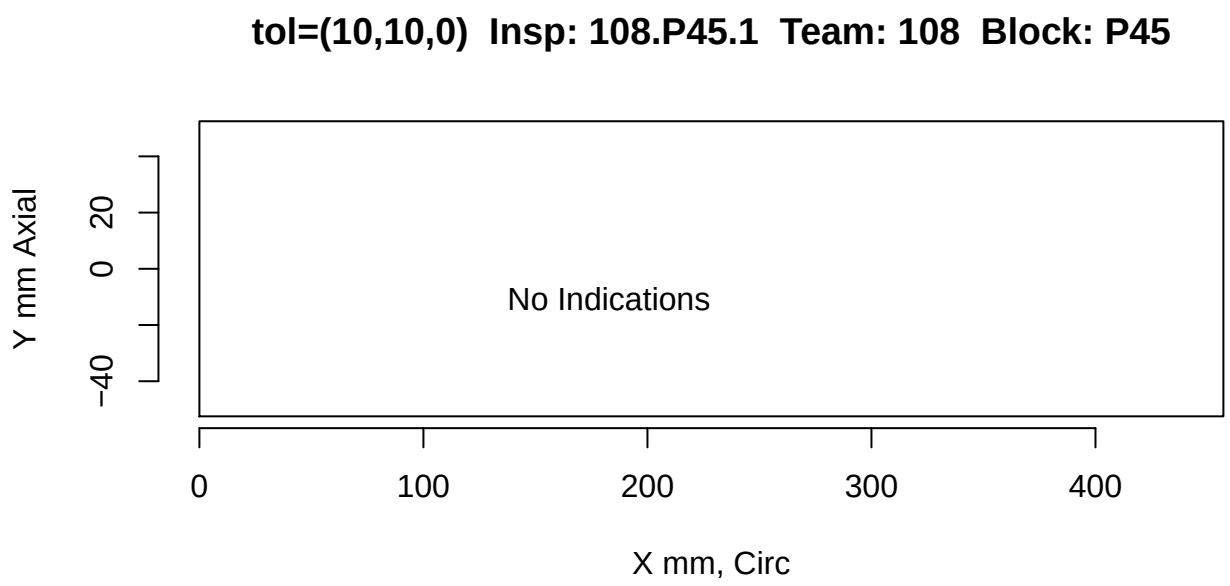
tol=(10,10,0) Insp: 108.P45.1 Team: 108 Block: P45
Y mm Axial
20
0
−40
No Indications
0
100
200
300
400
X mm, Circ

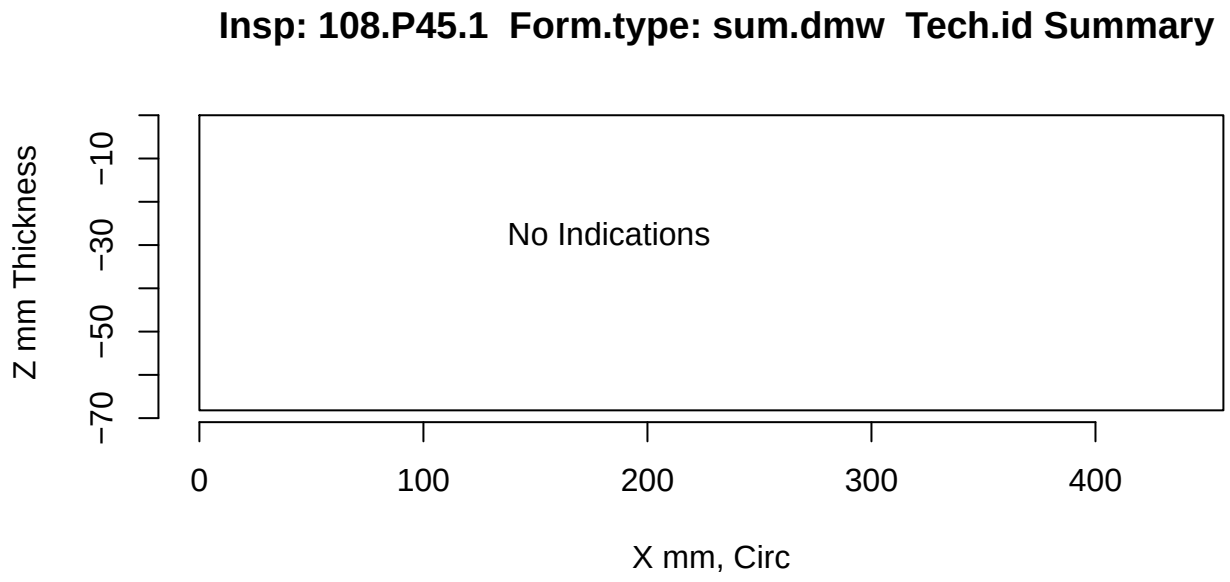
Insp: 108.P45.1 Form.type: sum.dmw Tech.id Summary
Z mm Thickness
−10
−30
−50
−70
No Indications
0
100
200
300
400
X mm, Circ

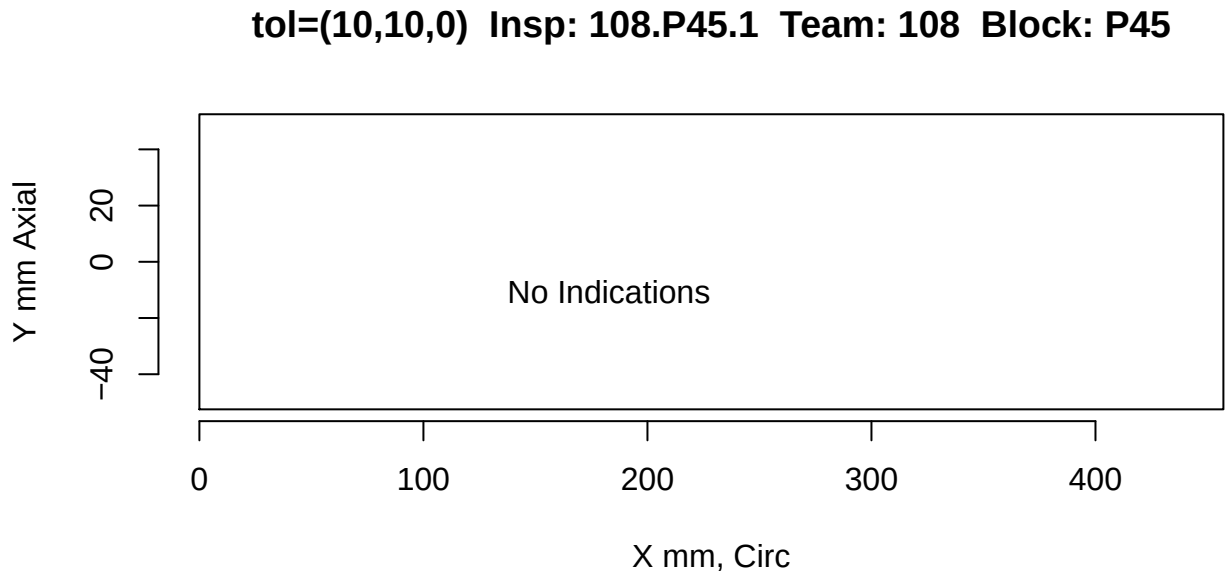
tol=(10,10,0) Insp: 108.P45.1 Team: 108 Block: P45
Y mm Axial
20
0
−40
No Indications
0
100
200
300
400
X mm, Circ

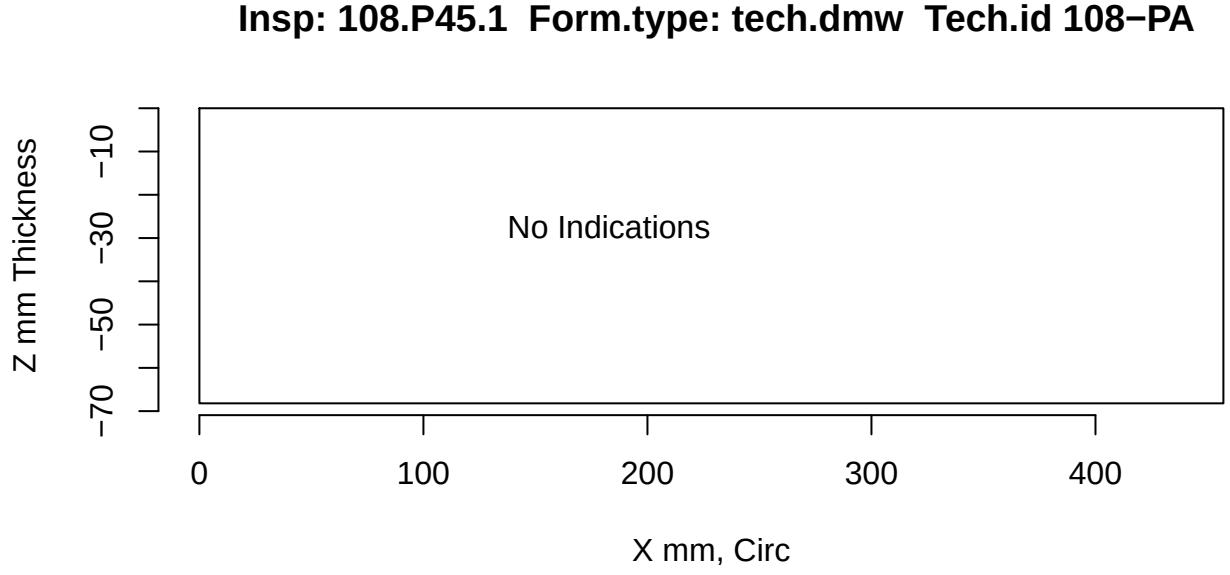
Insp: 108.P45.1 Form.type: tech.dmw Tech.id 108−PA
Z mm Thickness
−10
−30
−50
−70
No Indications
0
100
200
300
400
X mm, Circ

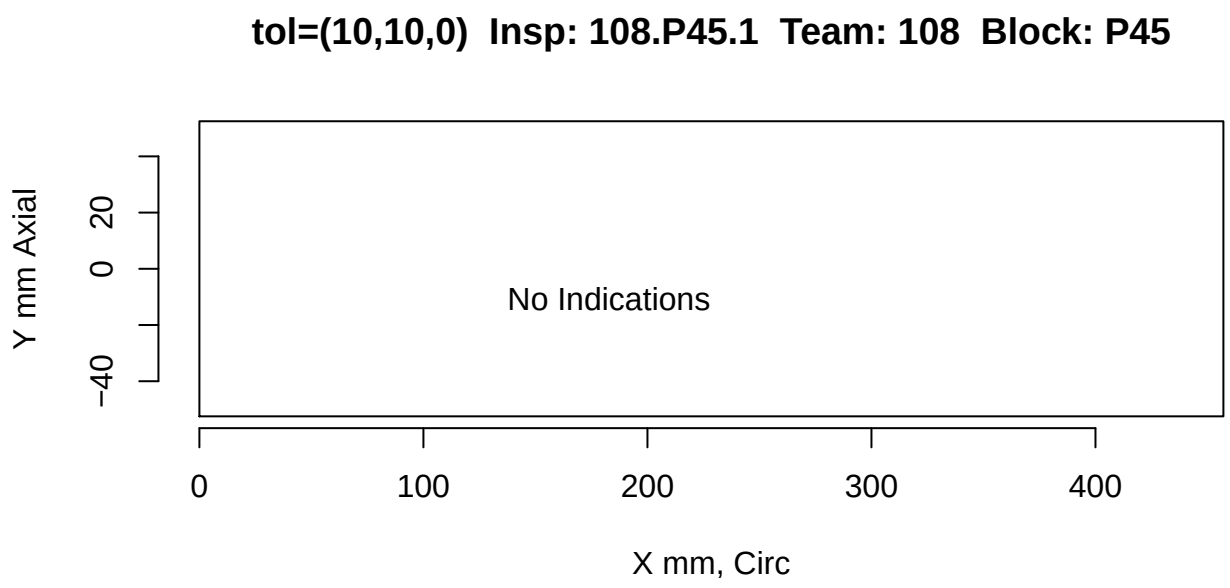
tol=(10,10,0) Insp: 108.P45.1 Team: 108 Block: P45
Y mm Axial
20
0
−40
No Indications
0
100
200
300
400
X mm, Circ

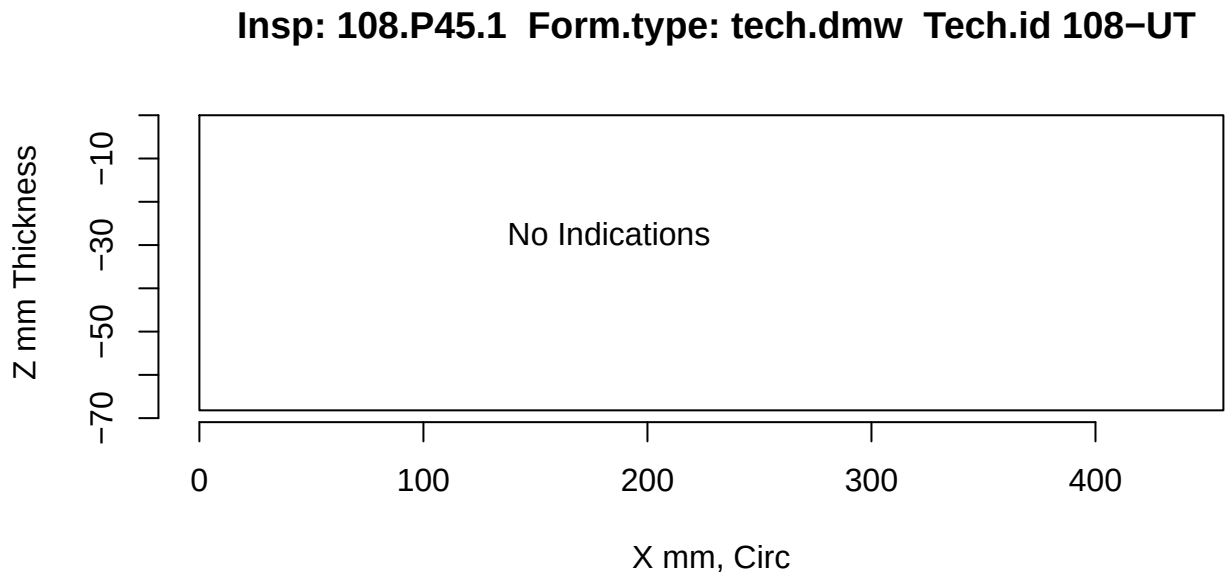
Insp: 108.P45.1 Form.type: tech.dmw Tech.id 108−UT
Z mm Thickness
−10
−30
−50
−70
No Indications
0
100
200
300
400
X mm, Circ

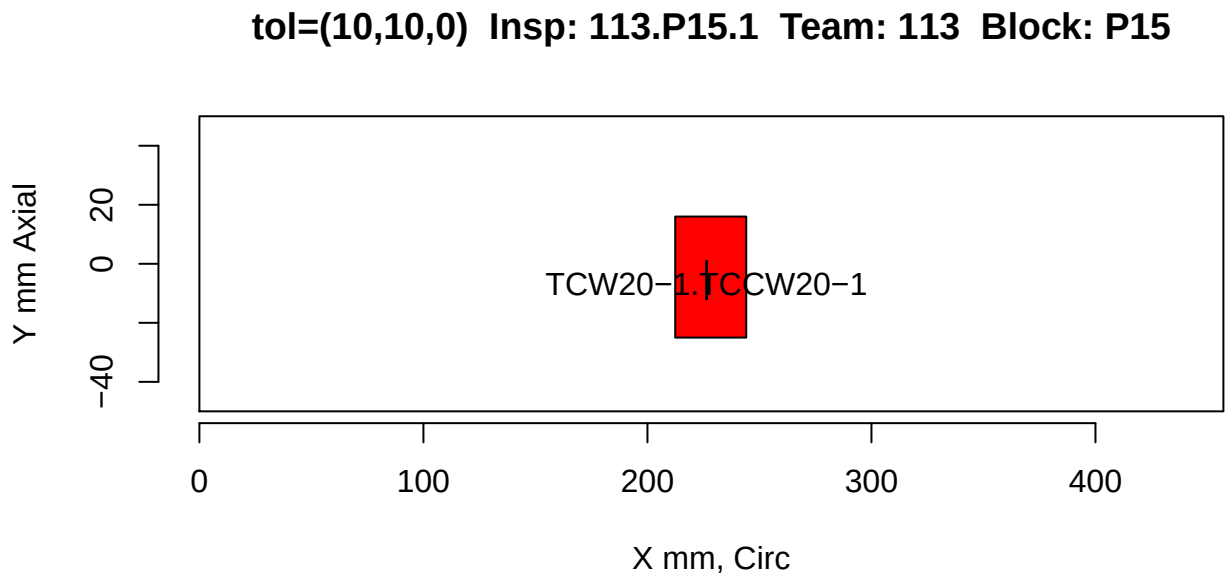
tol=(10,10,0) Insp: 113.P15.1 Team: 113 Block: P15
Y mm Axial
20
0
−40
TCW20−1.TCCW20−1
0
100
200
300
400
X mm, Circ

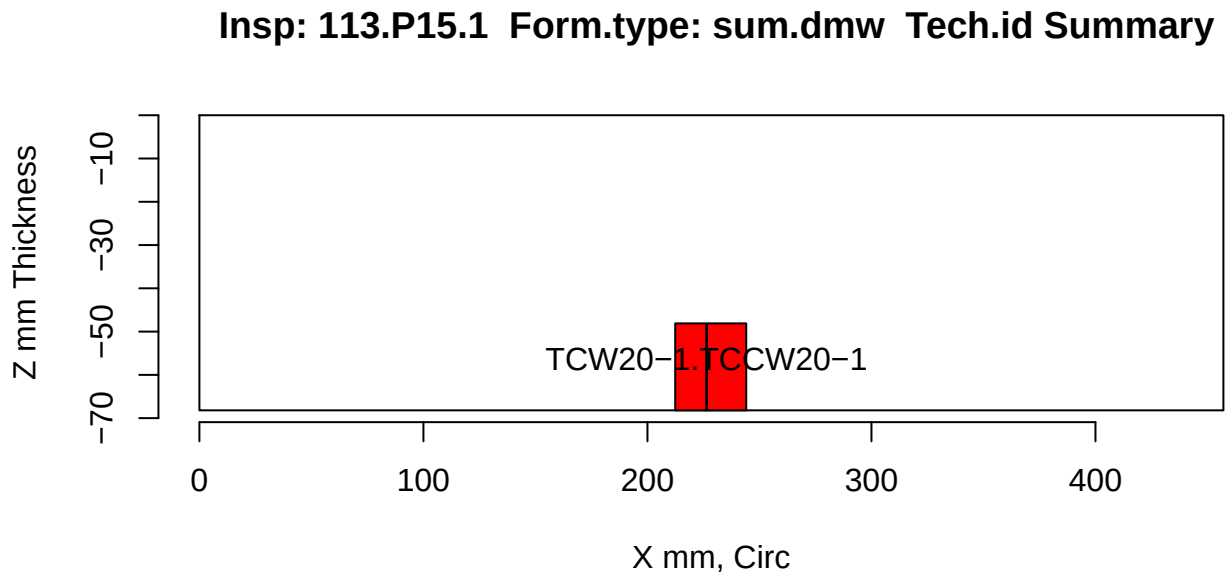
Insp: 113.P15.1 Form.type: sum.dmw Tech.id Summary
Z mm Thickness
−10
−30
−50
−70
TCW20−1.TCCW20−1
0
100
200
300
400
X mm, Circ

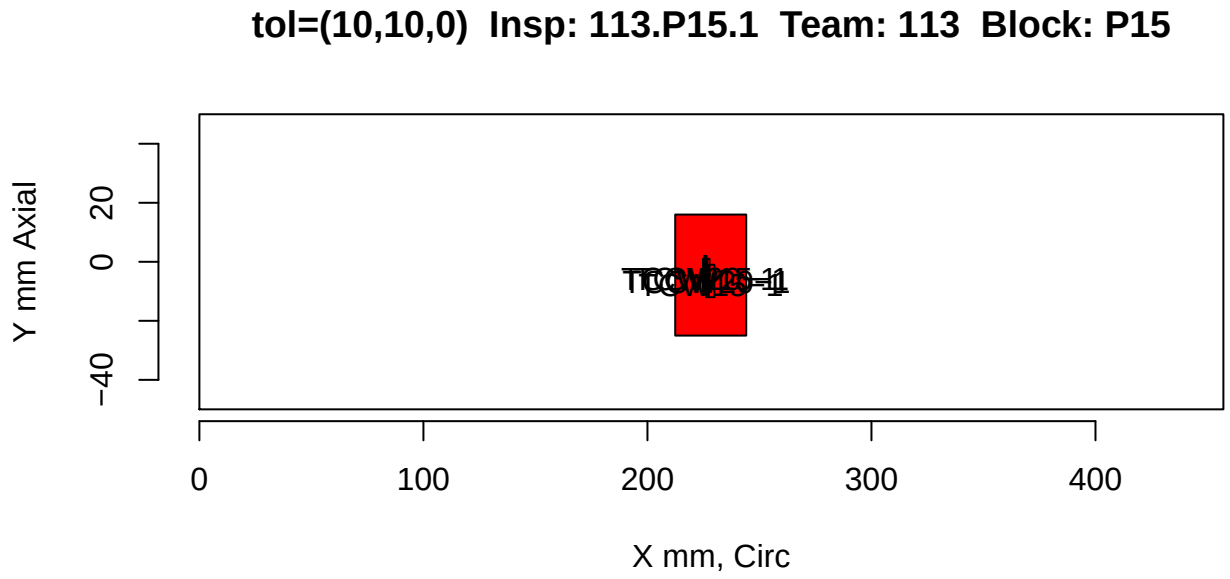
tol=(10,10,0) Insp: 113.P15.1 Team: 113 Block: P15
Y mm Axial
20
0
−40
0
100
200
300
400
X mm, Circ

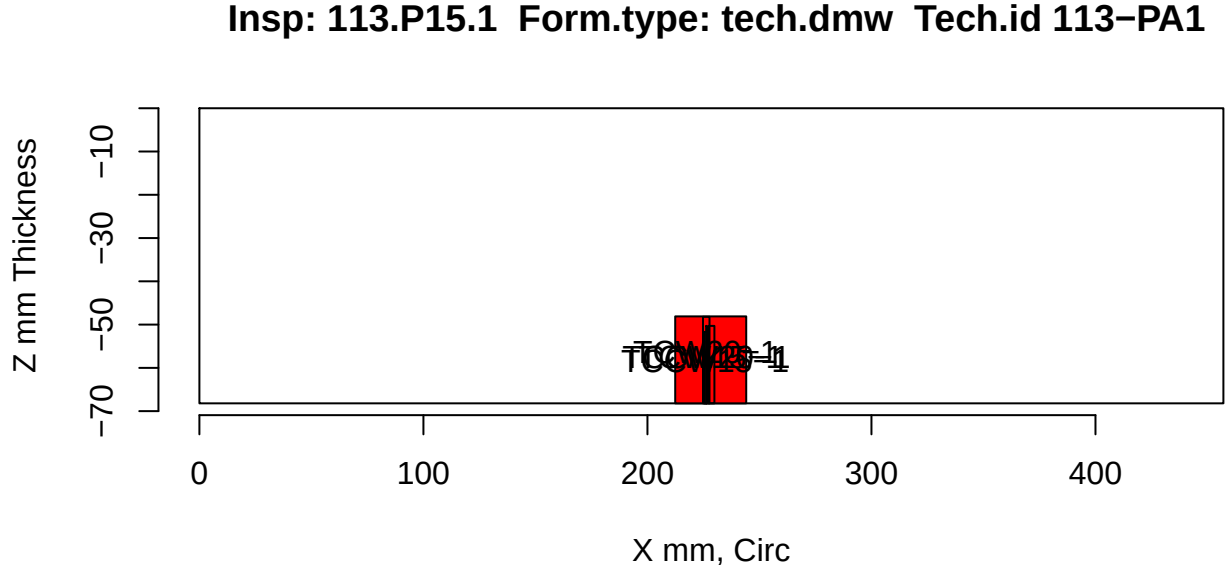
Insp: 113.P15.1 Form.type: tech.dmw Tech.id 113−PA1
Z mm Thickness
−10
−30
−50
−70
0
100
200
300
400
X mm, Circ

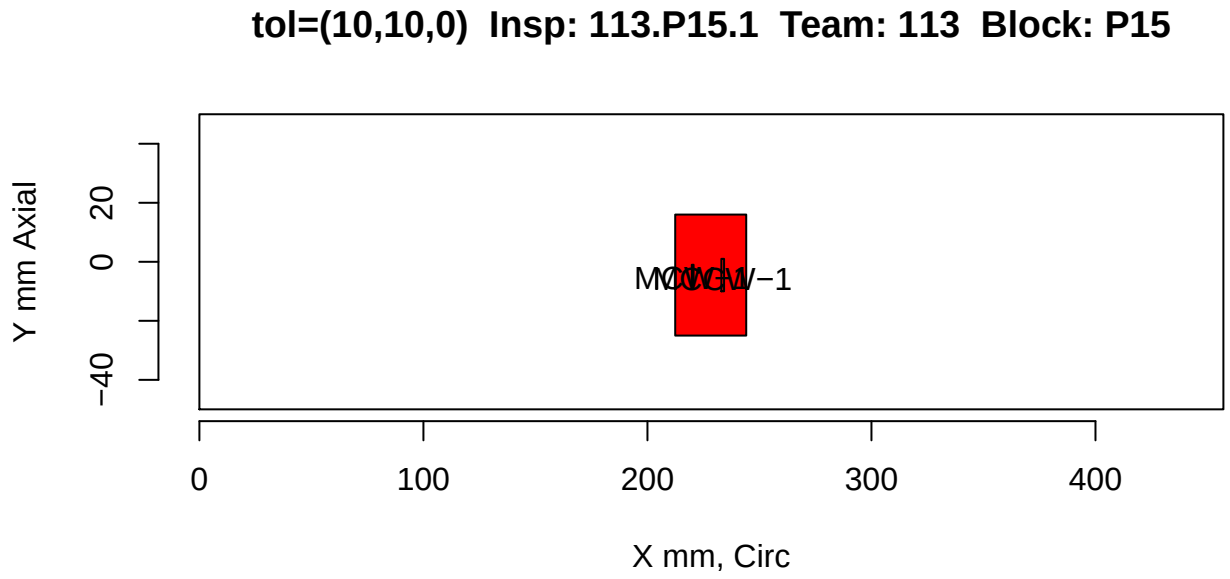
tol=(10,10,0) Insp: 113.P15.1 Team: 113 Block: P15
Y mm Axial
20
0
−40
0
100
200
300
400
X mm, Circ

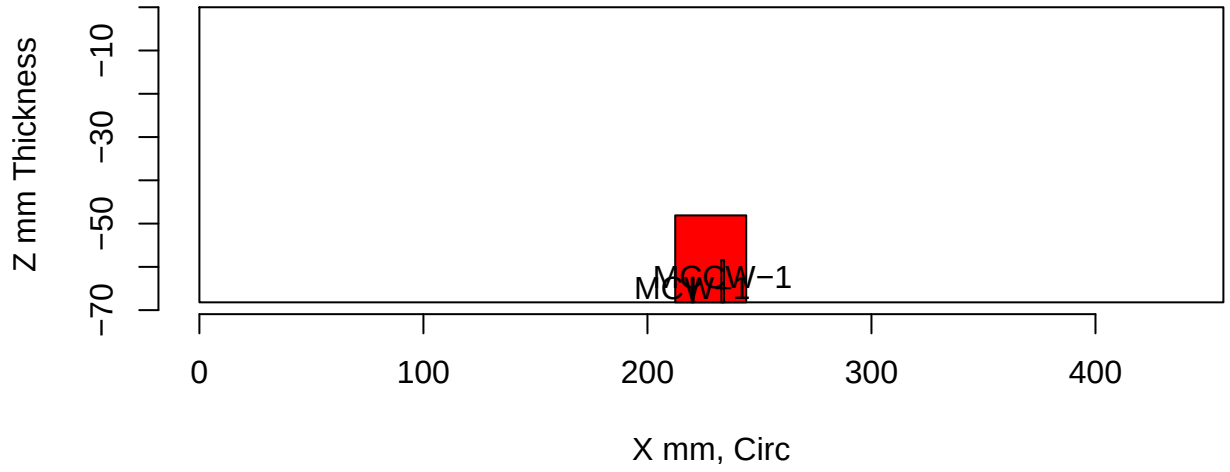
Insp: 113.P15.1 Form.type: tech.dmw Tech.id 113−PA2
Z mm Thickness
−10
−30
−50
−70
0
100
200
300
400
X mm, Circ

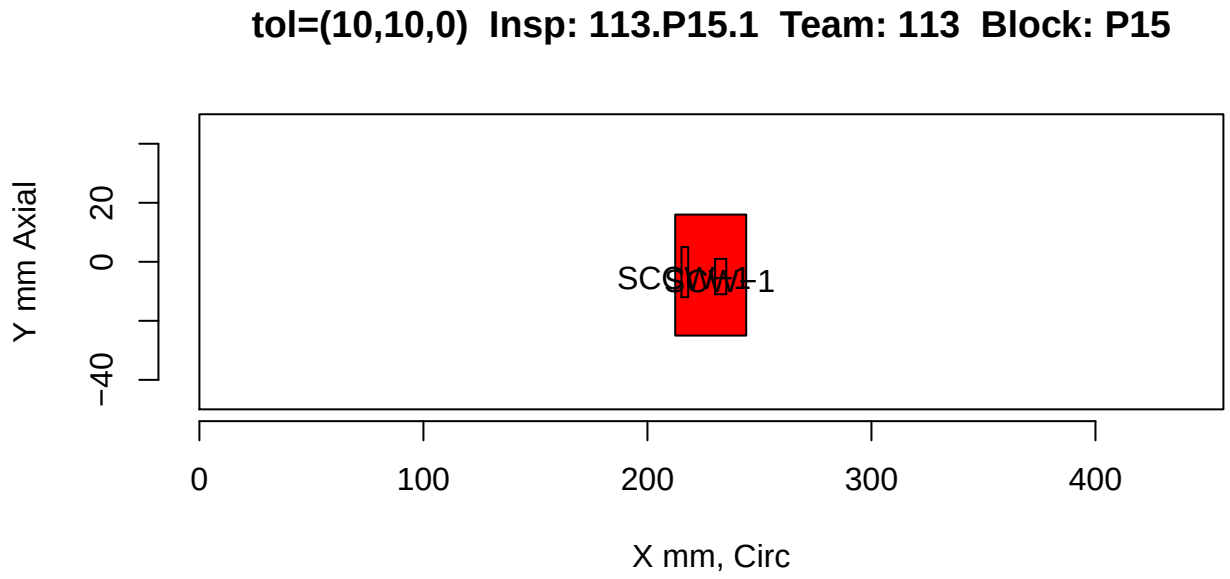
tol=(10,10,0) Insp: 113.P15.1 Team: 113 Block: P15
Y mm Axial
20
0
−40
SCW-1
0
100
200
300
400
X mm, Circ

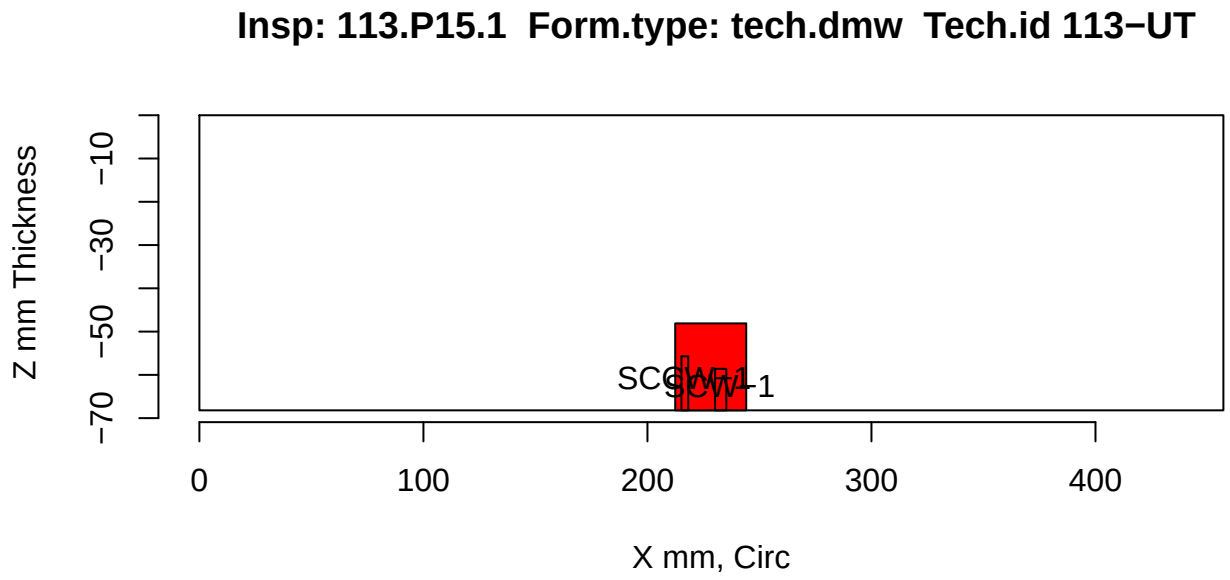
Insp: 113.P15.1 Form.type: tech.dmw Tech.id 113−UT
Z mm Thickness
−10
−30
−50
−70
SCW-1
0
100
200
300
400
X mm, Circ

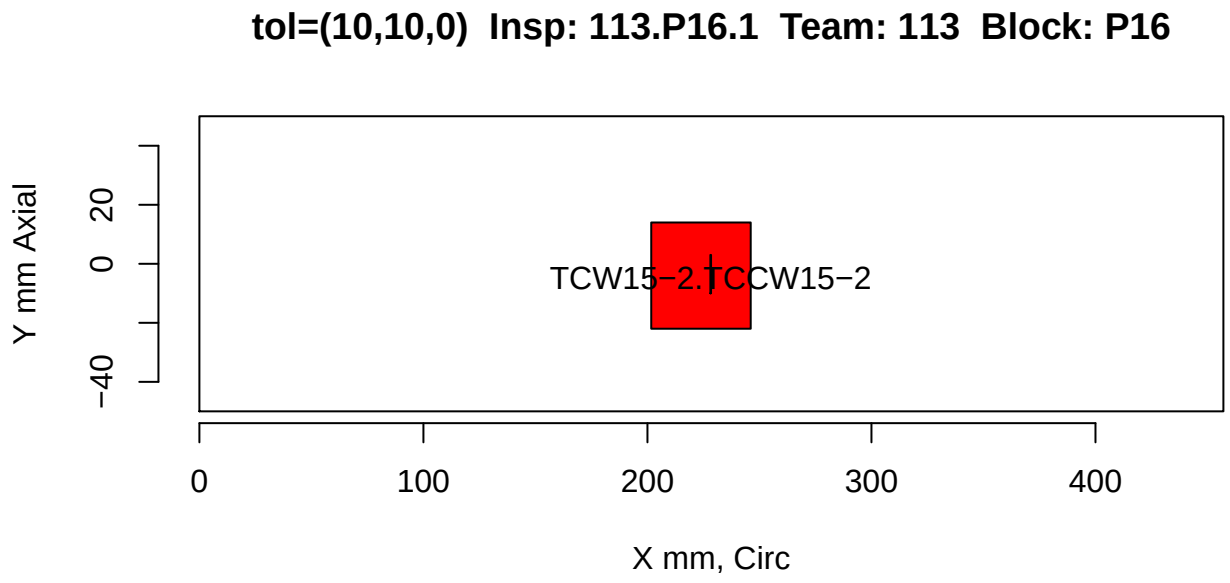
tol=(10,10,0) Insp: 113.P16.1 Team: 113 Block: P16
Y mm Axial
20
0
−40
TCW15−2.TCCW15−2
0
100
200
300
400
X mm, Circ

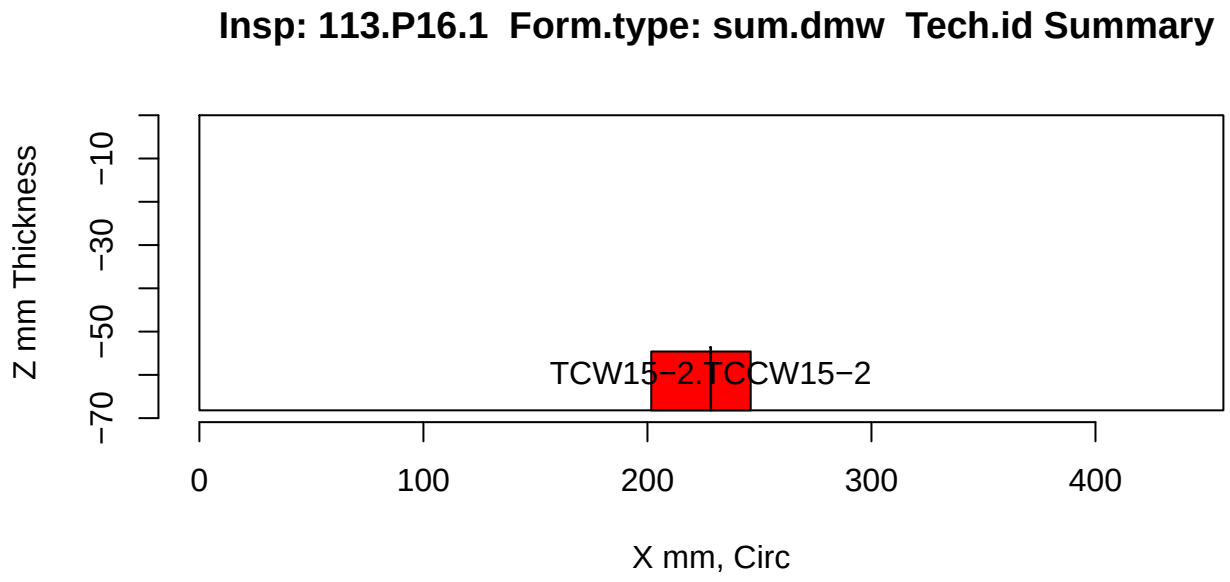
Insp: 113.P16.1 Form.type: sum.dmw Tech.id Summary
Z mm Thickness
−10
−30
−50
−70
TCW15−2.TCCW15−2
0
100
200
300
400
X mm, Circ

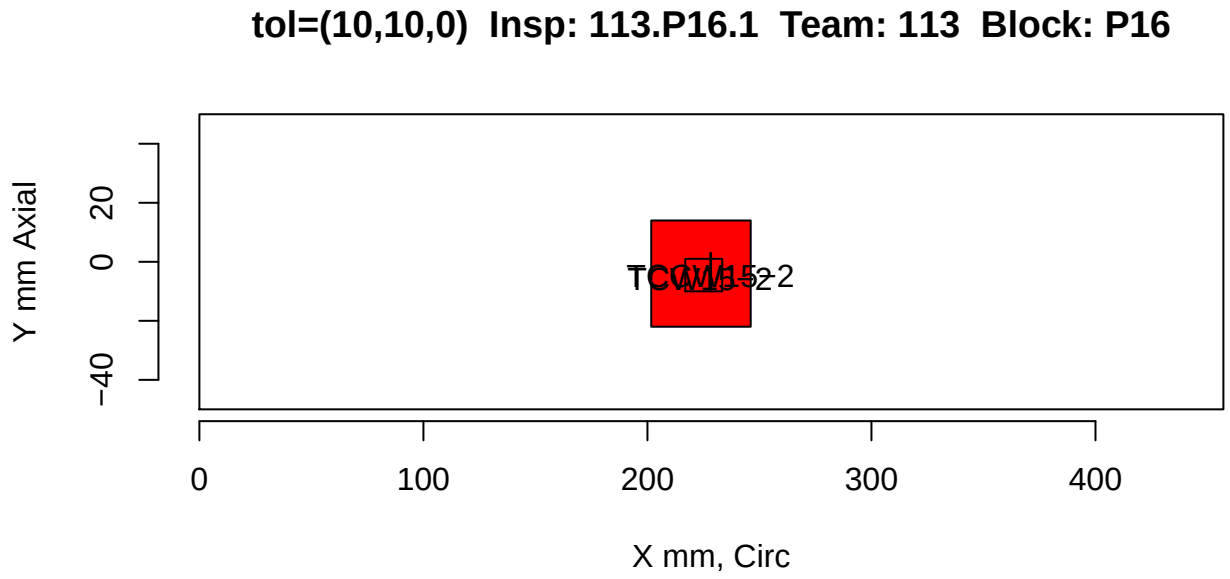
tol=(10,10,0) Insp: 113.P16.1 Team: 113 Block: P16
Y mm Axial
20
0
−40
0
100
200
300
400
X mm, Circ

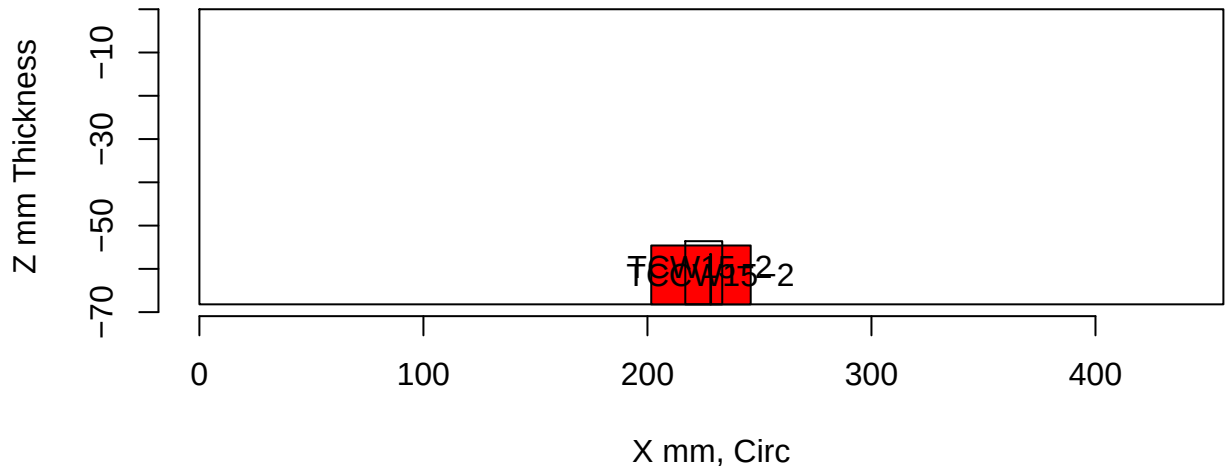
Insp: 113.P16.1 Form.type: tech.dmw Tech.id 113−PA1
Z mm Thickness
−10
−30
−50
−70
0
100
200
300
400
X mm, Circ

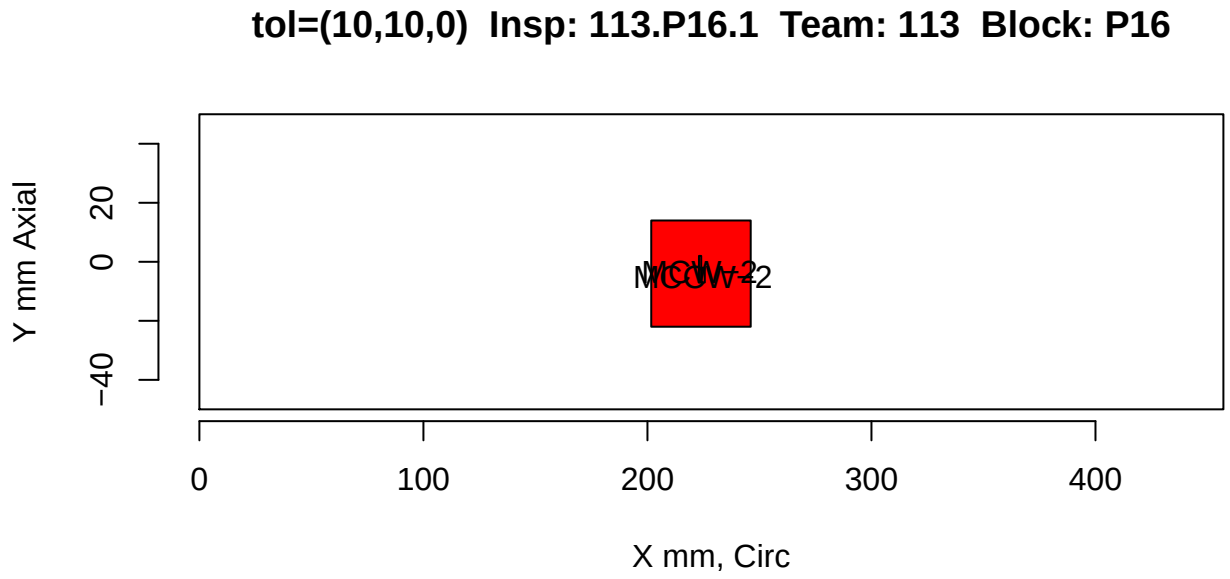
tol=(10,10,0) Insp: 113.P16.1 Team: 113 Block: P16
Y mm Axial
20
0
−40
MCOW-2
0
100
200
300
400
X mm, Circ

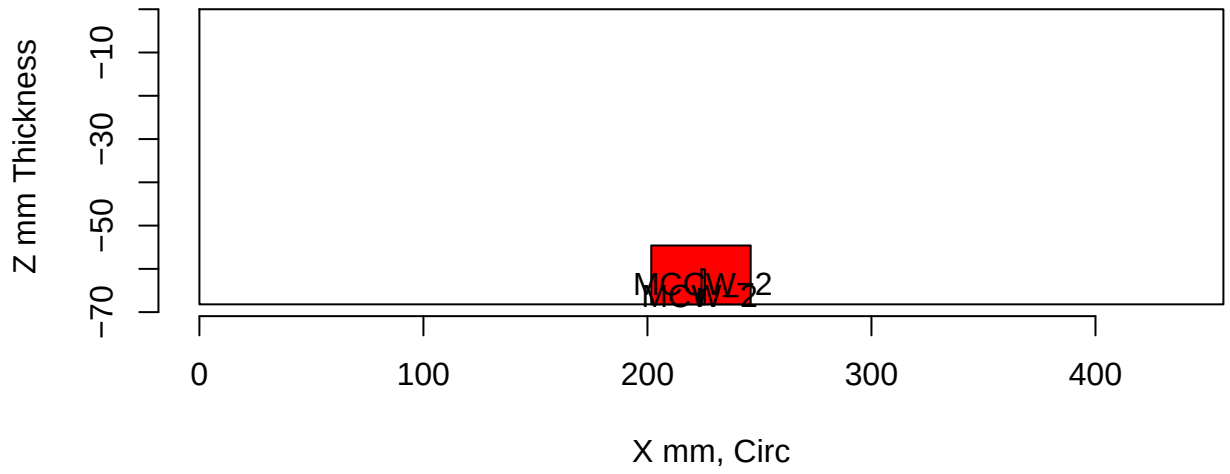
Insp: 113.P16.1 Form.type: tech.dmw Tech.id 113−PA2
Z mm Thickness
−10
−30
−50
−70
MCOW-2
0
100
200
300
400
X mm, Circ

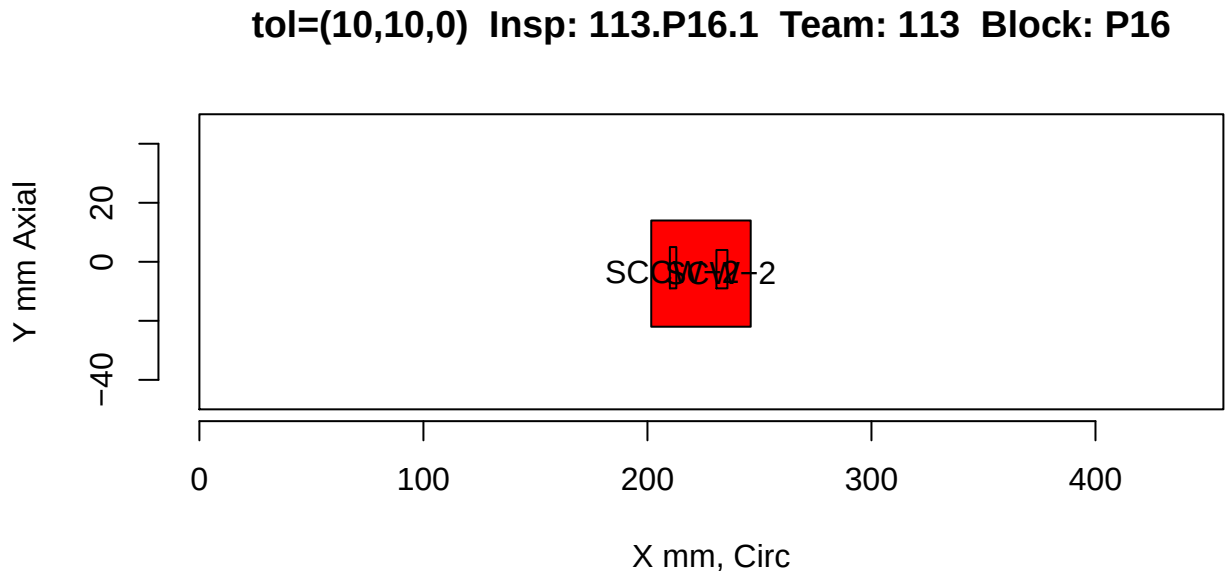
tol=(10,10,0) Insp: 113.P16.1 Team: 113 Block: P16
Y mm Axial
20
0
−40
SCC
SCW-2
0
100
200
300
400
X mm, Circ

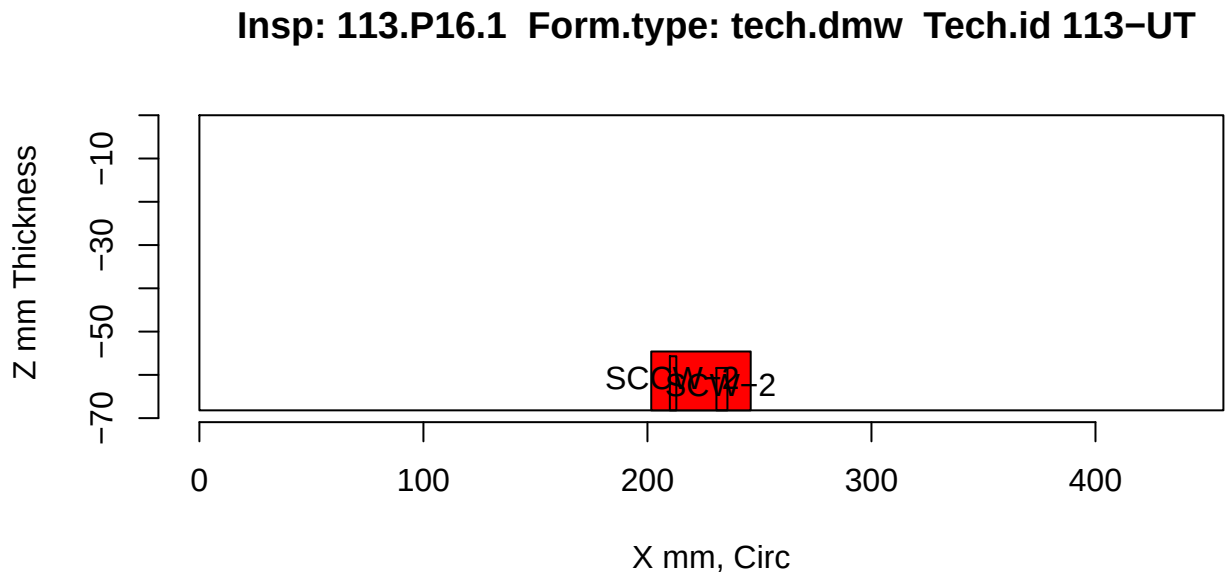
Insp: 113.P16.1 Form.type: tech.dmw Tech.id 113−UT
Z mm Thickness
−10
−30
−50
−70
SCC
SCW-2
0
100
200
300
400
X mm, Circ

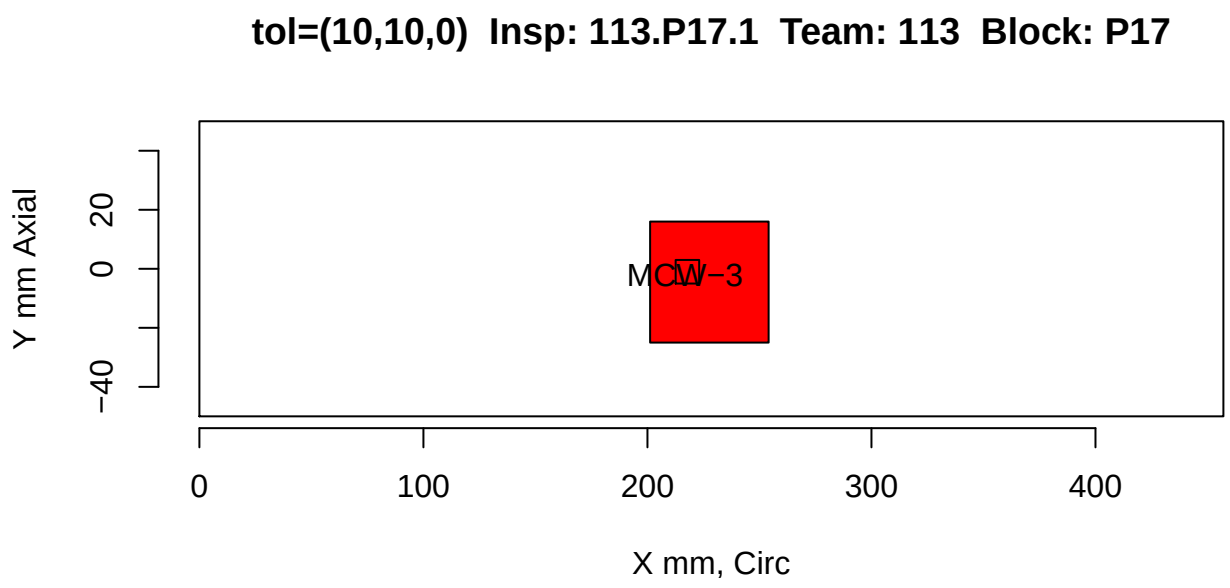
tol=(10,10,0) Insp: 113.P17.1 Team: 113 Block: P17
Y mm Axial
20
0
−40
MCW−3
0
100
200
300
400
X mm, Circ

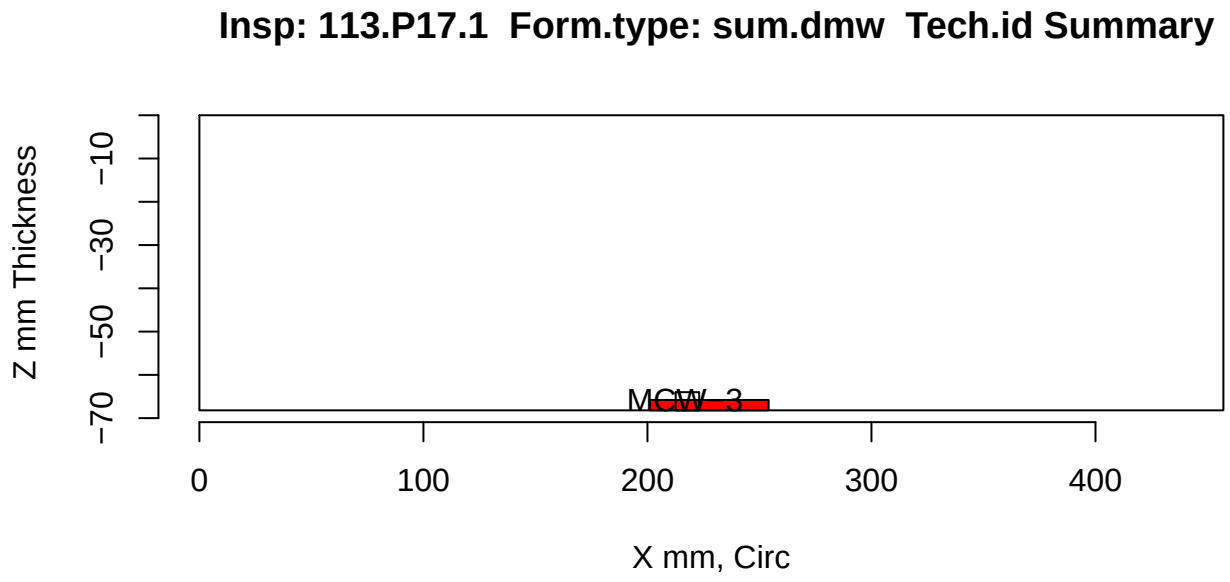
Insp: 113.P17.1 Form.type: sum.dmw Tech.id Summary
Z mm Thickness
−10
−30
−50
−70
MCW−3
0
100
200
300
400
X mm, Circ

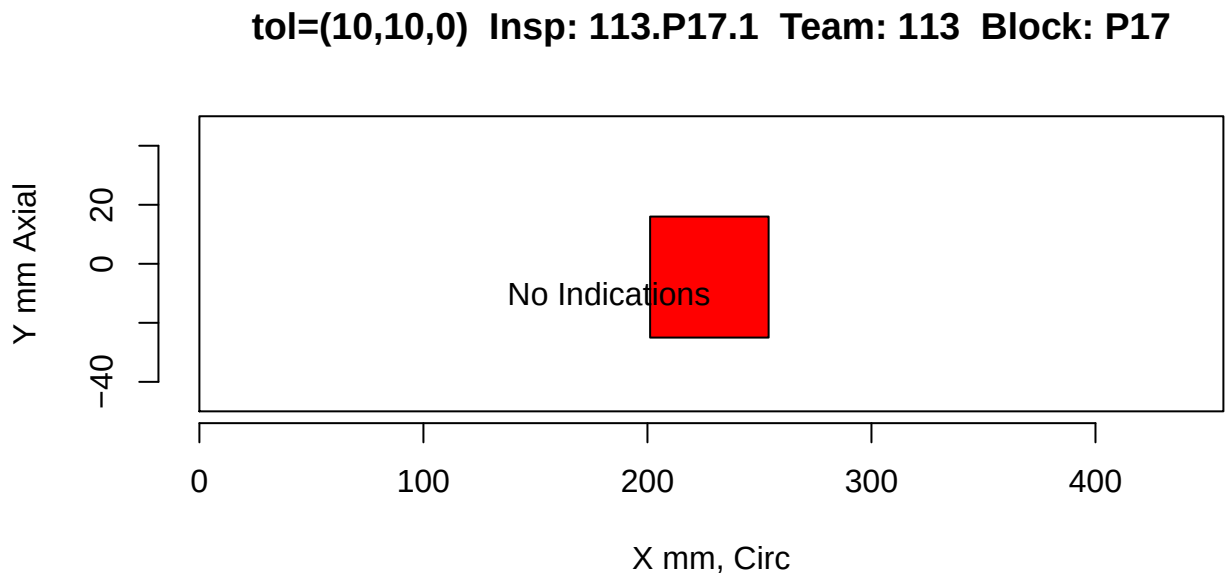
tol=(10,10,0) Insp: 113.P17.1 Team: 113 Block: P17
Y mm Axial
20
0
−40
No Indications
0
100
200
300
400
X mm, Circ

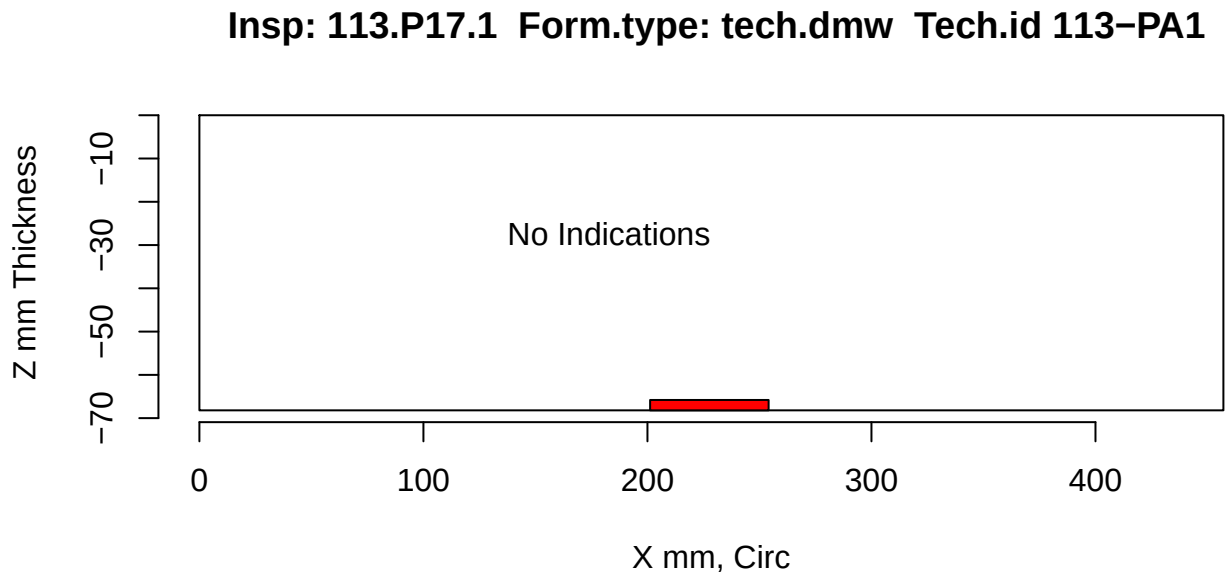
Insp: 113.P17.1 Form.type: tech.dmw Tech.id 113−PA1
Z mm Thickness
−10
−30
−50
−70
No Indications
0
100
200
300
400
X mm, Circ

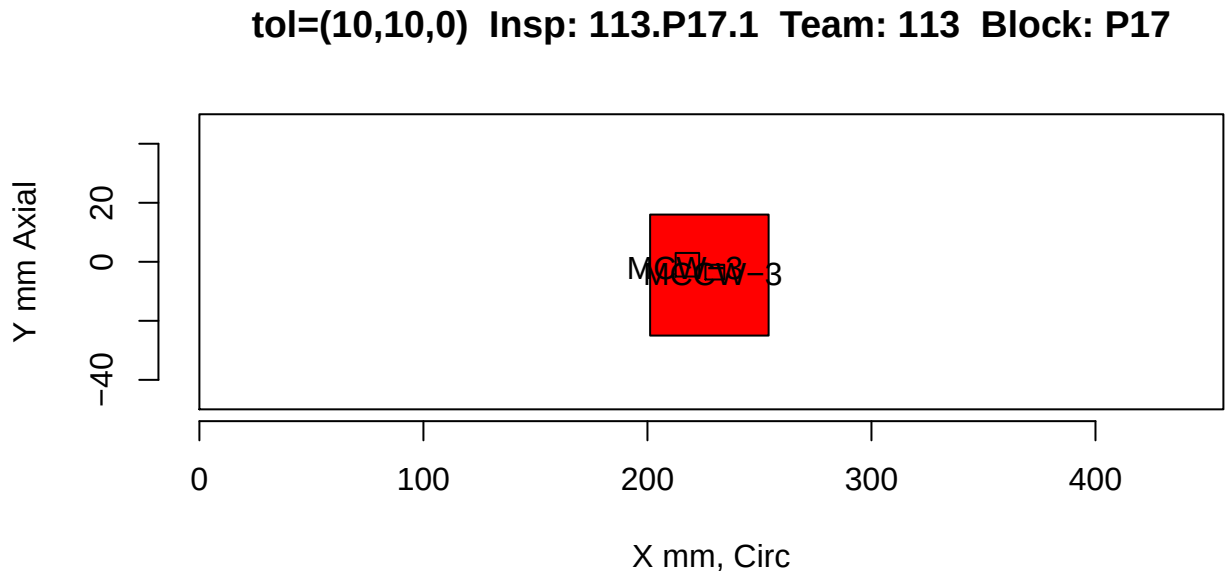
tol=(10,10,0) Insp: 113.P17.1 Team: 113 Block: P17
Y mm Axial
20
0
−40
MCCW−3
0
100
200
300
400
X mm, Circ

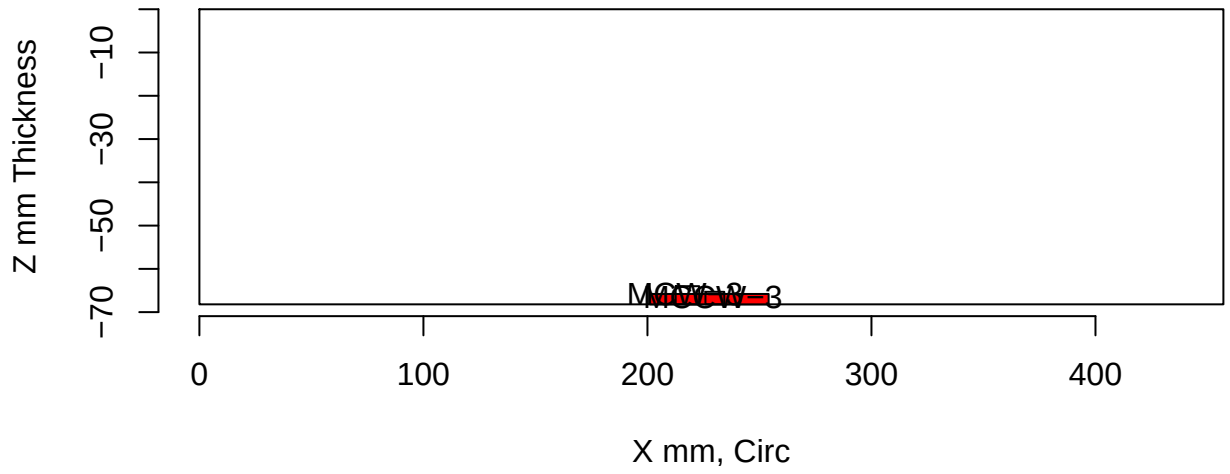
Insp: 113.P17.1 Form.type: tech.dmw Tech.id 113−PA2
Z mm Thickness
−10
−30
−50
−70
0
100
200
300
400
X mm, Circ

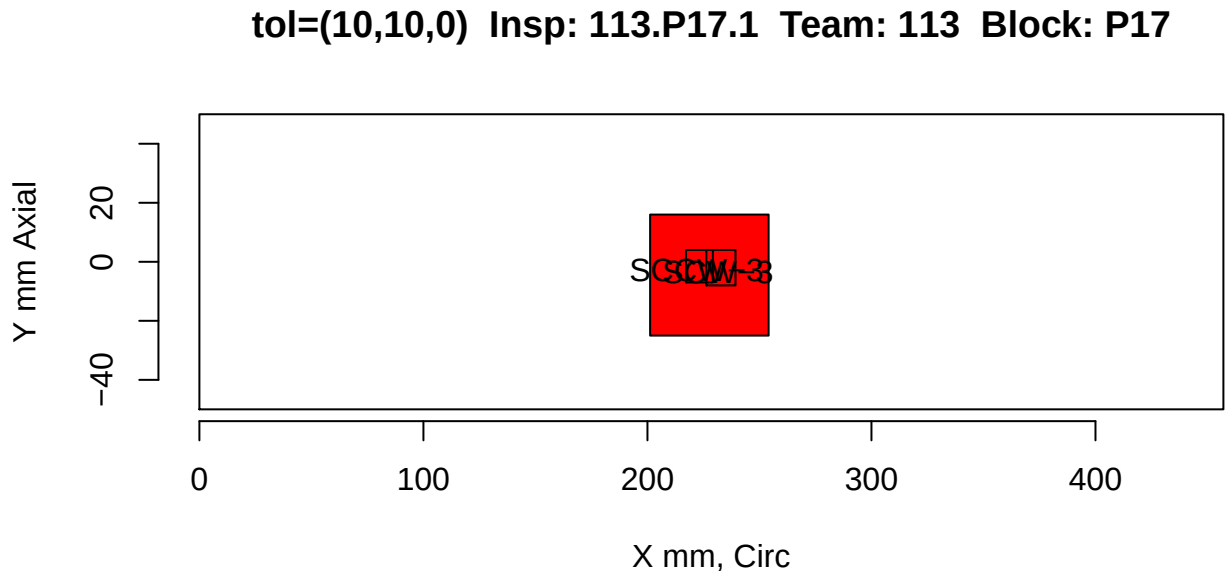
tol=(10,10,0) Insp: 113.P17.1 Team: 113 Block: P17
Y mm Axial
20
0
−40
0
100
200
300
400
X mm, Circ

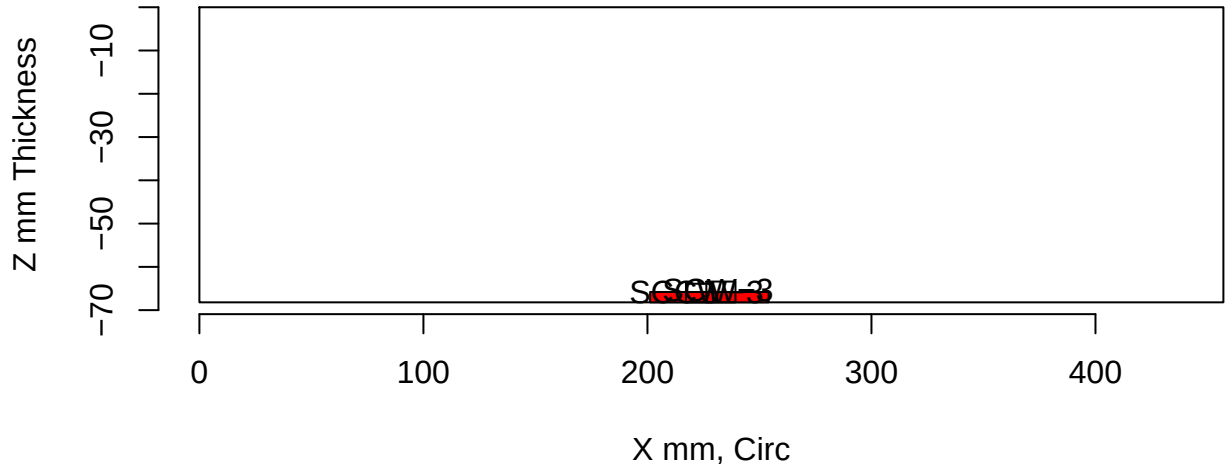
Insp: 113.P17.1 Form.type: tech.dmw Tech.id 113−UT
Z mm Thickness
−10
−30
−50
−70
0
100
200
300
400
X mm, Circ

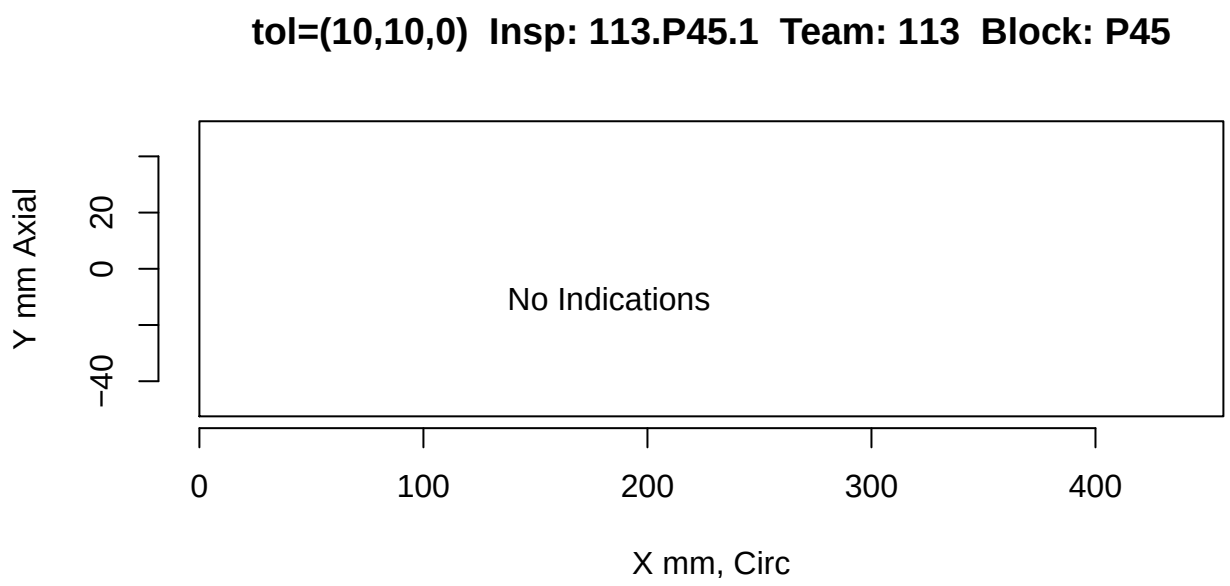
tol=(10,10,0) Insp: 113.P45.1 Team: 113 Block: P45
Y mm Axial
20
0
−40
No Indications
0
100
200
300
400
X mm, Circ

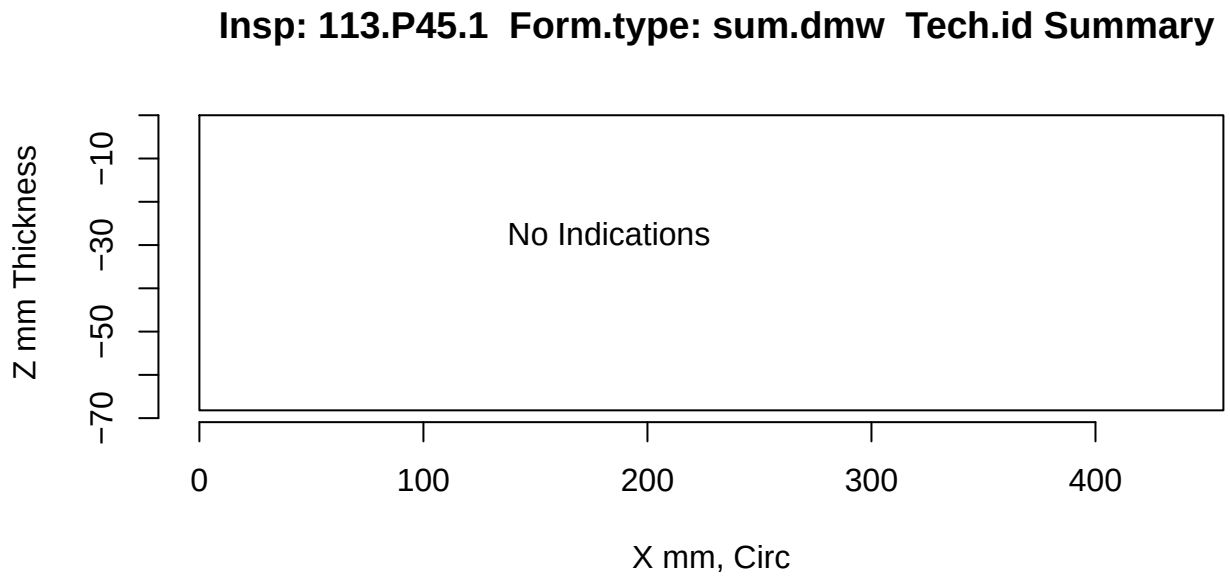
Insp: 113.P45.1 Form.type: sum.dmw Tech.id Summary
Z mm Thickness
−10
−30
−50
−70
No Indications
0
100
200
300
400
X mm, Circ

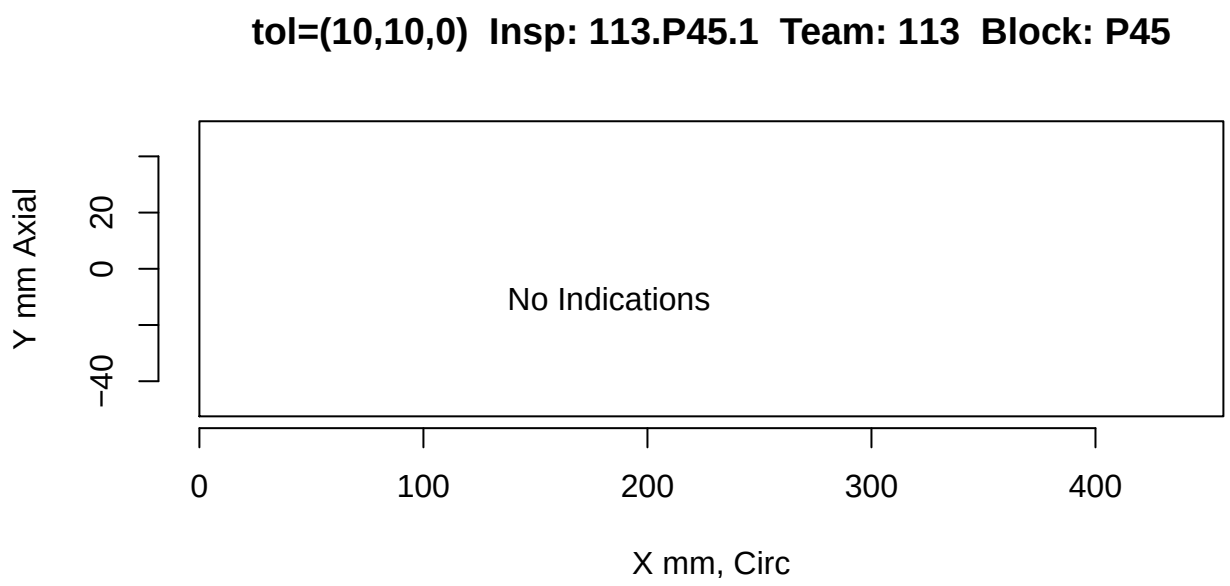
tol=(10,10,0) Insp: 113.P45.1 Team: 113 Block: P45
Y mm Axial
20
0
−40
No Indications
0
100
200
300
400
X mm, Circ

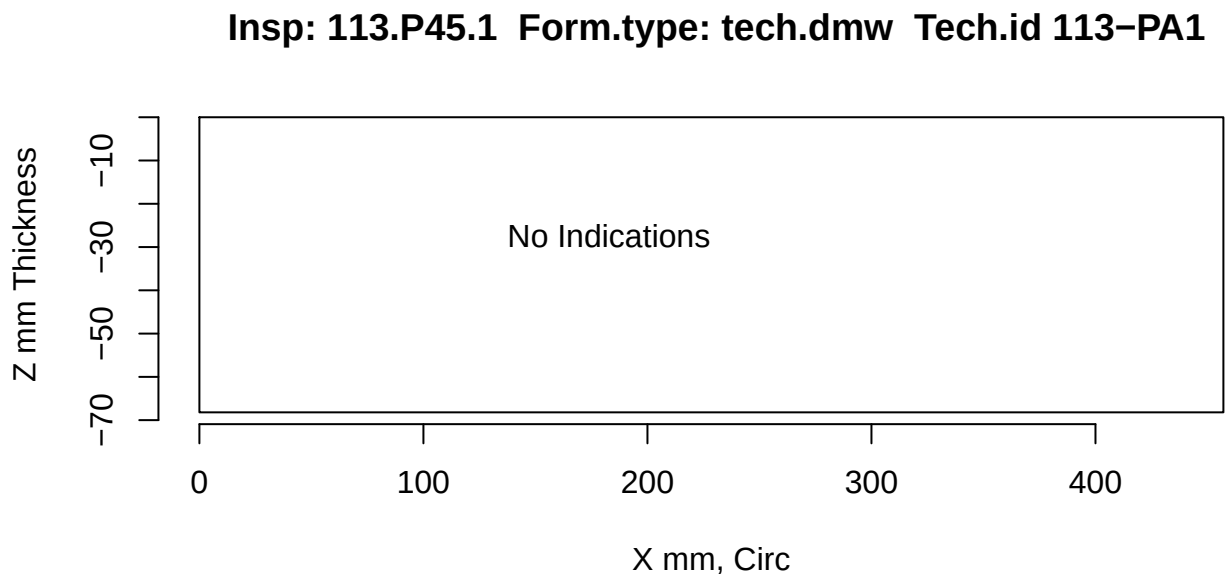
Insp: 113.P45.1 Form.type: tech.dmw Tech.id 113−PA1
Z mm Thickness
−10
−30
−50
−70
No Indications
0
100
200
300
400
X mm, Circ

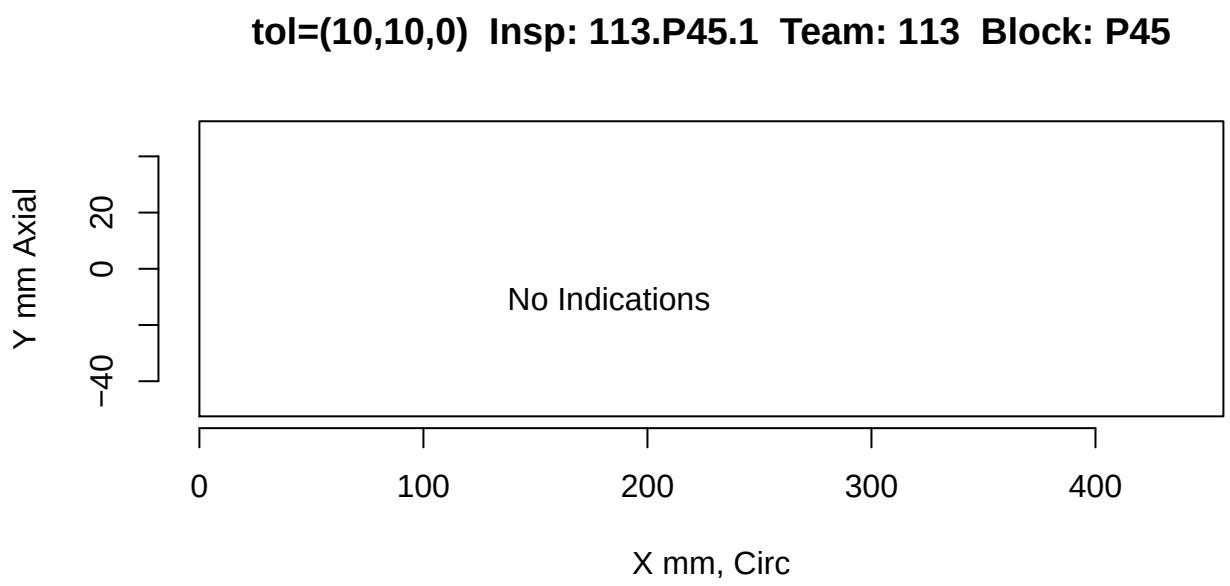
tol=(10,10,0) Insp: 113.P45.1 Team: 113 Block: P45
Y mm Axial
20
0
−40
No Indications
0
100
200
300
400
X mm, Circ

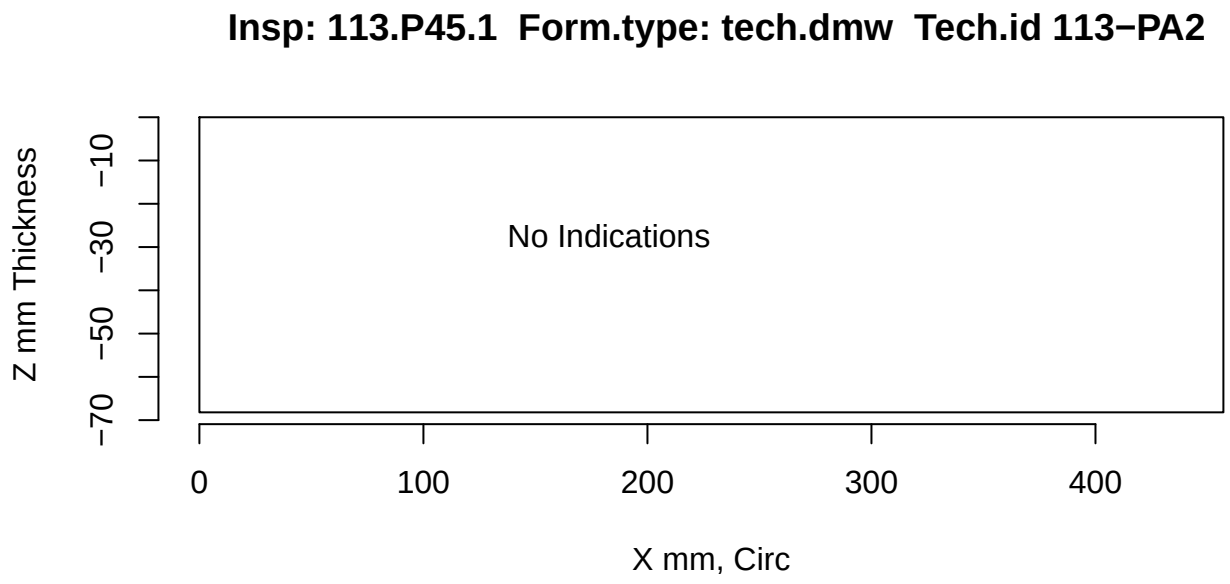
Insp: 113.P45.1 Form.type: tech.dmw Tech.id 113−PA2
Z mm Thickness
−10
−30
−50
−70
No Indications
0
100
200
300
400
X mm, Circ

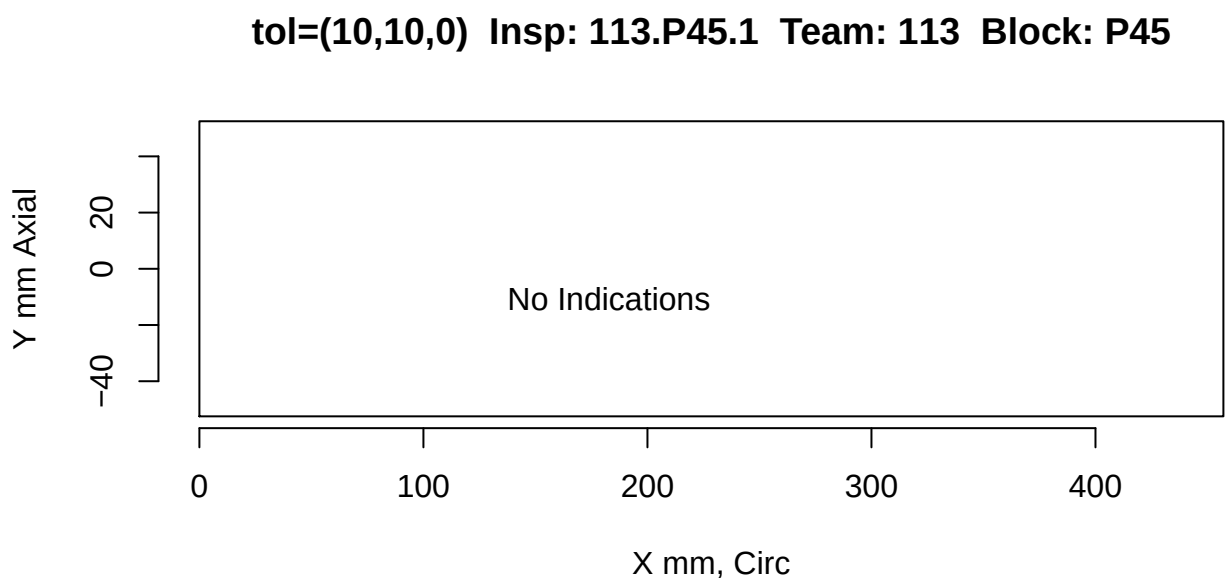
tol=(10,10,0) Insp: 113.P45.1 Team: 113 Block: P45
Y mm Axial
20
0
−40
No Indications
0
100
200
300
400
X mm, Circ

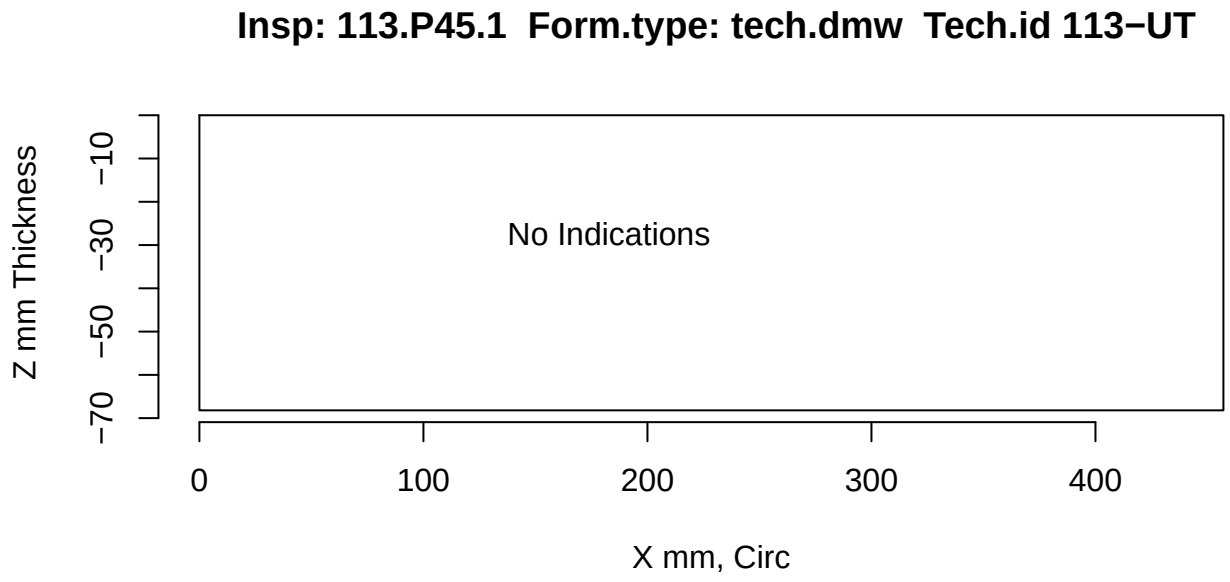
Insp: 113.P45.1 Form.type: tech.dmw Tech.id 113−UT
Z mm Thickness
−10
−30
−50
−70
No Indications
0
100
200
300
400
X mm, Circ

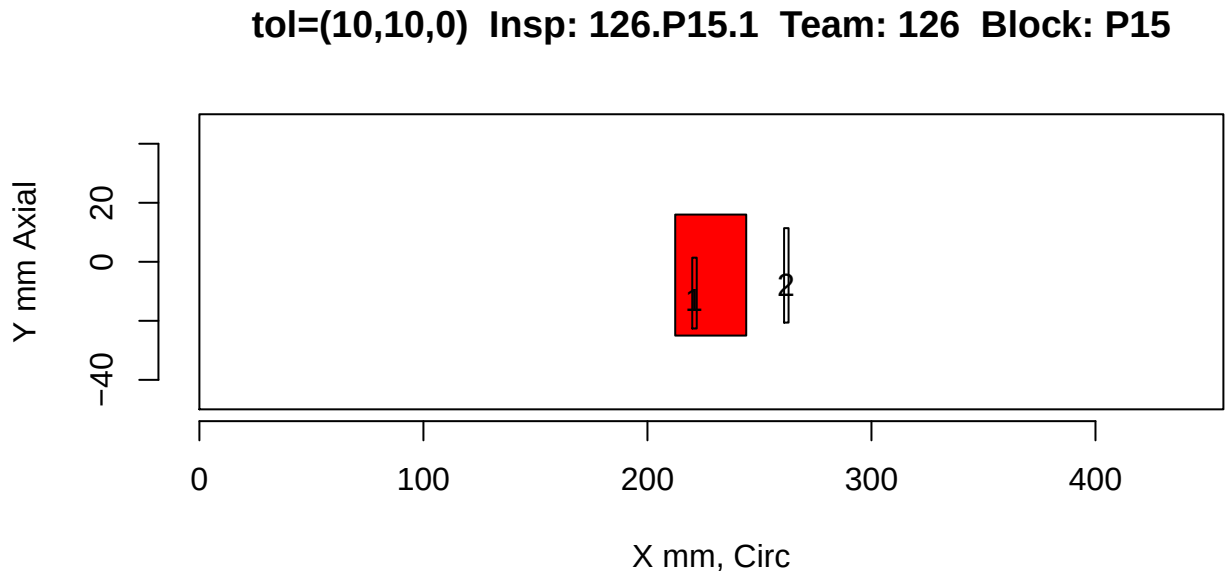
tol=(10,10,0) Insp: 126.P15.1 Team: 126 Block: P15
Y mm Axial
20
0
−40
1
2
0
100
200
300
400
X mm, Circ

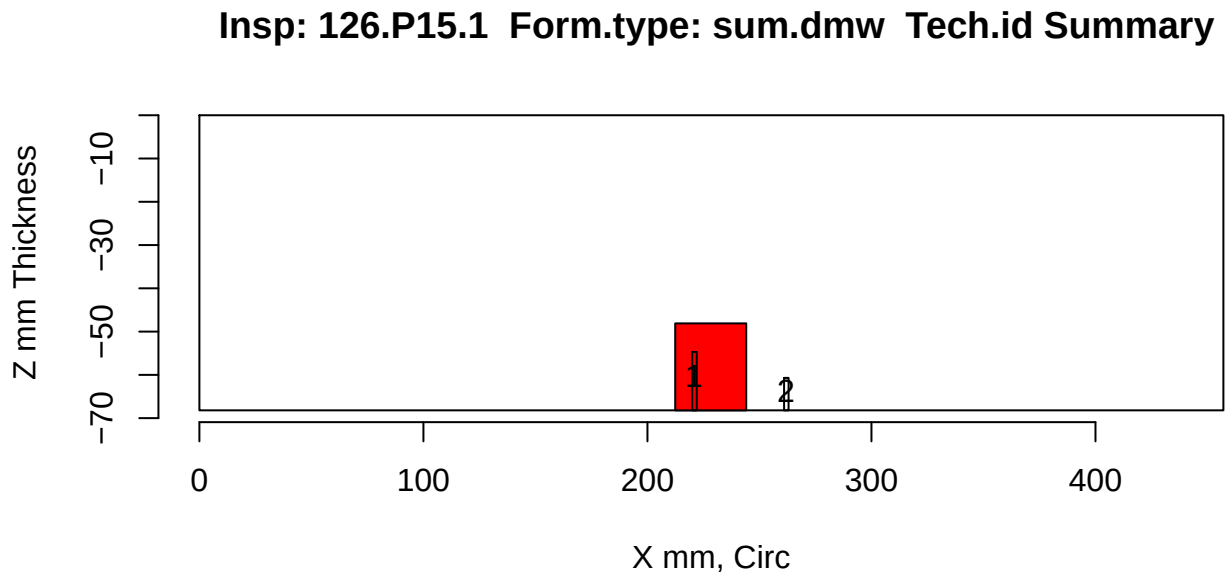
Insp: 126.P15.1 Form.type: sum.dmw Tech.id Summary
Z mm Thickness
−10
−30
−50
−70
1
2
0
100
200
300
400
X mm, Circ

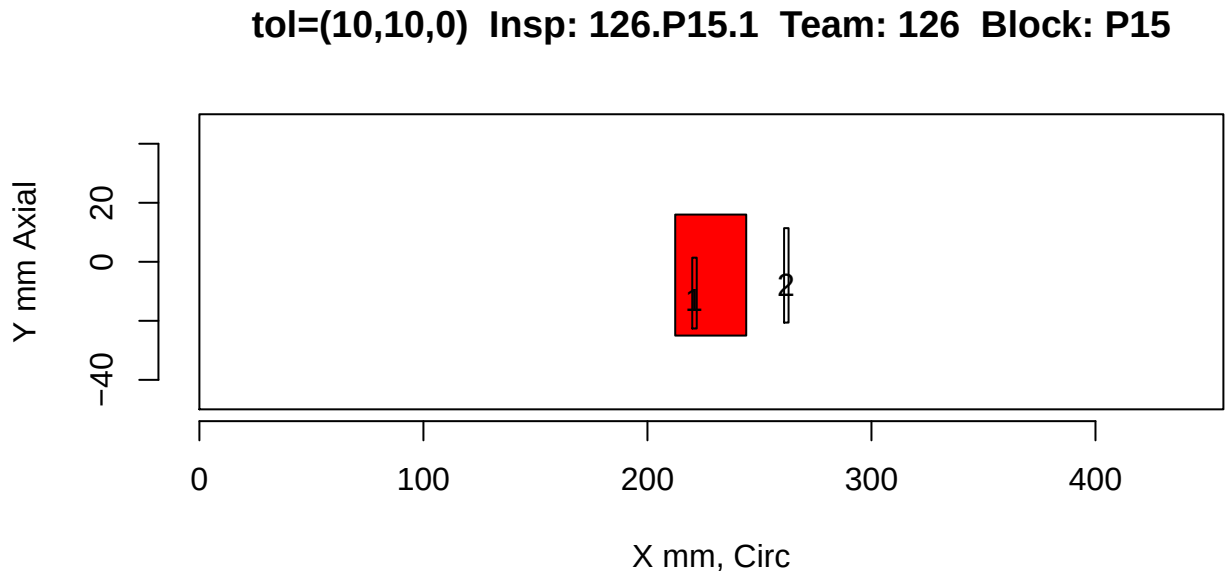
tol=(10,10,0) Insp: 126.P15.1 Team: 126 Block: P15
Y mm Axial
−40
0
20
1
2
0
100
200
300
400
X mm, Circ

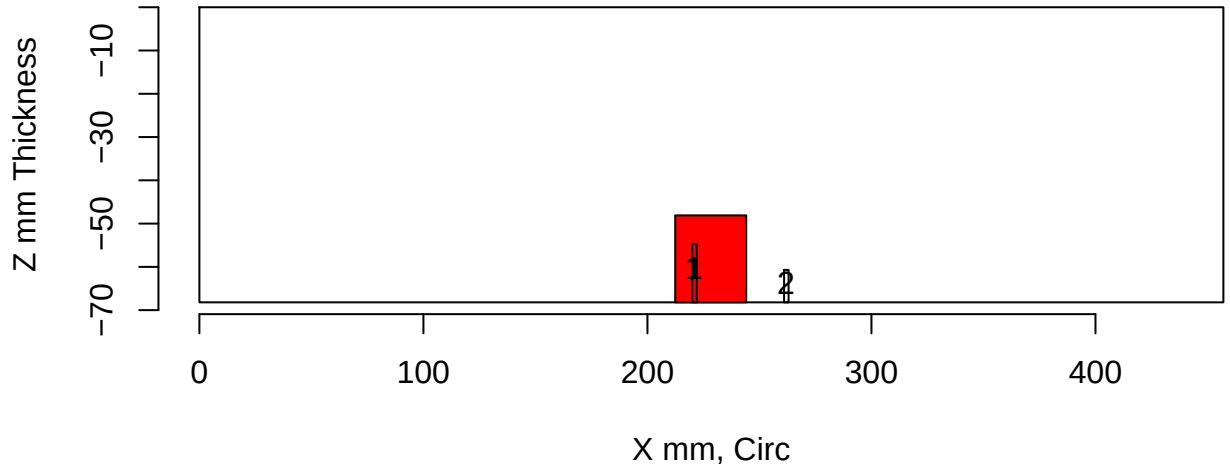
Insp: 126.P15.1 Form.type: tech.dmw Tech.id 126−PA
Z mm Thickness
−70
−50
−30
−10
1
2
0
100
200
300
400
X mm, Circ

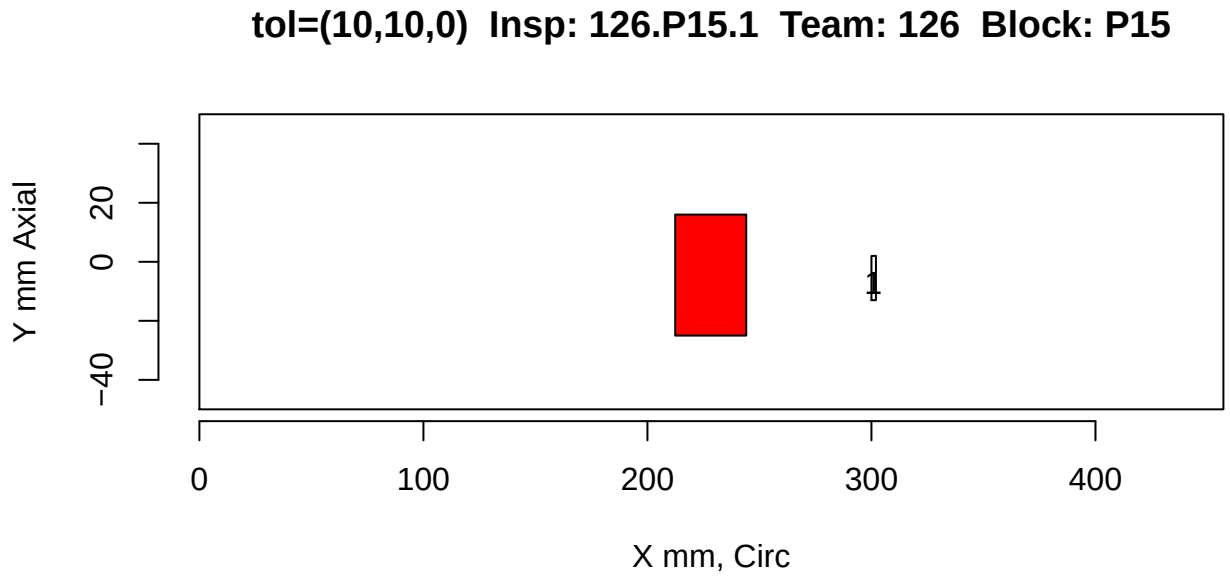
tol=(10,10,0) Insp: 126.P15.1 Team: 126 Block: P15
Y mm Axial
20
0
−40
1
0
100
200
300
400
X mm, Circ

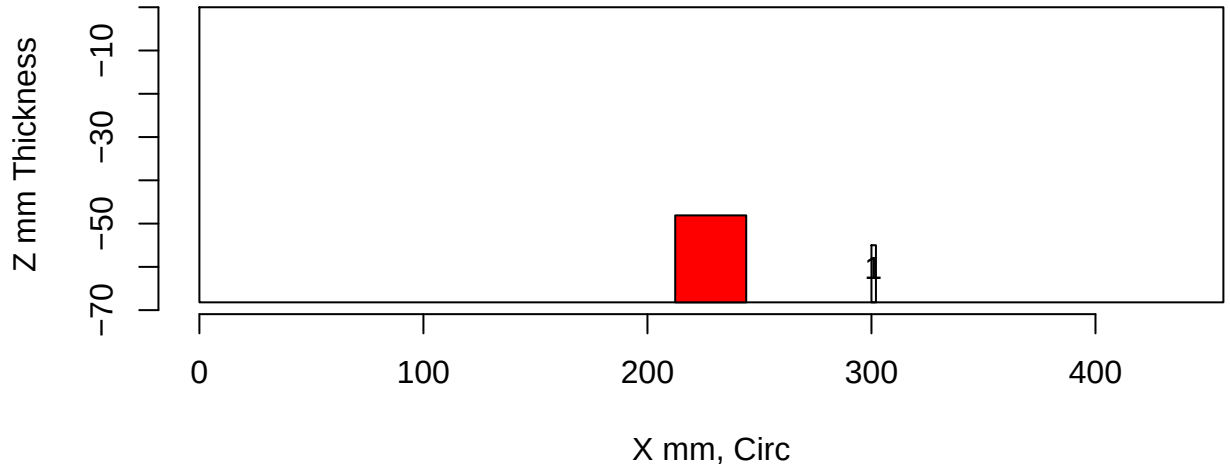
Insp: 126.P15.1 Form.type: tech.dmw Tech.id 126−UT
Z mm Thickness
−10
−30
−50
−70
1
0
100
200
300
400
X mm, Circ

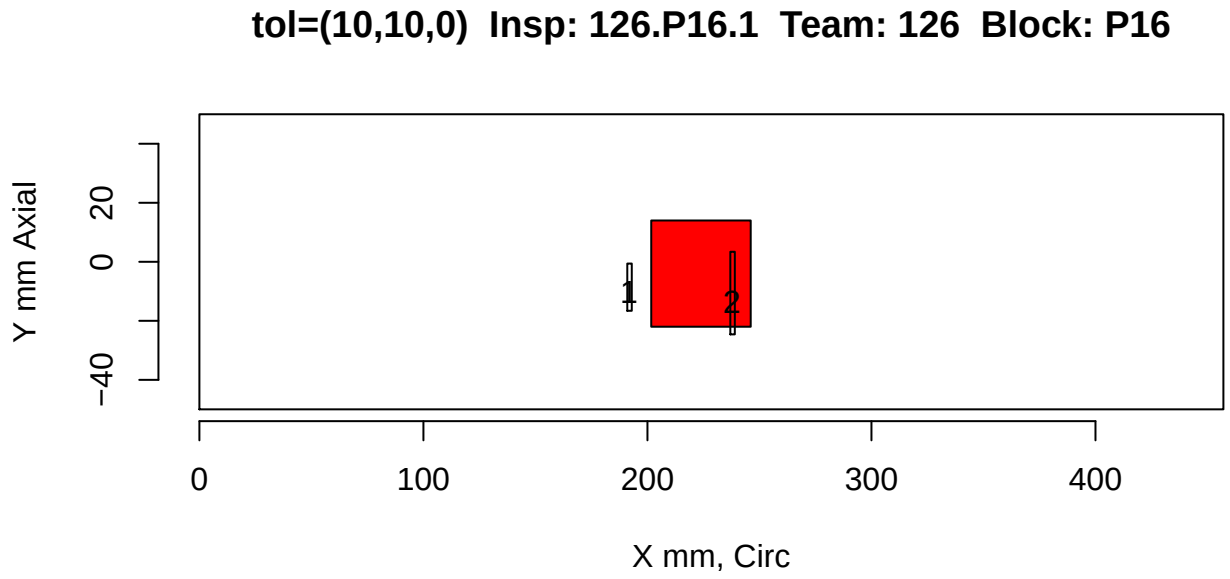
tol=(10,10,0) Insp: 126.P16.1 Team: 126 Block: P16
Y mm Axial
20
0
−40
1
2
0
100
200
300
400
X mm, Circ

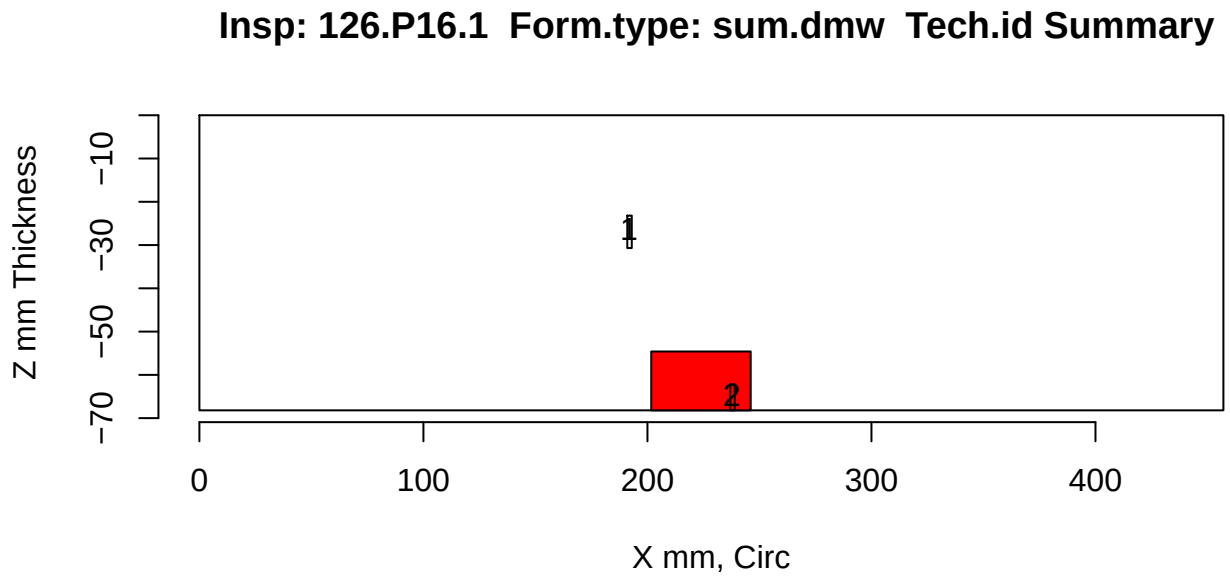
Insp: 126.P16.1 Form.type: sum.dmw Tech.id Summary
Z mm Thickness
−10
−30
−50
−70
1
2
0
100
200
300
400
X mm, Circ

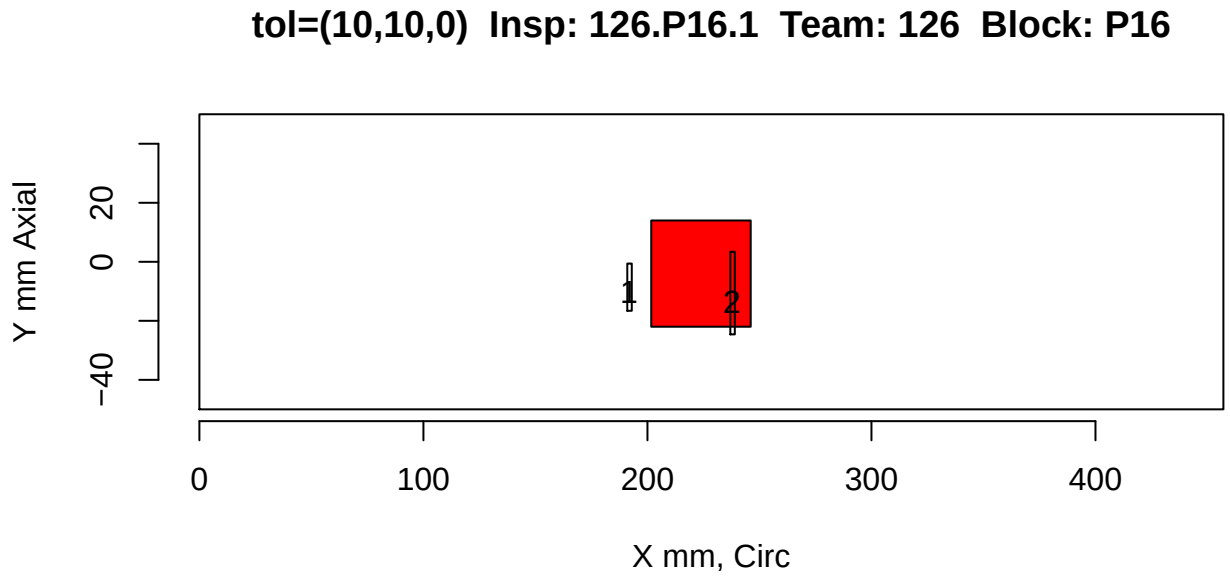
tol=(10,10,0) Insp: 126.P16.1 Team: 126 Block: P16
Y mm Axial
20
0
−40
1
2
0
100
200
300
400
X mm, Circ

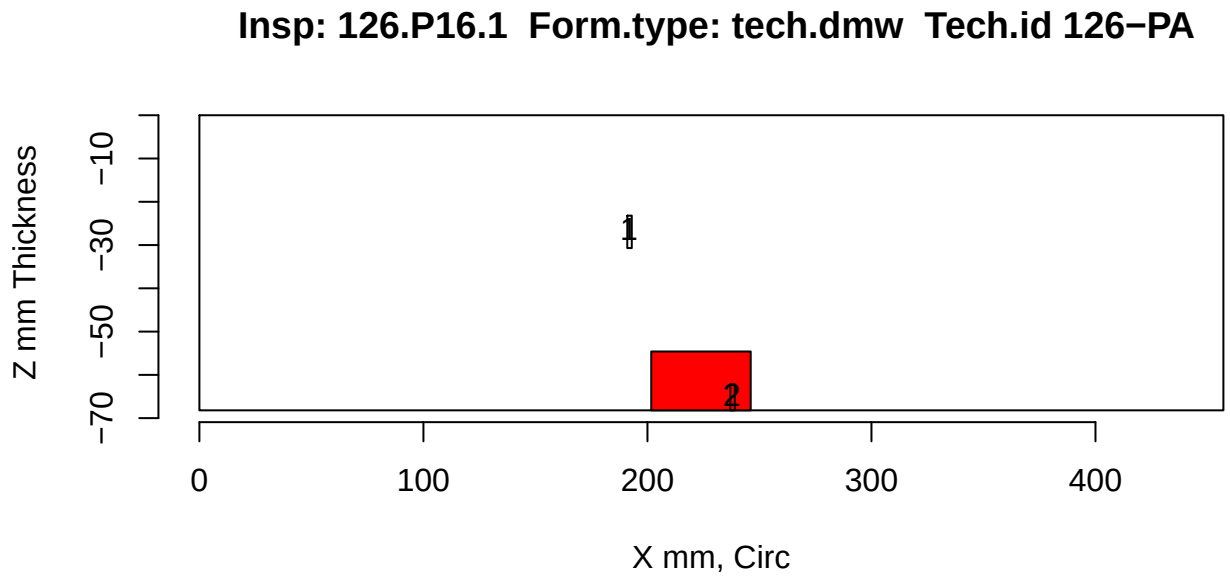
Insp: 126.P16.1 Form.type: tech.dmw Tech.id 126−PA
Z mm Thickness
−10
−30
−50
−70
1
2
0
100
200
300
400
X mm, Circ

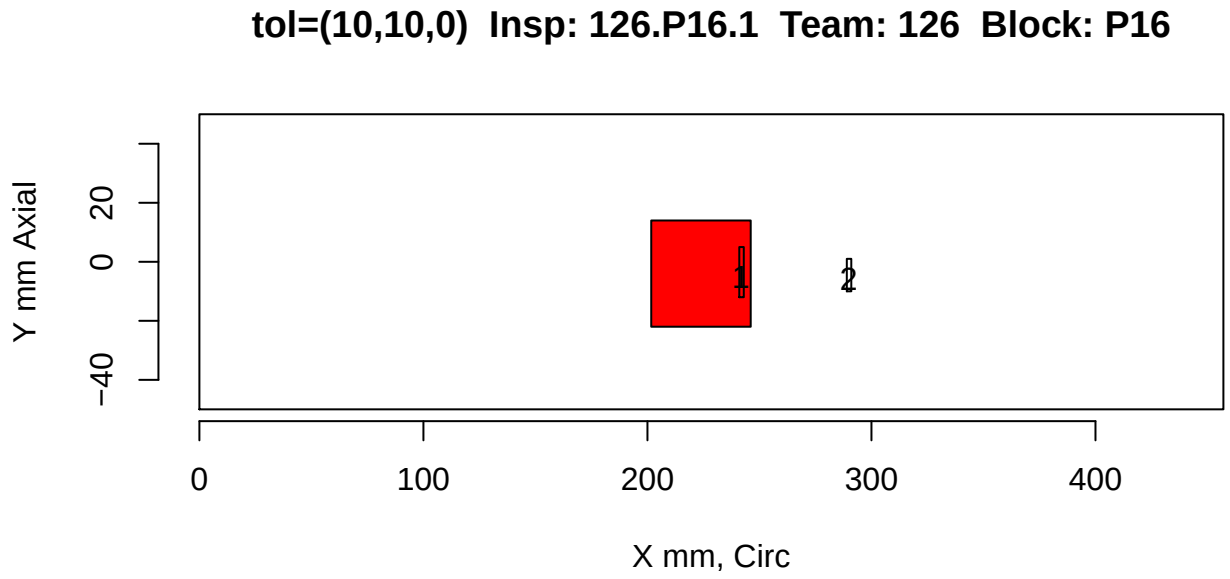
tol=(10,10,0) Insp: 126.P16.1 Team: 126 Block: P16
Y mm Axial
20
0
−40
1
2
0
100
200
300
400
X mm, Circ

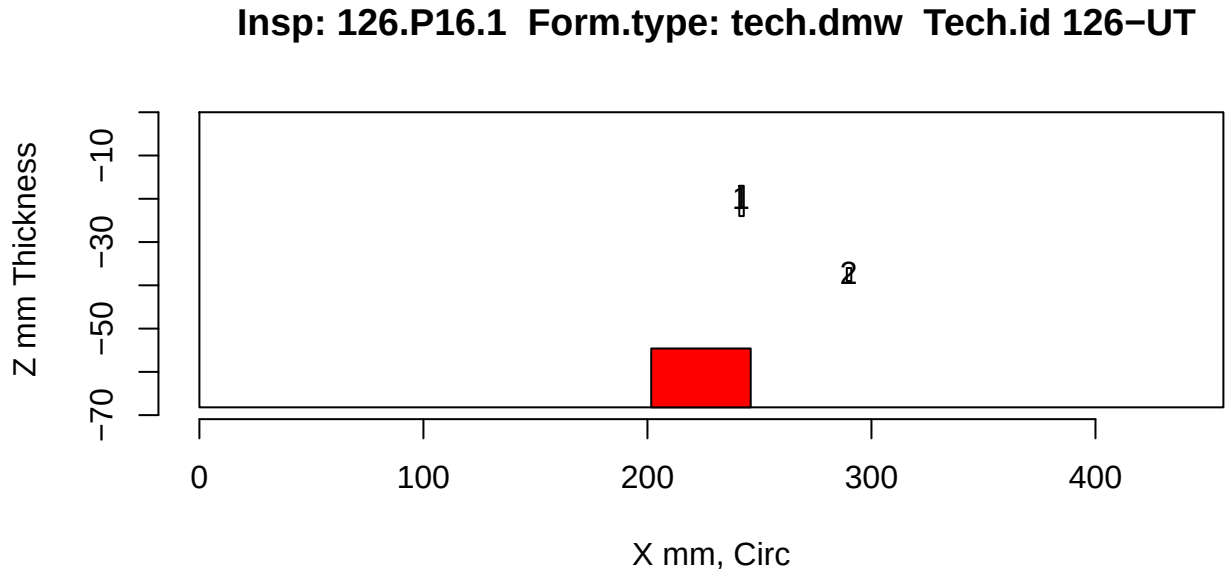
Insp: 126.P16.1 Form.type: tech.dmw Tech.id 126−UT
Z mm Thickness
−10
−30
−50
−70
1
2
0
100
200
300
400
X mm, Circ

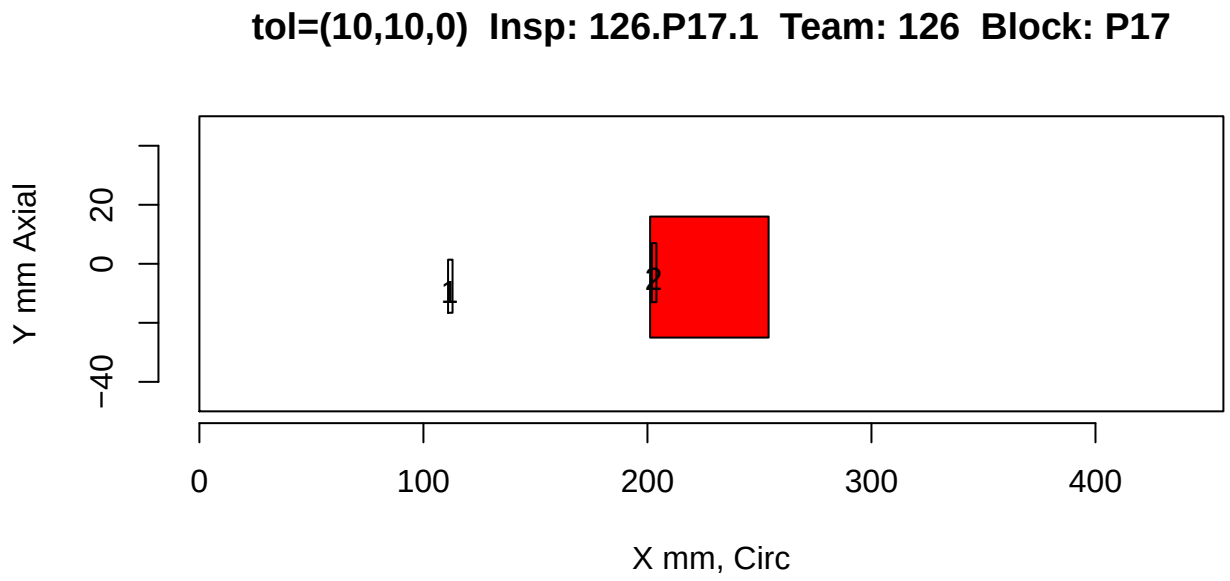
tol=(10,10,0) Insp: 126.P17.1 Team: 126 Block: P17
Y mm Axial
20
0
−40
1
2
0
100
200
300
400
X mm, Circ

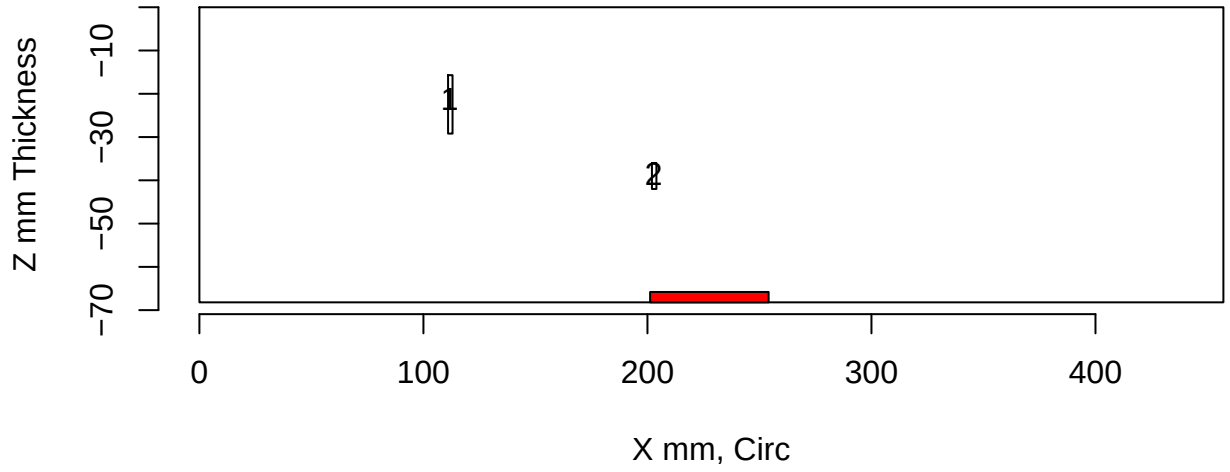
Insp: 126.P17.1 Form.type: sum.dmw Tech.id Summary
Z mm Thickness
−10
−30
−50
−70
1
2
0
100
200
300
400
X mm, Circ

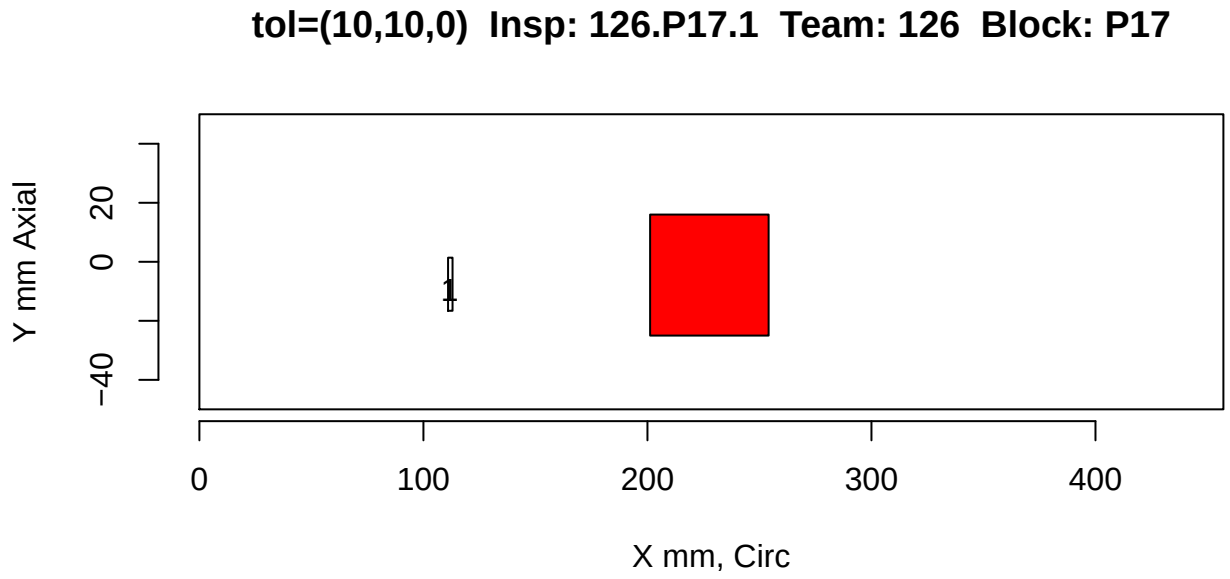
tol=(10,10,0) Insp: 126.P17.1 Team: 126 Block: P17
Y mm Axial
20
0
−40
1
0
100
200
300
400
X mm, Circ

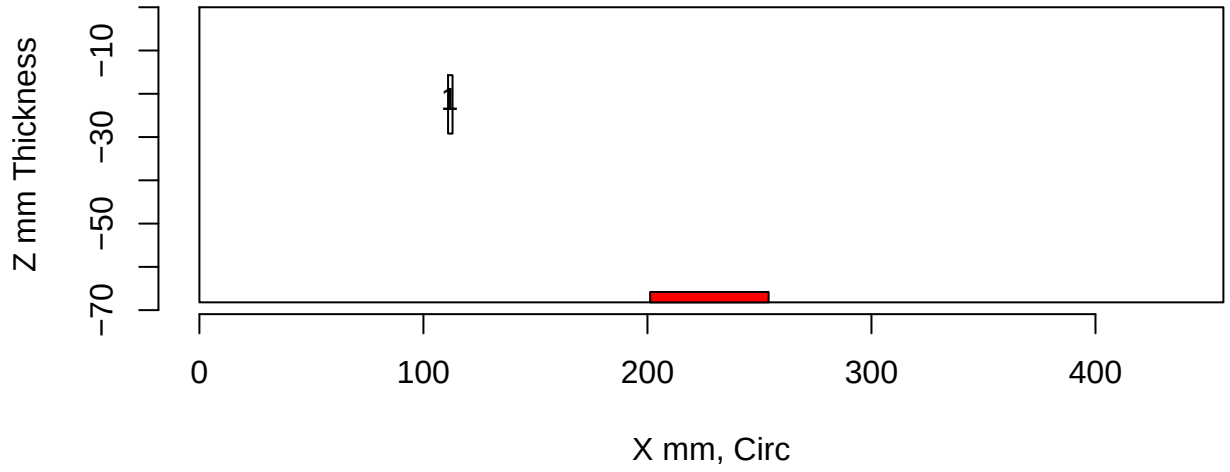
Insp: 126.P17.1 Form.type: tech.dmw Tech.id 126−PA
Z mm Thickness
−10
−30
−50
−70
1
0
100
200
300
400
X mm, Circ

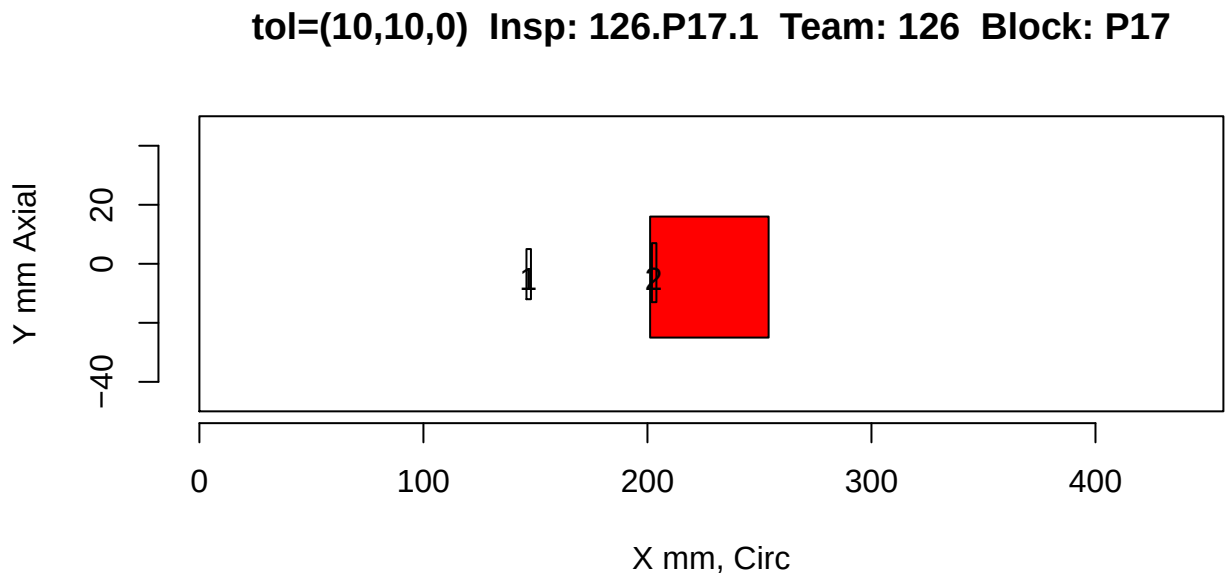
tol=(10,10,0) Insp: 126.P17.1 Team: 126 Block: P17
Y mm Axial
20
0
−40
1
2
0
100
200
300
400
X mm, Circ

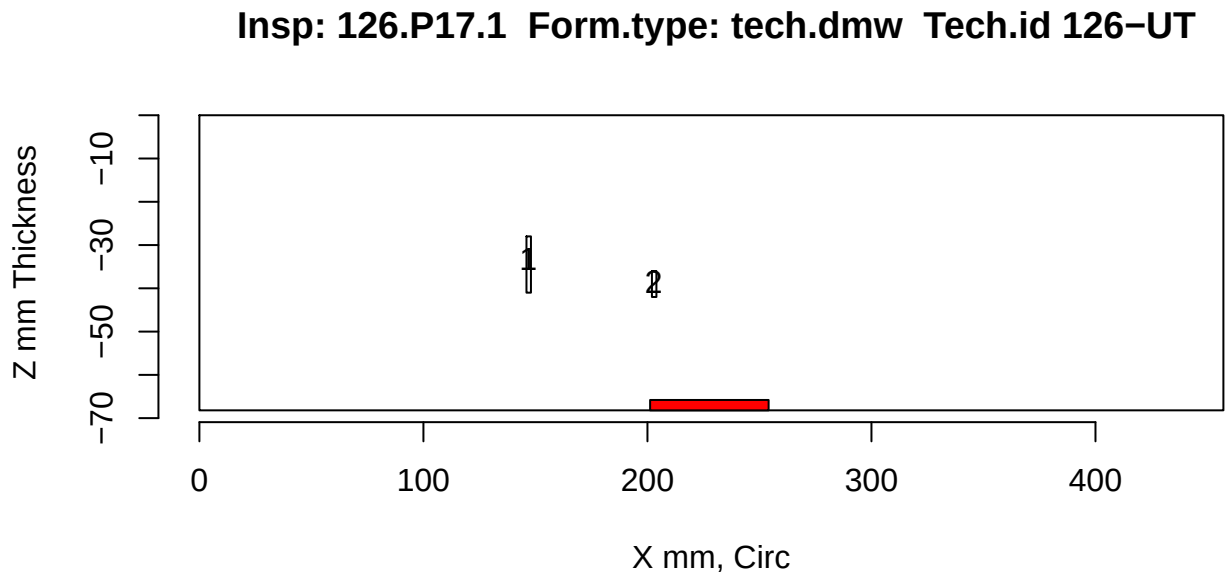
Insp: 126.P17.1 Form.type: tech.dmw Tech.id 126−UT
Z mm Thickness
−10
−30
−50
−70
1
2
0
100
200
300
400
X mm, Circ

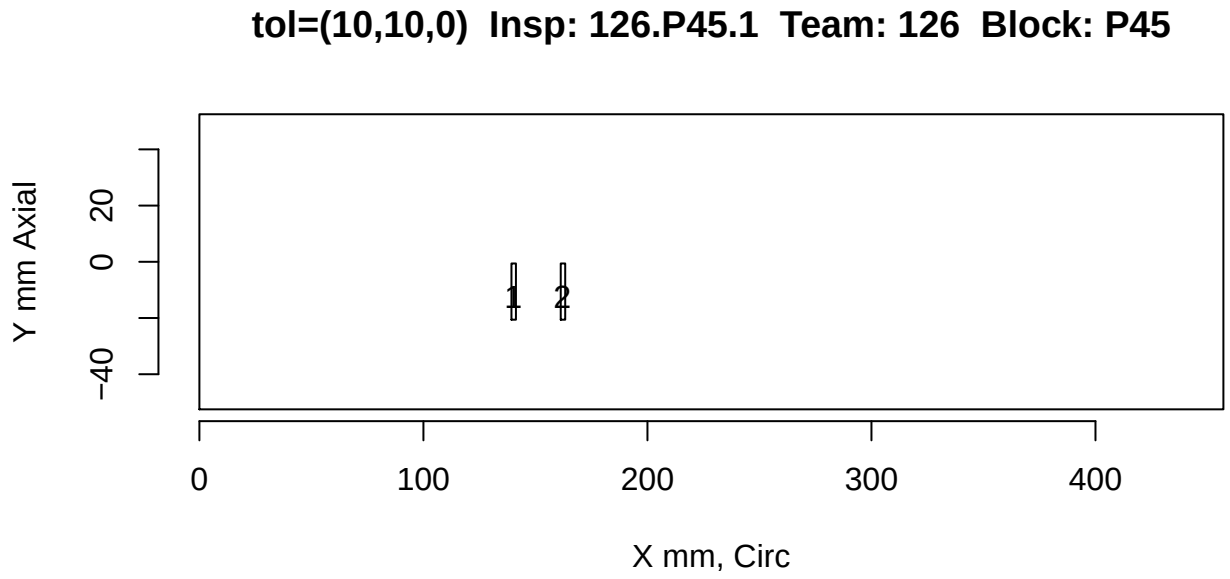
tol=(10,10,0) Insp: 126.P45.1 Team: 126 Block: P45
Y mm Axial
−40
0
20
1
2
0
100
200
300
400
X mm, Circ

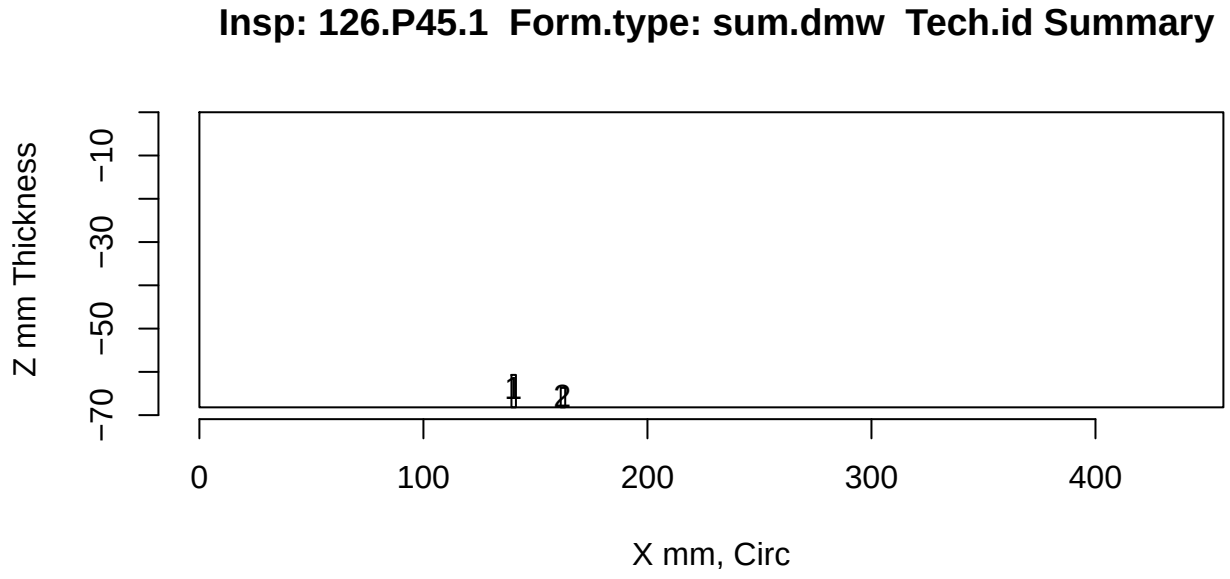
Insp: 126.P45.1 Form.type: sum.dmw Tech.id Summary
Z mm Thickness
−70
−50
−30
−10
1
2
0
100
200
300
400
X mm, Circ

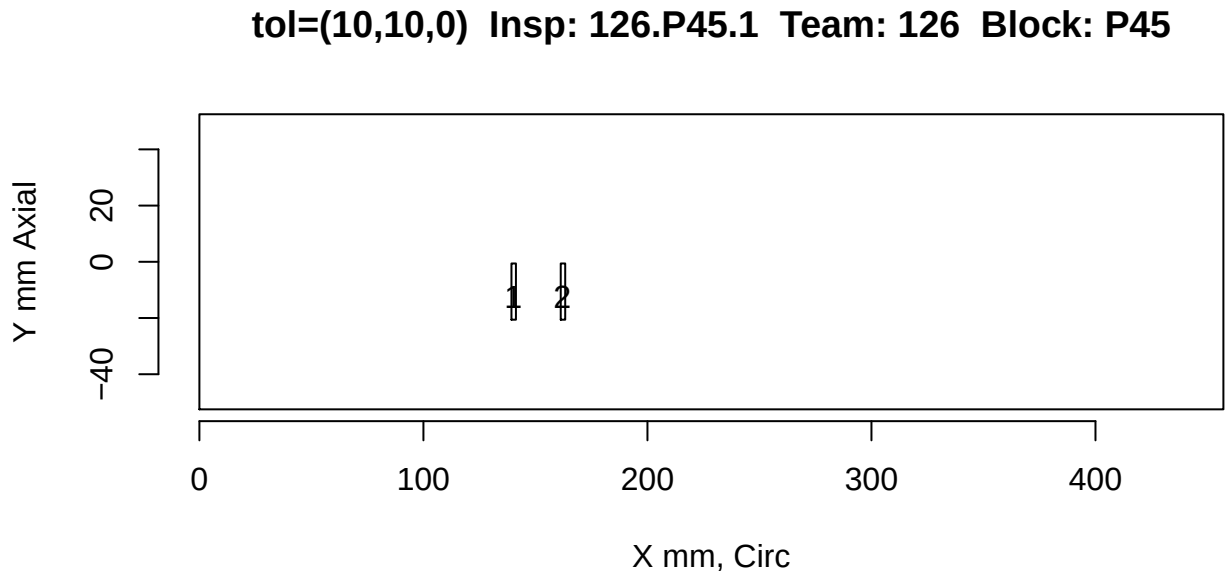
tol=(10,10,0) Insp: 126.P45.1 Team: 126 Block: P45
Y mm Axial
−40
0
20
1
2
0
100
200
300
400
X mm, Circ

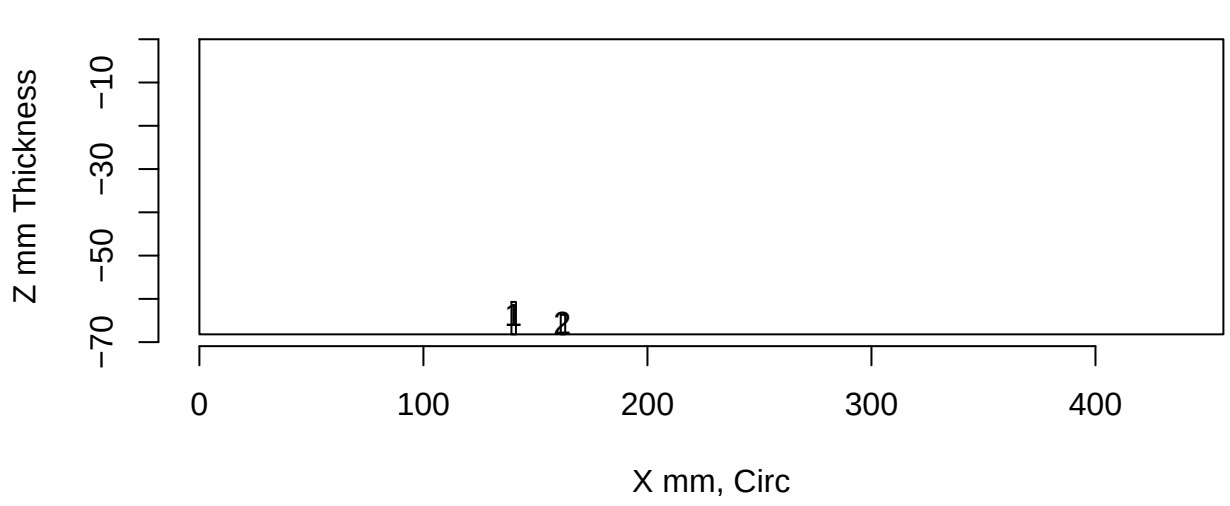
Insp: 126.P45.1 Form.type: tech.dmw Tech.id 126−PA
Z mm Thickness
−70
−50
−30
−10
1
2
0
100
200
300
400
X mm, Circ

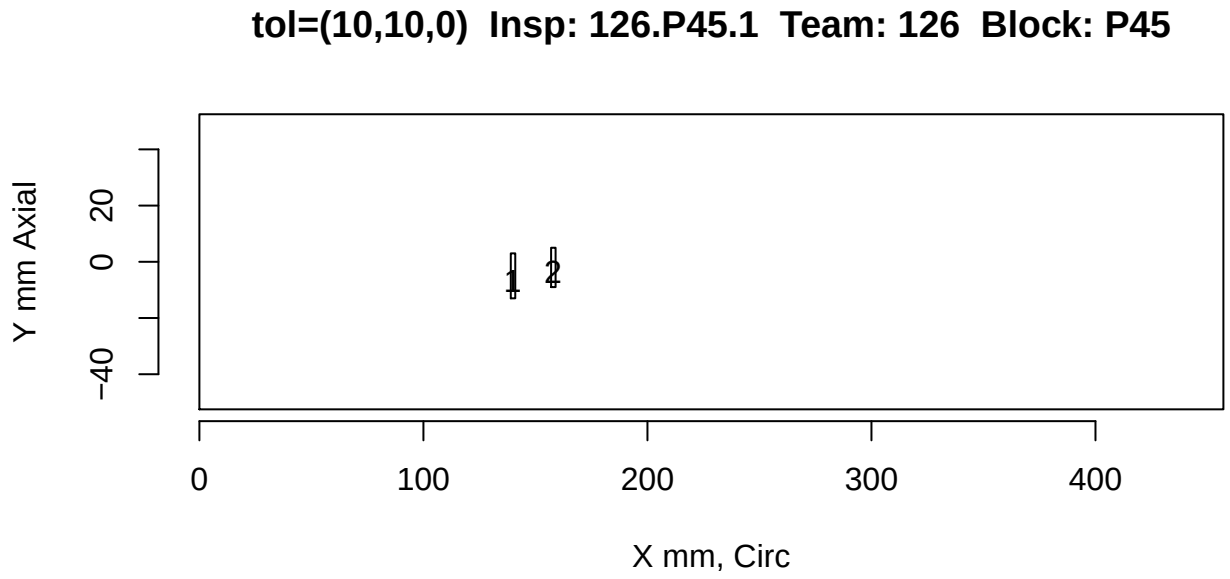
tol=(10,10,0) Insp: 126.P45.1 Team: 126 Block: P45
Y mm Axial
20
0
−40
1
2
0
100
200
300
400
X mm, Circ

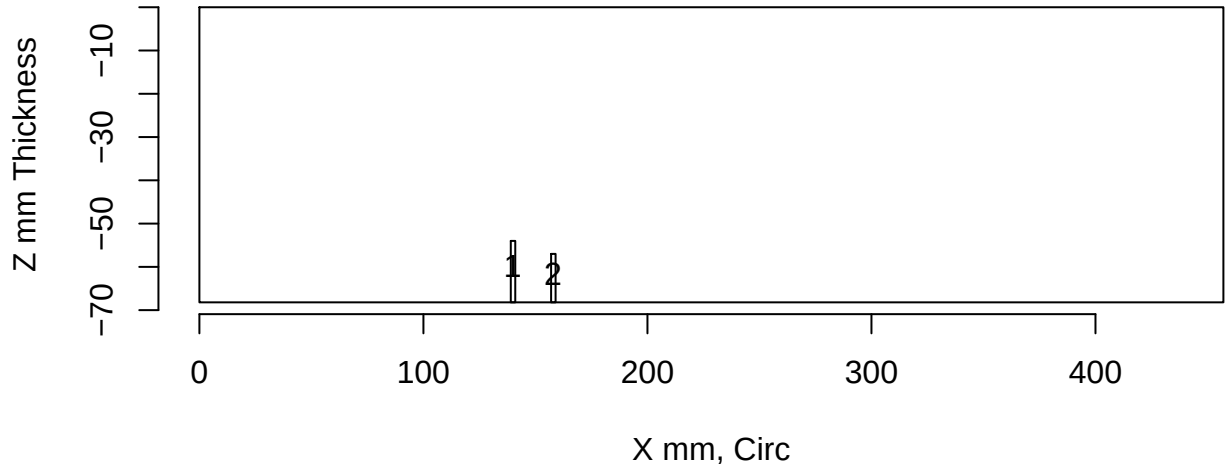
Insp: 126.P45.1 Form.type: tech.dmw Tech.id 126−UT
Z mm Thickness
−10
−30
−50
−70
1
2
0
100
200
300
400
X mm, Circ

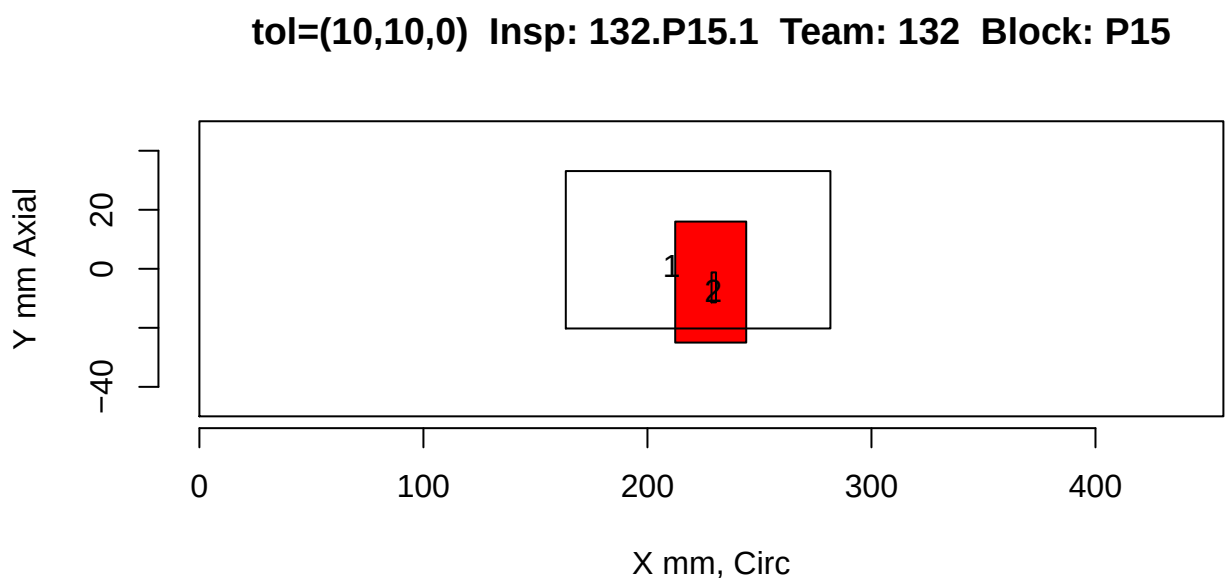
tol=(10,10,0) Insp: 132.P15.1 Team: 132 Block: P15
Y mm Axial
20
0
−40
1
2
0
100
200
300
400
X mm, Circ

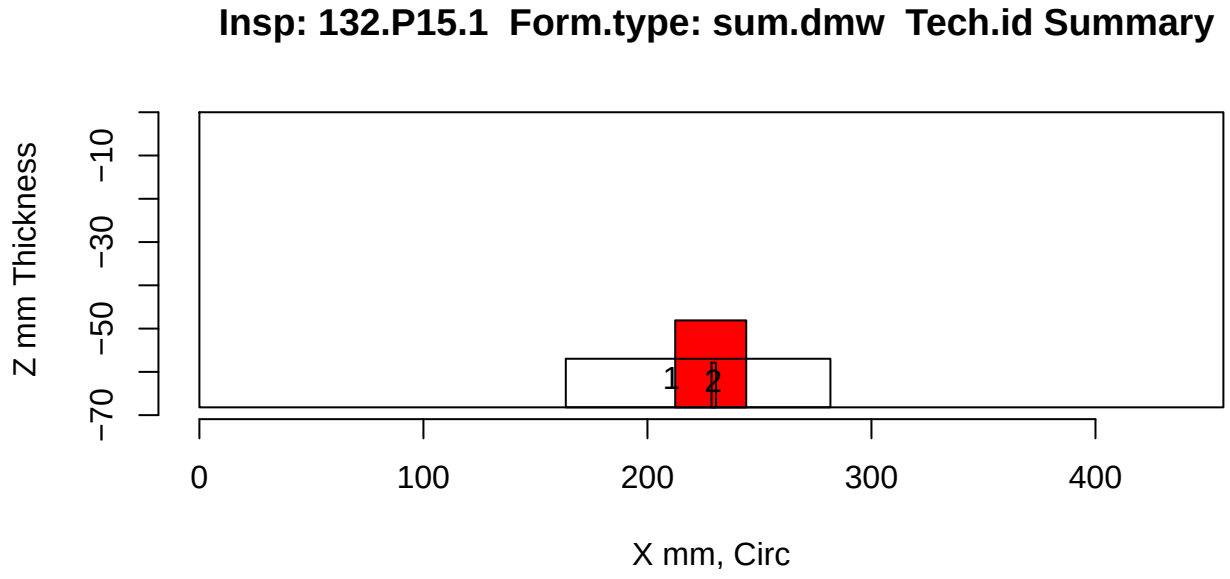
Insp: 132.P15.1 Form.type: sum.dmw Tech.id Summary
Z mm Thickness
−10
−30
−50
−70
1
2
0
100
200
300
400
X mm, Circ

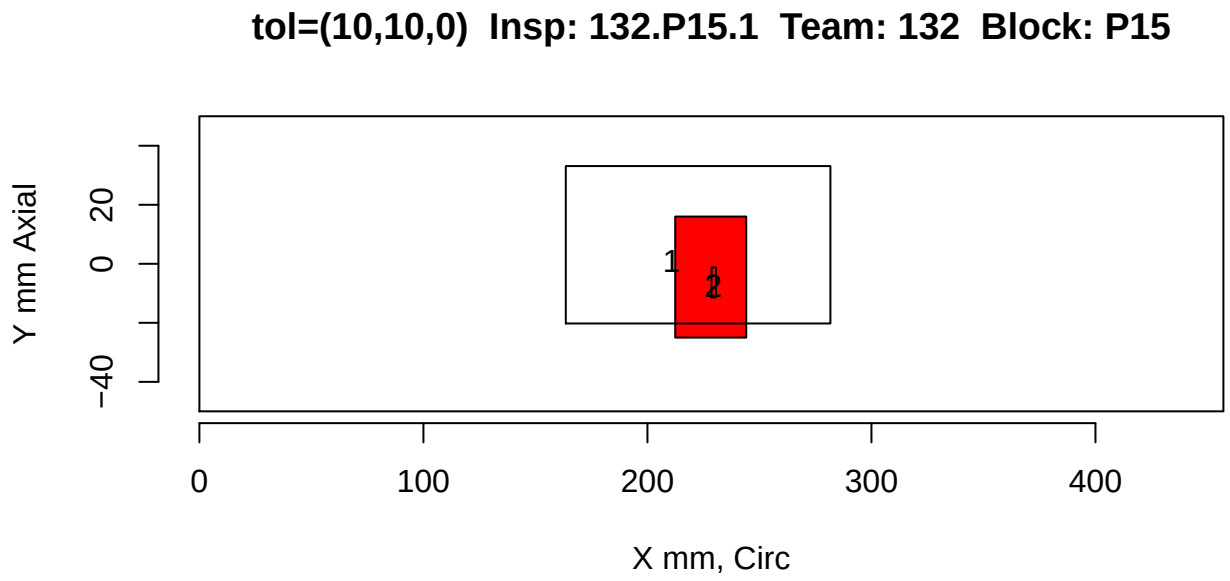
tol=(10,10,0) Insp: 132.P15.1 Team: 132 Block: P15
Y mm Axial
20
0
−40
1
2
0
100
200
300
400
X mm, Circ

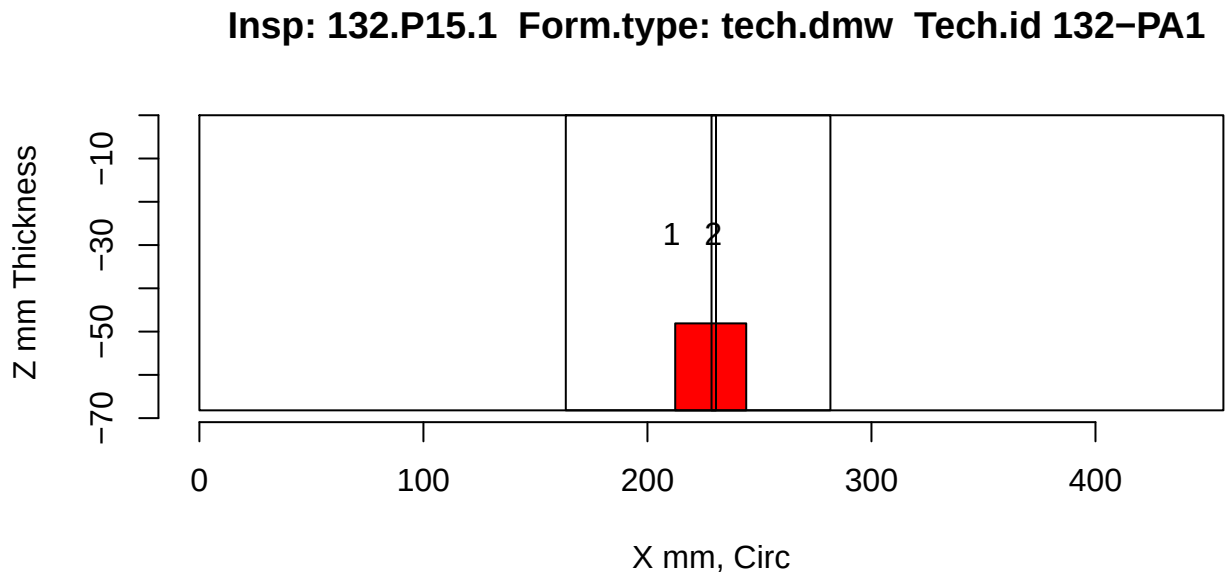
Insp: 132.P15.1 Form.type: tech.dmw Tech.id 132−PA1
Z mm Thickness
−10
−30
−50
−70
1
2
0
100
200
300
400
X mm, Circ

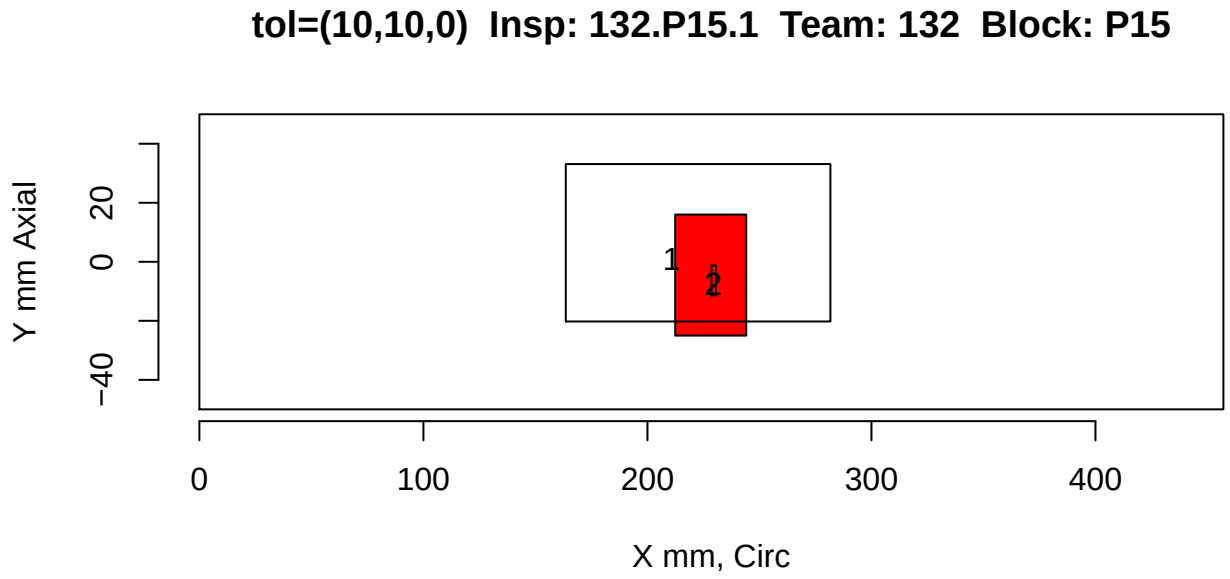
tol=(10,10,0) Insp: 132.P15.1 Team: 132 Block: P15
Y mm Axial
20
0
−40
1
2
0
100
200
300
400
X mm, Circ

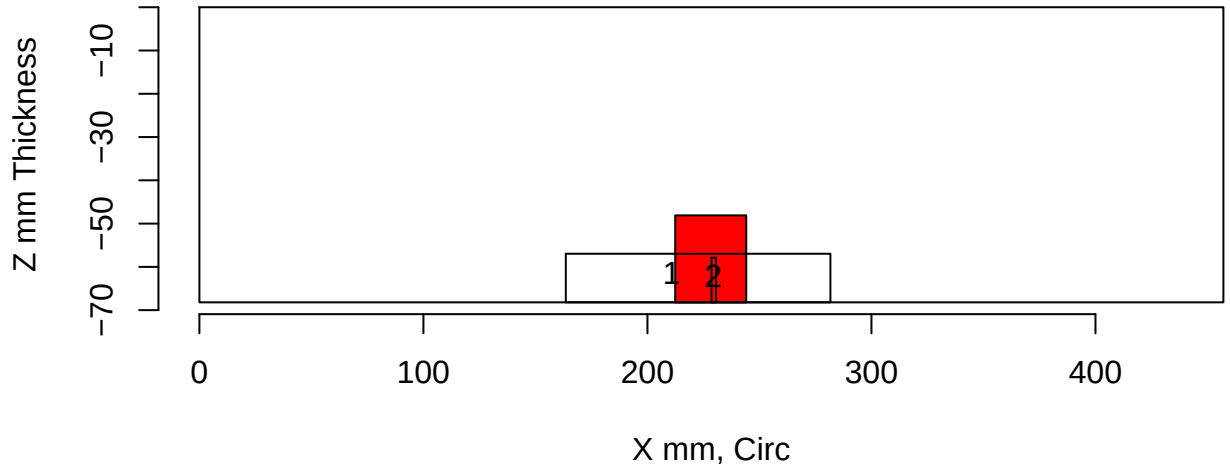
Insp: 132.P15.1 Form.type: tech.dmw Tech.id 132−PA2
Z mm Thickness
−10
−30
−50
−70
1
2
0
100
200
300
400
X mm, Circ

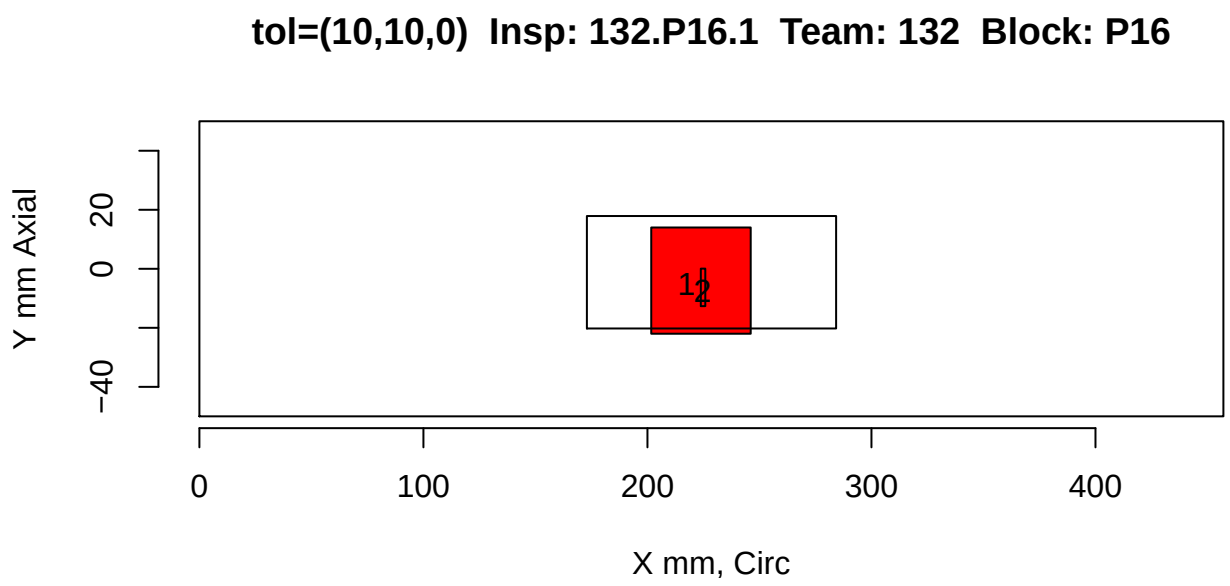
tol=(10,10,0) Insp: 132.P16.1 Team: 132 Block: P16
Y mm Axial
20
0
−40
12
0
100
200
300
400
X mm, Circ

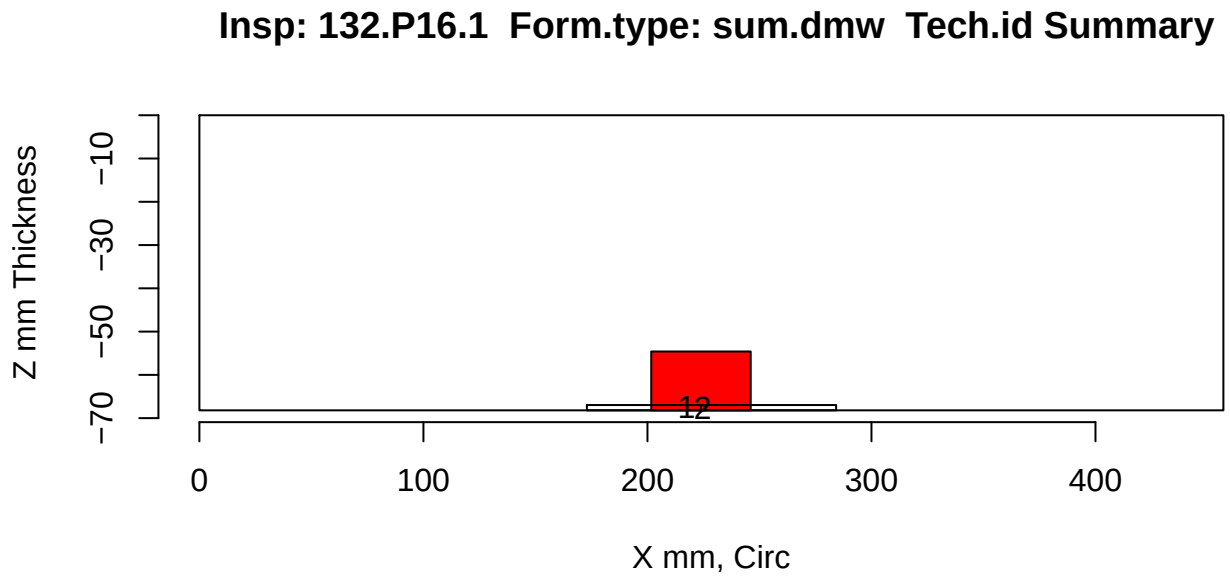
Insp: 132.P16.1 Form.type: sum.dmw Tech.id Summary
Z mm Thickness
−10
−30
−50
−70
12
0
100
200
300
400
X mm, Circ

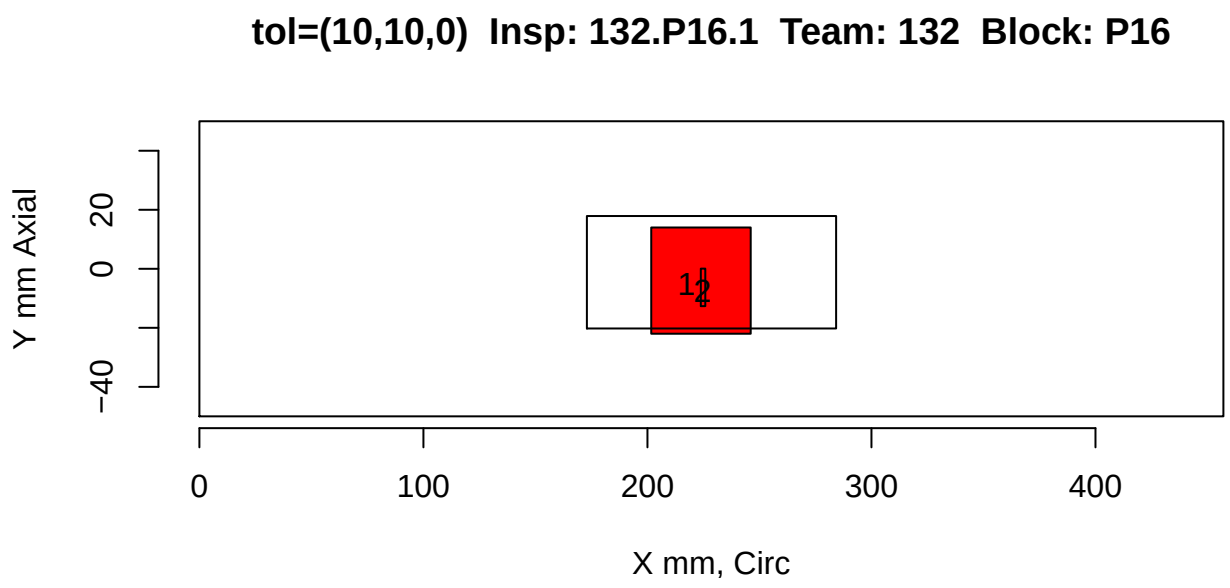
tol=(10,10,0) Insp: 132.P16.1 Team: 132 Block: P16
Y mm Axial
20
0
−40
12
0
100
200
300
400
X mm, Circ

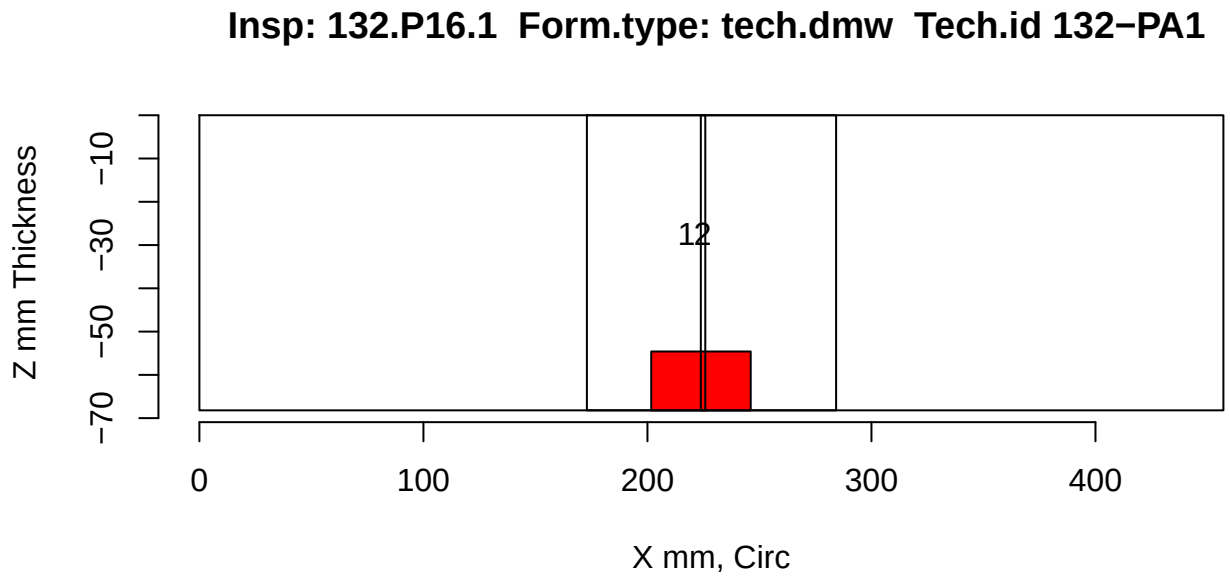
Insp: 132.P16.1 Form.type: tech.dmw Tech.id 132−PA1
Z mm Thickness
−10
−30
−50
−70
12
0
100
200
300
400
X mm, Circ

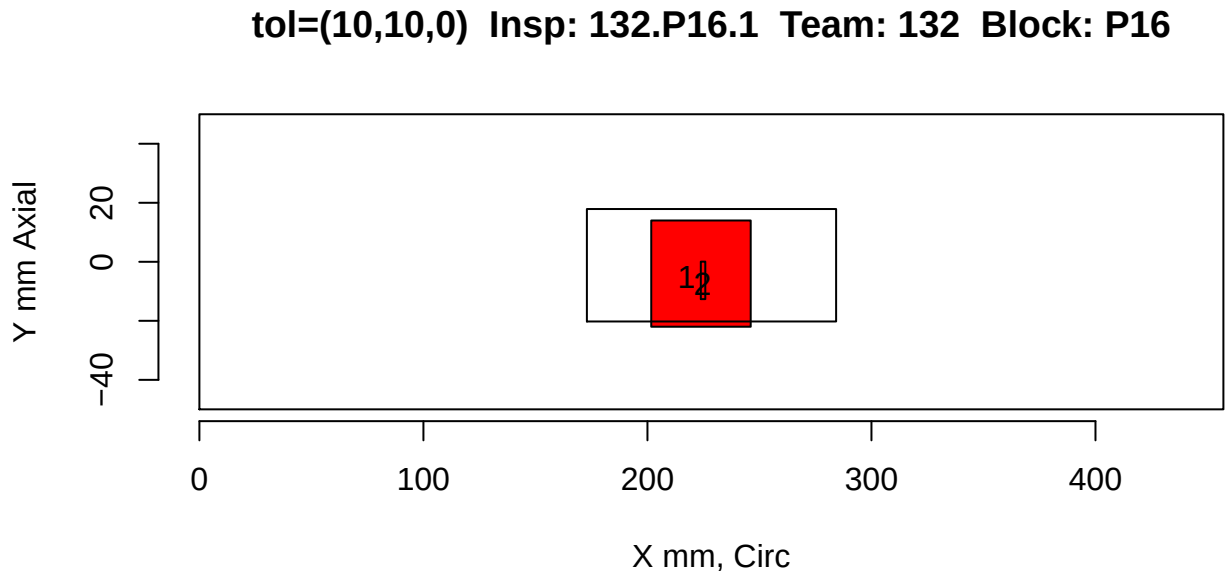
tol=(10,10,0) Insp: 132.P16.1 Team: 132 Block: P16
Y mm Axial
20
0
−40
12
0
100
200
300
400
X mm, Circ

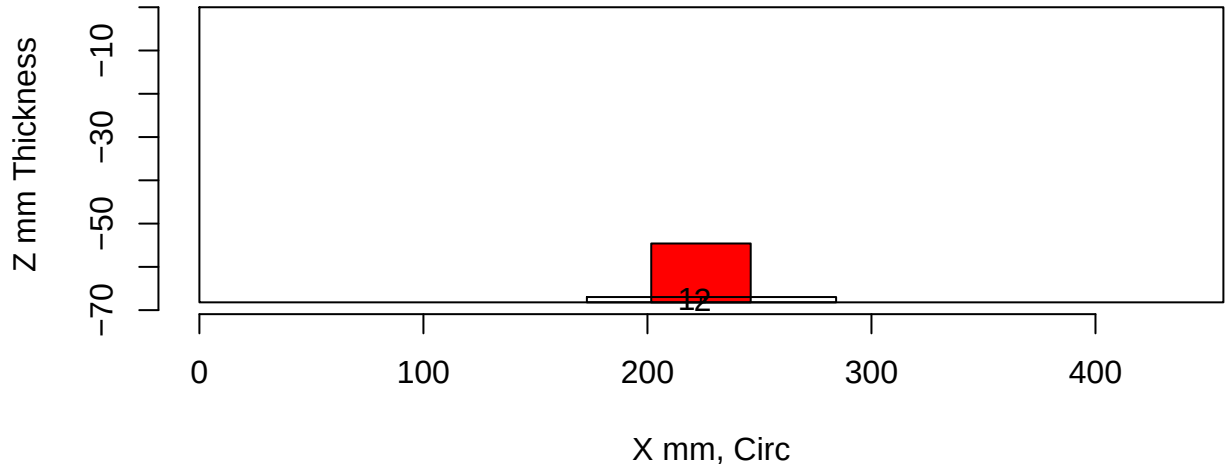
Insp: 132.P16.1 Form.type: tech.dmw Tech.id 132−PA2
Z mm Thickness
−10
−30
−50
−70
12
0
100
200
300
400
X mm, Circ

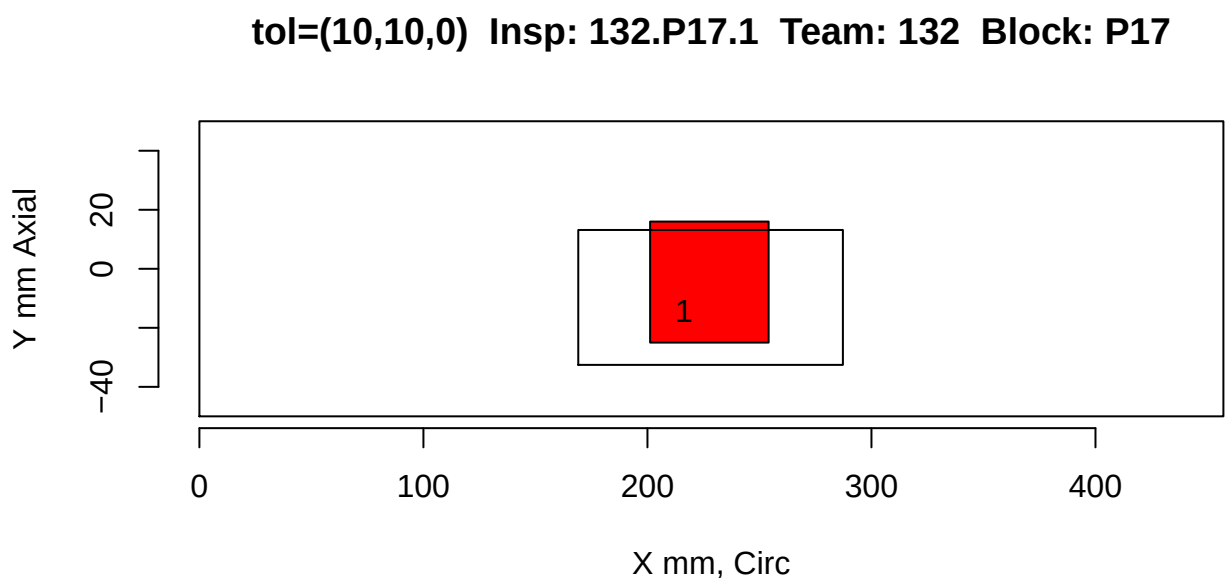
tol=(10,10,0) Insp: 132.P17.1 Team: 132 Block: P17
Y mm Axial
20
0
−40
1
0
100
200
300
400
X mm, Circ

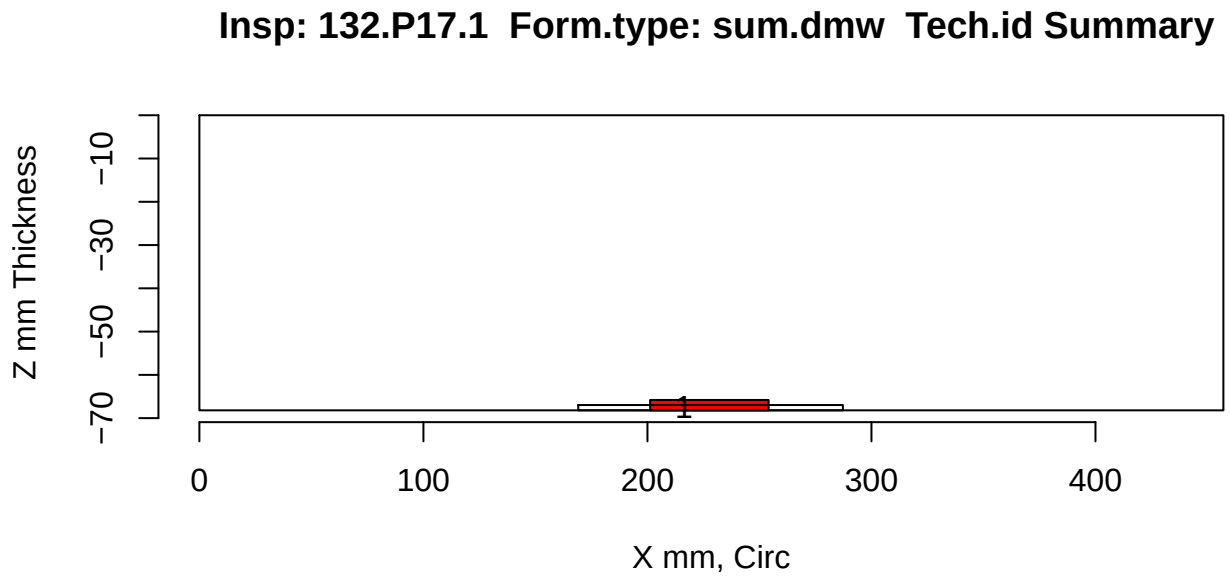
Insp: 132.P17.1 Form.type: sum.dmw Tech.id Summary
Z mm Thickness
−10
−30
−50
−70
1
0
100
200
300
400
X mm, Circ

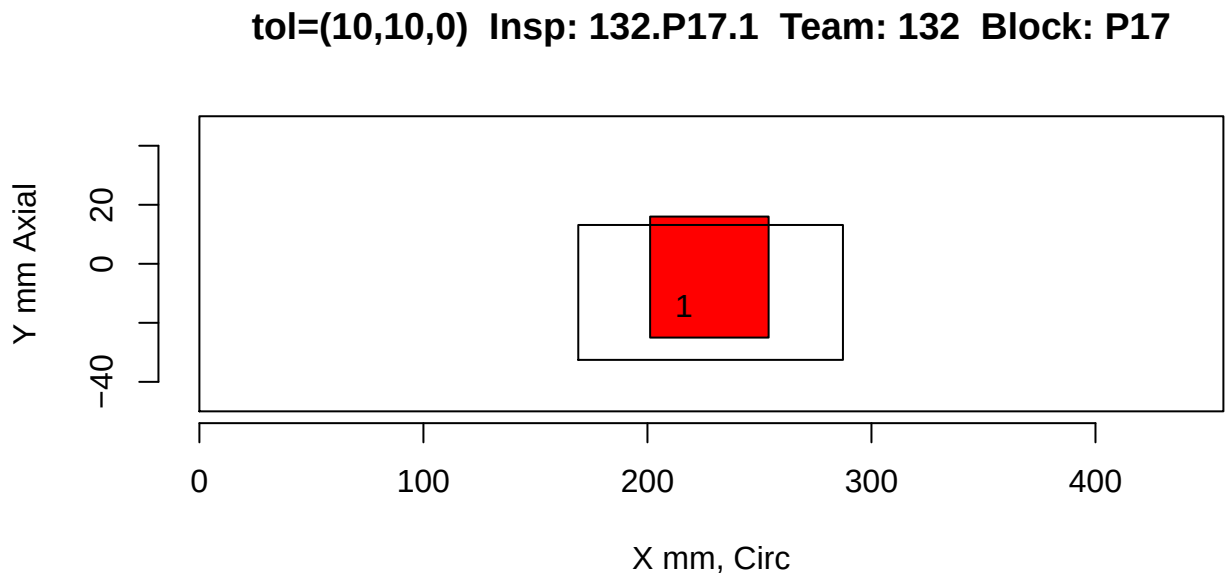
tol=(10,10,0) Insp: 132.P17.1 Team: 132 Block: P17
Y mm Axial
20
0
−40
1
0
100
200
300
400
X mm, Circ

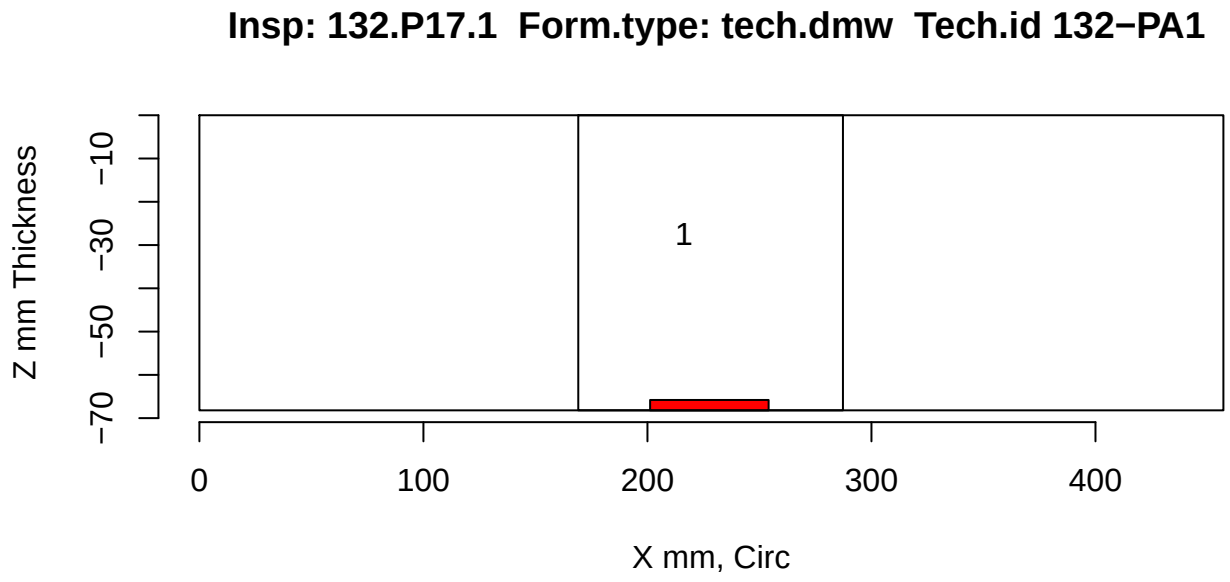
Insp: 132.P17.1 Form.type: tech.dmw Tech.id 132−PA1
Z mm Thickness
−10
−30
−50
−70
1
0
100
200
300
400
X mm, Circ

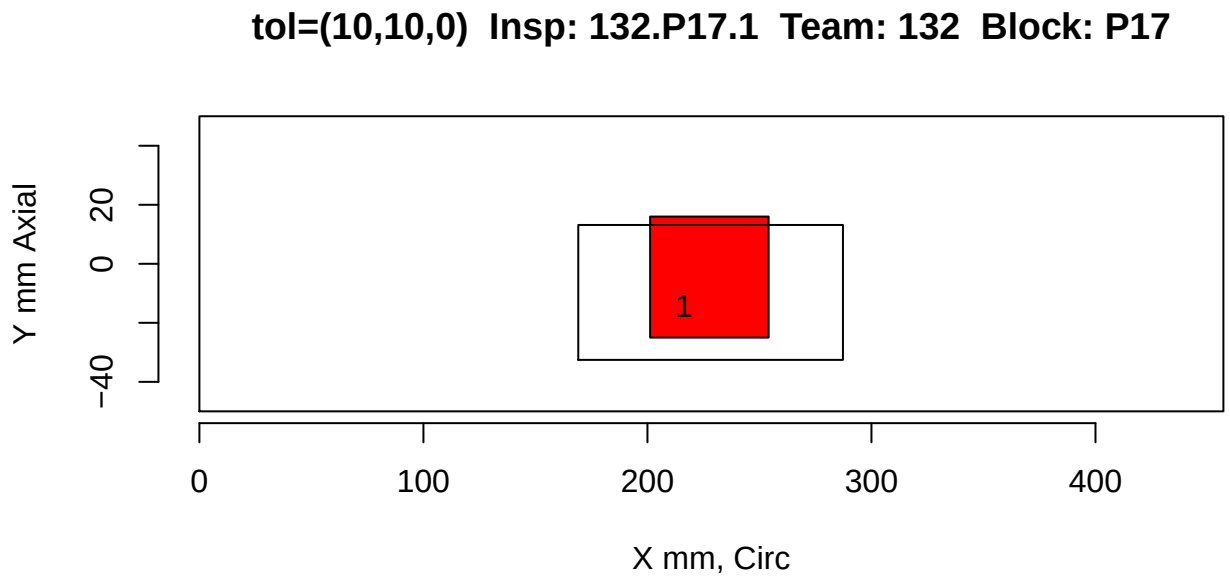
tol=(10,10,0) Insp: 132.P17.1 Team: 132 Block: P17
Y mm Axial
20
0
−40
1
0
100
200
300
400
X mm, Circ

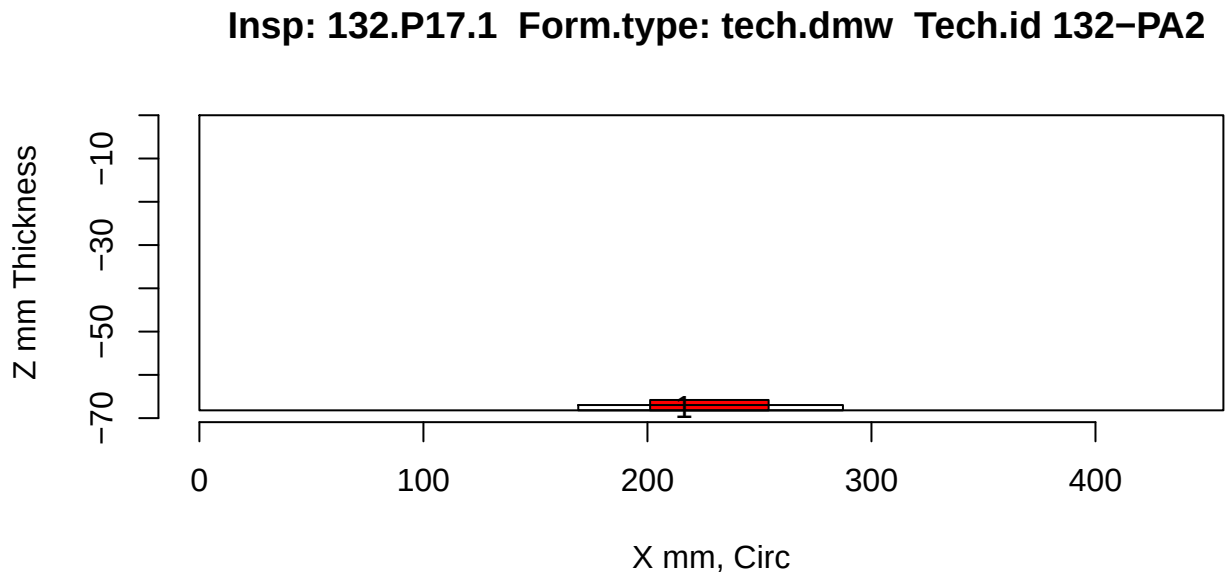
Insp: 132.P17.1 Form.type: tech.dmw Tech.id 132−PA2
Z mm Thickness
−10
−30
−50
−70
1
0
100
200
300
400
X mm, Circ

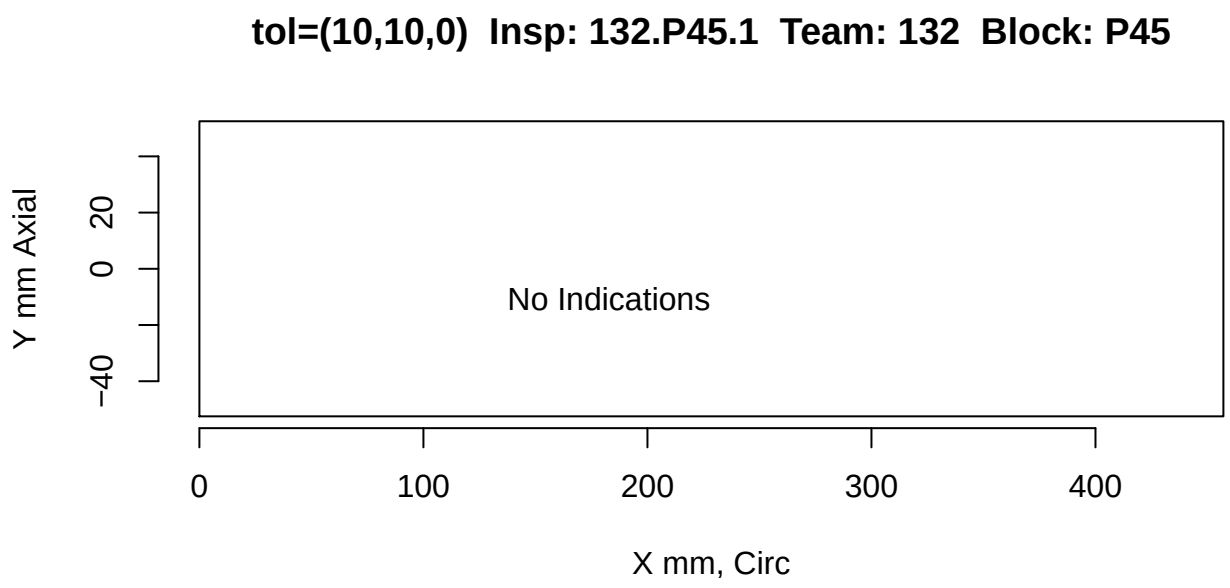
tol=(10,10,0) Insp: 132.P45.1 Team: 132 Block: P45
Y mm Axial
20
0
−40
No Indications
0
100
200
300
400
X mm, Circ

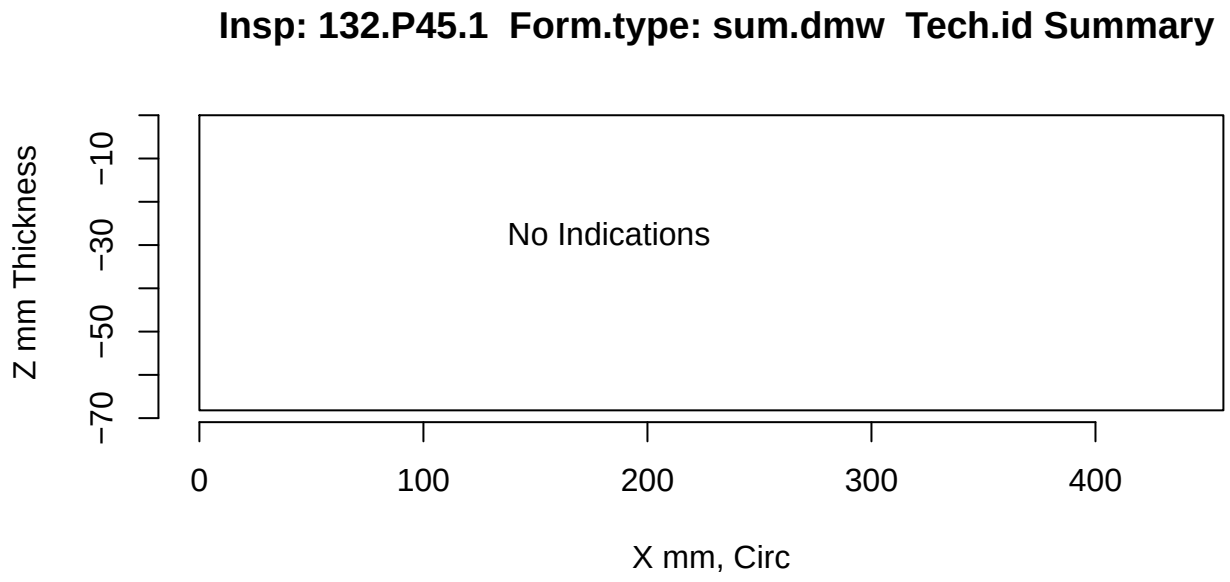
Insp: 132.P45.1 Form.type: sum.dmw Tech.id Summary
Z mm Thickness
−10
−30
−50
−70
No Indications
0
100
200
300
400
X mm, Circ

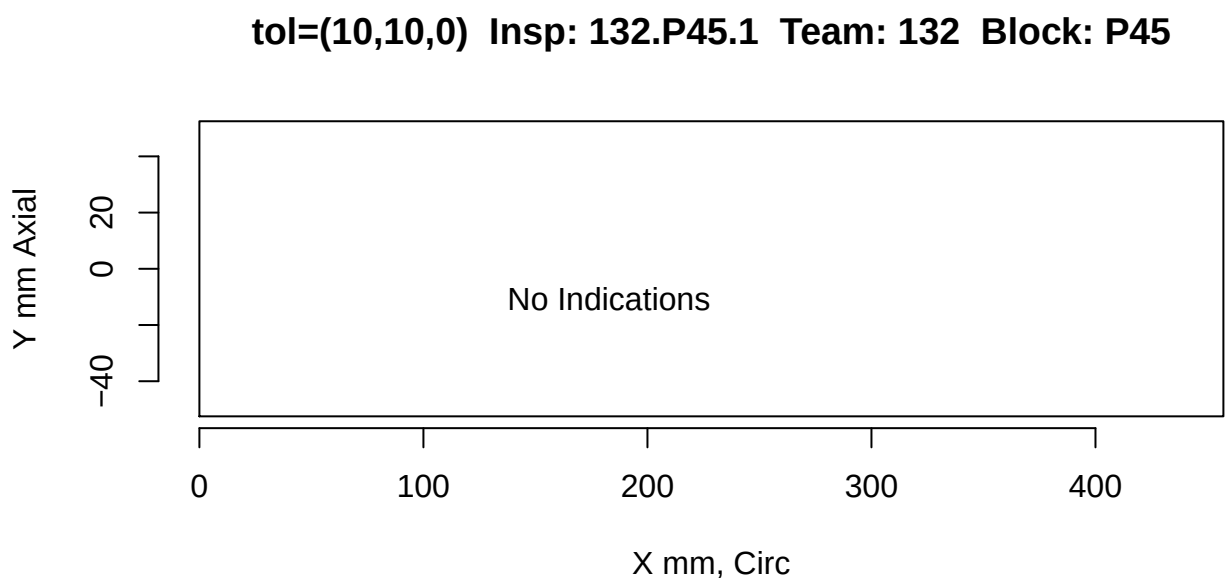
tol=(10,10,0) Insp: 132.P45.1 Team: 132 Block: P45
Y mm Axial
20
0
−40
No Indications
0
100
200
300
400
X mm, Circ

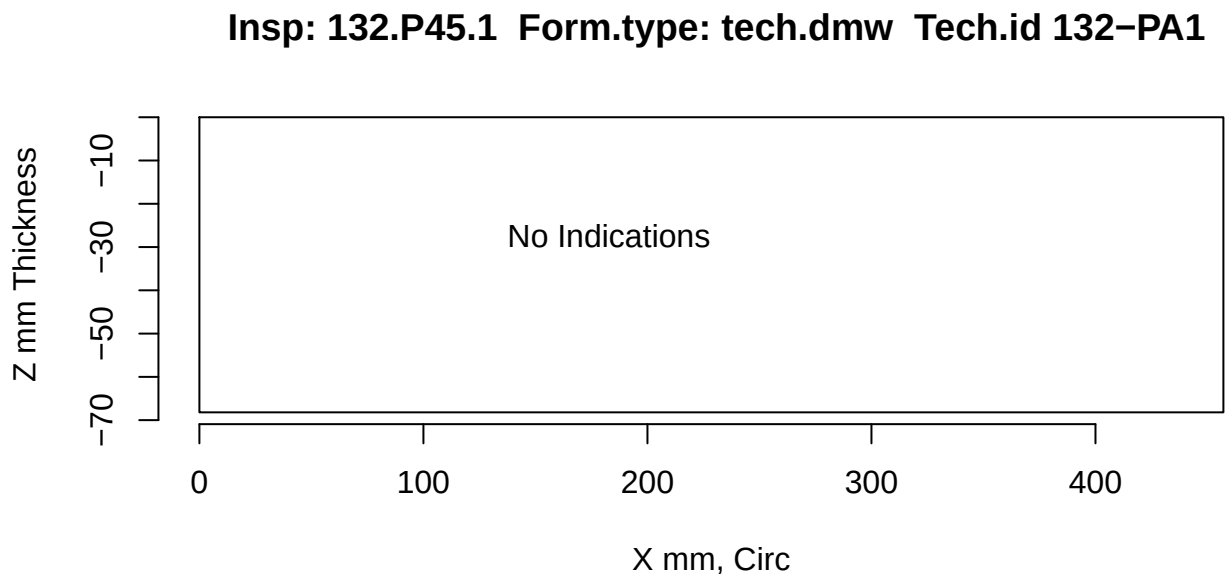
Insp: 132.P45.1 Form.type: tech.dmw Tech.id 132−PA1
Z mm Thickness
−10
−30
−50
−70
No Indications
0
100
200
300
400
X mm, Circ

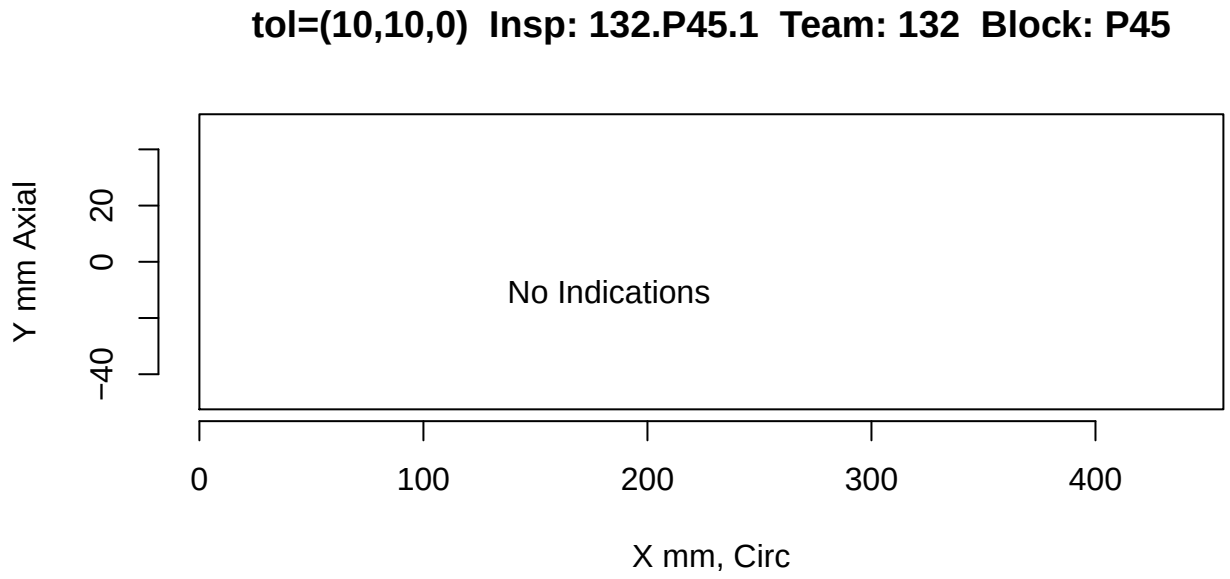
tol=(10,10,0) Insp: 132.P45.1 Team: 132 Block: P45
Y mm Axial
20
0
−40
No Indications
0
100
200
300
400
X mm, Circ

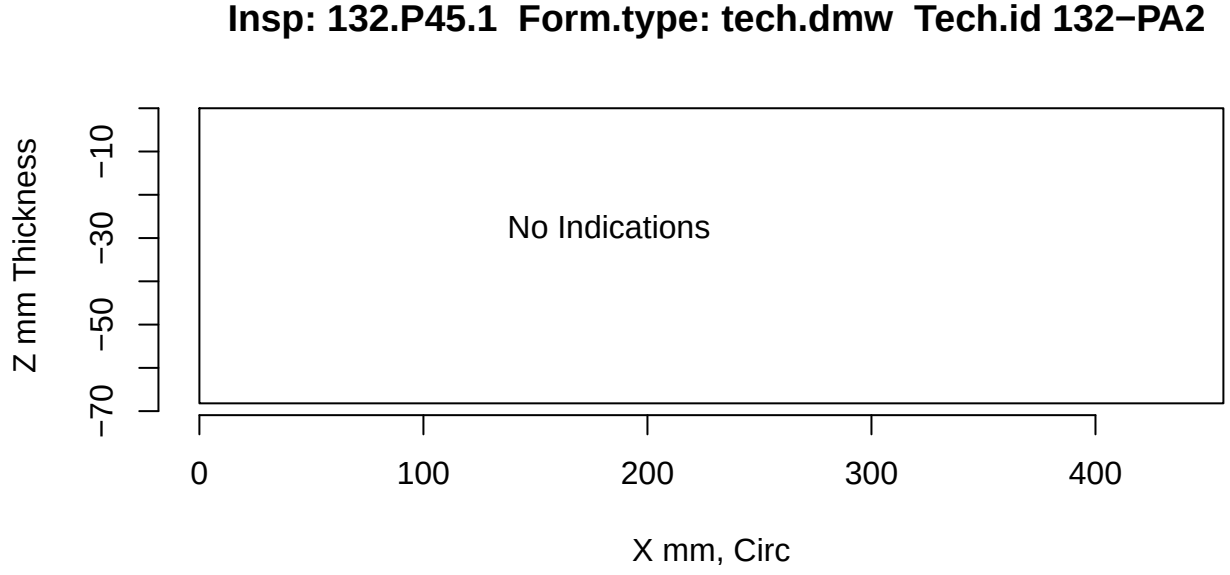
Insp: 132.P45.1 Form.type: tech.dmw Tech.id 132−PA2
Z mm Thickness
−10
−30
−50
−70
No Indications
0
100
200
300
400
X mm, Circ

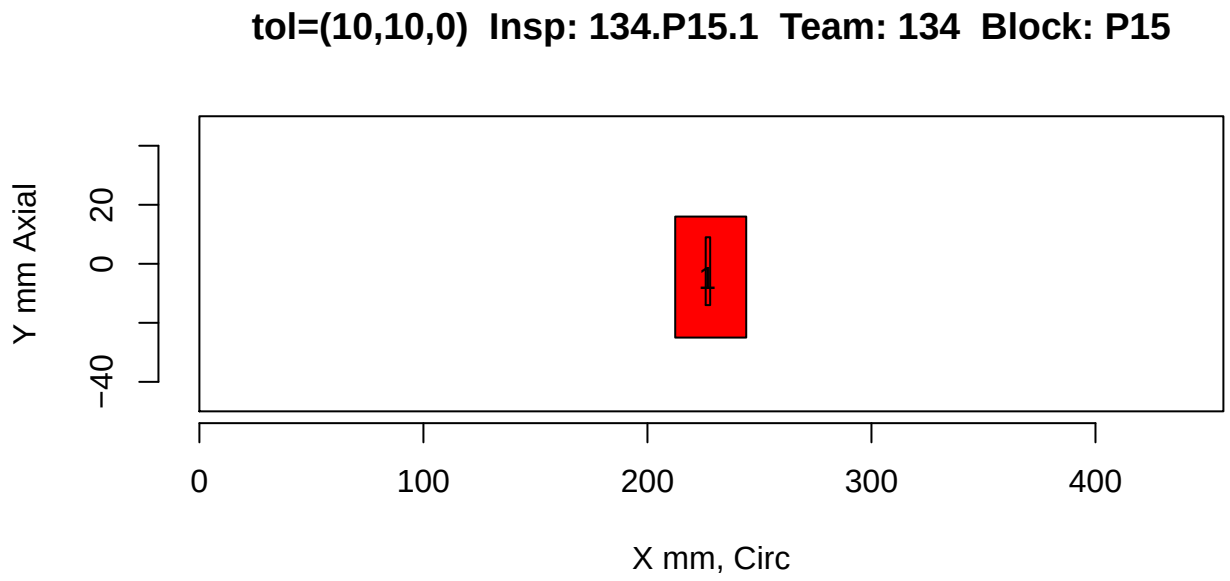
tol=(10,10,0) Insp: 134.P15.1 Team: 134 Block: P15
Y mm Axial
20
0
−40
1
0
100
200
300
400
X mm, Circ

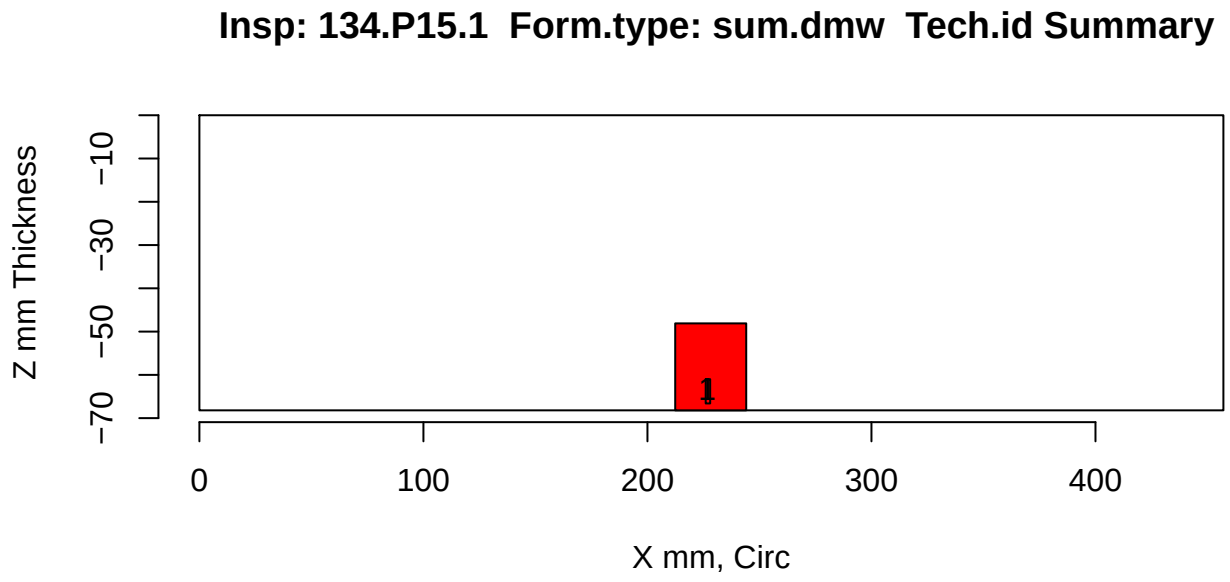
Insp: 134.P15.1 Form.type: sum.dmw Tech.id Summary
Z mm Thickness
−10
−30
−50
−70
1
0
100
200
300
400
X mm, Circ

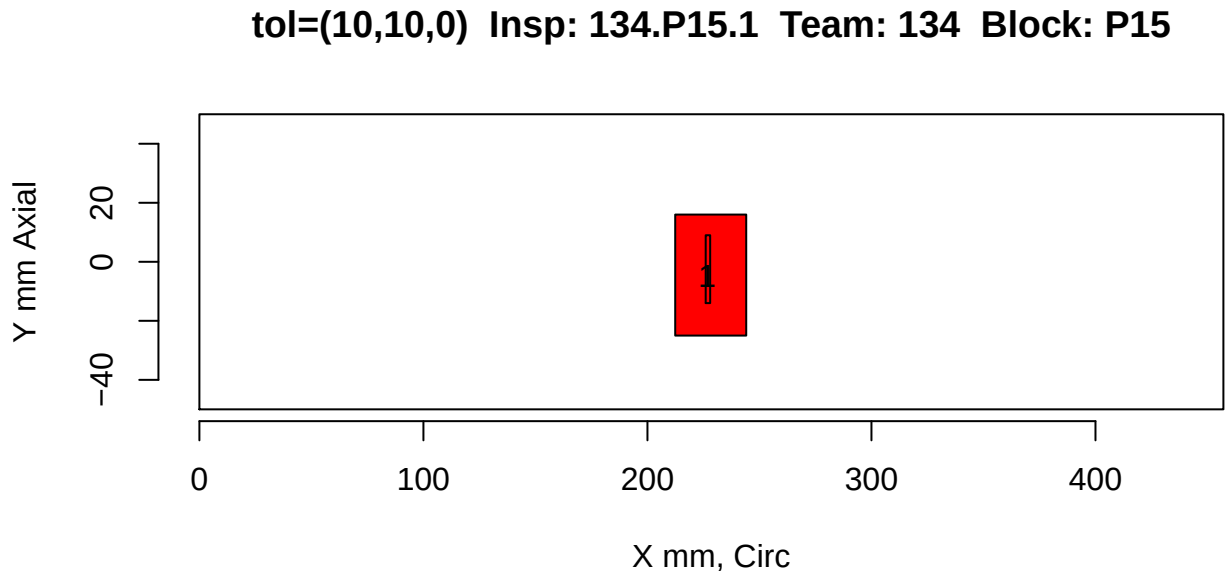
tol=(10,10,0) Insp: 134.P15.1 Team: 134 Block: P15
Y mm Axial
20
0
−40
1
0
100
200
300
400
X mm, Circ

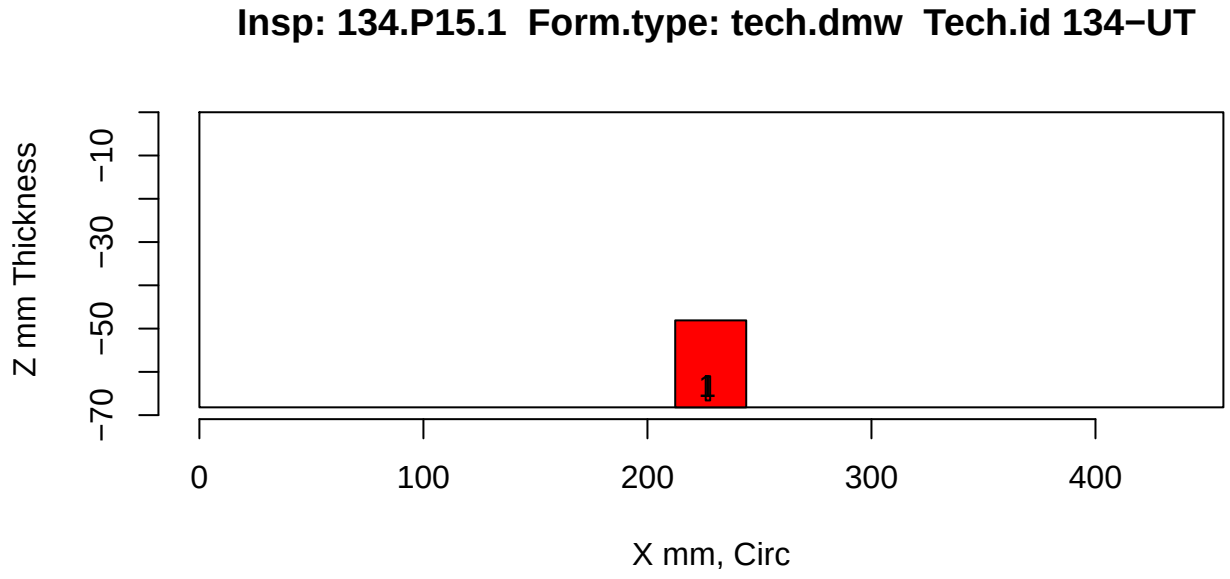
Insp: 134.P15.1 Form.type: tech.dmw Tech.id 134−UT
Z mm Thickness
−10
−30
−50
−70
1
0
100
200
300
400
X mm, Circ

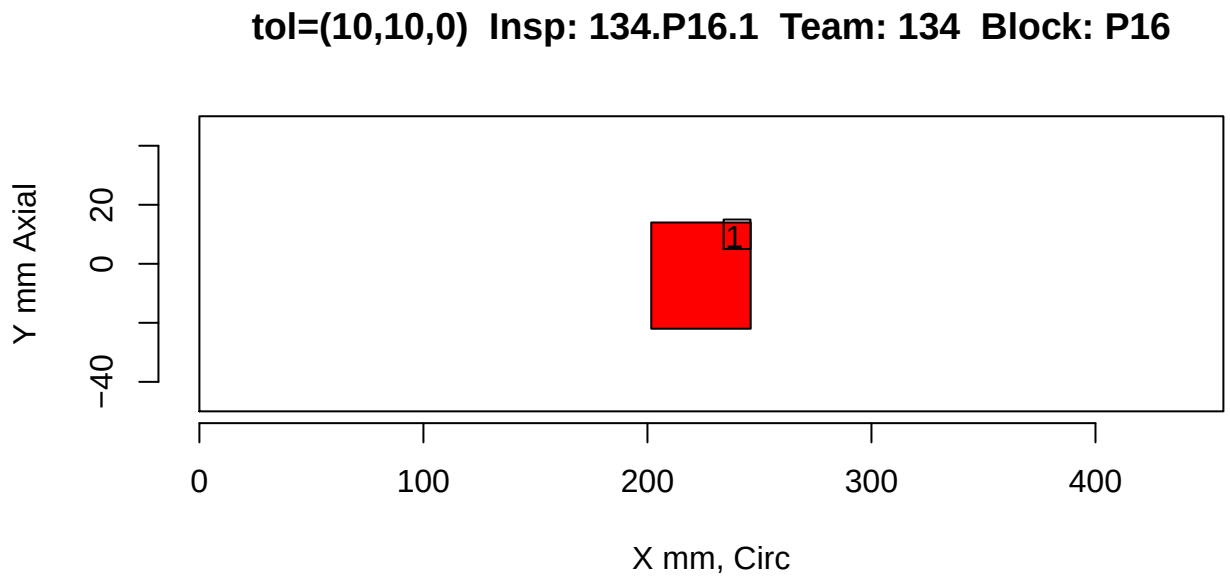
tol=(10,10,0) Insp: 134.P16.1 Team: 134 Block: P16
Y mm Axial
20
0
−40
1
0
100
200
300
400
X mm, Circ

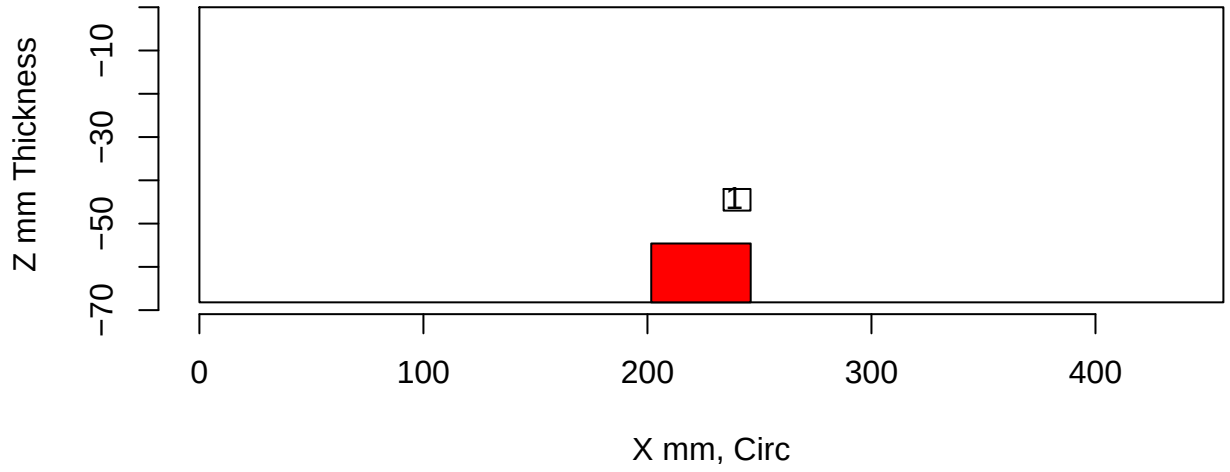
Insp: 134.P16.1 Form.type: sum.dmw Tech.id Summary
Z mm Thickness
−10
−30
−50
−70
1
0
100
200
300
400
X mm, Circ

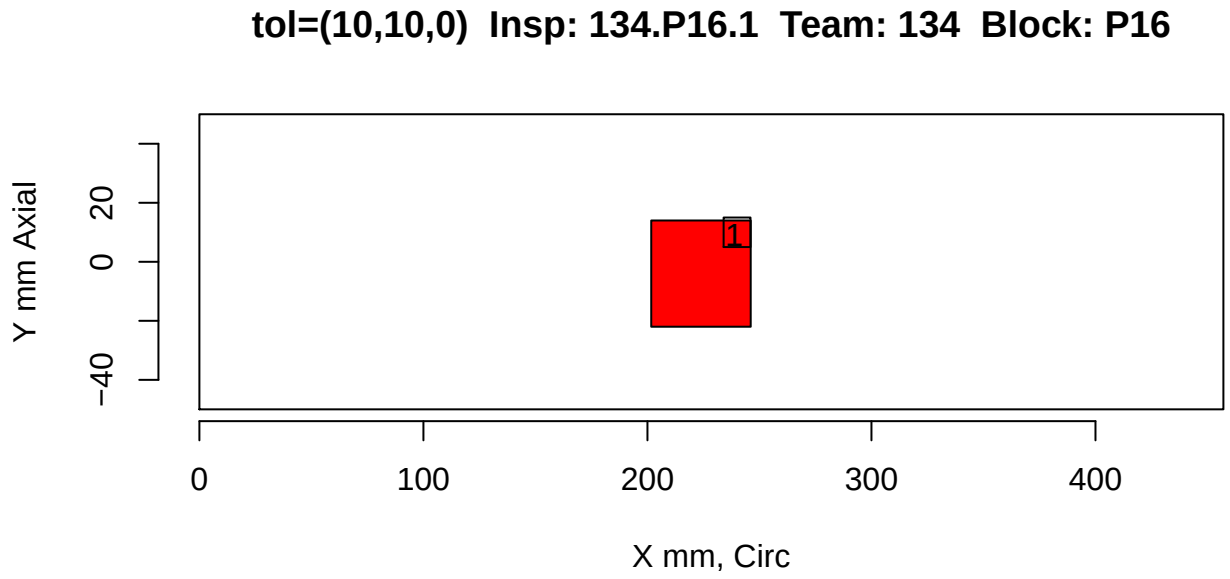
tol=(10,10,0) Insp: 134.P16.1 Team: 134 Block: P16
Y mm Axial
20
0
−40
1
0
100
200
300
400
X mm, Circ

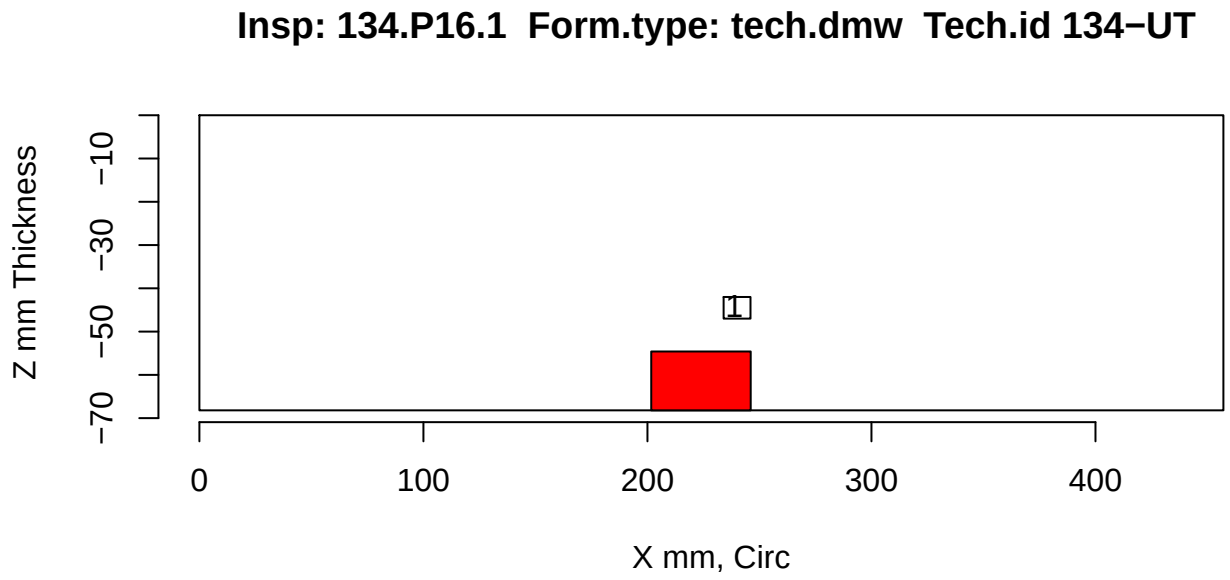
Insp: 134.P16.1 Form.type: tech.dmw Tech.id 134−UT
Z mm Thickness
−10
−30
−50
−70
1
0
100
200
300
400
X mm, Circ

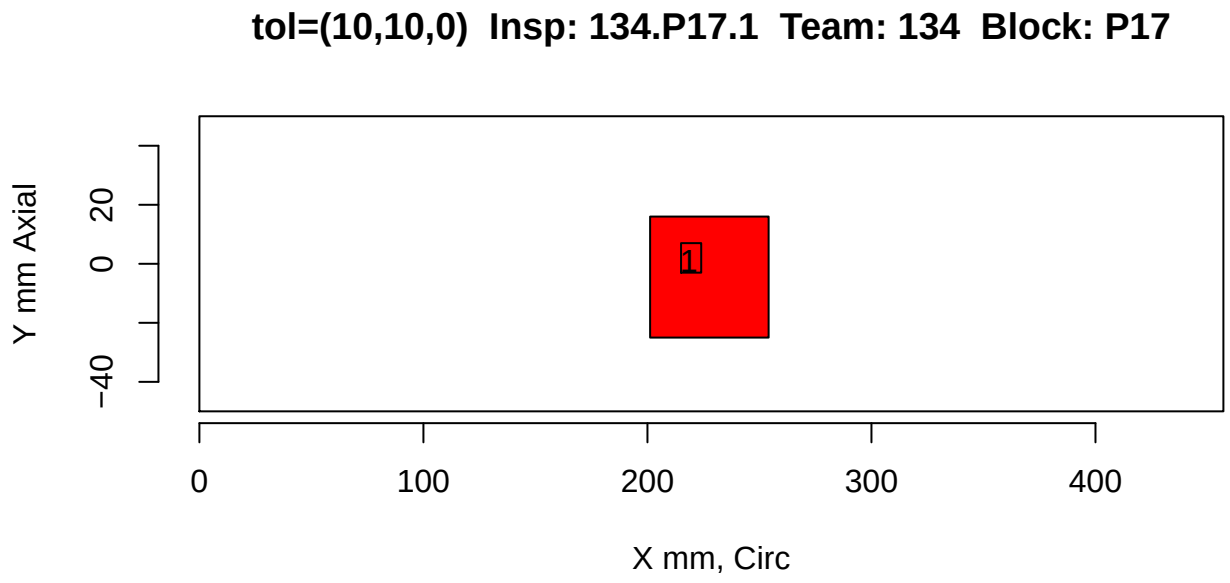
tol=(10,10,0) Insp: 134.P17.1 Team: 134 Block: P17
Y mm Axial
20
0
−40
1
0
100
200
300
400
X mm, Circ

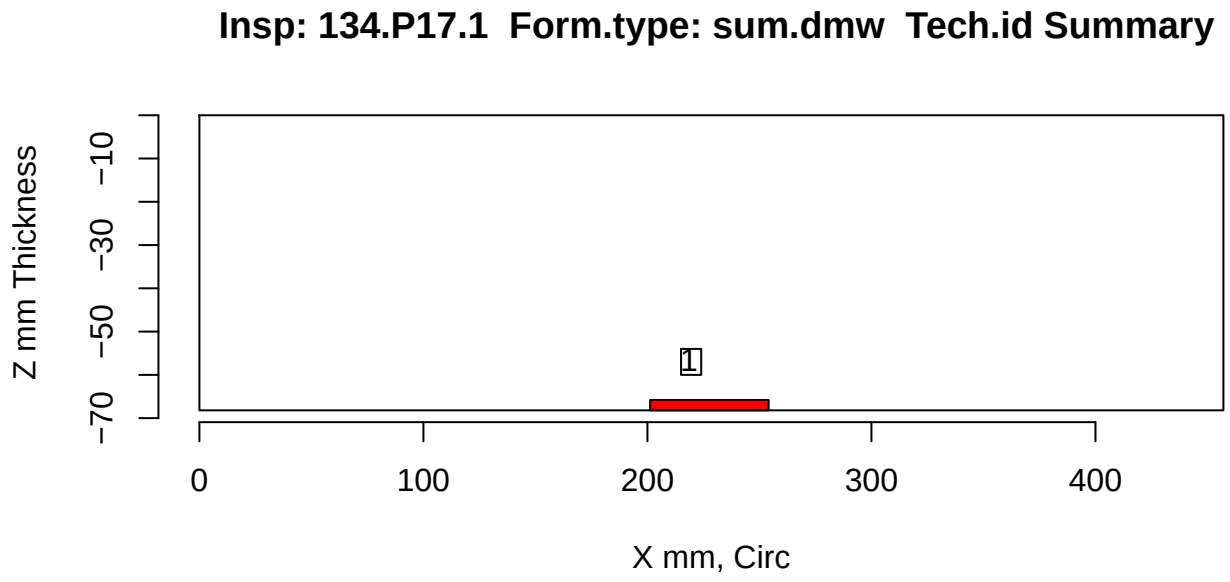
Insp: 134.P17.1 Form.type: sum.dmw Tech.id Summary
Z mm Thickness
−10
−30
−50
−70
1
0
100
200
300
400
X mm, Circ

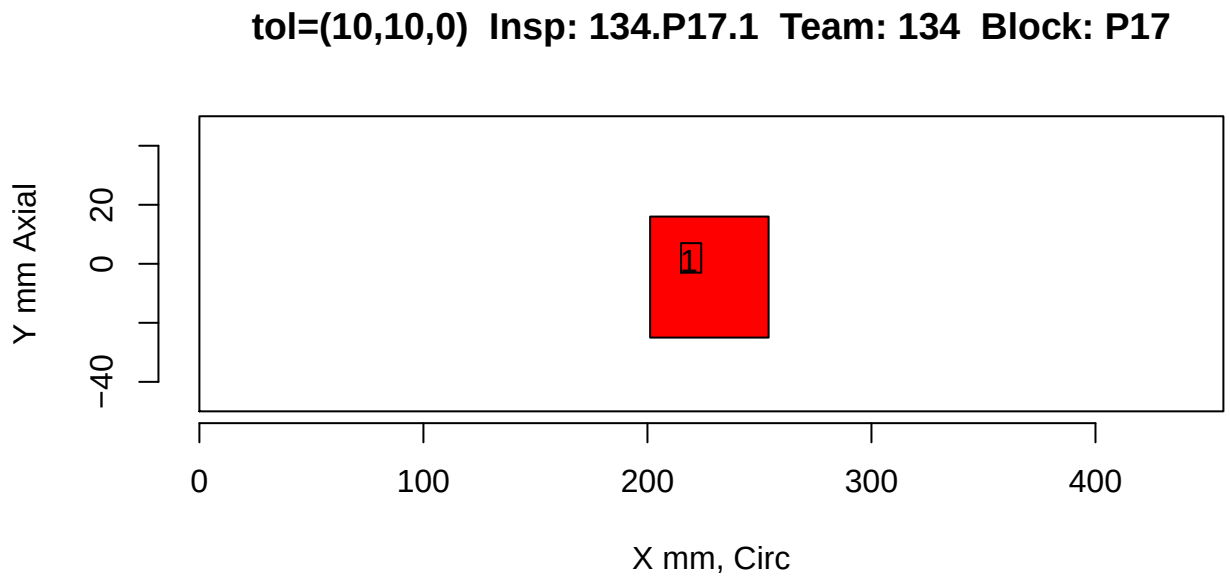
tol=(10,10,0) Insp: 134.P17.1 Team: 134 Block: P17
Y mm Axial
20
0
−40
1
0
100
200
300
400
X mm, Circ

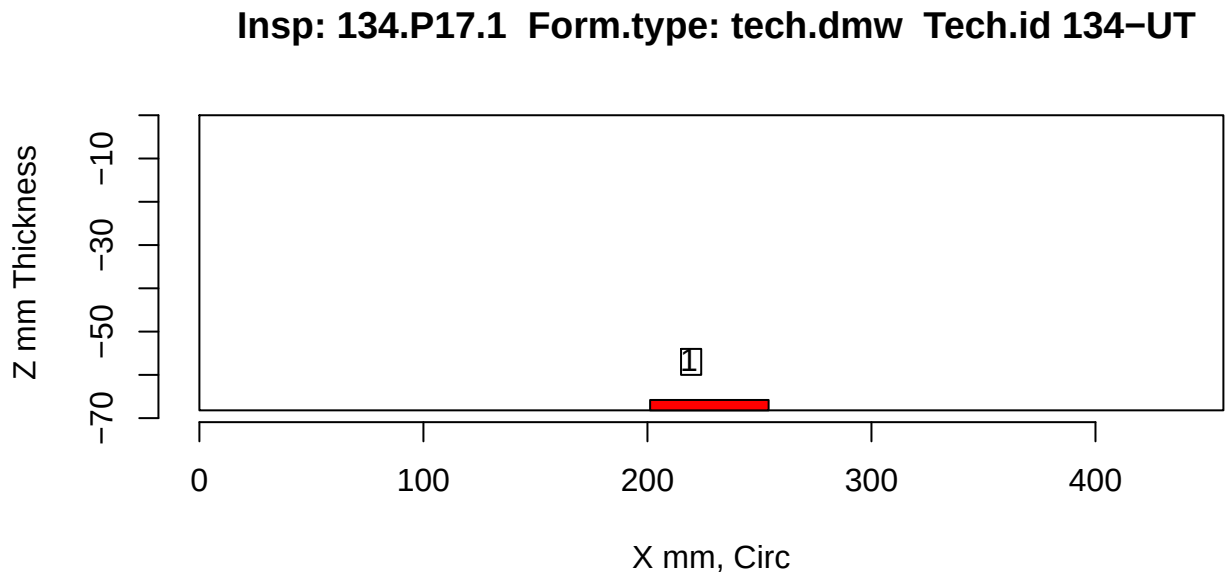
Insp: 134.P17.1 Form.type: tech.dmw Tech.id 134−UT
Z mm Thickness
−10
−30
−50
−70
1
0
100
200
300
400
X mm, Circ

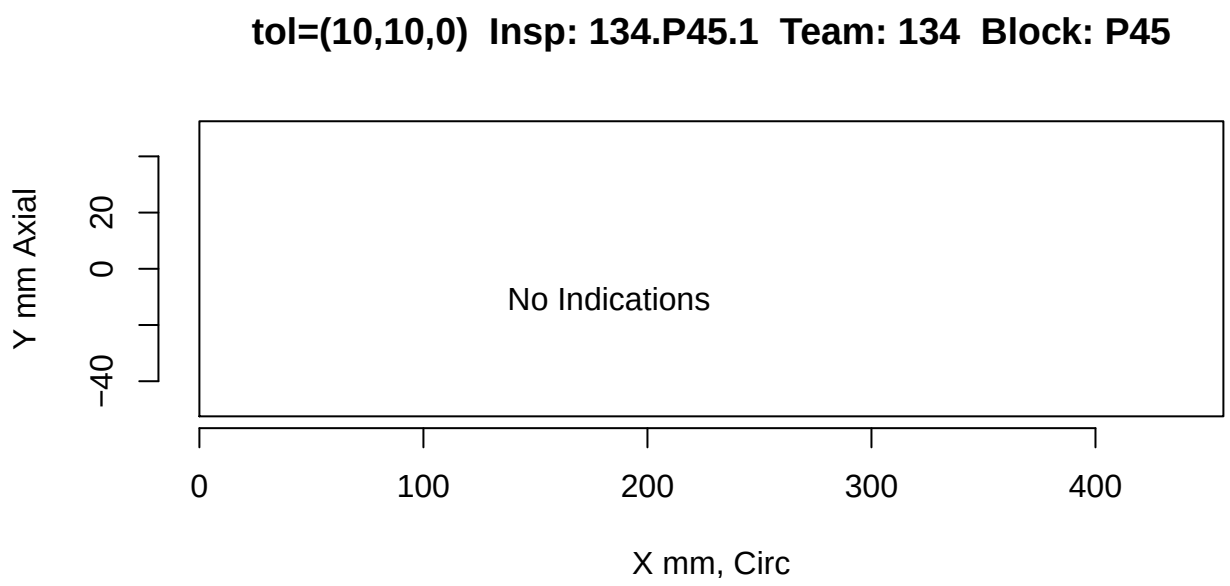
tol=(10,10,0) Insp: 134.P45.1 Team: 134 Block: P45
Y mm Axial
20
0
−40
No Indications
0
100
200
300
400
X mm, Circ

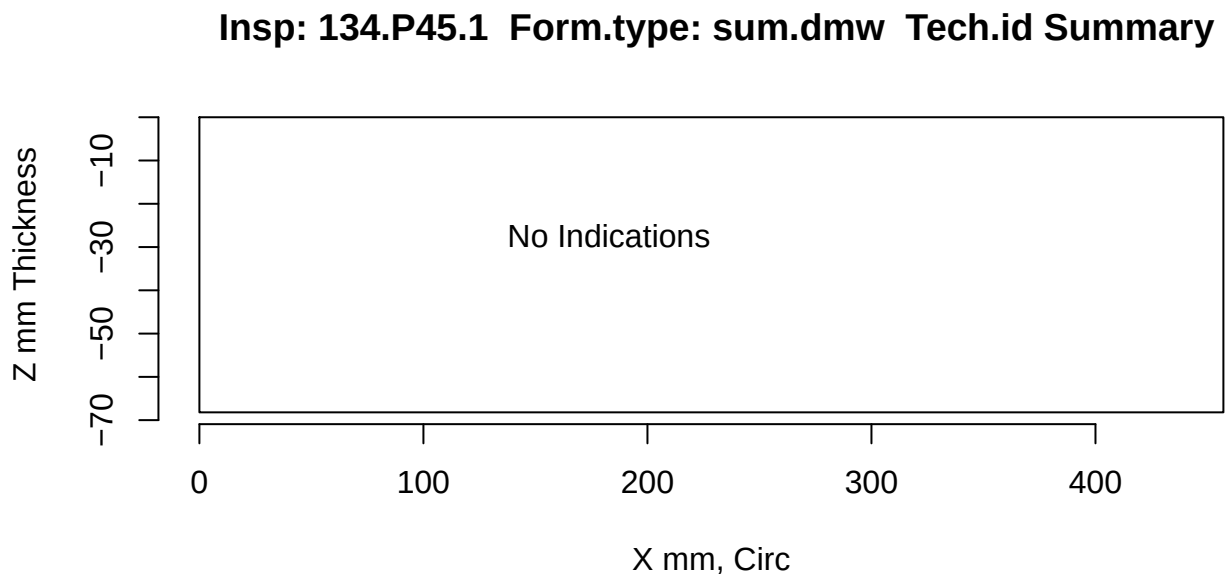
Insp: 134.P45.1 Form.type: sum.dmw Tech.id Summary
Z mm Thickness
−10
−30
−50
−70
No Indications
0
100
200
300
400
X mm, Circ

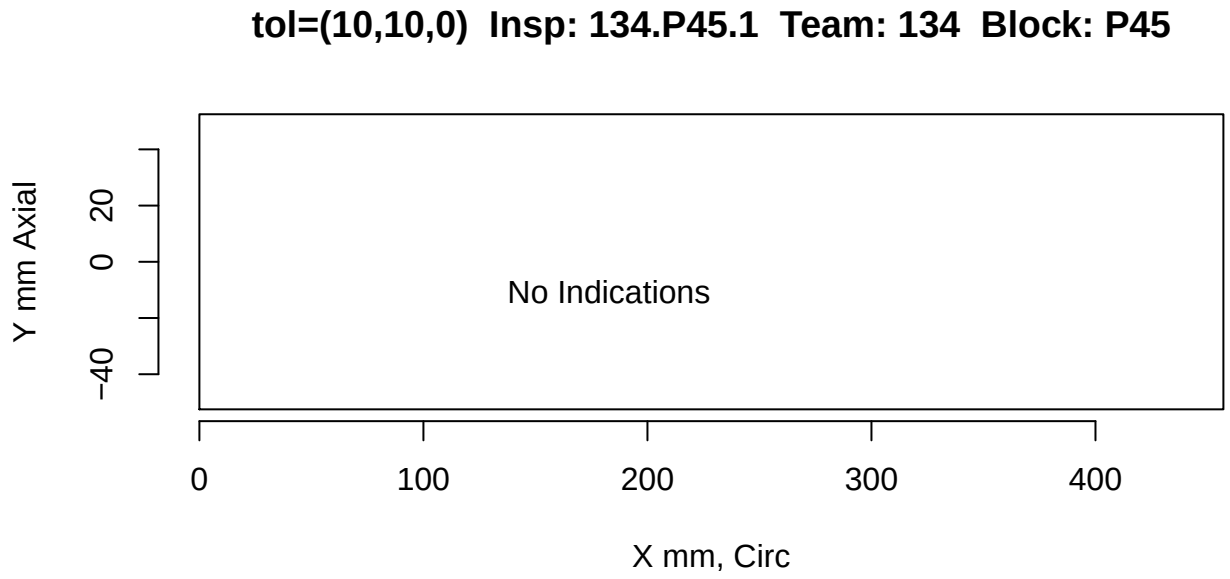
tol=(10,10,0) Insp: 134.P45.1 Team: 134 Block: P45
Y mm Axial
20
0
−40
No Indications
0
100
200
300
400
X mm, Circ

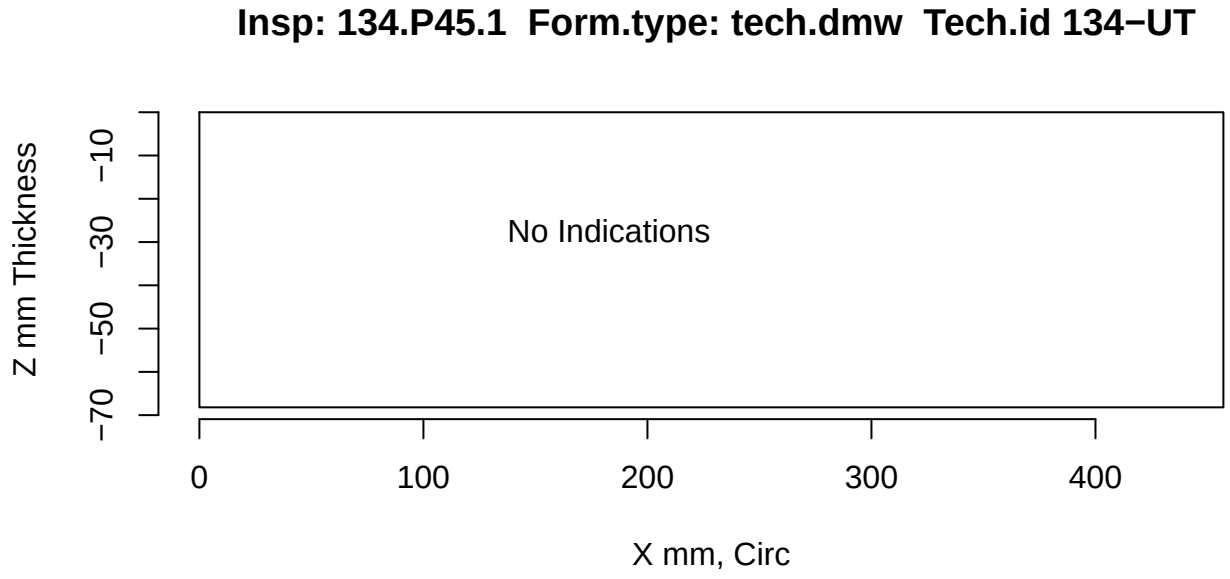
Insp: 134.P45.1 Form.type: tech.dmw Tech.id 134−UT
Z mm Thickness
−10
−30
−50
−70
No Indications
0
100
200
300
400
X mm, Circ

Pacific Northwest
NATIONAL LABORATORY

Proudly Operated by **Battelle** *Since 1965*

902 Battelle Boulevard
P.O. Box 999
Richland, WA 99352
1-888-375-PNNL (7665)

www.pnnl.gov

Prepared for the U.S. Nuclear Regulatory Commission
under a Related Services Agreement with the U.S. Department of Energy
CONTRACT DE-AC05-76RL01830

U.S. DEPARTMENT OF
ENERGY